Developing a method to include flood defenses explicitly in flood hazard maps based on limited available information.

Flooding in Limburg. Sem van der Wal ANP

Master Thesis Rapport

February 2022

Vincent G. Jilesen

TU Delft

Developing a method to include flood defenses explicitly in flood hazard maps based on limited available information.

Vincent G. Jilesen

This research has been done for the partial fulfillment of requirements for the degree of Master of Science in the field of Civil Engineering at the Delft University of Technology, Delft, The Netherlands

Delft, February 2022

Graduation Committee:

Prof. dr. ir. S.N. Jonkman	Delft University of Technology - Hydraulic Engineering Section
Dr. Ir. Matheus van Ledden	World Bank Group
Dr. Elisa Ragno	Delft University of Technology - Hydraulic Engineering Section
Dr. Ir. Olivier Hoes	Delft University of Technology - Water Management Section
Ir. Slobodan Kolaković	University of Novi Sad - Hydrotechnics and Geodesy

Contents

Preface

This rapport marks the final step to completion of my study in Hydraulic Engineering at the faculty of Civil Engineering at the Delft University of engineering.

I wish to thank the members of the graduation committee for their time and contributions during this thesis. In special I wish to thank Mathijs for his guidance and enthusiasm during this period.

Summary

Flooding is one of the most damaging natural disasters worldwide, and presents a significant risk for a large amount of the global population. For the development of flood disaster management strategies, policy makers make use of flood hazard maps to inform investment strategies to reduce risk. In many current flood hazard mapping methods, the role of embankments is either implicit or completely unaccounted for. However, these defense systems can play a key role in both the final extent of the inundation as well as in the development of the inundation. Limitations in available data are often the reason for the lack of explicit implementation of embankments. The goal of this study is the development of a method that can explicitly include the effects of flood defenses in a flood hazard map based on limited available data. Next, this has been tested for a low-lying riverine area and the Tisa river basin in Serbia was selected as a case study area for this purpose. First, an idealized approach has been followed to better understand the model behavior using settings resembling this river. Finally, the method has been applied with a more realistic river schematization.

To develop a method for a more explicit inclusion of flood defenses, an understanding of the different current approaches has been generated based on a literature review. On the scale of global flood maps, the failure probabilities of flood defenses are not used. Only with post-processing, certain areas are considered protected by removing inundation from the maps. Many studies of flood hazard mapping use the so-called bathtub approximation. Hereby is assumed that the complete floodplain will flood and that the inundation depth is found by extrapolating the water surface level outside of the embankments to the area inside of the embankments. The influences of the flood defenses on the inundation are not included. Regional flood hazard maps are still made without flood defenses in many cases. While the improved resolution allows for more detailed maps, the lack of available data still limits the implementation of flood defenses. Flood mapping methods exist that include failure probabilities for flood defenses but these require large amounts of data that is not available everywhere.

An idealized model based on the Tisa river characteristics is used to test a flood mapping method which includes explicitly the presence and potential failure of embankments. Based upon data on the river geometry, hydraulics as well as land-use in the floodplains, a model schematization has been set up with the SOBEK software. The embankments were simplified to a crown height for the purpose of overflow and an estimated failure probability. The breaching of the levee is simulated according to the Verheij-vdKnaap breach growth model. The estimation of the failure probabilities was based on historical failure rates of a comparable flood defense system along the Elbe River. The levees were schematized into segments based on the maximum breach width of the breaching model.

Based on the consequences of a breach, the defense system was split into different stretches. A breaching probability has been defined using the number of segments in a stretch and a binomial distribution. This probability can then be linked to the resulting inundation of the model scenario to create probabilistic flood hazard maps. It was found that multiple simultaneous breaches were necessary to capture the full range of potential scenarios. This leads to a large amount of model runs to provide a reasonable prediction of the inundation probability. A total of 66 computations have been simulated to cover the entire probability space of the base setup. These computations include different return periods (10, 100, 1000 years) and the breach possibilities.

The results of the idealized model scenarios are combined to provide flood hazard maps. Graphs and maps of the inundation depth based on a return period are also created. Also, sensitivity runs have been

carried out to test the influence of changing single parameters. By comparing these to the bathtub approximation, the variance between these methods has been determined. In addition to this, two ratios were presented to quickly determine how this method compares to the bathtub approximation. By taking the ratio between the volume of the flood wave that is available for inundation and the volume that flows through the breach the limiting factor can be found. This ratio indicates whether the inundation is supply limited or breach capacity limited. Secondly, the ratio between the breaching volume and the volume required to reach the inundation depth and extent of the bathtub approximation has been considered. If this ratio approaches or exceeds 1, it means that the bathtub fill approximation is a reasonable assumption.

The idealized modeling simulations have shown that the bathtub approximation should be used with care in large floodplains. Even if the size of the floodplain is restricted to a relatively small area along the river the inundation behaviour is quite different from the bathtub approximation. In all variations it was found that the breach discharge was the limiting factor for the volume that could enter the floodplain. There was more volume available in the river for inundation.

Following the idealized model exercise, the method was applied to a more realistic representation of the case study area. This model was made in HEC-RAS and due to the scale of the model, scenarios with multiple simultaneous breaches could not be simulated. The results of this model show a significant reduction in inundation depth and extent compared to the predictions of the bathtub approximation, see figure right.

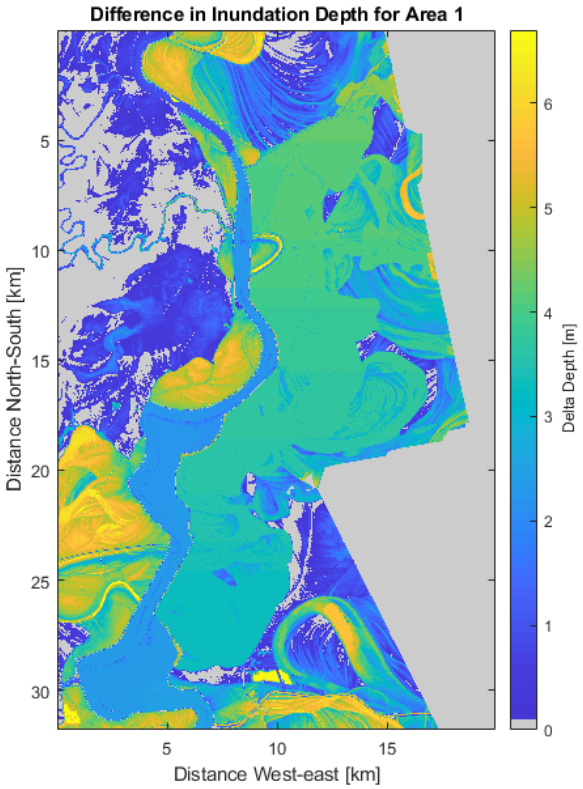

Figure 0.1: Difference in inundation depth for a 1000-year return period based on potential inundation depth from a bathtub approximation and the new method presented in this study including failure of embankments.

Based on the results of both the idealized model and the case study, it can be concluded that the inclusion of flood defenses adds additional information to the flood hazard maps. The bathtub approximation leads to a worst-case scenario and is very likely an upper limit of inundation for the situations considered in this study such as the Tisa River. As shown with the idealized and realistic case, the bathtub approximation will lead to conservative results for large floodplains such as the Tisa River. When the effect of breaching is included, the results of this case study show a much smaller inundation depth and extent. This pattern is likely more realistic given the flood volume and also the embankments built to provide protection against 100-year flood levels. The presented approach provides insight in the inundation probability which can be used by policy makers to plan flood risk management strategies

and prioritize interventions.

This scientific study has explored a new method to explicitly include the presence and potential failure of flood defenses in flood inundation mapping exercises. The Tisa River has been used solely as case study area to test this new modeling method. The findings of this study can serve as good grounds for further methodological considerations in the improvement of flood hazard mapping assessments in similar river basins in the future.

Chapter 1

Introduction

1.1 Relevance of flood mapping

Floods are some of the most damaging natural hazards and result in high impacts across the globe. According to a report by the United Nations (Wallemacq & House 2018) the total damage between 1998 and 2017 was 656 billion US dollars. It affected 2.0 billion people and caused the loss of over 140 thousand lives. Floods have occurred all over the world and throughout history. A recent example is the flooding of the Missouri river in 2019 in the Midwest of the US (Almukhtar *et al.* 2019). This flooding event lasted for more than two weeks and affected a large area along the river. With damage in excess of 2.9 billion US dollar and 30 casualties it shows that flood disasters remain relevant even in the wealthy regions of the world. In the same year an extreme amount of rainfall in the eastern part of Africa has led to widespread damage and destruction of harvests (OSHA 2019). This in turn has led to the outbreak of cholera and additional deaths. This flood has affected around 2.8 million people. These examples highlight the significant societal impacts of floods.

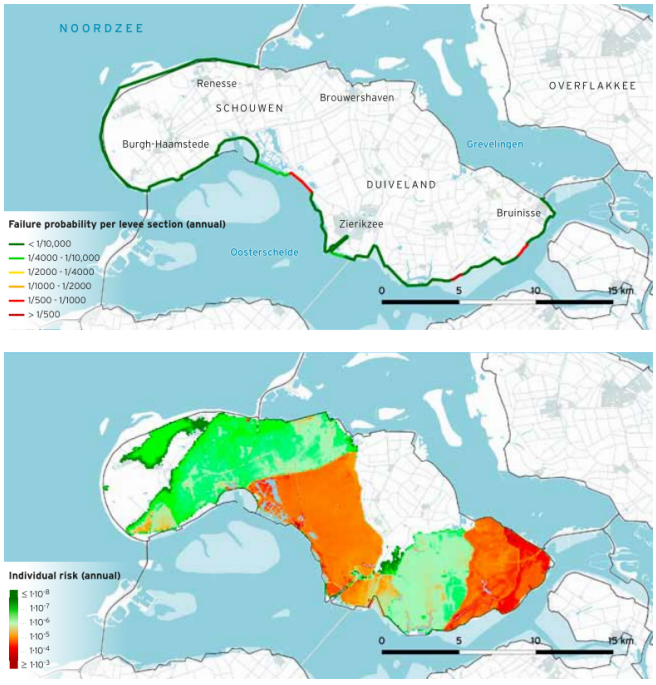

Figure 1.1: Flood risk map of Schouwen-Duivenland in the Netherlands as made as part of the VNK project. (Vergouwe 2014)

Knowledge of the potential extent of floods is therefore paramount for governments, private industry and citizens to reduce the risk of flooding. To be able to prepare accordingly to floods, it is required to predict the occurrence of flooding and the extent of inundation. Often the government will determine flood zones associated with a specific return period which are used to create evacuation plans and damage mitigation strategies (see Figures 1.1 and 1.3 for examples of these maps). Many countermeasures can be taken to mitigate potential damage in these flood zones. Structural interventions range from the construction of levees and drainage channels to the temporary placement of sandbags by property owners in front of their doors. In the United States, FEMA (Federal Emergency Management Agency) has created flood maps for use in its National Flood Insurance Program (NFIP). These maps are used to communicate the risk to citizens and

private companies. The insurance premiums are based on the flood hazard level of the area. These examples show that flood maps are an important input for flood-based disaster management strategies.

Being aware of the need to reduce risk, various countries across the globe have legislation in place in which flood mapping plays a central role. In 2007, the EU has presented the Floods Directive (Directive 2007/60/EC) requiring all member states to prepare flood risk management strategies for all relevant regions. The Floods Directive requires three flood hazard maps for short, medium and long return periods. These maps need to provide the extent of inundation, the flood depth and the flow velocity as well as flood propagation. With this information, predictions for the impacts of these floods on health, environment, economic activities and cultural heritages must be made. These impacts are visualized in flood risk maps. The flood hazard and risk maps are used by policy makers for developing a flood risk management strategy including structural interventions (e.g. embankments, etc.) and non-structural measures (e.g. emergency planning and land management).

Flood mapping is thus an essential ingredient to reduce risk and even a regular activity in many countries due to existing legislation. A flood hazard map is one of the simplest ways to communicate the threat of floods to citizens and businesses. By being aware of the potential danger that affects regions it is possible to take steps towards mitigating those risks.

1.2 Motivation for studying the role of embankments

Nowadays, flood hazard maps are created for different types of floods at different scales with a variety of models. There exist - broadly speaking - two different scales for flood maps, a global scale and a regional scale. The difference in models between these scales is often a matter of grid resolution. Modeling at higher resolution becomes increasingly feasible these days due to increased numerical computation power and the availability of detailed data sets (e.g. topography, land use).

Flood hazard maps are typically generated with numerical models using data from topography, hydrology, hydraulics, existing infrastructure, land use etc. as input. Long-term data series are required to determine storm surge or river discharge statistics and derive boundary conditions for flood hazard models. The topography is used to create a Digital Elevation Model (DEM) which is the basis for the modeling of flood routing and the level of inundation. Land use maps are generally converted to create land roughness maps for the flood computations. River hydraulic data is used both for flood routing and the determination of surges and flood waves. As an example the data structure of the GLOFRIS model is presented in Figure 1.2.

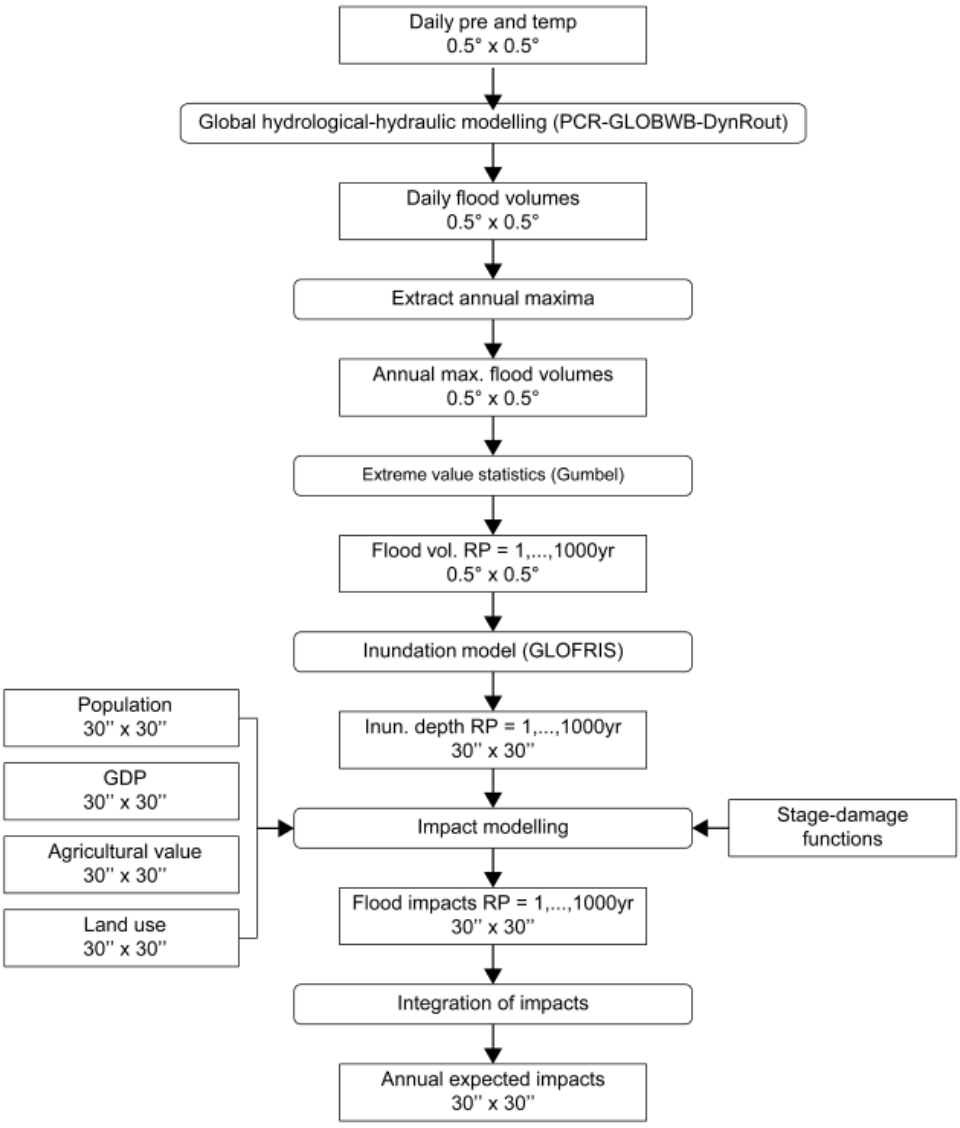

Figure 1.2: Data structure of the GLOFRIS global flood map (Ward *et al.* 2013)

For low-lying areas, making these maps is not straightforward because of the presence of embankments and their effects on the flood extent. In many flood hazard mapping projects, the inclusion of embankments is not very detailed. Levees are assumed to be effective to their crest or design water level. There is no consideration for the actual failure probabilities. This has resulted in flood maps where parts of the inundated area are removed by post-processing if these areas are protected by an embankment. The influence on flood routing that this step might have is not considered. In other projects, the area protected by flood defenses is marked as potential inundation area without any information on the probability of this occurring. In the Netherlands, all of the flood defense systems were modeled in a probabilistic way as part of the VNK project (Veiligheid Nederland in Kaart). Detailed flood hazard maps were made taking into account the failure probabilities of the embankments. An example has been included in Figure 1.1. This is an example of implementing flood defenses into flood

mapping while acknowledging the inherent uncertainty of their functioning. By not taking the flood defenses into account a large overestimation of the inundated area could occur. While simultaneously underestimating the inundation depth and overestimating the time for evacuation in the areas that will be flooded. This can be seen in Figure 1.3 where a large area of the low-lying area surrounding the Sava river has been predicted to be at risk of inundation.

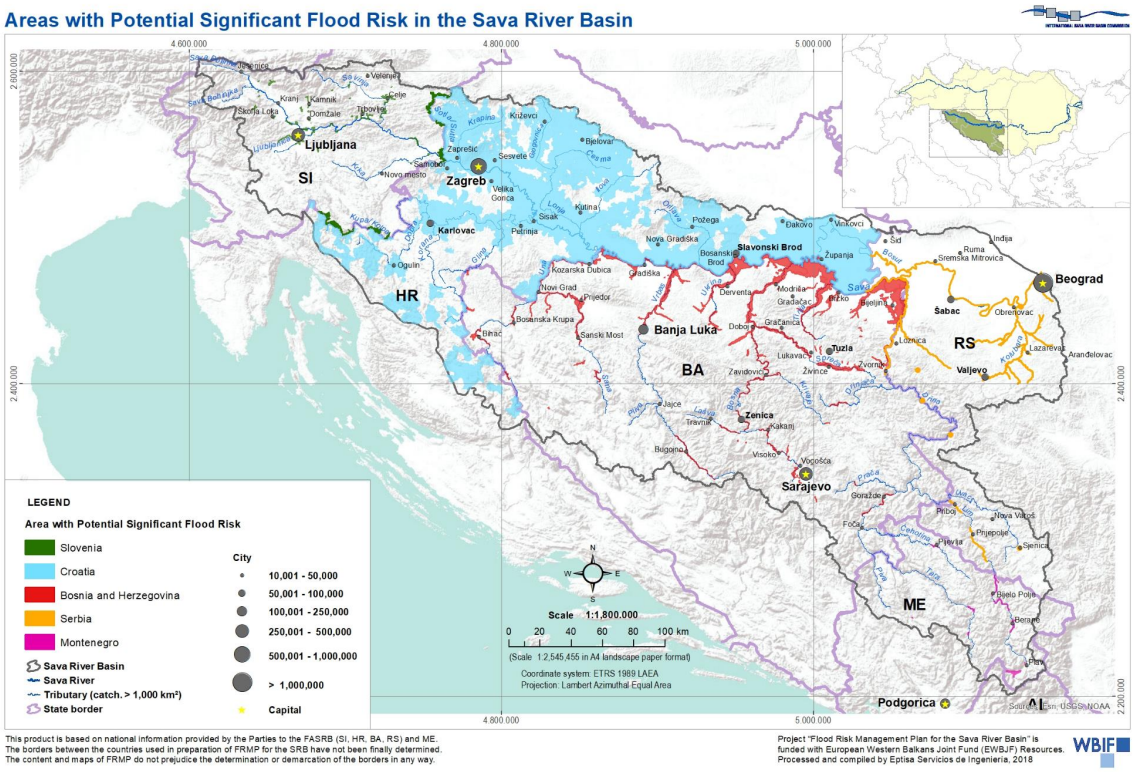

Figure 1.3: Flood risk map of the Sava river basin in Serbia from draft rapport. (Eptisa Servicios de Ingeniería S.L. 2018)

The role of embankments in flood protection is very clear but how to include this aspect into flood maps is an area which requires further research. The key problem in modeling of flood defenses is the inherent complexity of their function. There are different mechanisms which can lead to failure. To properly account for these mechanisms a large amount of information about the design and material of the levee is required. Many flood defense systems also include other works like sluices and drainage channels with have their own failure mechanisms. Even the properties of the underlying soil layers need to be known to accurately predict the performance of a system during a flooding event. Ultimately the lack of data available for these mechanisms makes it very difficult to provide accurate failure probabilities with any certainty. In this regard there is no perfect model or strategy to apply to determining the influence of a flood defense system.

1.3 Objective and scope

In most current flood mapping approaches, flood defenses are not included or only included in post-processing. Only in specific studies with large funding like the VNK and IPET studies, the explicit

modeling of flood defenses has been included. In global and local flood inundation maps the flood defenses are only included implicitly or not at all. Explicit inclusion refers to the use of probabilities to determine the influence of flood defenses on the flood hazard mapping. For global maps this is caused by a lack of data or the limited resolution. In local flood maps the resolution is not a problem but there is often still limited available data. The lack of explicit modeling of flood defenses leads to potential inaccuracies in the predictions of inundation extent, depth and the evacuation time.

The goal of this thesis project is to explore the development of a method to integrate the likelihood of failure of flood defenses into flood maps based on limited data. For this purpose, several research questions are defined:

1. What are the current methods of including the effects of levees and the possible failure of these structures in flood inundation maps?

2. What is the structure of a method to include the likelihood of levee failure into flood inundation maps considering an environment with limited available field data?

3. What can be learned from applying this method to various idealized cases about the importance of taking into account levee failure in flood inundation mapping?

4. How could this method be applied in practice to a real-world situation and what can be learned from this for application to other riverine areas around the world?

This study has been limited to fluvial flooding in low-lying areas protected by embankments. These areas are very relevant from a risk management perspective since a large part of the world population and GDP is concentrated along river floodplains with flood protection systems in place. Due to the topographic nature of floodplains in these areas flood extent is easily overestimated if embankments are not taken into account properly. Due to the limited data, the inclusion of structures as part of the flood defense system will not be considered in this study. A method based on limited data cannot perfectly model the complicated mechanisms that are involved. But a reduction in the inaccuracy, and an improvement to the reliability of flood hazard maps can be made.

1.4 Approach

1. What are the current methods of including the effects of levees and the possible failure of these structures in flood inundation maps?

The first research question has been answered in the literary review. Based on the initial study a lack of explicit modeling of flood defenses was found in most current strategies. The leading cause for these limitations are the lack of data on flood defenses and the low resolutions of the models. The literary review can be found in Chapter 2.

2. What is the structure of a simplified method to include levee failure into flood inundation maps considering an environment with limited available field data?

To answer the second research question, a simplified method for the modeling of flood inundation has been developed. The second part of the thesis study is the implementation of a simplified model for a river flood. This allows for the testing of individual parameters and to determine their influence on the results. The setup of this model can be found in Chapter 3.

Since the goal of this study is to improve on the modelling of flood defenses with limited data,

specific failure mechanisms are not studied. For the initial setup of the idealized model, an estimation of the failure rates has been made. Based on this estimation, the breaching probabilities have been determined and a fragility curve has been constructed. The initial estimates have been based on the order of magnitude found in historical data as described in (Kool *et al.* 2022).

To make use of this simplified model, data is required to define various model inputs. The forcing of the model requires water levels and flood duration for multiple return periods. These have been used to derive hydrographs as the input for the model. The hydrological model is a gauged flow model as a detailed cascade model is outside of the scope of this study. For the levees the height as well as an estimate for the used material are used.

In the VNK study (Vergouwe 2014) the flood defense systems have been split into different sections based on consequences and levee properties. This strategy has also been applied to this method. A 2D or quasi-2D hydraulic model has been used for this study. These also provide better accuracy for flood progression in low-lying areas. The model for the initial setup has been made in the SOBEK software made by Deltares. This program can combine a 1D channel with a 2D grid to represent the river and the floodplain respectively.

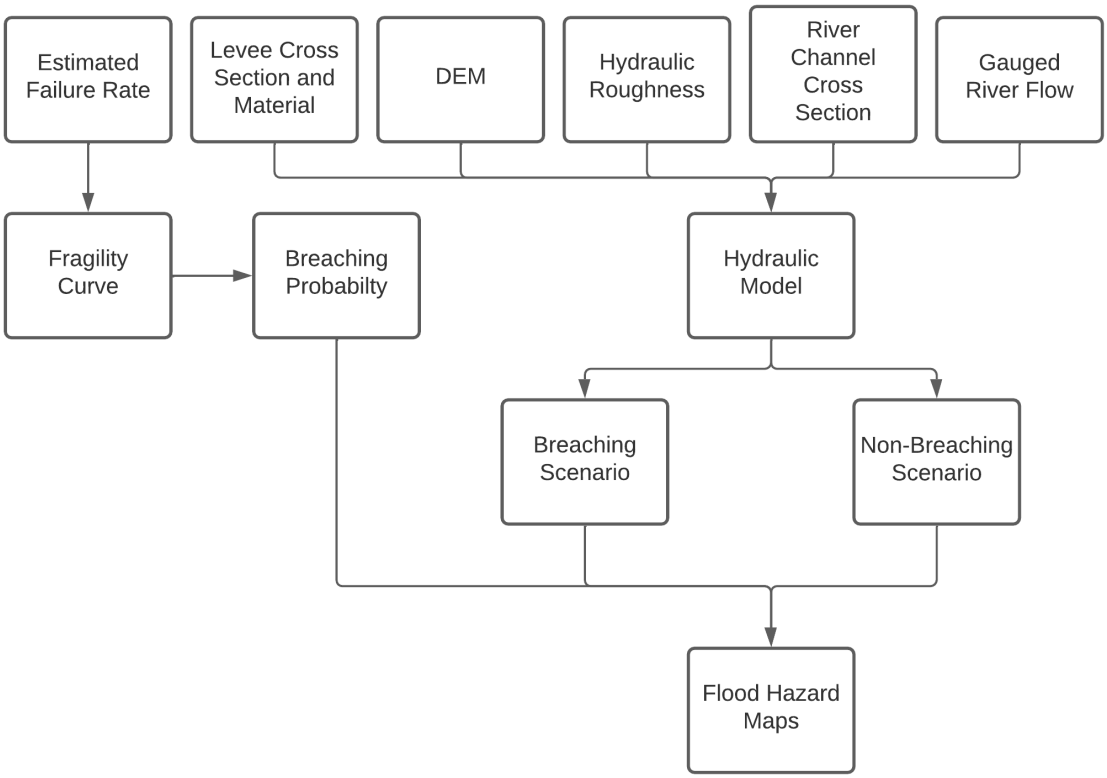

Figure 1.4: Proposed process flowchart

The results from the hydraulic software have been visualized to be usable for flood inundation maps. For this study the open-source QGIS software was used. The combination of different scenarios requires some calculations that are best done with a numeric calculation tool such as MATLAB.

3. What can be learned from applying this method to various idealized cases about the importance of taking into account levee failure in flood inundation mapping?

The third part of this thesis is the evaluation of the method applied to an idealized model. The EU Flood Directive requires flood maps of three different return periods. The medium return period has been used as a basic test for the function of the model. The model has been tested for a low return period to provide insight in the possible overestimation of these smaller floods. The high return period was studied to provide insight in the method's handling of large floods. As an initial selection the 10-year, 100-year and the 1000-year return periods have been studied herein.

To study the behaviour of the inundation for different circumstances an evaluation has been made of the idealized model. By changing certain parameters, changes in inundation behaviour could be found. Based on these changes, it is possible to predict how the method will behave for different cases.

This has led to a number of flood maps for different return times and parameter selections. By scaling the parameters their influence on the final flood extent has been visualized. These maps have been compared with a control map based on average values to study this in more detail. Flood maps are made by combining the breaching scenarios and the non-breaching scenario into a single map. The results of the idealized model are presented in Chapter 4.

4. How could this method be applied in practice to a real-world situation and what can be learned from this for application to other riverine areas around the world?

The fourth part is a real-world case study of the Tisa river. Currently the flood maps for this basin have been made using 1D flood models and the current flood defenses have not been included. This makes this area interesting to test in newly developed method and compare to the current maps. The new method can also be tested on performance based on a historical flood.

For the implementation of the model for the case study, the following data were required: gauged flow data for the upstream boundary condition of the river for several return periods, river profiles for the determination of flood development and profiles of the levees surrounding the river reach studied and a DTM of the area. The implementation and the results of the proposed method for a case study is presented in Chapter 5.

Chapter 2

Literature review

2.1 Introduction

This literature review has been made as the first part of a master thesis study on the inclusion of flood defenses in flood mapping. In this literature review the answer is sought for three main questions:

What methods are used in the creation of flood maps for different scales? The first goal of this literary study is to find out how flood maps are currently made. Which strategies are currently employed for different types of flooding? In this study the focus is on river and coastal flooding, as this is where most flood defense structure are built for.

How are flood defenses included in these maps? The second goal is to find out how flood defenses are modeled into the flood maps. The importance of embankments cannot be overstated in the development of accurate flood routing.

What kind of data is required to create these maps? The final goal of this study is to find out how the available data influences the creation of flood maps and especially the inclusion of flood defenses.

For this literary review scientific articles on the topic of flood mapping were sought in several journals relating to natural hazards and hydrology. These include the Journal of Flood Risk Management, Environmental research letters and Natural Hazards and Earth System Sciences with a focus on case studies and validation studies for flood mapping models. For the study of detailed inclusion of flood defenses in flood mapping, two specific projects were studied: the VNK project in the Netherlands and the IPET study of the hurricane protection system in New Orleans. Both of these projects have a detailed probabilistic approach to the modeling of flood defenses.

For additional insight in the process of flood mapping, publications of the World Bank Group, the United Nations Office of Disaster Risk Reduction (UNDRR) and the Global Facility of Disaster Reduction and Recovery (GFDRR) were studied.

The currently existing methods for flood inundation mapping can be roughly split into two scales and the influence of flood defenses can be included in both implicitly and explicitly. An overview is made in Figure 2.1. In Section 2.2 the focus is on global flood mapping. These are large scale methods that use implicit modeling of flood defenses. In Section 2.3 local flood mapping used by national governments is studied. Methods for these maps are made at a smaller scale with greater resolutions but the modeling of flood defenses remains implicit. Finally, in Section 2.4 a study is made on the explicit modeling of flood defenses by two major projects, the VNK and IPET project. Since the case study in this thesis focuses on the Tisa River in Serbia, a brief introduction of this river and the current flood mapping efforts is presented in Section 2.5.

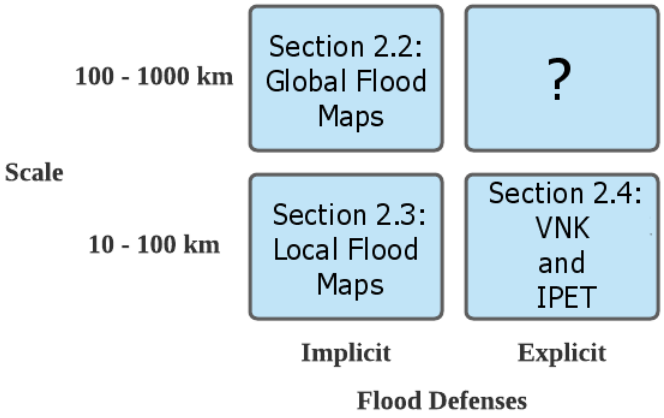

Figure 2.1: Inclusion of flood defenses and scale in flood mapping.

2.2 Global flood mapping

2.2.1 Introduction

Global mapping efforts are made to provide information to policy makers and citizens everywhere. These projects are mostly focused on data poor regions where local governments do not have the funding or expertise to create smaller scale maps on their own. Most of the currently available data sets provide several different products for different return periods. These products include primarily flood hazard maps with inundation extent, depth, velocity and propagation. As described in (Alphen *et al.* 2009), flood hazard maps are used for many different policies. Based on flood hazard maps flood risk maps can be made. These combine the hydraulic information with flood damage curves to predict the economic losses caused by a certain level of flooding. Even though creating maps of this scale leads to a limited resolution they can still provide a large amount of value.

Based on a recent study (Aerts *et al.* 2020) on the validation of global flood maps a selection of models was studied. The models will be compared on the difference in hydraulic modelling and the reliability of the resulting flood maps. These are presented in Table 2.1.

Global Flood Model	Model Resolution	Output Resolution	Forcing approach	Hydraulic approach
CaMa-UT	3 arcsec	18 arcsec	Cascade model	Complex 2D sub-grid
CIMA-UNEP	3 arcsec	32 arcsec	Gauged flow model	Simple 1D
ECMWF	3 arcsec	18 arcsec	Cascade model	Complex 2D sub-grid
JRC	30 arcsec	30 arcsec	Cascade model	2D hydrodynamic
GLOFRIS	30 arcsec	30 arcsec	Cascade model	2D volume
Fathom	3/30 arcsec	3 arcsec	Gauged flow model	2D hydrodynamic

Table 2.1: Overview of studied global flood map models.

Global models are focused on fluvial floods and do not include coastal flooding or the influence of sea levels to river dynamics. Where river floods fueled by precipitation and can be predicted with run-off models that use the same elevation data as flood routing models. Coastal floods are generated by a combination of tides, wind-induced surges and waves. The influence of the water level at the mouth of a river can be seen for a large distance. The inclusion of these effects requires a large amount of data on the occurrence of storms and wind. To properly model waves development detailed information on the bathymetry of the coastal area is needed. This information is often not available in less developed regions.

2.2.2 Data requirement

The first major components of all flood mapping efforts are hydrological data used to determine the forcing of the models. There are two models used to predict river floods. The first model is locally measured water levels and flow rates. Measuring station are found over the whole world but predominately in developed regions. A publicly available source for global river discharge data is Global Runoff Data Center (GRDC) (WMO 2021) sponsored by the World Meteorological Organization (WMO). The map of measuring stations, that are part of the data base, shows clearly that most of the data is center around Europe and the United States while a lot of the data in the rest of the world is somewhat out of date. The second model is to calculate the discharge of rivers with a runoff model and precipitation data. Global precipitation data is available from the Global Precipitation Measurement mission (GPM) from NASA. This data product has a spatial resolution of 10km and a temporal resolution of 30 minutes.

The second major component is elevation data and land properties. The use of the first of these is obvious. The elevation data is required to determine the depth and extent of inundation. This data is stored as a Digital Elevation Model (DEM). In certain cases, the terms Digital Surface Model (DSM) and Digital Terrain Model (DTM) are used. The DSM includes buildings and vegetation in its elevation while the DTM only includes the elevation of the terrain itself. The terms DEM and DTM are often used interchangeably. The global flood models studied all use data from STRM3 data set. This data set was created by the Shuttle Radar Topography Mission in 2000. This data has a resolution of 3 arc sec or roughly 90m. It is also provided at a 30 arc sec resolution. To properly predict

the propagation and extent of inundation more data is required. In addition to the elevation also the roughness of the bed material is required. The roughness is a key component for the determining of the momentum balance component of the hydraulic model. The slope of an area can be found from the elevation data. The slope is included in both the mass and the momentum balance. Often these data sets need to be corrected due to errors in the measurement of an innate measurement bias.

Flood defenses are simplified due to their relatively small scale compared to the rest of the model and the limited amount of data. Most flood defenses structures are far smaller than the 1 km resolution most global flood maps work with. Due to the resolution, these defenses are thus not visible in hydraulic modeling. Furthermore, the probabilistic modeling of flood defenses requires far more local data that cannot be found with remote sensing techniques. There is very limited globally available information on the existence and standards of flood defenses. An effort has been made to provide a global database for flood protection standards (Scussolini *et al.* 2016). FLOPROS is based on three different layers. The first layer is based on known data on flood defenses, the second layer on known policies and the third layer is estimated based on local GDP. With these three layers a complete overview of global protection standard is made. The influence of maintenance and climate change is not included and this can lead to uncertainty regarding the current state of the flood defenses. A standard is no guarantee for the proper implementation.

2.2.3 Methodology

The use of 1D, quasi-2D or 2D hydrodynamic models for inundation is common in global flood mapping. The key difference between these three models is how the DEM is included into the model. A study on the differences between these models was made in a master thesis (Betsholtz & Nordlöf 2017) based on the HEC-RAS software. In the case of a 1D model, the area surrounding the river is treated as an extension of its cross section. This is theoretically based on the 1D shallow water equations (St.Venant equations) for unsteady flow. This is a relatively low computational method since it treats the flow of the water parallel to the river axis only. A side-effect of this approach is that the inundated area is treated as a bathtub. This means that as soon as the water level crests a levee or any part of the cross-section the area behind is immediately assumed to have that same water level as seen in Figure 2.2. The effects of embankments or any other part of the terrain are unaccounted for.

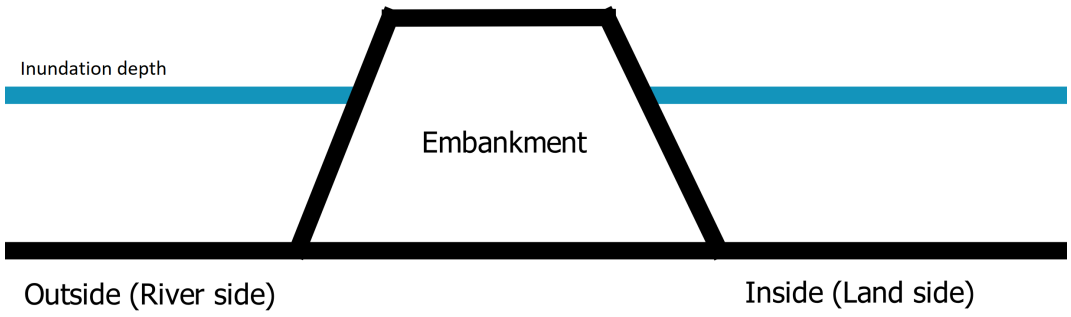

Figure 2.2: Bathtub approximation often results in water bypassing embankments without any breaching or overtopping.

The 2D model is based on a grid or cell map where each point has an elevation and roughness. These are then combined with the 2D hydraulic relationships to provide flow patterns varying in space and time. The relation between the flow and the water level are again based on shallow water equations. Most models apply a simplification in the form of the diffuse wave approximation. This simplification is based on the assumption that the momentum equation is dominated by the gravity and bottom friction terms. This model can provide more insight in the propagation of the flood as it no longer assumes parallel flow to the river and does not automatically fill the area behind levees. This type of model is computational far more intensive that the 1D models.

The quasi-2D approach combines the 1D model for the flow in the river with a 2D flood routing model as soon as the embankments are crested. This provides a reduction in computational requirement compared to a full 2D approach while reducing the issues caused by a fully 1D approach. Of interest is the coupling between these two models. There are two different methods. In the first, the 1D model provides the forcing for a 2D model in the case of overtopping or a levee breach. The incoming volume is then the forcing for the 2D model. In the second method the 1D model is used to provide the upstream boundary conditions for a 2D model at the area of interest.

Data is found at different resolutions and the global models are limited in resolution by computational power. CaMa-UT (Yamazaki, Kanae, *et al.* 2011) makes use of a global flow routing map based on the DEM and the Global Drainage Basin Database (GBDB) (Masutomi *et al.* 2009). In the ECWMF model (Pappenberger *et al.* 2012) the ERA-Interim (ERAI) reanalysis is used to model the run-off though the HTESSEL scheme. The ERAI is made with data from the Global Precipitation Climatology Project (GPCP).

Many data sets for gauged flow are limited in temporal resolution. The down scaling of this data to usable probabilistic values to provide good estimates for peak flows with a certain return period is complex and can be computationally demanding. The ECMWF model (Pappenberger *et al.* 2012) includes a standardized method to determine these.

There are two methods to determine the forcing of the hydraulic model: the climate cascade model and the gauged flow model. An overview is presented in Figure 2.3. The gauged flow model is purely based on historical water levels and flow rates measured in the past. While a long history of measurements exists in Europe and other wealthy countries, in major parts of the world this data is rather limited. In contrast, the climate cascade model is based on precipitation and run-off models to determine the water levels and flow rates in rivers downstream of the watershed. This model can be used worldwide with the use of satellite data for precipitation and a DEM. Of interest is the inclusion of climate change influence on these two different approaches. The gauged flow model is very limited in the study of the influence of different climate behavior or increased urbanization in its watershed. These effects can

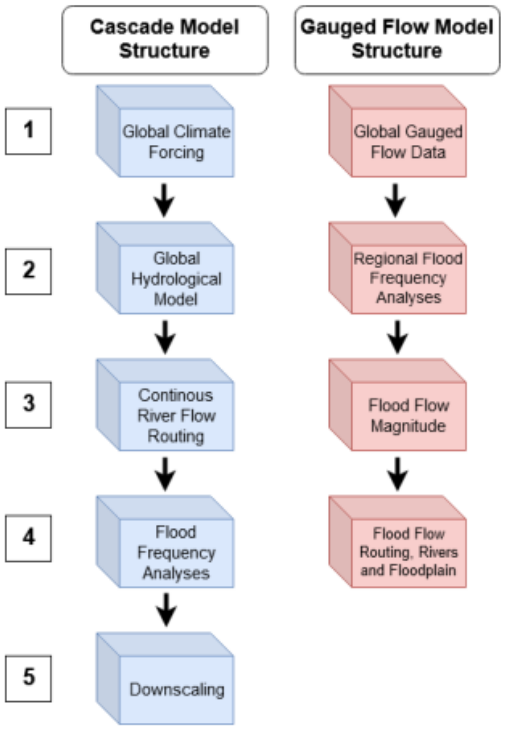

Figure 2.3: Workflow climate cascade model and gauged flow model by (Aerts *et al.* 2020).

be modeled into a climate cascade model. The drawback of a climate cascade model is the degree of uncertainty related to the influence of storage. The run-off is dependent on the storage of water in the soil. The storage capacity that is available is related to the weather over a longer period. Run-off modeling comes with its own uncertainties which should be considered.

Most models have flood defenses that are treated fully deterministic or included these only during post-processing. In the case of 1D modeling, the embankments adjacent to the river can be taken into account as part of the cross-section. But these extend only to the geometry. None of the failure mechanisms are only related to the crest level of the levee. By assuming that the levee is infallible the hazard would be strongly underestimated. It is remarked in (Ward *et al.* 2013) that the 2 year return period is assumed to not lead to overbank flooding and this volume is removed from the combined flood hazard maps. In addition, due to the lack of globally available data of flood protection these are not included in the model which will lead to an overestimation. In FATHOM (Sampson *et al.* 2015), the flood defenses are assumed to have failed but could be included as additional conveyance capacity. More detailed approaches are hindered by limited data and the small scale of the defenses compared to the resolution of the flood hazard maps. In the ECWMF model (Pappenberger *et al.* 2012) an algorithm is described predict the design return period for the flood defenses based on the local concentration of the GDP. Based on this an ellipse is placed over the GDP center and this area is excluded for flood hazards for flood up to the design return period.

For the studied global flood models the applied strategy is summarized here:

In CaMa-UT (Yamazaki, Kanae, *et al.* 2011) the rivers are simulated has having a simple rectangular geometry, and the channel width and bank height were estimated from the upstream runoff. The river and the flood plain are combined for the purpose of storage. For each point the river discharge, water depth and the inundated area are calculated based on the water storage. With the use of the diffuse wave simplification the flow is routed downstream with inclusion of backwater effects. The model generates maps of various resolutions where each pixel is one cell for the 2D hydraulic model. Each cell has been assumed to have only one downstream cell.

The CIMA-UNEP model (Rudari *et al.* 2015) makes use of a 1D hydraulic model. The roughness coefficient is variable over both the channel and the flood plains. Backwater effects in tributaries caused by the water level of the main river are included.

The ECMWF model (Pappenberger *et al.* 2012) combines the HTESSEL (Hydrology Tiled ECMWF Scheme of Surface Exchanges over Land) land surface model to provide the run-off values based on precipitation data. These are then combined with the CaMa-Flood model (Yamazaki, Kanae, *et al.* 2011) to produce flood mapping.

In the JRC model (Dottori *et al.* 2016) flood inundation is modeled with the CA2D 2D hydraulic model. This model makes use of a grid where the squares are model as octagons to link them to the both the orthogonality and diagonally adjacent cells. This leads to some measure of numerical inaccuracy but was found to provide a better prediction for real world flood events. The shape allows for better modeling of flow directions based on the DEM. The 2D equation are calculated with the Euler method. The channel and the floodplain are modeled with separate roughness values. The forcing is down scaled to hydrographs for each flood point and are used for the simulation of inundation. Flood points are placed at the outlet of the river basin and 10km upstream from the previous one.

The GLOFRIS model makes use of a DEM and a map of river cells of the same resolution. In this study (Ward *et al.* 2013) this was 30 arc sec. A grid is generated of a smaller resolution than the input data. From a single starting grid cell, the water level is raised by 10 cm. If the water level or elevation in adjacent cells is lower than the water level in this cell, the water level is raised to the starting level. This process is repeated till the total added volume is equal to the incoming flood volume.

The FATHOM model (Sampson *et al.* 2015) makes use of SRTM3 data which is corrected for vegetation and urbanization. The 3 arc sec version of the SRTM DEM is used to reduce noise. This will lead to a reduction of the bias of the DEM and a better approximation of the real-world terrain. Precipitation data is combined with the GRDC database to provide estimations for annual max discharge forecasts. The described method is still under study and therefore carries an additional degree of uncertainty. The noise of the 3 arc sec map used for the precipitation modeling is considered a more significant source of uncertainty. River characteristics are estimated based on local data if available or from the assumption that bankfull discharge occurs with a return period of 2 years. This can be combined with the channel width found through remote sensing and an estimate mate of channel slope based on the DEM. With Manning's equation then the channel depth can be determined. The inundation is then modeled with a 2D hydraulic model (LISFLOOD-FP). This is done on the 30 arc sec resolution to reduce the computation time significantly.

2.2.4 Discussion

The currently available global flood maps have many aspects in common in their approach. The methodology varies in the hydrological forcing as well as the hydraulic flood routing. The key problem

of the existing flow gauge data is the limited availability. While this data is of good quality in developed countries, the quality and the availability is limited in less developed regions. The cascade model makes use of watershed models and precipitation data generated by remote sensing. Uncertainty of the satellite data is caused by inherent biases and difficulty in validation of the data in areas with limited meteorological data collection on the ground. Run-off modeling is made more difficult by the presence of vegetation and the lack of information of groundwater storage in the watershed.

The data requirements of global flood models are relatively low but this results into increased uncertainty. The output resolution of most of the studied models was around 30 arcsec (roughly 920 meters at the equator) or 18 arcsec (roughly 550 meters at the equator). The models that run internally at a smaller resolution often include simplifications in the modeling. CaMa-UT simplifies the channel parameters and CIMA-UNEP makes use of a 1D hydraulic model. The uncertainty caused by the limited resolution can be seen in studies that compare different global flood maps with each other for a single area. In (Aerts *et al.* 2020) it is shown that the models have differences in flood extent up to a factor of 4 during a study of flooding extent in China. In (Bernhofen *et al.* 2018) the difference in estimates by different global flood maps was studied for Nigeria and Mozambique. The Critical Success Index (CSI) scores range between 0.45 and 0.70. This shows that the accuracy of the flood maps is rather limited and a large degree of uncertainty remain in the predictions of flooding.

Flood defenses are included in the models in different ways without really accounting for any failure probability or are not included at all. The limited resolution makes it impossible to determine the exact shape of embankments from remote sensing alone at a global scale. Due to this often estimates are made to provide a design return period for the flood defenses. In certain models an effort is made to reduce the overestimation for low return period events by removing part of the flood hazard area in a post-processing step. In these cases the flood defenses are modeled implicitly as fully deterministic. For large return periods, the flood defenses are assumed to fail which leads to some overestimation. While all of these techniques are logically sound, they introduce a large amount of uncertainty into the flood maps. This leads to problems with the development of mitigation strategies.

2.3 Regional and local flood mapping

2.3.1 Introduction

Regional models are often capable to provide more information on flood routing due to higher resolution and more local details. Compared to global flood models, the higher resolution provides more output data to create flood risk maps. The added value of this can provide far better insight in the design of mitigation measures.

There are many uses for local flood maps. One of the uses for regional flood maps is for insurance risk maps. These maps are used to determine the premium for flood insurance. In the USA, flood insurance is provided by the government through the National Flood Insurance Program (NFIP). For this reason, the Flood Risk Insurance Maps (FIRM) used are provided by FEMA. These maps are built up using smaller maps created by local organization according to FEMA guidelines. In many of these areas it is impossible to find a mortgage without a flood insurance policy. Flood insurance policies are mostly found in wealthy western countries like North and West Europe, Australia and Japan as well as in Mexico, Peru, Indonesia, Morocco and Nepal.

Most regional flood mapping efforts use models comparable to GFM, but are able to use local and historical data. The ability to use local information on the properties of river channels makes it possible to create more accurate models for river routing. These lead to better hydrographs that are

used for hydraulic modeling. The bias and noise that is inherent to DEM based on remote sensing can be corrected by making local measurements. Land-use and vegetation data can provide better estimates for Manning's roughness and therefore more accurate flood routing.

Coastal flood maps are not made on a global scale due to the lack of available information. The dependency on bathymetry and coastal morphology makes the estimation of wave behavior difficult at a global scale. Proper modeling for these requires a larger resolution than is usually used by open-source global models. There exist global storm surge models but these are not used for flood mapping and do not include any embankments or dunes. Flood hazard maps based on sea level rise due to climate change also exist but are based on a bathtub model. In these maps the inundation is set such that all land below that water level is flooded without acknowledging natural or manmade defenses.

2.3.2 Data requirements

Satellite data of topography and rainfall can be validated be local measurements to improve accuracy and correct for biases. DEM data sets can have significant biases but can be corrected with local survey data (Pakoksung & Takagi 2016). Local precipitation radar stations are often validated with local ground measurements are can provide better quality data. The run-off of precipitation is strongly influenced by the interception of vegetation.

The bathymetry of the rivers can be modeled with greater accuracy instead of assuming a standard shape for the cross section. Rivers come in many different types with different rates of entrenchment. By including local survey data, the river can be modeled in greater detail and the floods can be predicted with better accuracy.

Local survey data can provide information that cannot be found though satellite imaging. The geology of the watershed is important for the modeling of run-off and has significant influence on the discharge of rivers. Permeability cannot be determined from remote sensing data and requires in site testing. Hydraulic roughness is of importance to the flood routing in floodplains. The smaller scale and local surveys can provide better estimates for this property.

Historical data can be used to provide insight in the occurrences of floods and help validating flood maps. By comparing the inundation extent from recent floods with the projected inundation extent of the flood map further fine-tuning is possible.

2.3.3 Methodology

Fluvial flood maps at regional and local scale are produced with similar methods as global flood methods. The smaller areal scope allows for the use of higher resolution DEM data sets and more complicated numeric modeling. Without the need to average roughness values of area of an area with a small resolution a better estimation of flood routing can be provided. Simplification used in global flood models like rectangular river cross sections can be avoided. An advantage of the greater resolution is the ability to model roads and other infrastructure. In flat areas obstacles like roads often limit the extent of inundation.

Coastal flood maps are created based on morphology and bathymetry of the coastal area. The forcing is based on a combination of tidal surge, storm surge and wave height. An example is a workflow for the development of coastal flood maps is the Coastal Storm Modeling System (CoSMoS) (Barnard *et al.* 2019). This model uses several different numeric models in conjunction with each other. The first step is the modeling of large-scale wave generation (swell) based on global wind data. At a

regional scale the model includes the swell in combination with storm surge and tides. This can be modeled with the Delft3D and SWAN software. At a local scale the wave behaviour can be modeled and used to predict wave setup and run-up. From this data it becomes possible to provide a flood map with the Delft3D, SWAN and XBeach software.

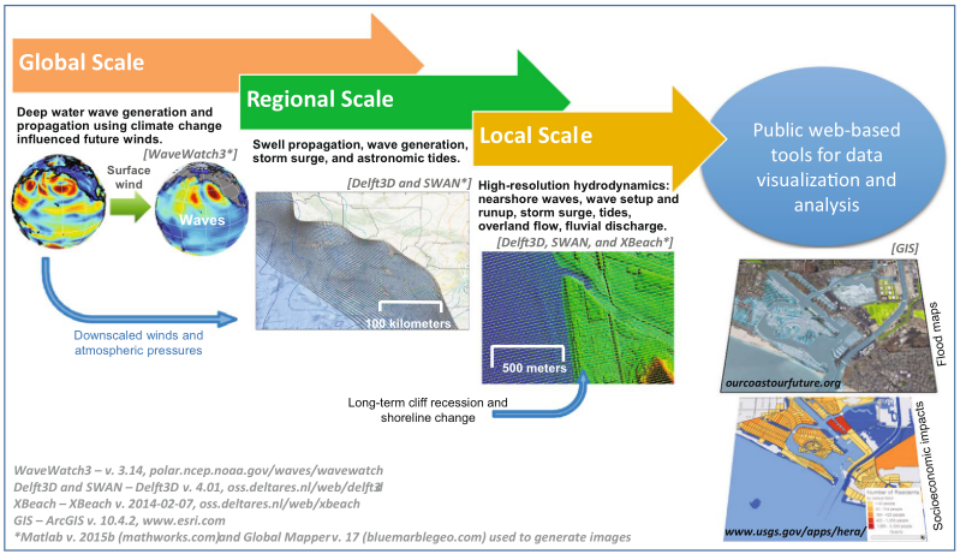

Figure 2.4: Workflow CoSMoS (Barnard *et al.* 2019)

The interaction between fluvial and coastal flooding is complicated and difficult to model. During a case study for the Shoalhaven River in Australia (Kumbier *et al.* 2018) the Delft3D model was used to create a flood hazard map with the use of a LIDAR data set for elevation with a resolution of 5m and a computational resolution of 25m. The forcing was a combination of gauged flow, weather and tidal data. The interaction between the different aspects of the forcing was found to determine large inaccuracies in the modeling of the flood.

In a study of flood risk modeling in eastern Canada (Didier *et al.* 2019) the difference between a bathtub model and XBeach was studied. Based on a historical flood the bathtub model has better prediction of inundation extent but has significant over prediction. However, the XBeach 2D model has a slightly better Critical Score Index. Both models score relatively close to each other with 51% against 48%. These scores are acceptable but not great. The bathtub model did lead to a large overestimation of the flood depth and therefore a far larger flood risk. Bathtub models are considered to be too inaccurate to use for coastal flood modeling.

The inclusion of flood defenses remains a difficult aspect of flood mapping even at this scale. In (Paprotny *et al.* 2019) the post-processing step of removing flood hazard from areas with protection was described. The protection was estimated on the basis of the FLOPROS data set. The modeling of coastal defenses requires detailed local studies which were not available for all of the European coasts. Another problem is that in less developed regions the embankments were built by locals and there is no exact information on their location or quality. To prevent underestimating the extent of flooding these embankments will not be included in the creation of flood maps. On the modeling side, the smaller scale makes it possible to include a break line in the grid to model a levee. This is possible in for example HEC-RAS. The surrounding grid cells will be given a non-standard shape to fit the break line into the grid. This allows for the deterministic modeling of the flood defenses and to test breaching scenarios but does not allow for probabilistic modeling.

The probabilistic analysis of dunes and natural protections in coastal areas is complicated, therefore a strong degree of uncertainty remains. Coastal morphology is a complicated process and the constant accumulation and erosion of dunes and banks make it difficult to make long term predictions.

2.3.4 Discussion

Regional and local flood maps are created using similar hydraulic models as global flood models but are often more capable of greater resolutions. The higher resolution maps provide better insight in the flood routing and allow for more accurate predictions. The required additional data for these resolutions are not always available in remote areas. This limits the advantages of these models. Advancement in remote sensing products have made higher resolution global data available. The inherent measurement bias in these data products needs to be corrected to provide the best accuracy. The smaller scale reduces the number of scenarios that need to be studied and allow for less simplifications in the modeling of flood routing. This further increases the accuracy of inundation modeling.

Coastal flood maps are made at this scale due to the nature of hydraulic mechanisms. Coastal flooding is a complex phenomenon that is often caused by storm surge and tides. In addition to this waves can damage coastal flood defenses. Waves are not included in global maps due to the sensitivity of wave breaking to small scale changes in the bathymetry. Tides and storm surge is easier to predict on a larger scale. The behavior of natural coasts is very difficult to predict in general and is often a large source of uncertainty.

The higher resolution makes it possible to include flood defenses in the flood map, but in most cases due to a lack of data no probabilistic analysis is included. At a higher resolution, flood defenses can be included in 1D and 2D models without much trouble. The probabilistic analysis remains often impossible due to a lack of data on the underlying soil structure. The designs of many embankments are not properly documented or built by local further complicating this. Most mapping efforts still make use of deterministic flood defenses in post-processing or by ignoring the structures all together. This results into maps for low-lying flood plain with extremely large inundation areas, as can be seen in for example the Sava river basin (Figure 1.3). In Serbia, flood maps were made mainly with 1D hydraulic models. While the models are suitable for certain areas, in low-lying regions this can lead to a potential overestimation of the inundation extent. An improvement in accuracy over global flood maps is achieved for most cases if use is made of higher-resolution modeling techniques in combination with a better technique to account for the failure of the protection systems. In many cases the uncertainties remain high due to lack of data and expertise.

To generate maps with greater certainty, data from local surveys is necessary to add to or validate remote sensing data. There exist a lot of global data sets with information on land use and vegetation cover. Biases in these data sets cause inaccuracies which can be prevented by validating these with local measurements and surveys.

2.4 Explicit modelling of flood defenses in flood mapping

Although explicit modelling of flood defenses is complicated, great efforts have been made. There are mapping efforts made that include these systems in great detail. In this study two of these projects were investigated. The first is the VNK project in the Netherlands which includes a strategy for probabilistic modeling of a basin surrounded by flood protections. The second project is the study of the flood defenses in New Orleans during the hurricane Katrina made by the IPET. This report includes probabilistic modeling of flood extent and depth based on incoming volume during the hurricane. The

volume not only depends on rainfall and the function of the drainage pumps but also include models for overtopping and breach events.

2.4.1 VNK

One of the most detailed flood maps is made in the Netherlands as part of the VNK project (Vergouwe 2014). It includes a full probabilistic analysis of the existing flood defense systems.

For the VNK project a very complete set of failure mechanisms was included for the flood defenses. These are described in the manual of the PC-Ring software (Vrouwenvelder *et al.* 1999a). The first modeled mechanism is overtopping. Overtopping is water that due to wave run-up flows over the crest of the dike and causes erosion on the inner slope or crest. This erosion can than lead to the formation of a breach. The determination of a critical overflow rate is the foundation of mechanism. The second mechanism studied is shearing of the levee. This failure probability is predicted according to the method of Bishop and is based on the drained strength parameters of the soil. The third failure mechanism is the occurrence of piping. The fourth mechanism is damage of the covering of the outer slope due to wave attack and following erosion. Two more failure mechanisms are studied for structures. The probability that the structure does not close when needed and failure of the system due to piping.

Methodology

The VNK program has focused on the failure of flood defenses as the primary cause of inundation. This means that only after a probabilistic calculation of the failure mechanisms a volume is determined which can be used to model the inundation. This is a different approach from most other models which determine flooding directly related to the forcing with the same software. This allows for the calculated for failure for multiple different scenarios and to combine these scenarios into a single flood hazard map for a given return period.

Due to the universal presence of surface water and flood defenses in the Netherlands the flood risk is determined for each system separately. Each protected area is treated as a basin surrounded by a dike ring. As described in (VNK2 project office 2012) the ring is split into segments with similar consequences. In this way the exact location of a breach is included into the modeling of inundation without having to perform a large number of simulations for each segment. This segment was further split into section of similar properties. For each of these sections the combined failure rate can be calculated which leads to the flood risk map for the segment. The maps for the segments can then be combined to provide a flood hazard map for the basin as a whole.

To limit the number of simulations required for each system, the concept of relief was introduced. This means that if failure occurs a segment the stress on nearby segments is reduced. This often the case in river floods due to the limited volume. There exist different approaches for this modeling assumption. In the case of no relief the number of simulation becomes extremely high causing problems with computations and lead to overestimation of the actual risk. By assuming that the weakest point or the point that is first loaded fails first the number of simulations is reduced but the actual risk ends up to be underestimated.

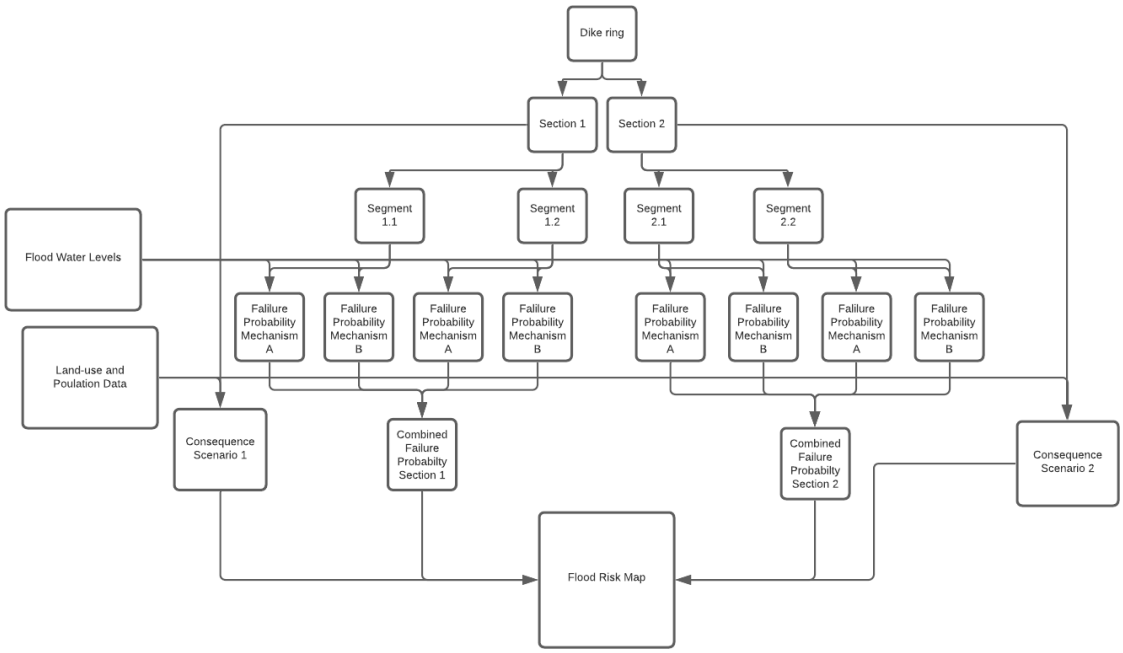

Figure 2.5: Schematized workflow for hazard calculation used in VNK.

To account for the uncertainty of geotechnical parameters length-effect correction are used to provide conservative strength values. It is common logic that a system fails at its weakest point. The problem is that it is often impossible to know where the weakest point is. For this reason, length effect are included for all sections to predict the strength of the weakest point. In this study a statistical model was used based on found strength parameters of the defenses. While the uncertainty cannot be removed completely due to the number of measurements that er needed, the reliability is improved over a deterministic approach.

The different failure models for each segment are combined into a single failure rate for the section of the flood defense system. As described in (VNK2 project office 2012) this is done with the Hohenbichler-Rackwitz method (Hohenbichler & Rackwitz 1982).

Data requirement

The VNK project uses a very large amount of data for the levees and other flood defenses. A complete description is found in (Vrouwenvelder *et al.* 1999b). For each of the studied failure mechanisms a list of different parameters is required. Each of these parameters is fitted to a probabilistic distribution to account for the unreliability of the measurements.

The forcing was based on water levels and wave run-up determined in the TRM2006 report (Witteveen+Bos 2006). In this report a norm value was provided as well as a "decimeringshoogte" for each point along the entire flood defense system. This is the difference between the norm value and a value for a return period 10 times higher or lower. For areas where wind is not a significant factor. only values for the water levels were provided. For areas where waves are important an additional a value for the wave run-up was made based on either a known levee profile or a standard profile.

2.4.2 IPET

After the disastrous consequences of Hurricane Katrina, a study was made on the functioning of the flood defenses in New Orleans. This study was performed by the Interagency Performance Evaluation Task Force (IPET). A task force of the US Army Corps of Engineers. The goal of this study was to evaluate the performance of the hurricane protection system during Katrina and determining what the actual risk was that the citizens were exposed to. The system had multiple problem including a lack of financial resources, maintenance and building code enforcement. The system consists of a series of flood defenses like levees and flood walls to combat storm surge and wave run-up and drainage channels and pumping stations to combat the pluvial flooding.

The IPET team used both theoretical models as well as empirical models to determine the failure probability of the flood defenses. The details of this approach are written in (IPET 2009) The IPET team used a event tree to determine the different scenarios in which water entered the different basins that make up New Orleans. A selection of different failure mechanisms was used; breaching without overtopping and breaching with overtopping for levees and flood walls. In addition, the reliability of structures and transition were included. Piping was not included due to the short time frame of the hurricane surge compared to seepage lengths. Other mechanisms were not included due to lack of data.

Methodology

For a hurricane the pluvial floods are difficult to prevent completely, but can be controlled through pumping stations. This leads to an approach where the incoming volume of water is key to determine the risk of inundation. The area that is protected by the system is divided into basin and sub-basins based on natural or manmade barriers which split the storage capacity of the area. Due to the nature of hurricanes, flash floods caused by precipitation are combined with storm surge at the coast. This means that some extent of inundation cannot be prevented. The hazard maps are based on the volume of water that enters and remains in the basins. The breach of a levee or flood wall is not considered a true failure of the system if the incoming water could be pumped out of the system before the inundation would lead to damage. The final volume in each sub-basin is based on the combined inflow and outflow caused by pumping.

The flood maps are based on several basins and sub-basins linked to each other over which the flood volume is distributed. Only if the water level reaches a high enough point in a basin, flow between different basins is possible. The sub-basins are modeled as a storage area. The border between two basins is assigned a certain height which when exceeded by one of the sub-basins will lead to flow between them. If both basins have a water level above the border the basins are treated as a single combined basin. Each basin has an inflow volume based on the precipitation during the event and potential breaches or overtopping of defenses.

This model includes most failure mechanisms that are common to levees but does not fully analyze all of them. Overtopping was based on the storm surge level and the commonly used weir flow equations. A probabilistic distribution was made for these properties. These were converted into a fragility curve and used to determine the expected overtopping volume for each section of flood defenses for a given surge level. The occurrence of breaches caused by overtopping were only studied based on empirical data due to the lack of an available erosion model. For this reason the required overtopping rates that would lead to failure is modeled with a different distribution for different soil types. Both the different breach types are assumed to be catastrophic and lead to a full levee height breach. The development of a breach in a levee is not directly modeled but included into the uncertainty analysis of this failure mechanism. The final water level in the basin is limited by the surge level outside of the system. This leads to a probabilistic distribution for the incoming volume for each section of the

system. Structures are modeled with similar distributions.

The flood map was created for each sub-basin based on a bathtub model. The local government of New Orleans had provided curves which link the stored volume with a inundation level for each basin. Based on these curves the final flood hazard maps were provided for different return periods and pumping capacities.

Data requirement

A review of the required data is based on (IPET 2009).

Modeling for hurricanes has a few extra steps compared to modeling for regular storms. The forcing on the system is based on hydrographs for the different parts of the hurricane protection system. These hydrographs are based on a combination of surge and wave modeling generated from the wind field of the hurricane. This can be predicted with the help of the Joint Probability Method (JPM) (Irish *et al.* 2008). This shows there is a relation between the size of the hurricane and the amount of storm surge generated in addition to just the effect caused by wind.

The flood defenses were studied by a combination of LIDAR data and surveys. The system was split into segments which are considered the same in cross section and forcing. The cross sections were studied on the basis of existing information combined with physical surveys and LIDAR elevation data with a resolution of 1ft. Further information on the properties of the underlying soil layer was used from the original construction of the project and additional tests at the sites of breaches.

The storage capacity for the basins were created by the local government. By simplifying the basin into a simple storage-elevation curve a large amount of detail is lost. This does allow for a low computation cost to model multiple different scenarios. Due to the effect of pluvial flooding, the 1D bathtub approach is not unreasonable to use in this case. By larger inflows of water during a breach the propagation is impossible to predict and cannot be used to determine evacuation plans or more detailed flood risk maps.

2.4.3 Discussion

The high detail mapping methods studied focus mainly on the probability of a flood occurring and use simplified methods to determine the inundation extent. This is viable due to a focus on smaller and mostly urbanized areas. In large flood plains, the flood propagation and the flow velocity are more relevant. For the production of flood risk maps in urban areas most damage is done by the inundation extent and depth. The small scale also leads to that relatively simple inundation curves as used in New Orleans are sufficient to predict the extent of the damage.

The focus on probabilistic analysis of the flood defenses leads to a rather complete inclusion of these into flood maps. In contrast to the methods described in Sections 2.3 and 2.2. The modeling of actual flood defenses allows for the determination of the local hazards for a certain return period with good accuracy and improved reliability. The location of a potential breach is also better predictable, which can help in the development of mitigation plans. The VNK study does not take the exact location of a breach into account as this is nearly impossible to predict but splits the dike rings in section based on consequences. In this way the method accounts for the location of breaches. The IPET study does not include the actual location or number of breaches at all and only focuses on the inundation volume generated. Relief is not taken into account but is also negligible for storm surges. Relief is dependent on the ratio of inundation volume and the incoming flood volume.

Even with the use of empirical models, the amount of survey data required is immense and it is unlikely that these projects could be performed in most parts of the world. To generate flood maps as was done in the VNK project or in the IPET study requires a large amount of funds and expertise. The IPET study had to make use of empirical models for their analysis of erosion of levees caused by overflow, as a proper model was not available. The IPET study had to perform additional surveys after the hurricane to provide additional data on the defense systems. The VNK study had to assume standard profile for some levees that were not documented completely. The uncertainty in measurements is always present but can be reduced significantly with large amounts of proper surveying and documenting.

2.5 Tisa river flood maps

As the case study in this thesis is based on the Tisa river in Serbia, the current available flood maps for this river are of interest. These are found in (COWI 2019) with the used approach and data.

2.5.1 Introduction

After the floods in 2014 the government of the Republic of Serbia approved a natural disaster risk management program. The program was set up with support of the European Union, the United Nations and the World Bank. As part of this program the World Bank has commissioned a study to prepare flood hazard and risk maps including the area around the Tisa river.

The Tisa river originates in the Ukraine at the confluence of the White Tisa coming from the Chornohorna mountain range and the Black Tisa coming from the Gorgany mountain range. It forms the borders between the Ukraine with Romania and Hungary before forming the border between Hungary and Slovakia. It than enters Serbia and joins with the Danube to which it accounts for 13% of its run-off.

The flood hazard maps for the Tisa were made with a 1D model and making use of a bathtub assumption for the floodplains. Maps were made for three return periods; 50 years, 100 years and 1000 years. The influence of climate change was studied based on the 100-year return period. For the 100-year return period some maps were made based on levee breaching in a 1D/2D model. The areas inside of the embankments is mapped with potential inundation due to uncertainty of the flood defenses. This is presented as an upper limit for the flooding. The potential inundation area is based on comparing the water surface elevation outside of the embankments and the terrain with the embankments.

2.5.2 Data

The first set of data used in the hydraulic input. This data is used to model the 1D river and can be used to help determine some of the inputs for the idealized case. The discharge used was based on data from several measurement stations along the Tisa including the Senta and Slankamen stations. The terrain for the 2D model was made with a DTM generated with the use of LIDAR technology. The roughness of the terrain has been determined based on urban-planning and land-use data.

2.5.3 Results

Based on the levee breach analysis that was made a series of maps with inundation arrival time were made. These maps show when the inundation reaches a certain point in the floodplain. The maps is created by taking snapshots of the inundation extent just before the breach, and 1 day, 1 week, 2 weeks and 3 weeks after the start of the breach. No information on the inundation depth or velocity is provided.

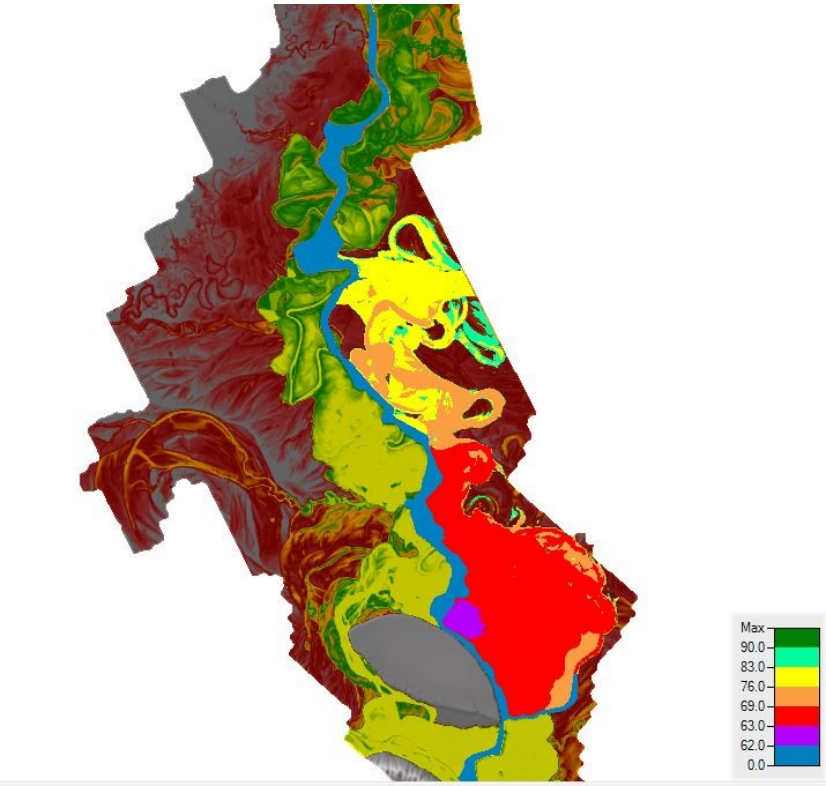

Figure 2.6: Inundation time map in hours for breach location "Zrenjanin" presented in COWI rapport.

Finally, based on the water levels found inside the levees a flood risk map was made for the Tisa river basin. The flood risk is split in real flood hazard in between the embankments and potential flood hazard at the protected side of the embankments. No estimates for the probabilities are provided.

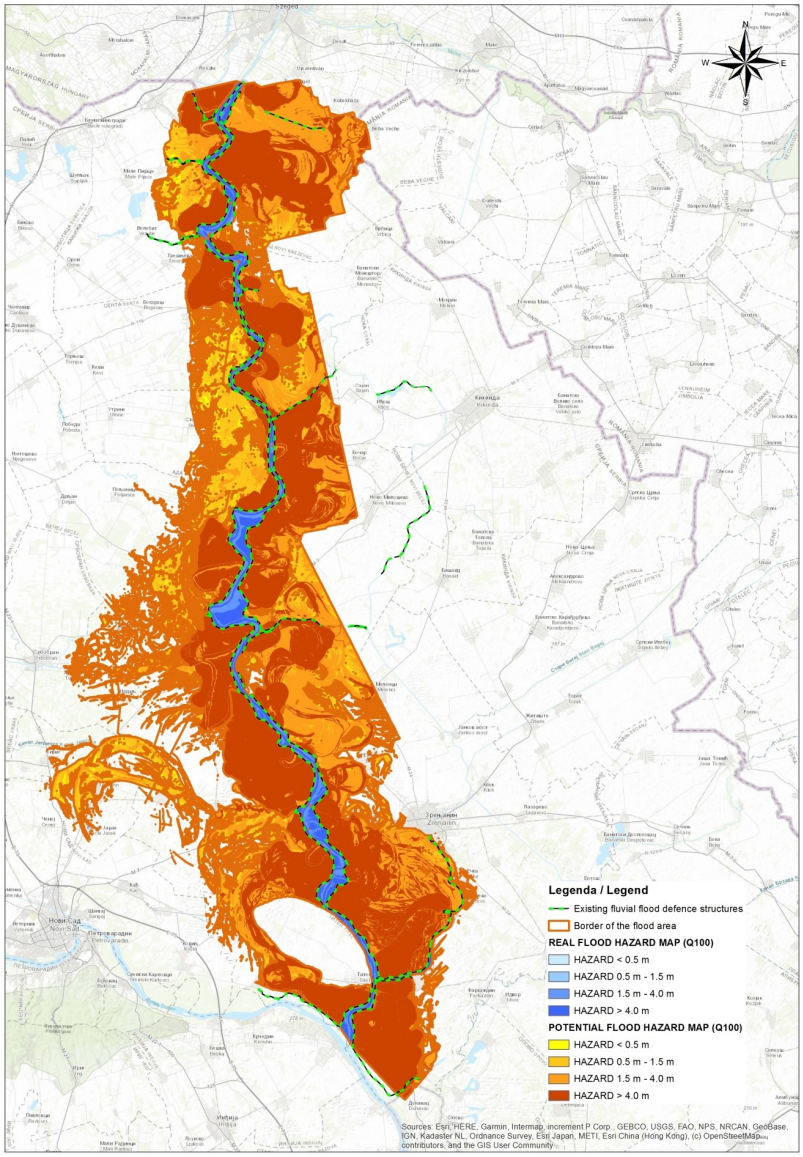

Figure 2.7: Flood hazard map for 100-year return period (COWI 2019)

Chapter 3

Setup of a idealized model for inundation along the Tisa river

3.1 Introduction

In this chapter an idealized model is presented to be used to develop flood hazard maps. This model includes explicitly the failure of levees and its effect on the inundation patterns. The development of a model for the creation of flood hazard maps is complicated by a large number of variables present in the river and the floodplain. As it is impossible to account for all of the variables, it is necessary to simplify the real world case. For this reason an idealized model is used to simplify the setup. This idealization allows for a better insight in the influence of certain parameters.

The idealized model is based on the Tisa river in Serbia due to interest in this area for the application of flood maps with flood protection included. The model was made in the SOBEK 2 software made by Deltares. This is a 1D/2D hydraulic modeling suite developed for several hydraulic applications like flood forecasting and drainage optimization. This software can be used to model the behavior of the idealized river as a 1D channel and the progression of the inundation over a 2D grid.

The model is split into three separate parts. The river, the floodplain and the breaches in the levees. The river is modeled as a straight 1D channel with a constant profile and friction coefficient. The floodplain is modeled with a 2D grid. The levees along the river are included in the 1D channel as part of the channel and in the 2D grid by raising the ground level of the cells to the crest height of the levees. The levees are assumed to be constant along the modeled river stretch. The breaches in the levee are modeled in SOBEK with a special type of channel known as a branch. The breaching process itself is modeled with the Verheij-vdKnaap formula which is built into SOBEK. This allows the width of the breach to be determined by the model itself based on the flow velocity through said breach.

This chapter is split into several sections. First, the schematization of the 1D and 2D parts of the model are explained in Section 3.2. In Section 3.3 the modelling of the levee breaches is explained. And in Section 3.4 the calibration of the model is found. Here, several calculation are made to ensure that the idealized model behaves in a similar way to a real world case.

3.2 Schematization of the river and floodplain

The structure of the model can be split into three different components. The schematization of the 1D channel that was used to model the river channel including the winterbed and the levees. The 2D grid used to model the floodplains behind the levees. And finally, the initial and boundary conditions used to model the river. These aspects are discussed below subsequently in the following subsections.

3.2.1 River as 1D channel

The channel is based on a relatively simple stretch of the Tisa river with a single conveying channel. The parameters used are based on a HEC-RAS model of the Tisa river used in a study on historical floods (Kolaković *et al.* 2016) as well as a study commissioned by the World Bank (COWI 2019). The Tisa river has a width that varies over the course of the river. A width of 150 meters was used as the basis for the simplified channel. The depth of the river varies between stretches but is on average around 12 meters. The HEC-RAS model splits the Tisa in four major stretches spanning multiple countries. This study focuses on the downstream part located in Serbia. The cross-sections used in the HEC-RAS model are shown in Figure 3.1.

The main channel is simplified as a trapezoid shaped channel shown in Figure 3.2. The floodplain is assumed to be horizontal till the levee. A decrease in ground level towards the levee can increase the amount of water that will flow through a possible breach. But this is an example of a parameter that adds complexity to the model and is neglected herein. The distance between the toes of the levees is set at 450 meters. The distance between the embankments varies greatly over the course of the river. There are several stretches along the river where large storage areas are available between the embankments. These areas are sometimes used as farm land. These are not included in this simplified model as their influence on the development of the water depth is not easy to determine over a long period.

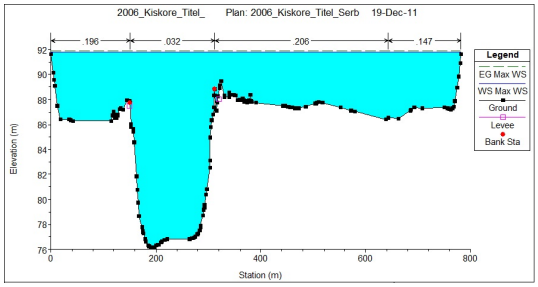

(a) Cross-section of the Tisa between Tisore and Szolnok in Hungary.

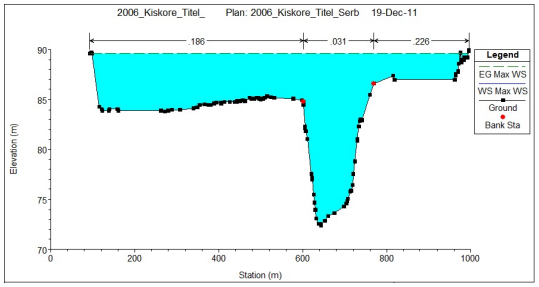

(b) Cross-section of the Tisa between Szolnok and Csongrad in Hungary

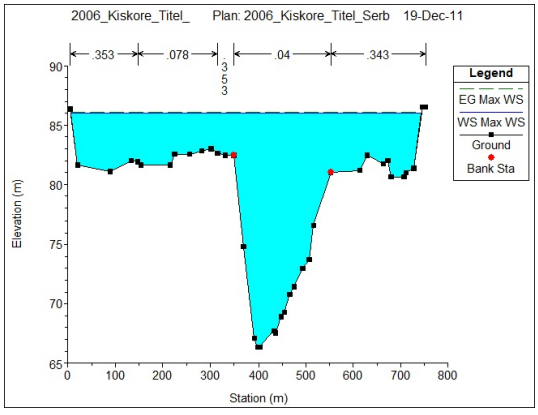

(c) Cross-section of the Tisa between Csongrad and Szeged in Hungary.

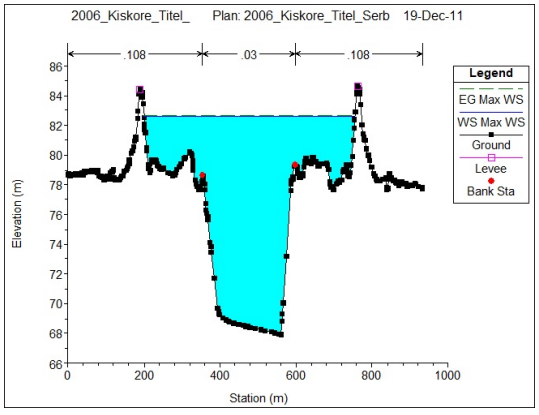

(d) Cross-section of the Tisa between Szeged and Titel in Serbia.

Figure 3.1: Selection of cross sections of the Tisa river similar to modeled cross section. Cross-sections are from the part of the Tisa river from Lake Tisa till it joins the Danube.

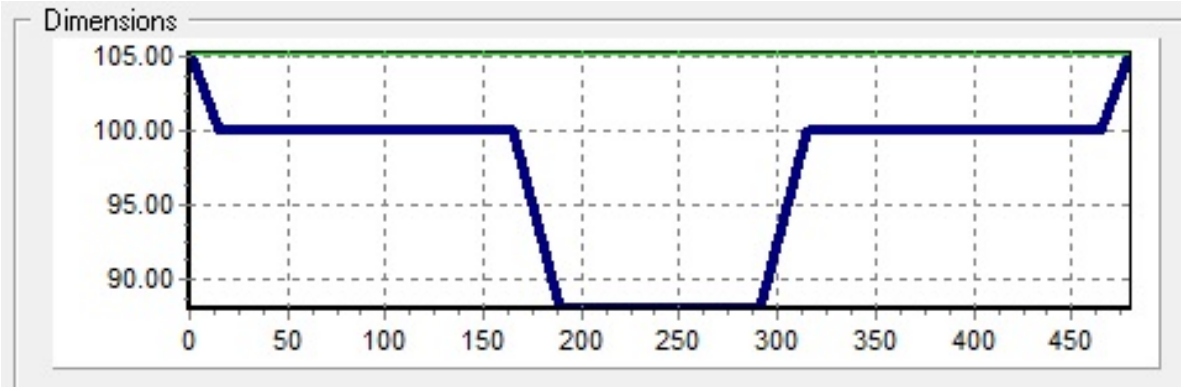

Figure 3.2: The cross section of the river channel profile implemented in SOBEK.

The bed slope is determined by the difference in bed level between the border with Hungary and the point where the river connects with the Danube river. The bed and water level difference between these points is both around 5.5 meter (see (COWI 2019)). This is rounded to 6 meter which combined with the length of the channel results into a bed slope of $6/150000 = 4e-5$ or 4 cm per kilometer.

The current levees around the Tisa were designed and constructed after a flood in 1967. They were designed based on the 100-year return period water levels. The levees have a height of 1 meter above this water level. Running the model results in value of around 4.3 meter above the floodplain was found for the 100-year return period discharge. The height of the levees was therefore assumed to be 5.3 meter above winterbed. These levees were implemented in the channel profile as seen in Figure 3.2. The river side levee slope along the Tisa is 1:3. The levee width used for the profile was rounded to 15 meter. This means the complete width of the channel is 480 meters. The 1D channel is set with the crown level of the levee as the ground level. The cells of the 2D grid over which the channel is routed have their ground level increased to the crown level of the levees. This prevents the water after a breach on one side of the river to flow to the floodplain on the other side. This is a technique that can also be automated in SOBEK, but was included manually to prevent problem with the modeling of breaches.

3.2.2 Floodplain as 2D grid

The floodplain has been schematized using a 2D grid with a cell size of 500 meters. This cell size is large enough to allow for short run times but still sufficiently small to capture the main topographic variations. For the flood plains, a distance of 25 kilometers perpendicular to the channel was prepared to include the entire area that can potentially flood. This is comparable to the average size of the floodplain surrounding the Tisa River in Serbia. The size of the 2D grid is therefore 302 by 52. SOBEK does not perform calculations on the cells at the edges of a grid. The area beyond the embankments is very flat and to properly study the extent of inundation a relatively large area is required.

The downstream slope of the terrain is assumed to be the same as the bed slope of the channel namely $4e-5$ or 4 cm per km. This simplifies the connection between the river and the floodplain and allows for more consistency over the whole length of the model. The bed slope translates to a drop of 0.02 meter per 500-meter cell. To limit the spread of extremely small inundation levels, such as the minimum value of 0.02 meter, a small slope was added to the 2D grid directed perpendicular to the channel. In the real world such small water depths would most likely be stopped by very minor obstacles. An increase of ground level of 0.01 meter per 500-meter cell was included to account for

this.

The friction of the bed and the floodplains are derived from earlier studies ((COWI 2019)). For the river bed a Manning roughness of $0.025 s/m^{1/3}$ was provided. The floodplains on the inside and outside of the defenses are assumed to have a constant Manning roughness of $0.045 s/m^{1/3}$. This Manning roughness corresponds to land being used for agriculture or livestock. The land use from the satellite images on google maps shows that the land around the Tisa is used for these purposes. This can be seen in Figure 3.3.

Figure 3.3: Google maps image of the Tisa river and surrounding area (Google, n.d.)

The edges of the grids are impassible for the inundation. At the downstream end of the 2D grid, this is realistic since the existence of the embankments of the Danube river will stop the inundation moving further downstream. This will result in an accumulation of water in in the floodplain. This is a realistic phenomenon that is commonly seen during flooding where infrastructure (roads, inner levees) can block the flow. The edge of the grid at the upstream side will be little influence on the results due to the slope of the land.

3.2.3 Initial and boundary conditions

The first boundary condition that is determined is the discharge at the northern boundary point. Here the incoming discharge is defined in the model. To estimate the discharges that correspond to the different return periods, an extreme value analysis has been made. There are two methods to make this analysis. The block maxima method and the peak over threshold method. Since the discharge through the Tisa has periodic seasonal discharge peaks, the block maxima method is selected.

The upstream discharges were determined from the Senta measuring station from GRDC database (WMO 2021). Senta is located around halfway between the border and the connection with the Danube. From the daily discharge records that were available for a period from 1971 till 2010 the annual maximum discharges were determined. These were fitted with a Normal, Log-normal and Generalized Extreme Value distribution. The CDF's of these distributions and the empirical CDF of the data are shown in Figure 3.4. All of these distributions seem to fit well to the data. To determine which has the best fit an one-sample Kolmogorov-Smirnov test was performed with a threshold of 5 %. The Kolmogorov-Smirnov test compares an empirical CDF of the studied sample to the CDF of a probabilistic distribution. The MATLAB implementation of this test compares the probability p of a deviation as least as large as the provided sample to a significance level α. If the p value is larger than the α value the null-hypothesis is rejected and it is acceptable to assume that the sample could be generated by the probabilistic distribution. The larger the probability the better the fit. The results of this test are summarized in Table 3.1.

The results in Table 3.1 show that all of the distributions are accepted. The Generalized Extreme Value distribution has the best fit. The Log-normal also has an very good fit just behind the GEV. The fit of the Normal distribution is also good but the difference is larger than of the other two. Based on these distributions the discharge for the return periods are estimated. The estimations are presented in Table 3.2 and a plot for the different distributions is presented in 3.5. Here it can be seen the GEV fit is closer the empirical values for the lower return periods but the Log-normal fits better

for the larger return periods. These results were validated by comparing them to the values used in a recent study ((COWI 2019)). It is important to be aware of the limited size of the data set used. Only 40 years of data was available which means that the values of the 100y and especially the 1000y return period have high uncertainty. This can be seen in the large differences in the values found from the different distributions. To allow for easier comparison for the current flood maps presented in the recent flood mapping study ((COWI 2019)), the discharge values from that report have been used for the modelling herein. The discharge starts and ends at a value of 1800 m3/s. This discharge leads to a water depth of around $11.5m$ in the channel and represents a large but still relatively common discharge.

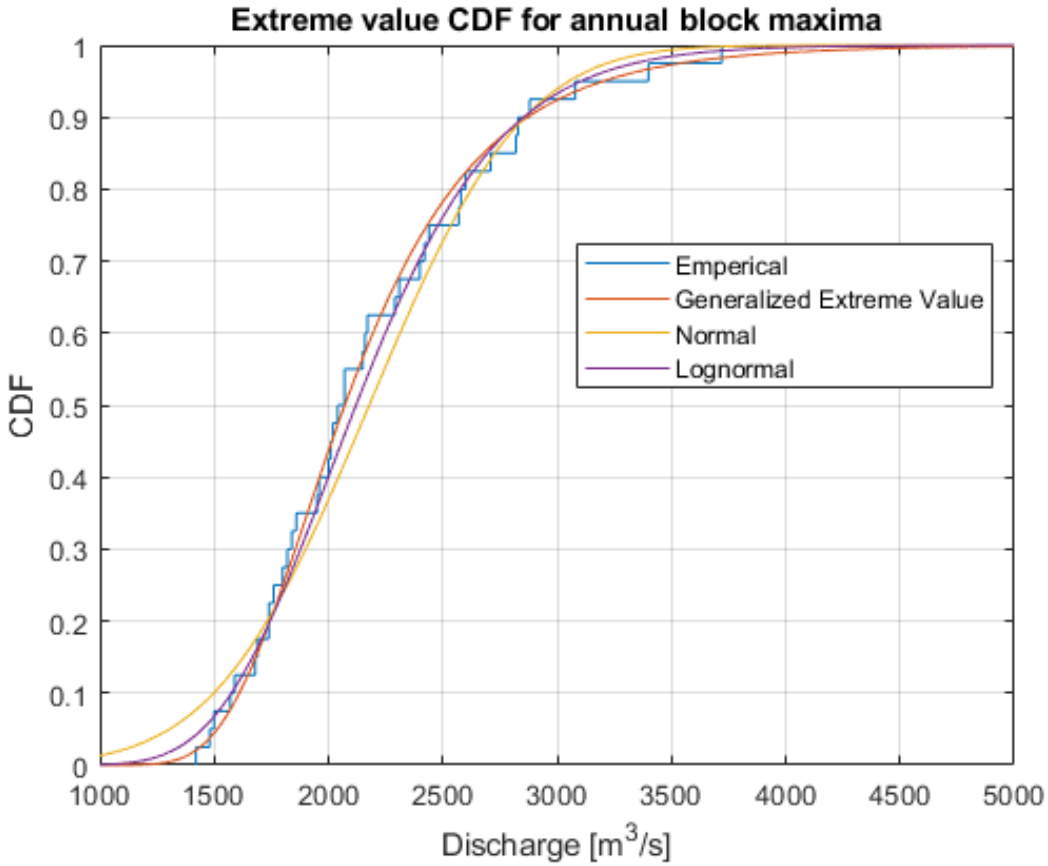

Figure 3.4: CDF plots for annual block maxima analysis.

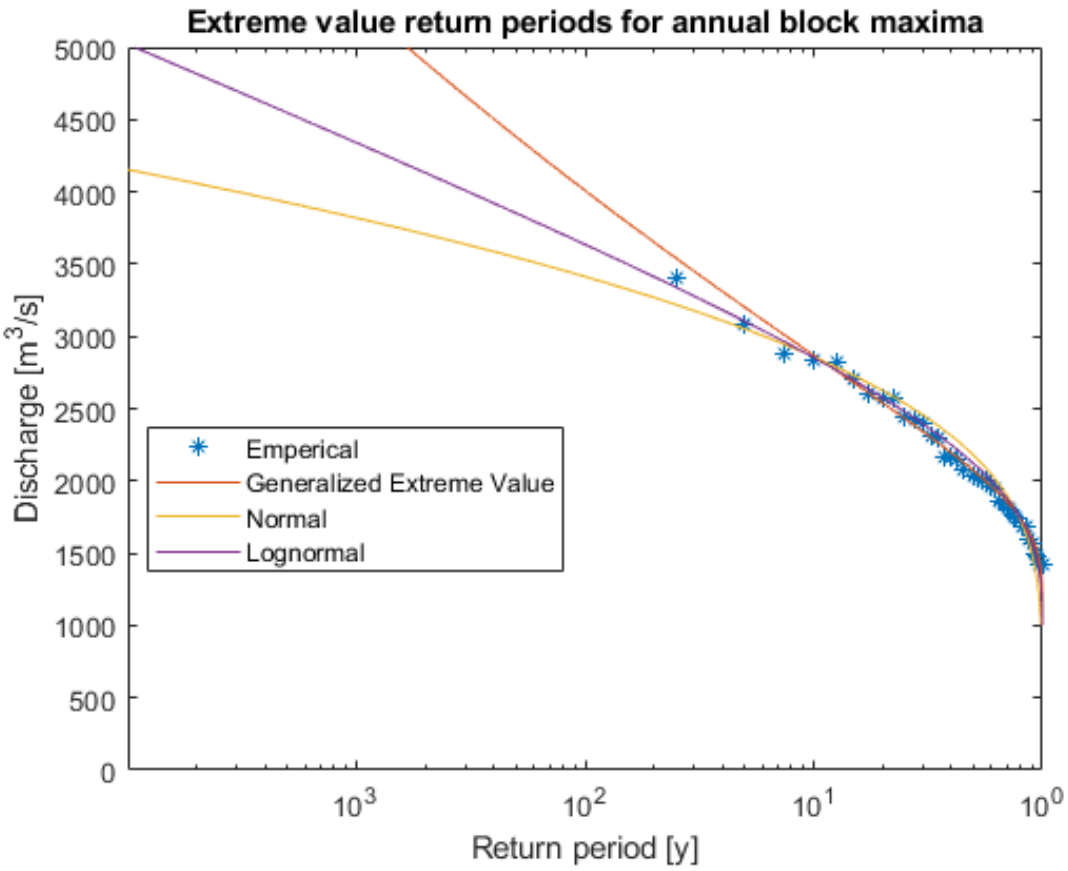

Figure 3.5: Return period plots for annual block maxima analysis.

Distribution	p	α	h
GEV	0.9955	0.05	0
Log-Normal	0.8608	0.05	0
Normal	0.4562	0.05	0

Table 3.1: Results of Kolmogorov-Smirnov test.

Return period	GEV	Normal	Log-normal	COWI
10 y	$2870m^3/s$	$2859m^3/s$	$2854m^3/s$	$2900m^3/s$
100 y	$4009m^3/s$	$3414m^3/s$	$3636m^3/s$	$3800m^3/s$
1000 y	$5304m^3/s$	$3819m^3/s$	$4340m^3/s$	$4600m^3/s$

Table 3.2: Discharges found based on extreme value analysis and the COWI report.

The initial state of the model is the same over the whole river channel. The initial discharge is set at $1800m^3/s$. This leads tot a initial water depth of $11.5m$. The initial conditions are used to define the model at the start of the scenario. These conditions ensure that the river is in a equilibrium state

before the discharge gets increased. Without this the results would less stable between the different return periods.

The downstream boundary condition is defined in SOBEK as a specific water level determined by the discharge that is conveyed. The table used for this is presented in table 3.3. These values were found by running the model with a no-breaching scenario for different discharges.

Discharge$[m^3/s]$	Water depth$[m]$
1800	11.5
2000	12.2
2900	14.6
3800	16.3
4600	17.3

Table 3.3: Summary of the southern boundary conditions.

The hydrograph is assumed to have a simple triangular shape. This shape is normal for river flooding events and is based on the historical water depths found at the Senta measurement station. The model runs over a time period of 50 days and the peak discharge is found in the middle of this period. The hydrographs for the different return periods are found in Figure 3.6. The water depths in the cross section can be seen in Figure 3.7. The time frame selected is 50 days and the peak discharge is found in the middle. The starting point for the model is on 1 January at 0:00. The peak enters the channel on 26 January at 0:00 and the end point is 20 February at 0:00. To limit the running time of the model the time step for outputs is set at 2 hours. This results in a total number of outputs of 600. The internal time step used in the calculations is 5 min.

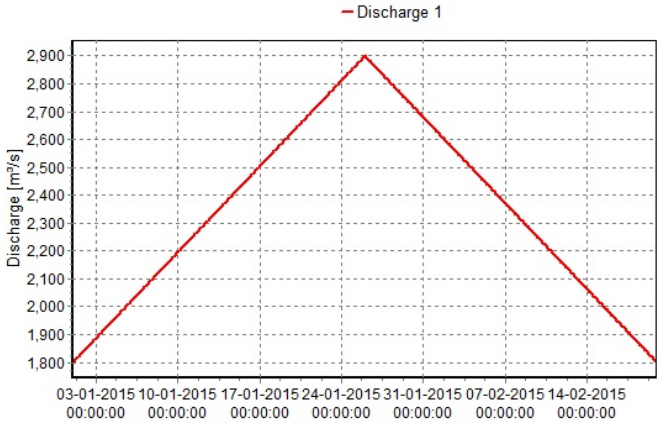

(a) Hydrograph for the 10y return period.

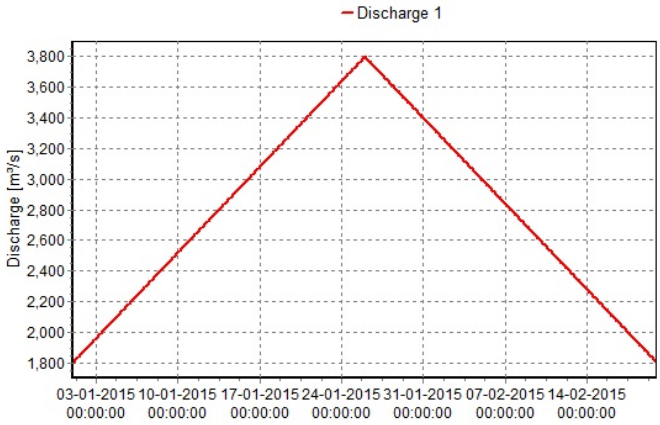

(b) Hydrograph for the 100y return period.

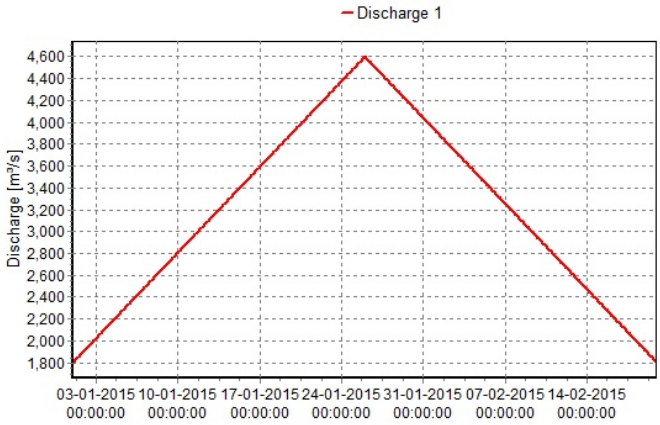

(c) Hydrograph for the 100y return period.

Figure 3.6: Hydrographs at the northern boundary point.

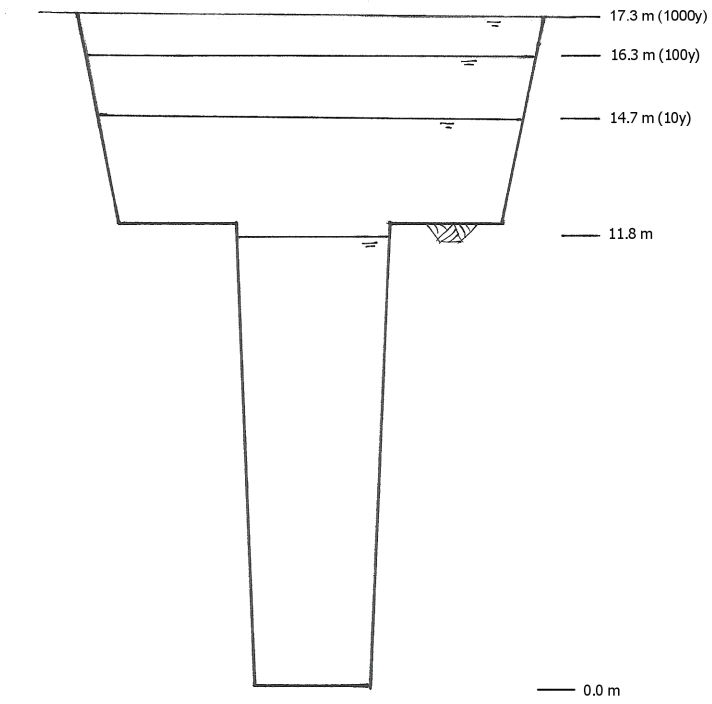

Figure 3.7: Water depths in the cross section for different return periods.

3.3 Levee breaching

A key component of the model is the breaching of the levees. Through these breaches, water can leave the channel and lead to inundation in the floodplains. There are two aspects of this that require modeling. The failure probability of the levee segment. And the formation and development of the breach when a failure occurs.

3.3.1 Levee failure probabilities

To determine the probability of a breach occurring anywhere in the levee along the idealized river, a probabilistic approach has been followed. This is partly based on (Kool *et al.* 2022). The levee along the entire idealized river was split in nine different stretches based on the resulting inundation of a breach. This inundation was based on initial test runs. It is unnecessary to model a breach in every potential location if the result will be the same. For this reason the levee was split in 15km long stretches. The stream-upward and stream-downward ends were not included as the edges of the modeled floodplain interferes with the results. Additional breaches in these areas do not provide additional insights. Each of these stretches was split in 200 meter wide section as this is the assumed maximum width of a breach that can be formed based on the Verheij-vdKnaap formula. This leads to 75 potential breaching locations per stretch.

The annual failure probabilities are represented with a fragility curve. If the loading on the levee increases so will the probability of failure. For this model the curve is idealized to three values for the three return periods. Based on historical data of a comparable river system, estimates were made for the failure probabilities. Three sets of estimated values were made. One set with average reliability, one with good reliability and one with poor reliability. These estimates are found in the first column of Table 3.4.

To determine failure probabilities from historical breaches both the state of the levee and the water levels are required. Even minor changes in the design or subsoil can impact the failure probabilities greatly. Often a flood defense system will only have a limited number of historical breaches leading to difficulty in extrapolation to greater return periods. Breaches are often found at local weak points in the levee. When a different system is used for the estimation of failure probabilities the relative presence of weak spots should be taken into account. Ultimately it remains difficult to make a reliable estimation for the failure probability. The process is visualized in Figure 3.8.

Based on a binomial distribution a chance of the occurrence of at least a single breach in a stretch can be made. By making an estimate for the failure chance of the levee sections for different return periods a fragility curve is formed. This curve can be used to determine the chance of breaching for a stretch.

$$P_b = 1 - (1 - P_f)^N$$

$$P_{b,k}(k) = \binom{N}{k} P_f^k (1 - P_f)^{N-k}$$

With P_b the chance of at least a single failure and P_f the chance of a breach in a section. $N = 750$ is the number of sections in a stretch and k is the number of breaches in a stretch. $P_{b,k}$ is the probability of exactly k breaches occurring. With the following assumed values the breaching probabilities are calculated. The results are presented in Table 3.4. In the first column the assumed failure rates of an individual section. In the second column the resulting breaching probability based on the binomial distribution. With that distribution the probabilities for one single breach ($P_{b,1}$) or two breaches occurring ($P_{b,2}$). This represents the chance of having multiple breaches in a single stretch.

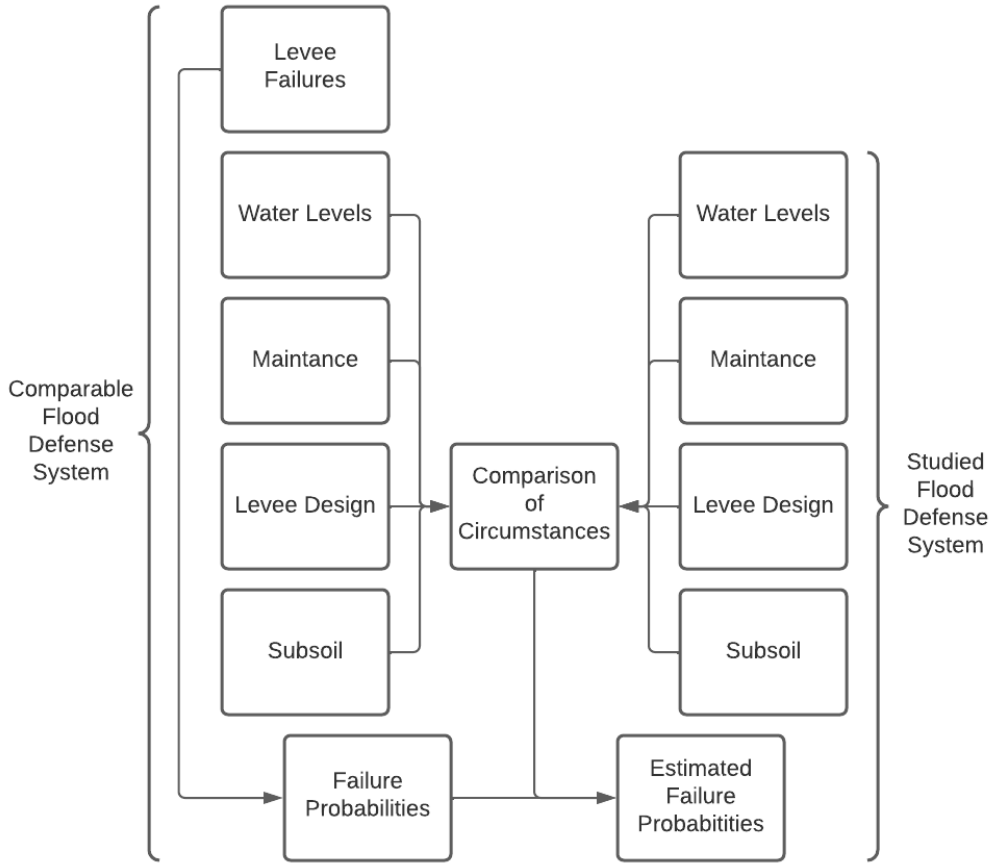

Figure 3.8: Flowchart of the process of making an estimation of the failure probabilities based on historical data of another system.

	P_f	P_b	$P_{b,1}$	$P_{b,2}$	$P_{b,1} + P_{b,2}$	$P_{b,1}/P_b$	$P_{b,2}/P_b$
10y	$1.00 * 10^{-5}$	$7.50 * 10^{-4}$	$7.49 * 10^{-4}$	$2.77 * 10^{-7}$	$7.50 * 10^{-4}$	1.00	0.00
	$2.00 * 10^{-5}$	$1.50 * 10^{-3}$	$1.50 * 10^{-3}$	$1.11 * 10^{-6}$	$1.50 * 10^{-3}$	1.00	0.00
	$5.00 * 10^{-5}$	$3.74 * 10^{-3}$	$3.74 * 10^{-3}$	$6.91 * 10^{-6}$	$3.74 * 10^{-3}$	1.00	0.00
100y	$1.00 * 10^{-4}$	$7.47 * 10^{-3}$	$7.44 * 10^{-3}$	$2.75 * 10^{-5}$	$7.47 * 10^{-3}$	1.00	0.00
	$2.00 * 10^{-4}$	$1.49 * 10^{-2}$	$1.48 * 10^{-2}$	$1.09 * 10^{-4}$	$1.49 * 10^{-2}$	0.99	0.01
	$5.00 * 10^{-4}$	$3.68 * 10^{-2}$	$3.61 * 10^{-2}$	$6.69 * 10^{-4}$	$3.68 * 10^{-2}$	0.98	0.02
1000y	$1.00 * 10^{-3}$	$7.23 * 10^{-2}$	$6.96 * 10^{-2}$	$2.58 * 10^{-3}$	$7.22 * 10^{-2}$	0.96	0.04
	$2.00 * 10^{-3}$	$1.39 * 10^{-1}$	$1.29 * 10^{-1}$	$9.59 * 10^{-3}$	$1.39 * 10^{-1}$	0.93	0.07
	$5.00 * 10^{-3}$	$3.13 * 10^{-1}$	$2.59 * 10^{-1}$	$4.81 * 10^{-2}$	$3.07 * 10^{-1}$	0.83	0.15

Table 3.4: Assumed failure probabilities and outcome of the binomial distribution calculation for breaching probability. Includes the probabilities for exactly one or two breaches, their sums and their ratios to the probabilities of at least one breach.

Based on the values found in Table 3.4, one breach is in most cases enough to encompass the realistic scenarios. For the 1000y return period the results show that there is a real chance of having two breaches in a single stretch. This calculation does not account for any relief effect. For this idealized model, it is assumed that multiple breaches will result to an relief effect, i.e. once a breach occurs, the other levee segments will not fail due to a lowering of the pressure against the entire levee system. Thus the total breaching width will remain similar.

The conditional fragility curves for both the failure of a single segment and the occurrence of breach in a stretch are plotted in figure 3.9. Fragility curve 1 ($FC1$) is based on the assumption of levees with good reliability, fragility curve 2 ($FC2$)is based on levees with average reliability and fragility curve 3 ($FC3$) is based on levees with poor reliability.

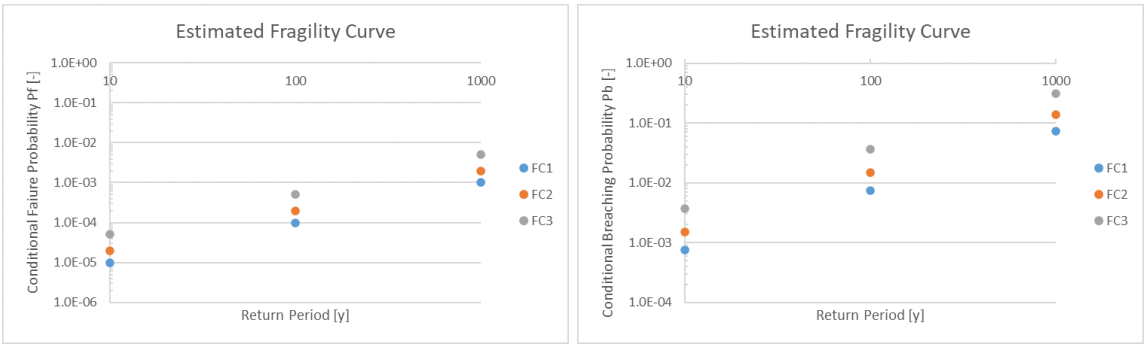

(a) Conditional estimated failure probabilities for the sections.

(b) Conditional estimated breaching probabilities for the stretches.

Figure 3.9: Graphs of the fragility curves.

Based on the breaching probability found, the chance for breaches in multiple stretches can be determined. This is done with the same binomial distribution. The results are presented in Table 3.5 in combination with the expected value and the standard deviation. Here N is the number of breaches.

	10y	10y	10y	100y	100y	100y	1000y	1000y	1000y
	FC1	FC2	FC3	FC1	FC2	FC3	FC1	FC2	FC3
N /Pb	$7.50 * 10^{-4}$	$1.50 * 10^{-3}$	$3.74 * 10^{-3}$	$7.47 * 10^{-3}$	$1.49 * 10^{-2}$	$3.68 * 10^{-2}$	$7.23 * 10^{-2}$	$1.39 * 10^{-1}$	$3.13 * 10^{-1}$
0	$9.93 * 10^{-1}$	$9.87 * 10^{-1}$	$9.67 * 10^{-1}$	$9.35 * 10^{-1}$	$8.74 * 10^{-1}$	$7.13 * 10^{-1}$	$5.09 * 10^{-1}$	$2.59 * 10^{-1}$	$3.39 * 10^{-2}$
1	$6.71 * 10^{-3}$	$1.33 * 10^{-2}$	$3.27 * 10^{-2}$	$6.33 * 10^{-2}$	$1.19 * 10^{-1}$	$2.45 * 10^{-1}$	$3.57 * 10^{-1}$	$3.77 * 10^{-1}$	$1.39 * 10^{-1}$
2	$2.01 * 10^{-5}$	$8.00 * 10^{-5}$	$4.91 * 10^{-4}$	$1.91 * 10^{-3}$	$7.19 * 10^{-3}$	$3.75 * 10^{-2}$	$1.11 * 10^{-1}$	$2.45 * 10^{-1}$	$2.54 * 10^{-1}$
3	$3.52 * 10^{-8}$	$2.80 * 10^{-7}$	$4.31 * 10^{-6}$	$3.35 * 10^{-5}$	$2.53 * 10^{-4}$	$3.35 * 10^{-3}$	$2.02 * 10^{-2}$	$9.25 * 10^{-2}$	$2.71 * 10^{-1}$
4	$3.97 * 10^{-11}$	$6.31 * 10^{-10}$	$2.43 * 10^{-8}$	$3.78 * 10^{-7}$	$5.75 * 10^{-6}$	$1.92 * 10^{-4}$	$2.36 * 10^{-3}$	$2.25 * 10^{-2}$	$1.85 * 10^{-1}$
$E(N\|f)$	0.01	0.01	0.03	0.07	0.13	0.33	0.65	1.25	2.82
$\sigma(N\|f)$	0.082	0.116	0.183	0.258	0.363	0.565	0.777	1.039	1.391

Table 3.5: Overview of probabilities for multiple breaches and the expected number of breaches.

For the first fragility curve ($FC1$) only a single breach occurring at the same time is a reasonable assumption based on the expected value and standard deviation. For the second fragility curve ($FC2$) the assumption of a single breach hold for the 10-year and 100-year return period. For the 1000-year return period two breaches should be taken into account based on the expected value. For the third

fragility curve ($FC3$), two breaches are required for the 100-year return period. The 1000-year return period would realistically require more than three breaches simultaneously. The number of model runs required to model a large number of breach combinations grows very quickly. A summary is presented in Table 3.6. To put a limit on the amount of run time required to run the idealized model, a maximum number of simultaneous breaches of three is used. In summary there are $N_{r,1} = 10 + 10 + 10 = 30$ runs required based on $FC1$. While for $FC2$, $N_{r,2} = 10 + 10 + 46 = 66$ runs are needed. And finally for $FC3$, the total number of model runs required has reached $N_{r,3} = 10 + 46 + 130 = 186$.

Breaches	Runs	Sum Runs
0	1	1
1	9	10
2	36	46
3	84	130
4	126	256
5	126	382
6	84	466
7	36	502
8	9	511
9	1	512

Table 3.6: Number of runs required for different number of simultaneous breaches.

3.3.2 Schematization of breach development

Based on initial testing runs of this model the distance between potential breach locations was set to $15\,km$. As can be seen in Figure 3.10, this leads to some overlap between the breaches. While in theory there are a infinite amount of potential breach locations, many of these lead to the same result. For this reason the total amount of breach locations can be reduced. The model was split into 9 stretches of $15\,km$ which led to 9 potential breach locations. There are no breaches modeled at the upstream and downstream boundaries of the river as these do not provide different result compared to the closest breach location. An overview of the breach locations is found in Figure 3.11.

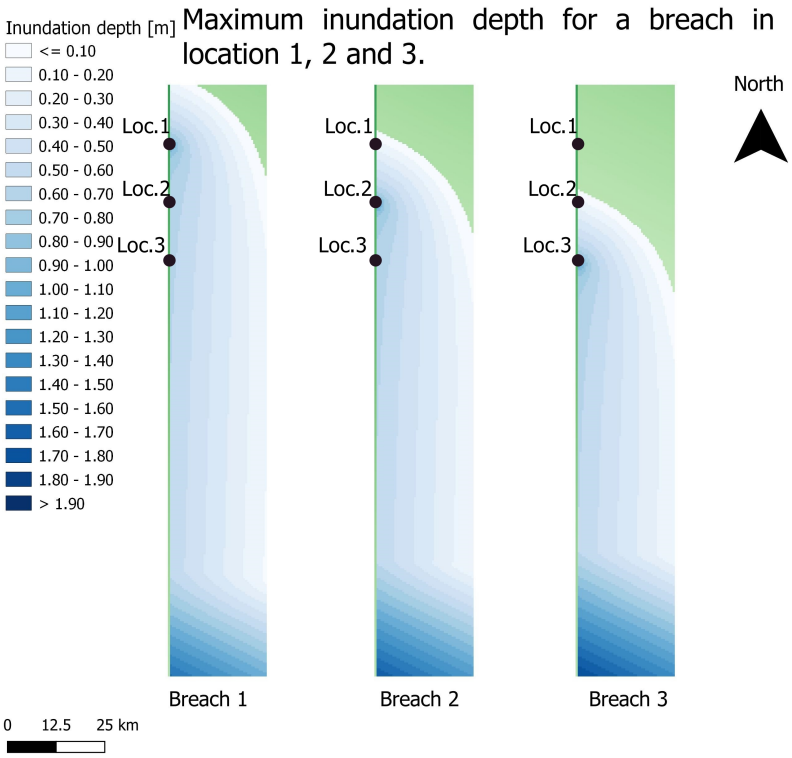

Figure 3.10: Maximum inundation depths for a breach in location 1, 2 and 3. The river is located at the west side of the floodplain.

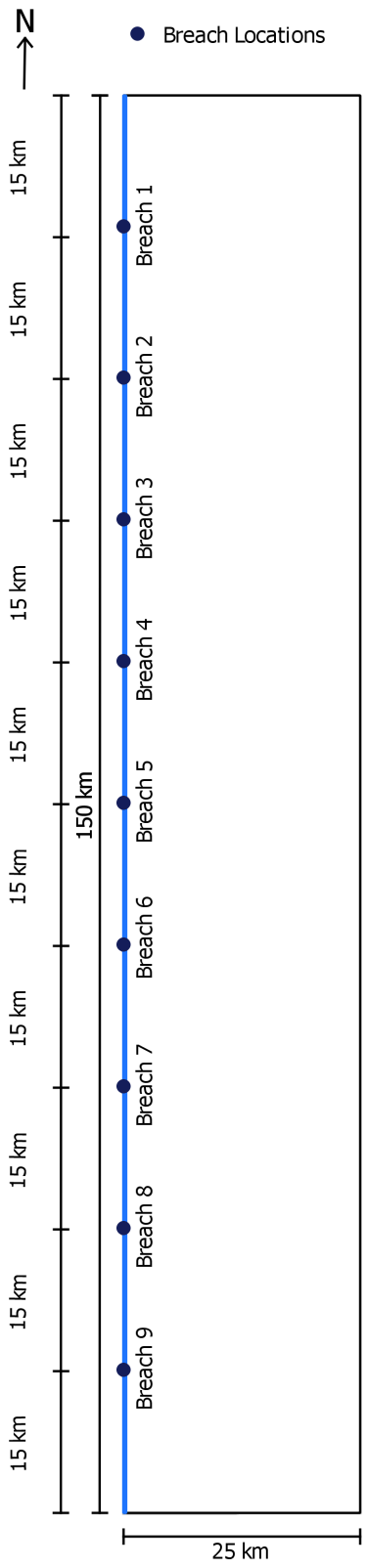

Figure 3.11: Sketch breach locations.

The breaching of the levees is schematized with a so-called branch. This is a part of the river network that only is modeled under certain circumstances. In SOBEK these are used to model breaches in levees or dams. There are two different formulas that can be used to model the breach itself. The vdKnaap (2000) formula or the Verheij-vdKnaap (2002) formula. In the idealized model the Verheij-vdKnaap formula is used. The initial crest height is logically set equal to the height of the levee. The minimal crest height was set to the ground level behind the levee. It is possible for erosion to reduce the bottom height of the newly formed channel to below the ground level but was not included in this initial model. This process consists of two phases.

The first phase is the initial creation of the breach. An initial width of the breach of 10 meters was assumed. This is small enough to allow the formula to decide what the actual final width is but also allows for a significant discharge to flow trough directly from the start. This process takes an amount of time that needs to specified in the branch properties. For this model a time period of 4 hours is assumed. The initial and theoretical maximum width of the breach are shown in Figure 3.12. Some graphs of the development of the breach can be found in3.14.

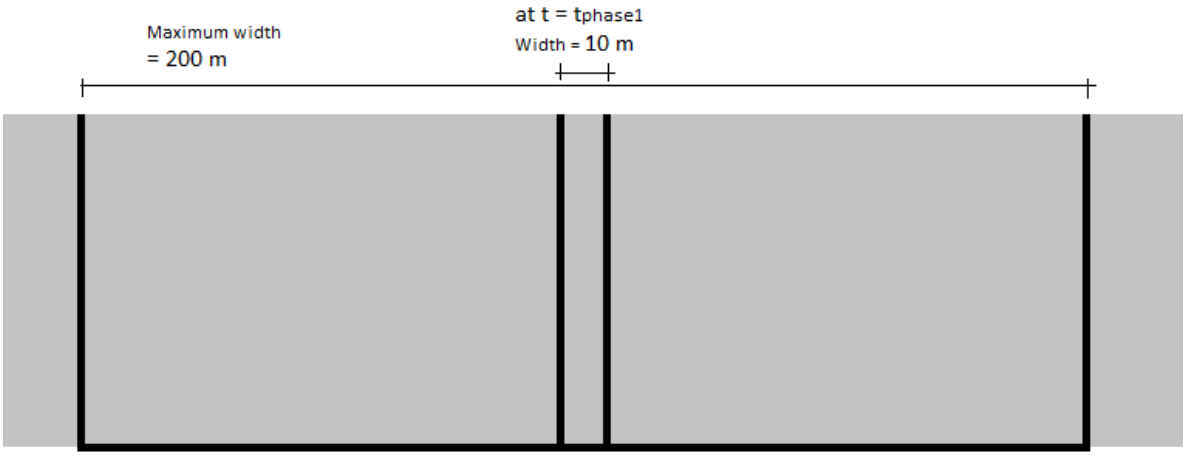

Figure 3.12: Sketch of the initial and maximum breach of the idealized levee

After the initial development of the breach the second phase begins. Here the width of the breach is increased if the flow velocity is larger than a constant critical flow based on the material of the levee. For the idealized model, a levee constructed out of sand was used. This leads to a standard value for the critical flow of $0.2\,m/s$.

$$For \quad T_{start} < t < t_{phase1}$$

$$B(t) = B_0 \quad z(t) = z_{crest} - (\frac{T_{start} - t}{t_{phase1}}) * (z_{crest} - z_{min})$$

$$For \quad t > T_{start} + t_{phase1}$$

$$z(t) = z_{min}$$

$$B(t_{i+1}) = B(t_i) + \Delta t(\frac{\delta B}{\delta t})_{ti}$$

$$(\frac{\delta B}{\delta t})_{ti} = \frac{f_1 f_2}{LN(10)} \frac{(g(h_{up} - max(h_{down}, z_{min})))^{\frac{3}{2}}}{u_c^2} \frac{1}{1 + \frac{f_2 g}{u_c}(t_i - t_0)} \quad if \quad |u| > u_c$$

$$(\frac{\delta B}{\delta t})_{ti} = o \quad if \quad |u| < u_c$$

3.4 Comparison to analytical formulas

To ensure that the model represents a real-life river with reasonable accuracy, some calibration calculations need to be performed. For the non-breaching scenarios, the water depths and the velocity of the flood wave can be studied. For the breaching cases the velocity in the breach itself should correspond to analytical calculations.

3.4.1 River channel

The water depth over the winterbed should correspond to values observed in comparable sections of the Tisa river. The following properties for the main channel can be determined: the depth d, discharge Q, the wet surface area of the cross section A, the wet perimeter P and the hydraulic radius R. The final one of these can be calculated with $R = \frac{A}{P}$. The results are listed in Table 3.7. The water depths were found by allowing SOBEK to run with a constant discharge until the equilibrium water depths were found.

Return period	d	Q	A	P	R
10y	$14.7m$	$2900m^3/s$	$2732m^2$	$471.9m$	$5.79m$
100y	$16.3m$	$3800m^3/s$	$3460m^2$	$481.5m$	$7.18m$
1000y	$17.3m$	$4600m^3/s$	$3976m^2$	$487.5m$	$8.16m$

Table 3.7: Overview of several properties of the profile for different water depths

The flow velocity in the channel for a given discharge should be the same as a value found analytically. A simple formula to calculate these velocities is:

$$U_f = \frac{Q}{A}$$

Here A is the wet surface area in the channel for the given depth and Q the discharge in the channel. This formula only upholds if the Reynolds number is large enough that the velocity can be assumed uniform over the cross section. This would require $Re = \frac{\rho U R}{\mu} => 4000$. With the dynamic viscosity μ equal to $1.002 Ns/m^2$ and the density ρ equal to $1000 kg/m^3$. The different values found in the model and calculated can be found in table 3.8.

Return Period	A	Re	U_f	U_m
10 y	$2732m^2$	5894	$1.02m/s$	$1.08m/s$
100 y	$3460m^2$	7811	$1.09m/s$	$1.09m/s$
1000 y	$3976m^2$	9447	$1.16m/s$	$1.14m/s$

Table 3.8: Model and calculated velocities

The flood wave in the model should move with a comparable velocity in the numerical model as in analytical models. The velocity of the flood wave can be determined with two different methods. The first method is based on the equation of motion and the continuity equation. This approach is based on chapter 3 of (*Syllabus River Dynamics 1* 2018).

$$B\frac{\delta h}{dt} + \frac{\delta Q}{\delta x} = 0$$

$$\frac{\delta Q}{\delta t} + \frac{\delta}{\delta x}(\alpha\frac{Q^2}{A}) = -gA\frac{\delta h}{\delta x} - \frac{gQ|Q|}{C^2A^2}$$

By scaling the different parameters, the parts of the equation that dominate can be found. For the scaling the following value were used. The discharge Q is of the scale of $2000m^3/s$, the height of the flood wave is of the scale of $5m$, the wave length is similar to the length of the channel and is set at 10^5m, the wave period is set at a scale of 1 day or 10^5s, the wet area A is scaled at $2000m^2$, the storage width is scaled at $500m$, the Chezy resistance parameter C is scaled at 50 and the hydraulic radius R is scaled at $5m$.

Scaling the continuity equation:

$$\frac{BHL}{QT} = \frac{500 * 5 * 10^5}{2000 * 10^5} = \frac{5}{4} = 1.25$$

Scaling the equation of motion:

$$\frac{QL}{gHAT} = \frac{2000 * 10^5}{10 * 5 * 2000 * 10^5} = \frac{1}{50} = 0.02$$

$$\frac{Q^2}{gHA^2} = \frac{2000^2}{10 * 5 * 2000^2} = \frac{1}{50} = 0.02$$

$$\frac{Q^2L}{C^2A^2RH} = \frac{2000^2 * 10^5}{50^2 * 2000^2 * 5 * 5} = \frac{8}{5} = 1.6$$

Based on these scaled parts of the equation of motion, it can be assumed that the flow is dominated by resistance and gravity. The advection term of the equation can be neglected. The order of the dominating term of the equation of motion should be the same as the order of the continuity equation. This approach only holds for rivers with a small Froude-number. $\frac{U}{\sqrt{gd}} = \frac{1.02}{\sqrt{9.81 * 11.6}} = 0.096$.

$$c_{HW} = \frac{Q}{A} + 0.5\frac{Q}{BR}$$

Here the B is the width of the river over the winterbed which is 450 meter. The results are summarized in table 3.9.

Return Period	Q	A	R	c_{HW}
10 y	$2900m^3/s$	$2732m$	$5.79m$	$1.61m/s$
100 y	$3800m^3/s$	$3460m$	$7.18m$	$1.67m/s$
1000 y	$4600m^3/s$	$3976m$	$8.16m$	$1.74m/s$

Table 3.9: High-water wave celerity values calculated

The second way to determine the celerity of the high-water wave is by making use of a formula based on the flow velocity for the provided discharge. The result are summarized in Table 3.10

$$c_{HW} = 1.5U$$

Return Period	U	c_{HW}
10 y	$1.08m/s$	$1.62m/s$
100 y	$1.09m/s$	$1.63m/s$
1000 y	$1.16m/s$	$1.74m/s$

Table 3.10: High-water wave celerity values based on flow velocity

Finally, these values can be compared to the results of the model itself. As can be seen in Figure 3.13 there is a short time interval between the peak water depths in the north and south boundary. Due to the time step of 4 hours, it is impossible to determine the exact time between these two peaks. But as a rough estimate, the time between the peaks for the 10 and 100 year return period can be taken as between 24 and 28 hours. This leads to a flood wave celerity between $\frac{150000}{24*3600} = 1.74m/s$ and $\frac{150000}{28*3600} = 1.49m/s$. The calculated values fall in this range. For the 1000 year return period, the period between the two peaks can be estimated at 16 to 24 hours, which will lead to a celerity between $1.74m/s$ and $\frac{150000}{16*3600} = 2.60m/s$. This is potentially larger than the calculated value. The 1000 year return period was determined for a profile with higher levees to prevent the overflow from interfering with the results. Even if the value is large the flood wave remains diffuse and the height of the wave would be reduced less at the southern boundary.

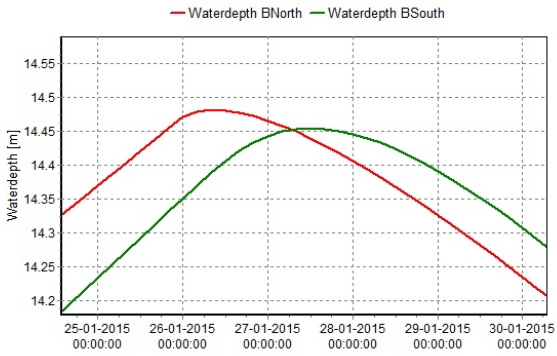

(a) Water depth peaks at the boundaries for 10 year discharge

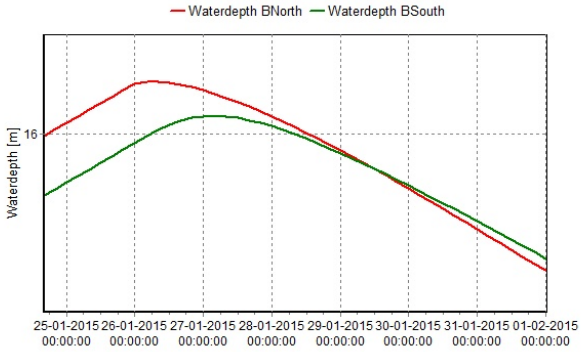

(b) Water depth peaks at the boundaries for 100 year discharge

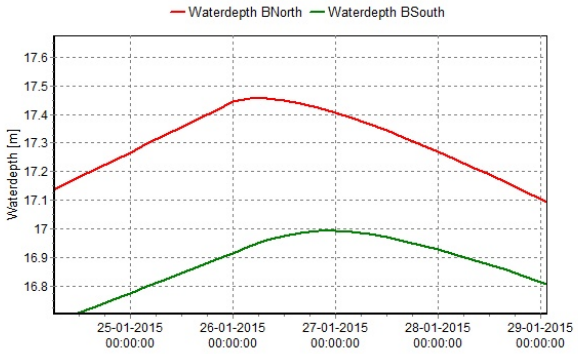

(c) Water depth peaks at the boundaries for 1000 year discharge

Figure 3.13: Peak water depths at the boundaries for the different return times.

3.4.2 Levee breaching

The discharge in the breaches should be similar to a value one could expect from analytical equations. The breach-growth is modeled in SOBEK with the Verheij-vdKnaap formula. For these calibration calculations the case for breach 1 is used. The following formulas are used in SOBEK for a Verheij-vdKnaap breach growth model (Verheij & Van der Knaap 2002). This method is described in the SOBEK manual (Deltaris 2018).

The development of a breach is split into two phases. The first phase is independent from the discharge trough the breach. But the second phase should behave according to the assumed relation between the width of the breach and the flow velocity through the breach. As long as the flow velocity is larger than the critical flow velocity of $0.2m/s$ the width of the breach increases. This can easily be read from the graphs of the width and flow velocity of the breach.

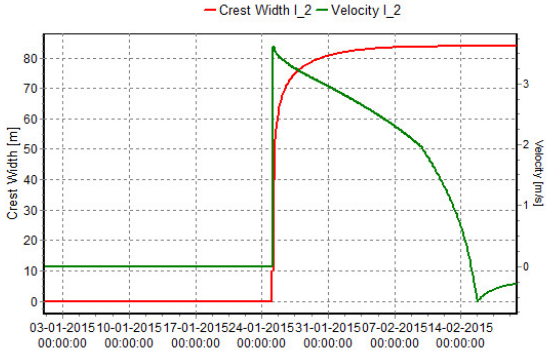

(a) Flow velocity and breach (crest) width for breach 1 during 10y return flow.

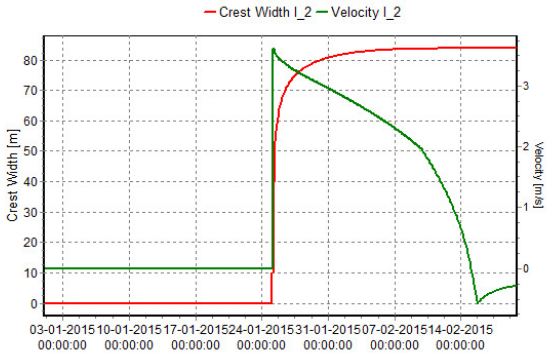

(b) Flow velocity and breach (crest) width for breach 1 during 100y return flow.

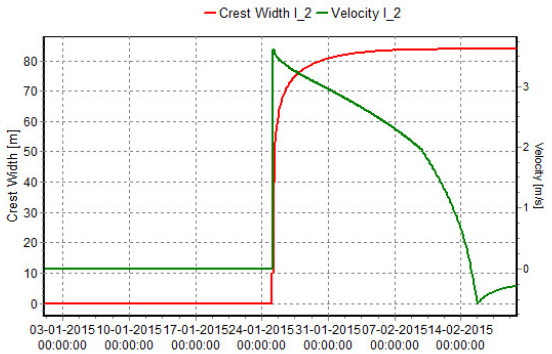

(c) Flow velocity and breach (crest) width for breach 1 during 1000y return flow.

Figure 3.14: Flow velocities and breach width over different return periods.

Chapter 4

Results and evaluation of the idealized model

4.1 Introduction

In this chapter, the results of the flood model with explicit inclusion of levee breaching are presented. The model schematization made in SOBEK replicates the Tisa River in Serbia but in an idealized way. For example, all geometric river characteristics (river, floodplain and levee cross-sections) are constant along the river axis and vary with a constant slope in downstream direction. The flood model accounts explicitly for levee breaching by taking into account the levee breaching probability and breach growth in time. The details of this model setup have been described in Chapter 3.

The purpose of this idealized model is to investigate the resulting inundation at the protected side of the embankments as a result of levee breaching. It also allows to study parameter variations and investigate how these influence the results. In Section 4.2 the outcomes of the baseline model are presented. Based on the outcomes the baseline setup, a recommendation for further evaluations is made. In Section 4.3 the different parameter variations are made and evaluated. The detailed results are collected in Appendix B. Finally, a discussion of and conclusions based on the evaluation are provided in Section 4.4.

4.2 Results for base setup

Running the baseline model with SOBEK for the Tisa river generates a large amount of data. The baseline computation consists of in total 66 1D-2D computations to account for all possible combinations of levee breaches along the Tisa River and different upstream discharge (10, 100, 1000 years). Each computation covers a period of 50 days. The total computation time on is around 10 hours.

To provide better insight to this data, first a set of maps is made to determine the chance of a depth above a certain value. This is referred to as the chance of wet feet. In addition, several plots were made of the water level that exceeds a 100-year and 1000-year return period. The base setup is based on the second fragility curve in Section 3.3.1. This fragility curve includes some influence of multiple simultaneous breaches. The amount of cases that have to be run in the model is still relatively low.

4.2.1 Methodology

In Section 3.2 the schematization of the used model is presented. In this section the setup of the different cases that are combined into the results are presented. The base setup consists of 66 different

cases. The cases are split among the three different return periods that are studied. For the case for purely overflow there is 1 case per return period. For the cases with a single breach occurring in the levees along the river there are 9 different cases per return period. The 1000-year return period has a high enough chance of breaching so that cases with two simultaneous breaches should be included. This leads to an additional 36 cases for this return period. Therefore a total amount of 66 cases are run. The probabilities for the occurrence of each case are found in Table 4.1. These value are found by dividing the probabilities in Table 3.5 with the number of different combinations as found in Table 3.6.

Return Period	10y	100y	1000y
P_{Event}	0.09	0.009	0.001
Non-Breach	$8.88 * 10^{-2}$	$7.86 * 10^{-3}$	$2.59 * 10^{-4}$
1 Breach	$1.20 * 10^{-3}$	$1.07 * 10^{-3}$	$3.77 * 10^{-4}$
2 Breach	$7.20 * 10^{-6}$	$6.47 * 10^{-5}$	$2.45 * 10^{-4}$
3 Breach	$2.52 * 10^{-8}$	$2.28 * 10^{-6}$	$9.25 * 10^{-5}$

Table 4.1: Overview of annual breaching probabilities for FC2.

The map of the probability of a water depth exceeding a specific depth is created by accumulating the different outputs of the 66 cases. If the overflow would reach a depth of more than 0.10 meter over the levee, the cell would have been colored in the map. It is assumed that the different breaching cases are mutually exclusive. If the breaches would be caused purely by overflow erosion, the breaches would occur fully dependent. If the breaching would be assumed to be caused by the underlying soil, the breaches would be independent. The influence of independent breaching is already included in the fragility curves. These methods of combining probability, for the purpose of creating a map, are described in more detail in a rapport made by Stichting Flood Control (*Onzekerheden in overstromingsrisico's* 2009).

In a MATLAB script the results of the 66 computations are combined to derive an annual probability of exceedance for a given water depth. It is assumed that the breaching scenarios are mutually exclusive. The chance for the different breaching cases is assumed to be the same. This simplifies the combining of different cases. In Table 4.1 the different annual probabilities are presented. The total sum of the different probabilities will be 0.1 as discharges with a return period of less than 10 years are assumed to be unable to trigger a levee breach.

By finding the water depths that are exceeded for a hundred and thousand year return period over the cells in the 2D grid, a estimation for the water levels can be made. The maximum water depths for each of the cases were collected for each cell and ordered by height. Then the corresponding probabilities were used to find the depth that would be exceeded 0.1 % or 1.0 % of the time. These values were found by ordering the maximum water depths found in the different cases and ordering these from largest to smallest. By counting back from the total studied annual probability of 10%, the value just below the target probability was found. This leads to a conservative estimation of the water depths in the cells. By plotting these values for a cross section of the flood plain these can be compared to the water levels between the embankments. Three cross sections were chosen for this analysis. The cross section at 75km ($X = 150$) represents the middle of the studied river between two breach locations. At 120km ($X = 240$) is the second to last breach location and combines the influence of the breach with the accumulation of water from stream upwards breaches. And finally, at the southern edge of the model ($X = 300$). At this location, most of the water ends up at the end of the simulation as this is the lowest point and the highest water levels are found. The locations of these cross sections are shown in Figure 4.1.

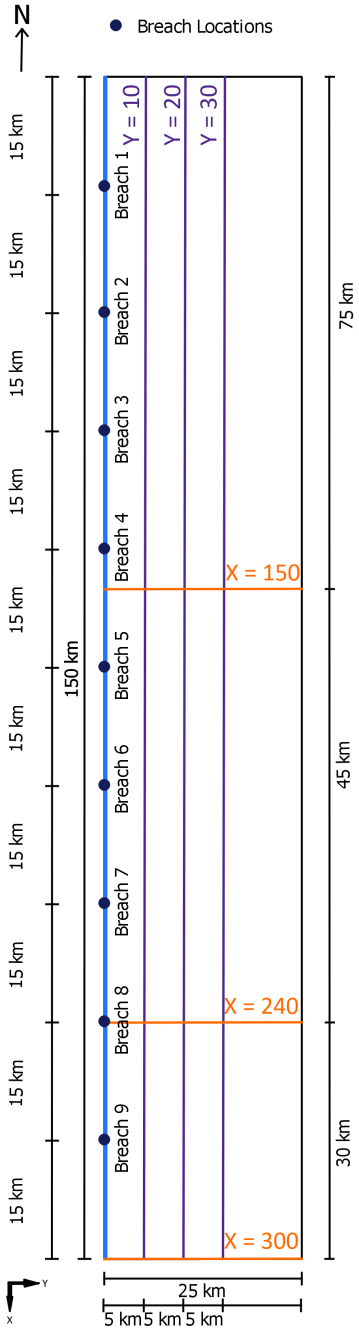

Figure 4.1: Sketch breach locations with cross sections.

4.2.2 Chance of wet feet

In the following Figure 4.2 the maps for a water depth of 0.1 meter, 0.3 meter, 0.5 meter and 1.0 meter have been provided. The values were created by comparing the maximum water depth found in the cell of the 2D grids to a specified value and summing the probabilities of the cases that equal

or exceed it. These maps provide some insight in the influence of the breaching locations and how the slope of the flood plain cause water to accumulate in the lowest areas. The probability of reaching certain water depths increase in downstream direction. The southern edge of the floodplain is assumed to be a large impenetrable obstacle. In the real world version of the Tisa, the levee of the Danube is present here which causes the water to accumulate in the lowest point. The lowest point is found in the bottom left corner of the floodplain.

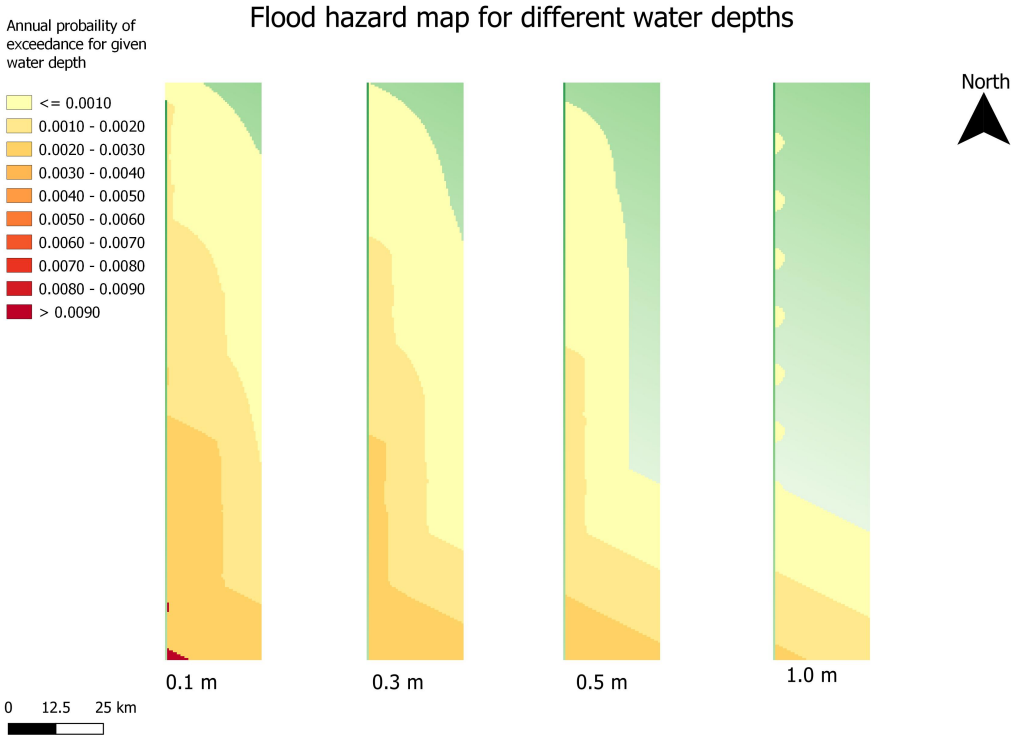

Figure 4.2: Wet feet map for the base setup.

4.2.3 Exceedance water levels

In Figure 4.3 the plots over the north-south cross sections are presented. A relatively low water level is found after around a third of the total river reach. The water level here is approximately $0.3m$. Further downstream the water has accumulated and formed a horizontal plane. The highest water level is found at the very edge of the model and is around $2.0m$. The difference between the different cross sections is minor. The water level decreases slightly further away from the levee. This is caused by a increase of the ground level. The 1.0% water level is only visible in the very bottom left corner of Figure 4.3a.

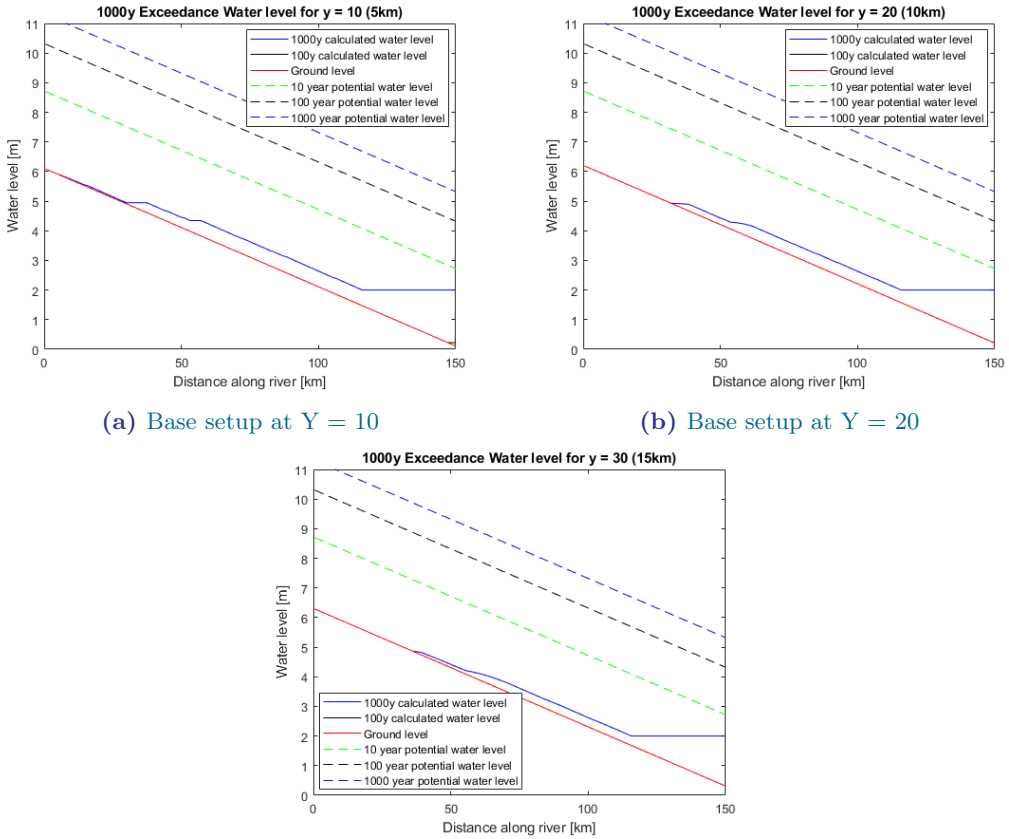

(a) Base setup at Y = 10

(b) Base setup at Y = 20

(c) Base setup at Y = 30

Figure 4.3: Plots of 100 year and 1000 year return period exceedance water levels along the north-south cross sections at 5km, 10km and 15km away from the river.

In the plots of Figure 4.4 the water levels are seen at different west-east cross sections. As already seen in the previous plots the highest water level is found at the southern edge of the model at $X = 300$. Here the water reaches a height of around $2.0m$ above the ground level. In the other two plots the heights are relatively low compared to the water level inside of the levees. In Sub-figure 4.4a the water level tapers of at the end. This implies that some of the inundation caused by the upstream breaches do not reach over the complete width of the floodplain at this cross section. The 100 year return period water level is only visible in sub-figure 4.4c.

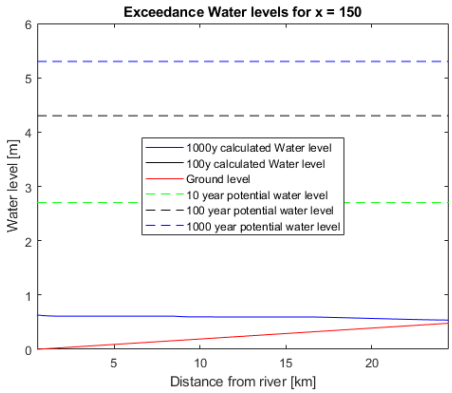

(a) Base setup at X = 150

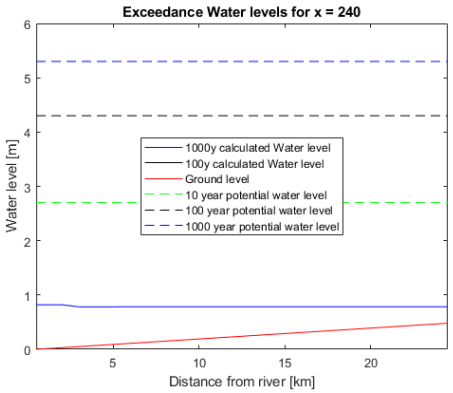

(b) Base setup at X = 240

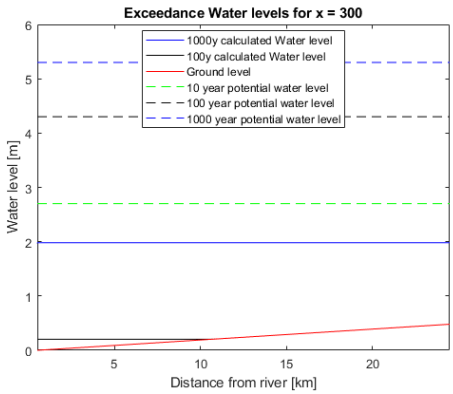

(c) Base setup at X = 300

Figure 4.4: Plots of 100 year and 1000 year return period exceedance water levels along the west-east cross sections.

4.2.4 Discussion base setup

By extrapolating the water surface level between the embankments over the flood plains, the inundation volume becomes extremely large. While the actual river discharge results in a volume that is often far smaller. The behaviour of the model depends on these volumes and their ratios.

To study these relations between the available volume and the stored volume in the floodplain several dimensionless ratios can be determined. These ratios can provide insight in the influence of variations in the model on the actual inundation volumes that can be expected.

Three different volumes are important in this situation. First, the total volume that enters the river and is conveyed through the winterbed. This volume is the total amount of water that can potentially flow into the flood plains. These values were found for the different return periods by first taking the sum of all discharges which led to a depth of over 12.0 meters reduced by the discharge that led to a depth of around 12.0 meter. This was for the currently used profile $2000\,m^3/s$. This can than be multiplied with the time step to find the volume. The resulting volumes can be used as a reasonable estimate for the total available volume for inundation.

$$V_{r,10y} \approx 1.589 * 10^9\, m^3, \quad V_{r,100y} \approx 3.480 * 10^9\, m^3, \quad V_{r,1000y} \approx 5.211 * 10^9\, m^3$$

The second volume is the sum of the positive discharge trough the breach. Negative flow caused by higher water levels outside of the levee or the reduction of the water level inside of the levees is removed. By doing this it is possible to determine to maximum amount of water in the floodplain during a breach event. This does not account for inundation caused by overflow. That can potentially be estimated in the same way as the volume conveyed over the winterbed. The exact volume that flows through a breach varies per location but they are very similar. Only at the southern breach locations the volume is reduced due to the increased water depth at the other side of the breach. This limits the head difference and thereby the discharge. The detailed overview of the different breaching volumes is provided in Table A.1.

And finally, the third volume of interest is the amount of water that can be stored in the flood plain given a certain depth. This can simply be found by multiplying the area of the floodplain with the desired depth. The available storage in the flood plain depends on the selected water level. If the water level of the related return period is continued over the floodplain a certain storage volume is found. This can be found by calculating the area A_x of the cross section underneath the 10 year return period water level over the flood plain as can be seen in Figure 4.4.

$$V_{f,10y} = A_x L = 150000 * 24500 * (2.70 - \frac{0.48 - 0.00}{2}) = 9040500000 \approx 9.0 * 10^9 m^3$$
$$V_{f,100y} = A_x L = 150000 * 24500 * (4.30 - \frac{0.48 - 0.00}{2}) = 9040500000 \approx 1.5 * 10^{10} m^3$$
$$V_{f,1000y} = A_x L = 150000 * 24500 * (5.30 - \frac{0.48 - 0.00}{2}) = 9040500000 \approx 1.9 * 10^{10} m^3$$

Two different ratios were determined with these volumes. The Breach-River-Ratio to describe the relation between the total available volume for inundation and the volume that could pass to a breach. The close the ratio gets to 1 the more of the supplied volume was able to flow trough the breach. The Breach-Floodplain-Ratio to describe the relation between the volume that enters the flood plain and the available storage.

$$BRR = \frac{V_b}{V_r}$$
$$BFR = \frac{V_b}{V_f}$$

The calculated values of the ratios are presented in Appendix A in Tables A.2 and A.3. The ratios are also presented as scatter plots in Figure 4.5. In the plots it can be seen that all of the points are found on a single line. This is caused by the fact that the storage volume (V_f) and the river volume (V_r) are the same for all of the points in a plot. Only the breaching volume (V_b) changes between the different points.

The scatter plots for the base setup show that the values of both the BRR and BFR are relatively low. The points remain in the bottom left quadrant. For further evaluation it is interesting how these ratio are linked to the model behaviour. It is unlikely that the BRR will reach a value above 0.5. To reach this value it would mean that half of the water that flows above the winterbed exits through breaches. The BFR on the other hand can most likely be increased to 1 for a smaller floodplain.

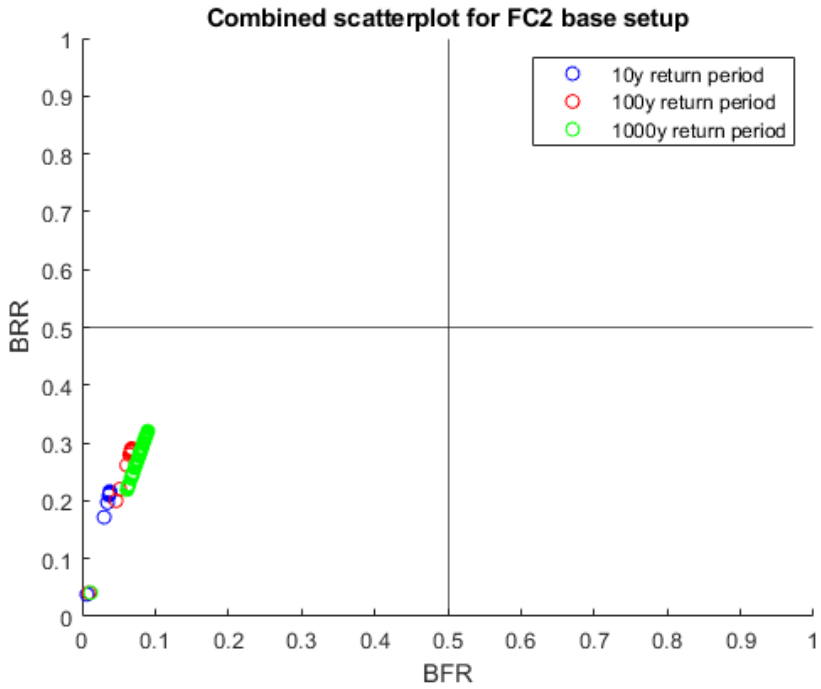

Figure 4.5: Scatter plots of the BFR and BRR ratios.

Based on these ratios it is clear that the breach is the limiting factor for the volume that can enter the defensed floodplains. The bathtub approximation is based on extrapolating the water levels from outside the defenses to the floodplain inside the defenses. If this approximation is applied the BFR would be equal to 1.0. Based on the results of the base case setup this seems to be an overestimation. The volume that flows through the breach needs to increase almost tenfold to reach the required volume stored over the floodplain that would be expected based on the extrapolation.

4.2.5 Applicability of BFR for other cases

An estimation of the BFR can be used to predict whether a bathtub approximation is sufficient or if more detailed method would be warranted. To study this two example cases in the Netherlands were studied. To determine this ratio three parameters are required in combination with an assumption for the breach width.

1. The surface area of the protected zone.
2. An estimation of the surface level elevation of the protected zone.
3. A water surface elevation outside of the defenses.

The breach is assumed to reach a width of $50\,m$ and that the flooding event will last for one week. For the determination of the breaching volume a conservative calculation will be used based on free flow over a broad weir with a discharge coefficient of $m = 0.55$. The water surface elevation are based

on (Waterdienst 2008). The surface elevation levels were determined based on the MERIT DEM (Yamazaki, Ikeshima, *et al.* 2017) via an online tool[1].

The first case studied is dike ring 49, IJsselland. The water surface elevation outside of the levee is $11.4m$, the land surface elevation is estimated at $10m$. The surface area A_{49} of this zone is 8700 hectares.

$$H_{49} = 11.4 - 10 = 1.4m$$
$$Q_{49} = mBH_{49}\sqrt{2gH_{49}} = 0.55 * 50 * 1.4 * \sqrt{2 * 9.81 * 1.4} = 202\, m^3/s$$
$$V_b = Q_{49} * 7 * 24 * 3600 = 1.22 * 10^8\, m^3$$
$$V_f = H_{49}A_{49} = 1.4 * 8700 * 100^2 = 1.22 * 10^8\, m^3$$
$$BFR_{49} = 1.0$$

Based on the results of these simple calculation the bathtub approximation can be used. The value for the breaching volume is very conservative.

The second case studied is dike ring 43, Betuwe. The water surface elevation outside of the levee is $14.9m$, the land surface elevation is estimated at $11m$. The surface area A_{43} of this zone is 66000 hectares.

$$H_{43} = 14.9 - 11 = 3.9m$$
$$Q_{43} = mBH_{43}\sqrt{2gH_{43}} = 0.55 * 50 * 3.9 * \sqrt{2 * 9.81 * 3.9} = 938\, m^3/s$$
$$V_b = Q_{43} * 7 * 24 * 3600 = 5.67 * 10^8\, m^3$$
$$V_f = H_{43}A_{43} = 3.9 * 66000 * 100^2 = 2.57 * 10^9\, m^3$$
$$BFR_{43} = 0.22$$

Based on these simple calculations even with a very conservative value for the breach volume the bathtub approximation would not be a reasonable strategy. Not enough volume can enter the protected zone to reach those water levels.

4.3 Evaluation of different variations of the idealized model

To further study the influence of certain parameters on the results of the idealized model, a number of evaluations were made. The focus is on parameters which potentially lead to significant changes in the behavior of the model. Of particular interest are the BFR and BRR ratios which were defined to provide insight in the behaviour of the model. For each of the selected parameters two different setup are tested.

The new setups for the idealized model of the Tisa river are compared to the base setup used in Section 4.2. The influence is studied based on a wet feet map, the plots of the exceedance water level over various cross sections and on scatter plots of the BFR and BRR. These can be found in their completion in Appendix B. Some of the more interesting results have been included in this section.

[1] "https://nl-be.topographic-map.com/", last referenced at 21-Feb-2022

The following setups are studied to determine the influence on the behaviour of the idealized model. The other fragility curves that were defined in Section 3.3.1 are studied as the first variation.

Secondly the influence of increased breaching depth is studied. In the base setup the depth was limited to the ground level of the floodplain. It is sensible to assume that the erosion that increases the width of the breach can also increase its depth.

The third studied variation is the width of the flood plain. The bathtub approximation is often used for smaller basin. In flood mapping this approximation is often also used for larger basins. In the results of Chapter 3 the water level plots show already significant differences with this assumption. A smaller floodplain area should result in water level plots that are closer to the assumed values if this approximation holds.

The fourth studied variation is a change in the depth of the floodplain. The flow velocity in the breach is driven by a head difference between the water level on the inside and outside of the embankments. By decreasing the ground level on the outside the head difference should be influenced.

The fifth variation is made by splitting the flood plain into two parts by adding effectively a wall in the flood plain perpendicular to the river channel. This wall represents a road or the levee of a side channel. Does the inclusion of this wall change the total discharge through the breaches or just change where the water ends up.

And finally for the sixth variation the starting time of the breach is brought forward. This lead to the breach forming before the peak water depth is reached at their location and also leads to more time for the breach to convey the water to the floodplain.

4.3.1 Different fragility curves

In this section the difference between the different fragility curves is studied. The fragility curves are defined in Section 3.3.1. The probabilities that are used to combine the results for the different cases are presented in Table 4.2. These are used for both the wet feet maps as the water level plots over the cross sections.

As an initial hypothesis the fragility curves based on a higher initial failure rate of the levee sections will lead to larger probabilities in the wet feet map. The influence on the water level plot is most likely minor. These are influenced less directly by the breaching probabilities. The BRR and BFR ratios will change with additional breaches. These will most likely cause higher breaching volumes and therefore higher values for the ratios.

Return Period	10y	10y	10y
Fragility Curve	FC1	FC2	FC3
P_{Event}	0.09	0.09	0.09
Non-Breach	$8.94 * 10^{-2}$	$8.88 * 10^{-2}$	$8.70 * 10^{-2}$
1 Breach	$6.04 * 10^{-4}$	$1.20 * 10^{-3}$	$2.94 * 10^{-3}$
2 Breach	$1.81 * 10^{-6}$	$7.20 * 10^{-6}$	$4.42 * 10^{-5}$
3 Breach	$3.17 * 10^{-9}$	$2.52 * 10^{-8}$	$3.88 * 10^{-7}$
Return Period	100y	100y	100y
Fragility Curve	FC1	FC2	FC3
P_{Event}	0.009	0.009	0.009
Non-Breach	$8.41 * 10^{-3}$	$7.86 * 10^{-3}$	$6.42 * 10^{-3}$
1 Breach	$5.70 * 10^{-4}$	$1.07 * 10^{-3}$	$2.21 * 10^{-3}$
2 Breach	$1.72 * 10^{-5}$	$6.47 * 10^{-5}$	$3.38 * 10^{-4}$
3 Breach	$3.02 * 10^{-7}$	$2.28 * 10^{-6}$	$3.01 * 10^{-5}$
Return Period	1000y	1000y	1000y
Fragility Curve	FC1	FC2	FC3
P_{Event}	0.001	0.001	0.001
Non-Breach	$5.09 * 10^{-4}$	$2.59 * 10^{-4}$	$3.39 * 10^{-5}$
1 Breach	$3.57 * 10^{-4}$	$3.77 * 10^{-4}$	$1.39 * 10^{-4}$
2 Breach	$1.11 * 10^{-4}$	$2.45 * 10^{-4}$	$2.54 * 10^{-4}$
3 Breach	$2.02 * 10^{-5}$	$9.25 * 10^{-5}$	$2.71 * 10^{-4}$

Table 4.2: Overview of annual breaching probabilities for different cases.

In figures 4.6, 4.7 and 4.8 the wet feet maps for the different fragility curves are shown. The total inundation has increased in the maps of the second fragility curve compared to the maps of the first fragility curve. The total inundation area has increased also in the maps of the third fragility curve but this increase is very minor. The dark red areas remain the same size for all three the fragility curves. The rate of increase of the probabilities went up for the higher fragility curves.

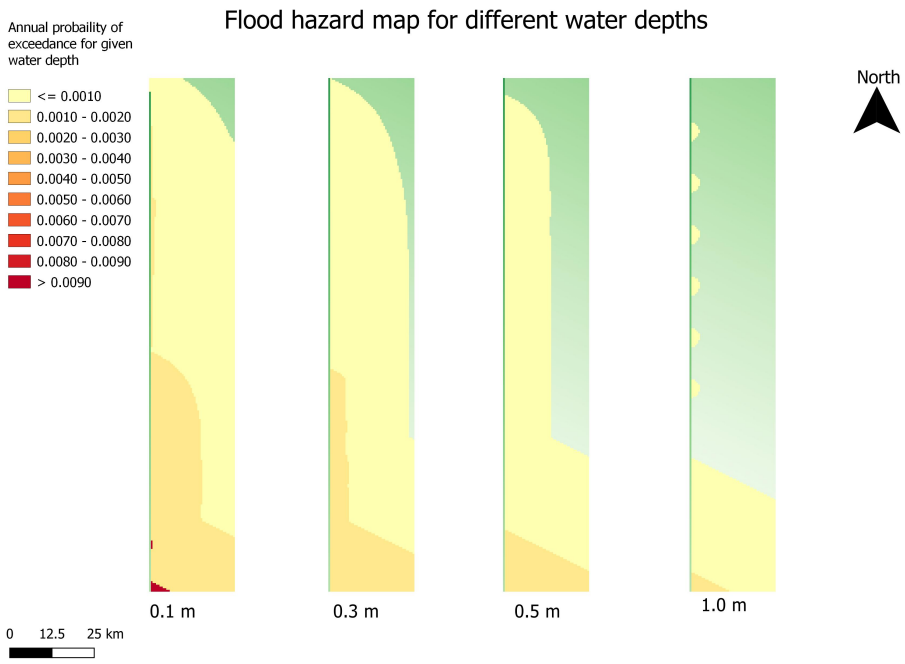

Figure 4.6: Wet feet map for fragility curve 1

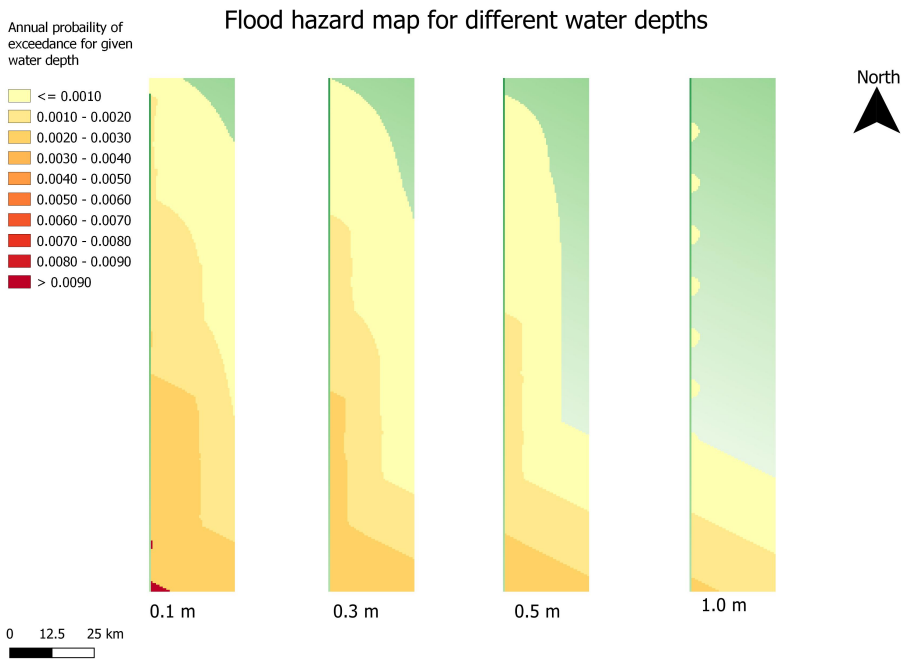

Figure 4.7: Wet feet map for fragility curve 2

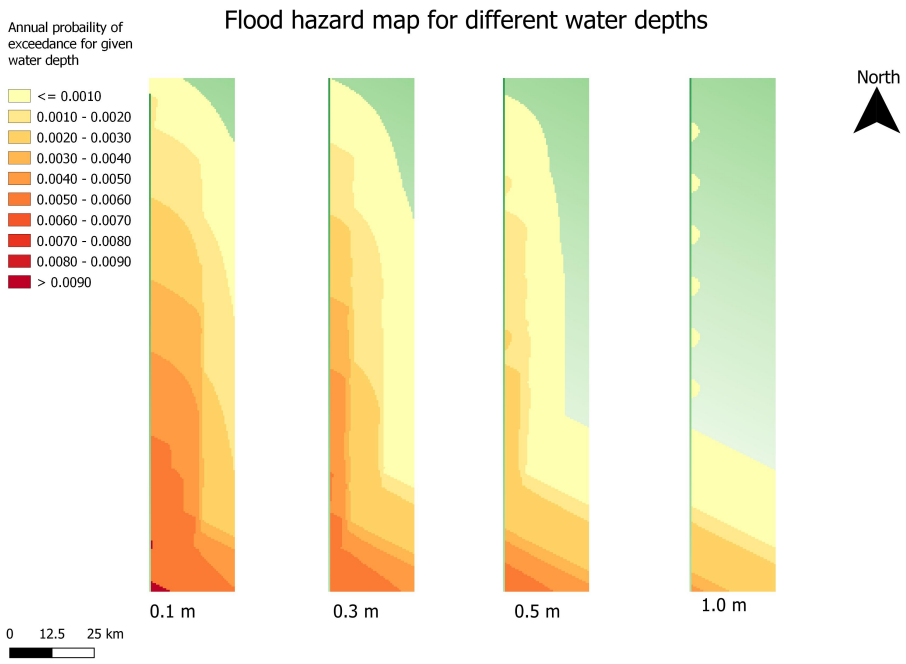

Figure 4.8: Wet feet map for fragility curve 3

In Figure 4.9 the water level plots are presented over the north-south cross sections. There are two differences visible between the different fragility curves. The first is the increased water levels at the southern edge of the floodplain. For the first fragility curve these remain relatively low at around $1.2m$. The plot is only visible for the second half of the river reach. For the rest of the reach the annual probability of exceedance is to small. For the second and third fragility curves, the plot is visible for a far larger part of the river reach. Only the first sixth of the reach has no of a minimal water level that is exceeded at a 1000y return period. The water level at the southern edge has increased only a small amount compared to the second fragility curve.

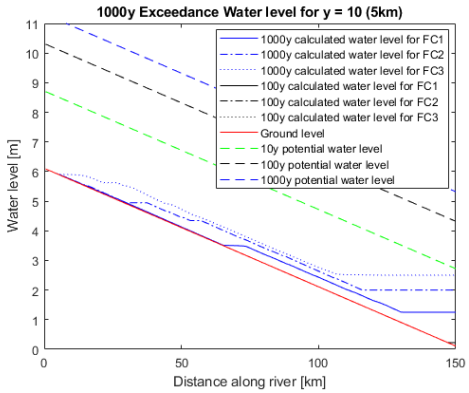

(a) Different fragility curves at Y = 10

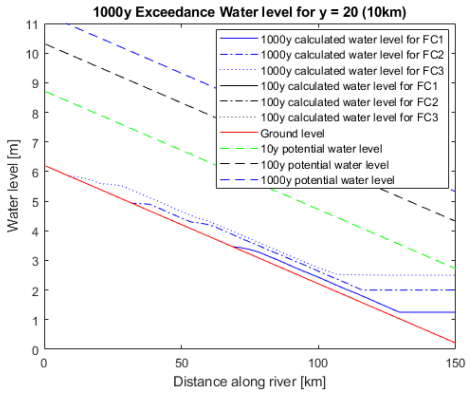

(b) Different fragility curves at Y = 20

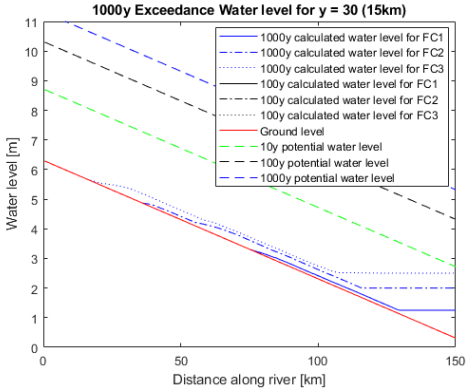

(c) Different fragility curves at Y = 30

Figure 4.9: Plots of the 100 year and 1000 year return period exceedance water levels along the north-south cross sections for 5km, 10km and 15km away from the river. For all three fragility curves.

In Figure 4.10 the plots of the water levels over the west-east cross section are shown. As also was seen in the previous plots the water level at the $X = 300$ has increased strongly between the first and second fragility curve. The difference between the second and third fragility curve is very minor. The water levels for the first fragility curve at $X = 240$ are very low and do not reach the full width of the floodplain. At $X = 150$ there is no plot visible at all. These values correspond to the plot in sub-figure 4.9a.

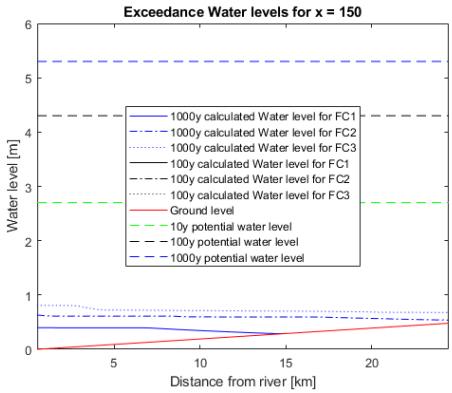

(a) Different fragility curves at X = 150

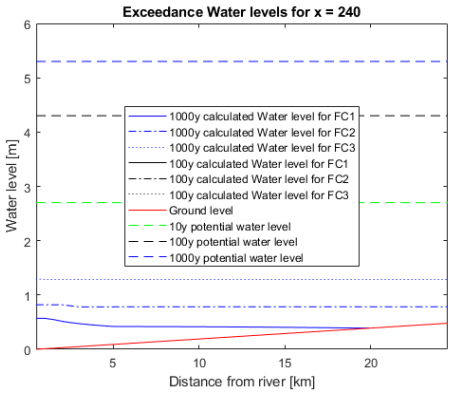

(b) Different fragility curves at X = 240

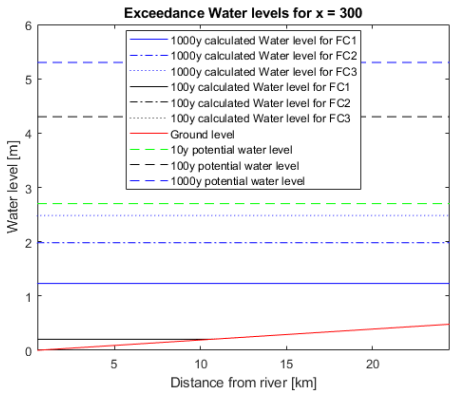

(c) Different fragility curves at X = 300

Figure 4.10: Plots of 100 year and 1000 year return period exceedance water levels for the different fragility curves, along the west-east cross sections at 75km, 120km and 150km downstream from the begin point.

The maps of the 1000 year return period inundation depth are presented in Figure 4.11. The inundation extent increases as the breaching probabilities become more unfavorable. The same applies to the inundation depths at the stream downward end of the floodplain.

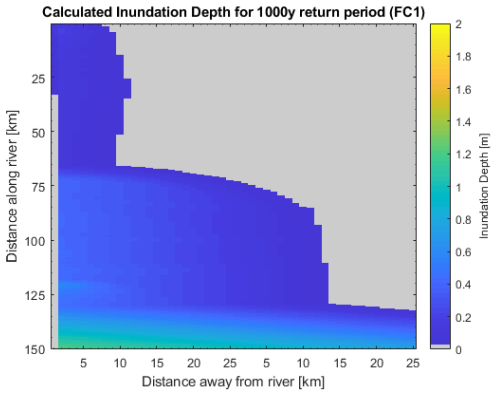

(a) 1000y return period exceedance depth for FC1

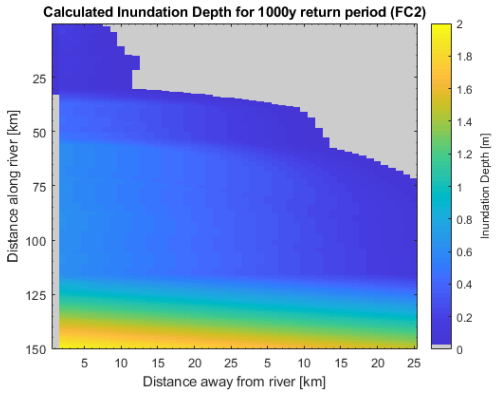

(b) 1000y return period exceedance depth for FC2

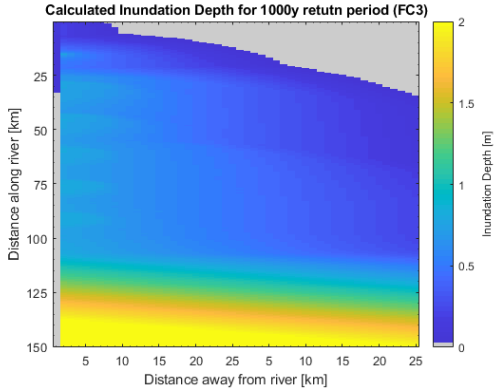

(c) 1000y return period exceedance depth for FC3

Figure 4.11: 1000y return period exceedance depths for the increased breaching depth setups.

In Figure 4.12 the scatter plots of the BRR and BFR are presented for the different fragility curves. The 10-year return period plots are all the same as well as the 100-year return period plots for the first and second fragility curve. For the 100-year return period the inclusion of multiple breaches has resulted in larger values of the breaching volume. The effects for the 1000-year return period plots are less noticeable. The breaching volume has increased compared to the first fragility curve but the three simultaneous breaches have had less of an impact on the breaching volume. The exact values of the breaching volume, BRR and BFR can be found in appendix A.

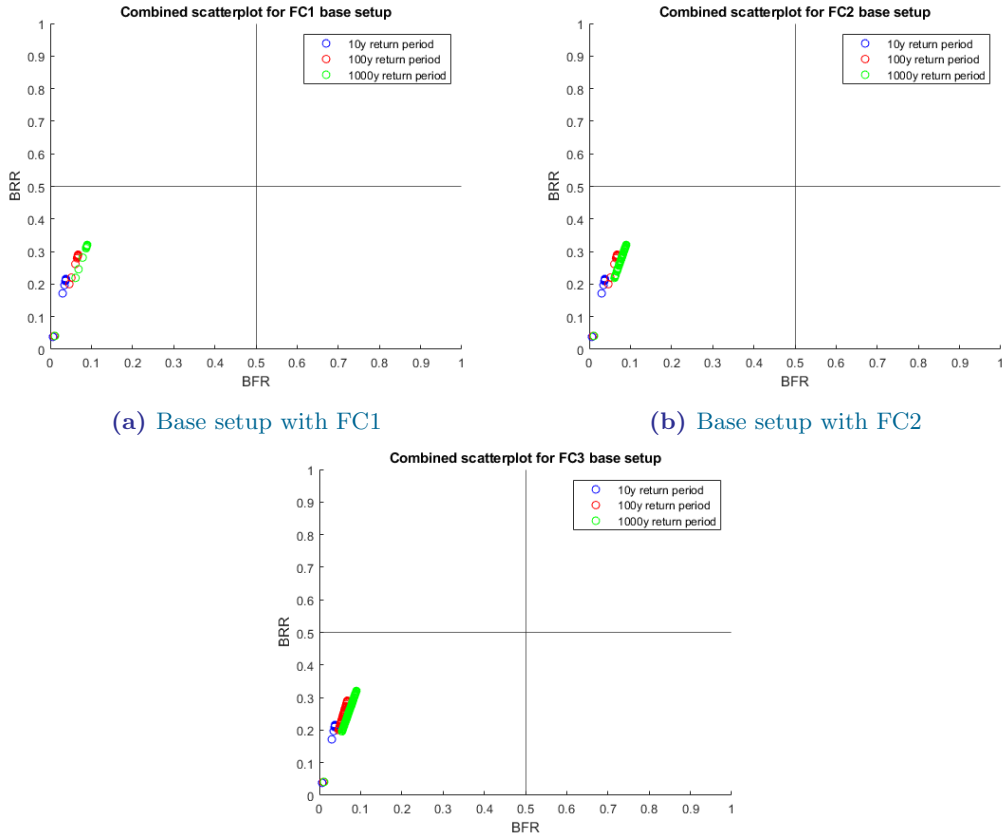

(a) Base setup with FC1

(b) Base setup with FC2

(c) Base setup with FC3

Figure 4.12: Scatter plots of the BFR and BRR ratios for the Base case for all three fragility curves.

4.3.2 Influence of breach depth

The first parameter studied is the depth (Z_b) of the breach that is formed. In the base setup the lowest point of the breach was assumed to be at the ground level of the winterbed and floodplain. That is to say $Z_b = 0$. In a real life scenario it is not unreasonable to assume that the erosion will lead to increased depth. To study this influence the depth has been lowered with $5m$ for the first setup. Thereafter the depth is increased with another $5m$ to a level of $10m$ below the winterbed. By taking big steps the influence will be more clearly visible if any influence is found. If nothing is seen in the results, it is more likely that their is no influence than that the variation was to minor to have any influence.

As an initial hypothesis, it is expected that the increased depth will lead to a larger flow initially but that over the whole time frame the discharge will end up very similar. The most important factor for the flow velocity in the breach is the head difference between the inside and the outside of the embankments.

As can be seen in figure B.1 the total area that is covered by the different water levels is very similar. Some differences in the probabilities are visible however. If the leftmost maps ($0.1m$ exceedance) of the three figures are compared it is clearly visible that in Sub-figures B.1b or 4.13 the higher exceedance probabilities occur further north than in Sub-figure B.1a. Especially further away of the river. In B.1c

the effect far away from the river is reduced. For the third map ($0.5\,m$ exceedance) the covered area is increased slightly with a increase in breach depth. In the final map ($1.0\,m$ exceedance) the areas around the stream upwards breach location are larger. The borders of the higher probabilities in the area have also moved north.

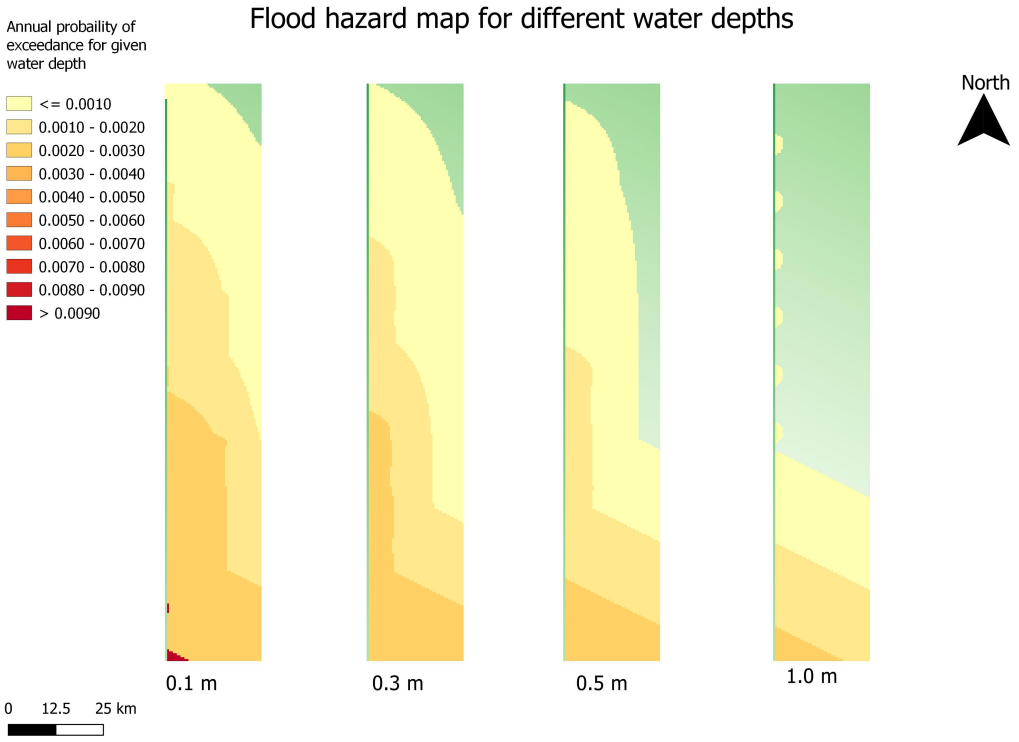

Figure 4.13: $Z_b = -5m$ setup wet feet map.

Based on the final map it can be seen that a increased breach depth leads to an larger initial discharge. This would explain the larger area around the breach locations. The borders between the third and fourth color provide some insight in the shape of the inundations caused by stream upwards breaches. This combined with the increased probabilities for the $1.0m$ exceedance implies that a larger amount of water enters the floodplain at the start of the breach. Supporting the hypothesis of a larger initial discharge. The total areas for the inundation imply that the total discharged volume is similar to that of the base setup. The $10m$ increase in depth seem to have a reduced the influence of the wet feet map compared to the $5m$ increase. This seems to imply that there is a also a negative influence on the discharge from an increased breaching depth.

The plots for the west-east cross-sections are presented in Figure B.2. The $10\,m$ increase does not result in higher water levels than the $5m$ increase. This mirrors the results seen in the wet feet maps of B.1c.

The maps of the 1000 year return period inundation depth are presented in Figure 4.14. The inundation extent and inundation depth ant the stream downward side of the floodplain have increased for a deeper breach. Additional depth after this point seems to reduce the increase compared to the base setup.

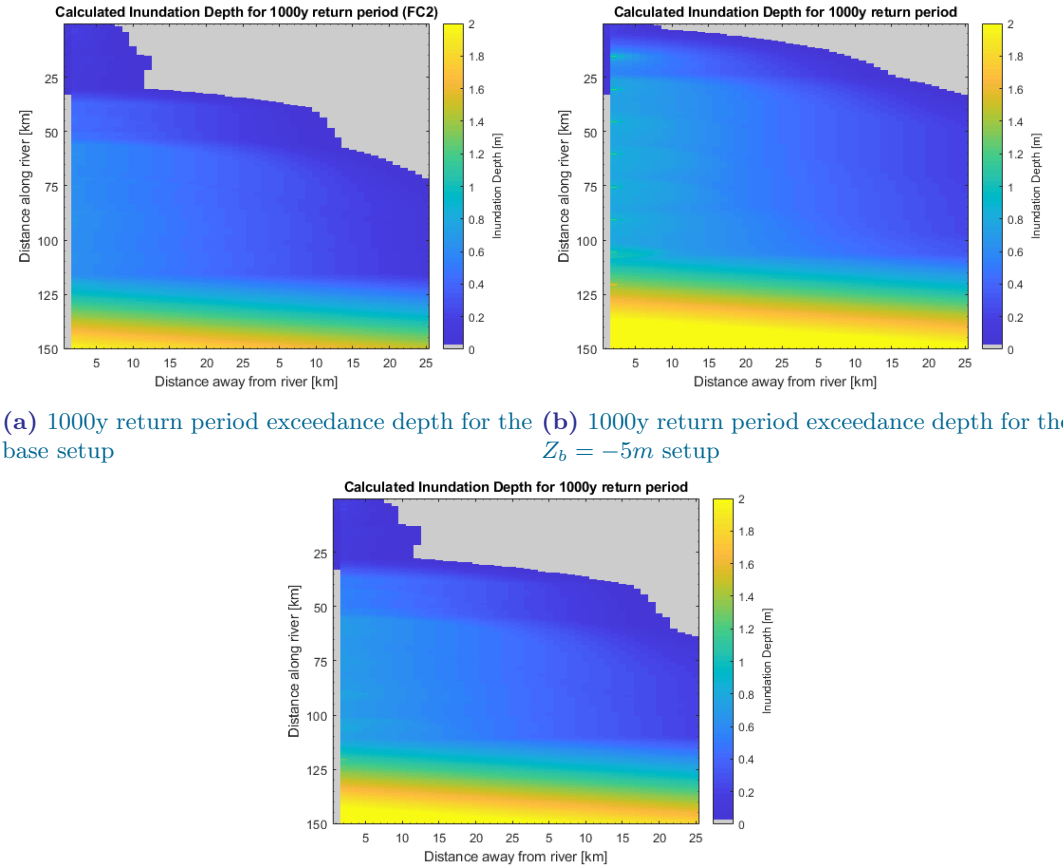

(a) 1000y return period exceedance depth for the base setup

(b) 1000y return period exceedance depth for the $Z_b = -5m$ setup

(c) 1000y return period exceedance depth for the $Z_b = -10m$ setup

Figure 4.14: 1000y return period exceedance depths for the base setup.

The water levels as seen along the north-south cross sections are shown in Figure B.3. As seen in the other selection of plots in Figure B.2 the water level has risen slightly and the additional depth of the $10\,m$ setup does not seen to result in higher water levels.

The scatter plots of the BRR and BFR in Figure B.4 confirm some of the things seen in the previous sections. The BRR is increased with additional breaching depth which means more of the available water in the river could enter the floodplain. This has lead to a equivalent change in the BFR. Again the difference between the $5m$ and the $10m$ increased depth are minimal. The 2 simultaneous breaches for the $1000y$ return period do also fall in line with the single breach scenarios. The $1000y$ return period scatter plots are included in Figure 4.15.

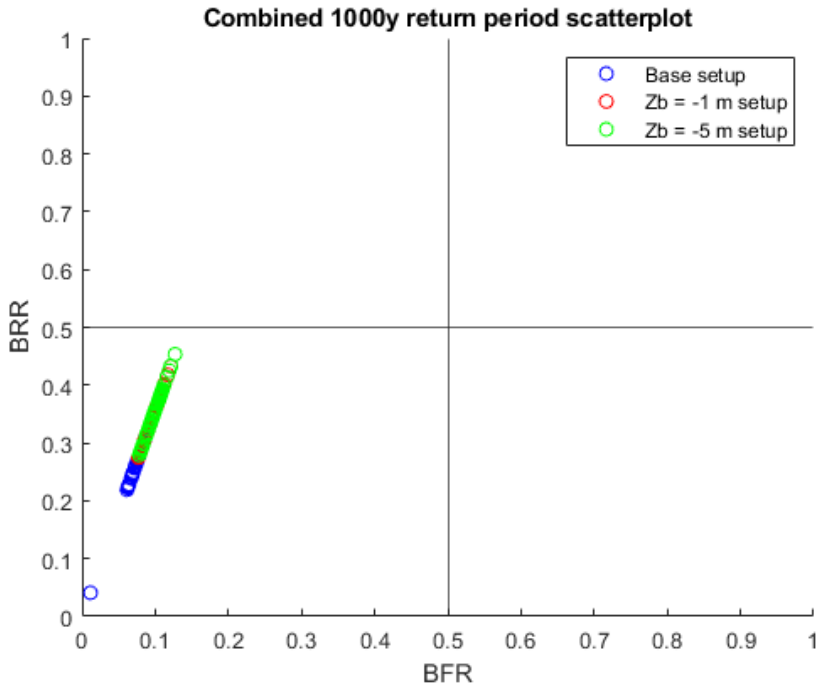

Figure 4.15: Scatter plots of the 1000y return period for the base setup and the increased breach depth setup.

4.3.3 Influence of floodplain width

The second variation studied is the influence of the width of the floodplain. That is to say the distance between the river levee and a undefined obstacle. By reducing this width the surface area of the floodplain will also decrease and due to that the storage volume. The width of the floodplain was first reduced to 8 km with a additional 500 m for the river itself. The 2D grid is now 302 by 19 (Including the zero value cells along the border). The second setup tested has an even smaller width of 2km excluding the river itself. The total size of the 2D grid is now 302 by 7.

The initial hypothesis is that reducing the storage volume will lead to an increase of the BFR. Simultaneously the BRR will decrease as higher water levels outside of the levee will reduce the discharge in the breaches. The water levels in the levee will be higher.

The influence of the reduced width is very visible in the maps presented in Figure B.5. Almost the whole floodplain is flooded for the lower water depths. Only for the 0.5 m and 1.0 m in B.5b there is still uncovered area in the flood plain. The probabilities of these depths occurring have increased as the borders between the different colors have moved northward. The probabilities near the southern edge are larger than in the base setup. The 2 km setup in B.5c shows similar probabilities as in the 8 km setup.

The plots along the west-east cross sections are presented in Figure B.6. A clear increase of the water levels can be seen. In is of notice that only in B.6i or 4.16b the assumed water level is reached for a 1000-year return period. In B.6f or 4.16a the water level remains well below the assumed 100y return period level.

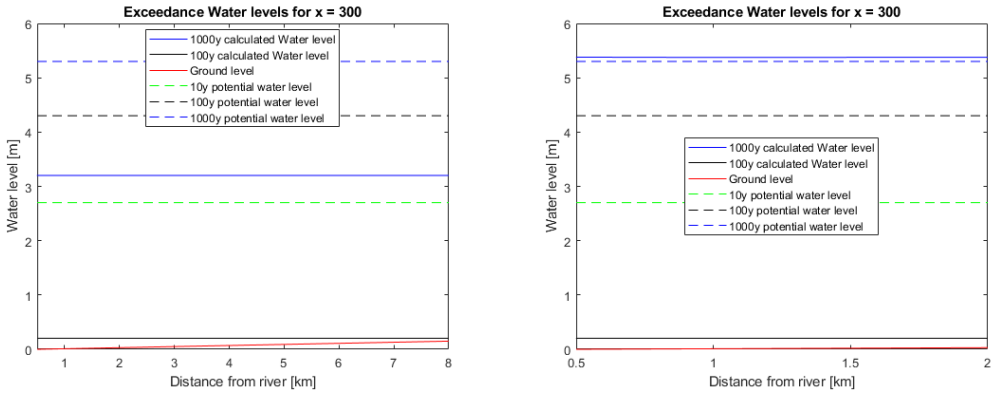

(a) 8km floodplain width setup at X = 300 **(b)** 2km floodplain width setup at X = 300

Figure 4.16: 100 year and 1000 year return period exceedance water levels at X = 300 for the reduced floodplain width.

The water levels in B.6h and B.6g remain far below the assumed levels even at a very small flood plain. It seems that the length has a strong impact on the height of the water levels in the flood plain. A more clear insight of this can be given based on Figure B.7 in the next section.

Due to the small width of the floodplain the regular set of cross section plots could not be made. Therefore only the Y10 version of the base setup can be compared to the plots of the variations. For the $2\,km$ setup a plot at Y = 3 has been made or $10\,km$ away of the river. These plots are presented in Figure B.7.

While the water levels have increased, a key difference can be seen in the plots compared to the assumed water levels. The shape of the plots are very different. This was visible in previous maps but is most clear in B.7c or 4.17. The assumption that a water level in the river can be continued on over the floodplain seems to not hold for floodplains that have a slope directed parallel to the river. As all floodplains that are sufficiently large will have at least a small slope. It seems that this assumption can only be used for relatively small contained floodplains.

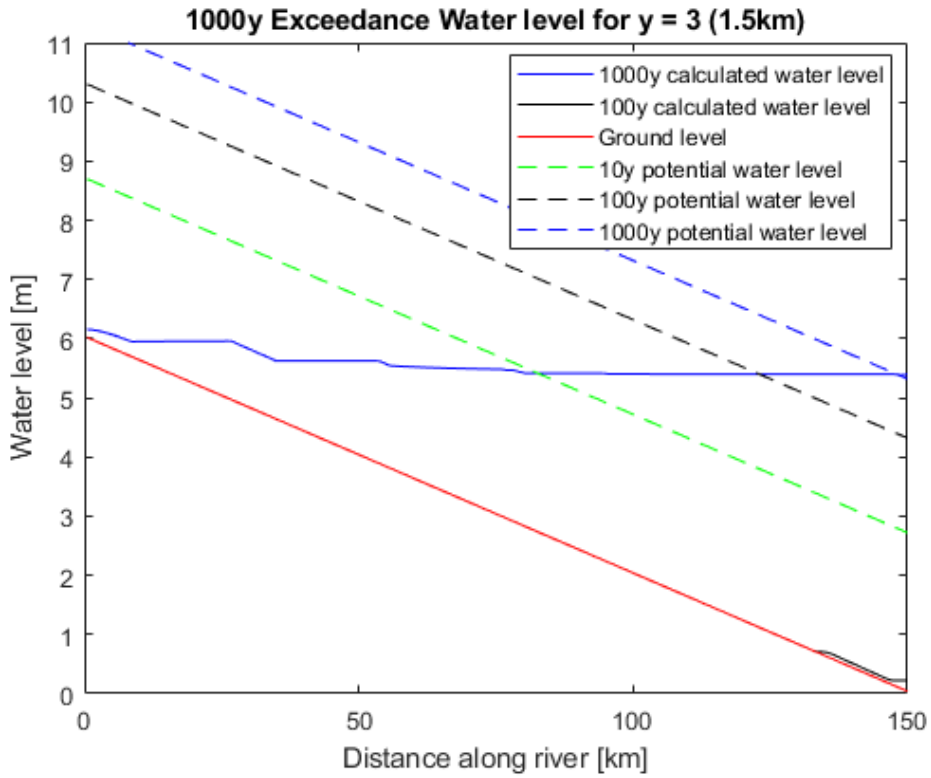

Figure 4.17: 1000 year and 100 year return period exceedance water levels for the 2km floodplain width setup

The maps of the 1000 year return period inundation depth are presented in Figure 4.18. The 8 km width setup looks similar to the base setup map. The inundation depths have increase at the stream downward side of the floodplain. In the $2\,km$ width the difference to the base setup is more pronounced. The complete floodplain is inundated and the depth have increased significantly.

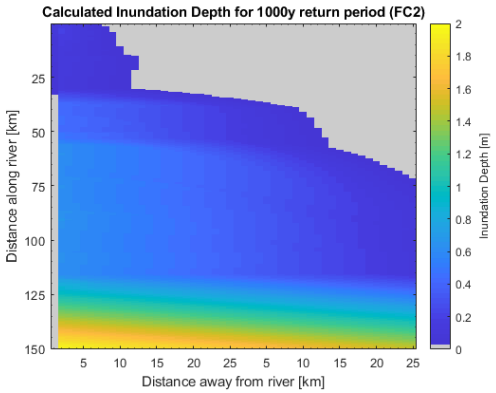

(a) 1000y return period exceedance depth for the base setup

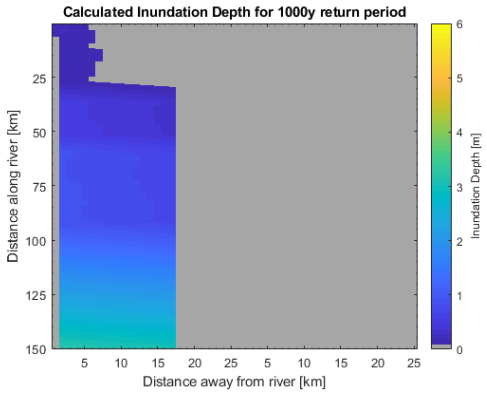

(b) 1000y return period exceedance depth for the 8 km width setup

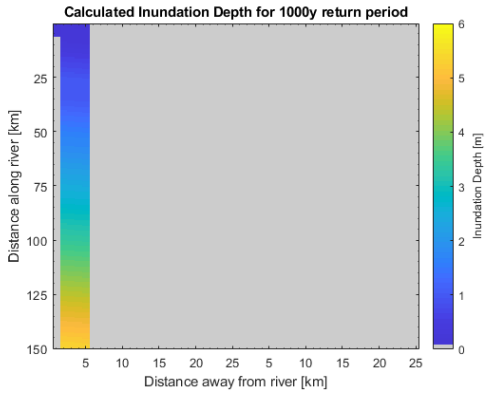

(c) 1000y return period exceedance depth for the 2 km width setup

Figure 4.18: 1000y return period exceedance depths for reduced width setups.

The scatter plots of the BRR and BFR are presented in figure B.8. The BRR is decreased by the limited width of the flood plain. This can be explained by the reduction of discharge caused by the increased water levels on the outside of the levees. The BFR has increased substantially by reducing the width of the floodplain. It is unsurprising that the highest values are found for breaches which are far upstream. Here the water level remains lower than at the downstream breach locations.

As the reduction of the floodplain width decreases both the discharge volume and the storage volume the change of the angle of the points in the scatter plot can show which effect is more dominant. As the angle decreases the reduction in storage volume is dominant. This can be seen best for the 1000-year return period. These scatter plots are presented in Figure 4.19.

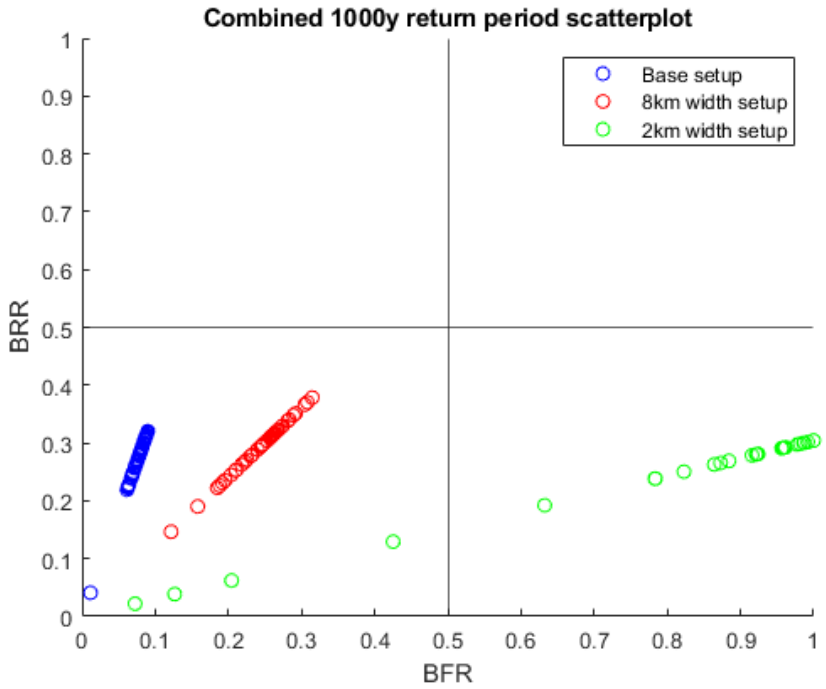

Figure 4.19: Scatter plots of the 1000y return period for the base setup and the reduced floodplain width setups.

It seems as if the BFR reaches past the soft limit of 1.0. By extending the plot the higher values become visible. As shown in Figure 4.20. For a significant amount of cases more water enters the floodplain than was assumed based on the water level inside of the levees.

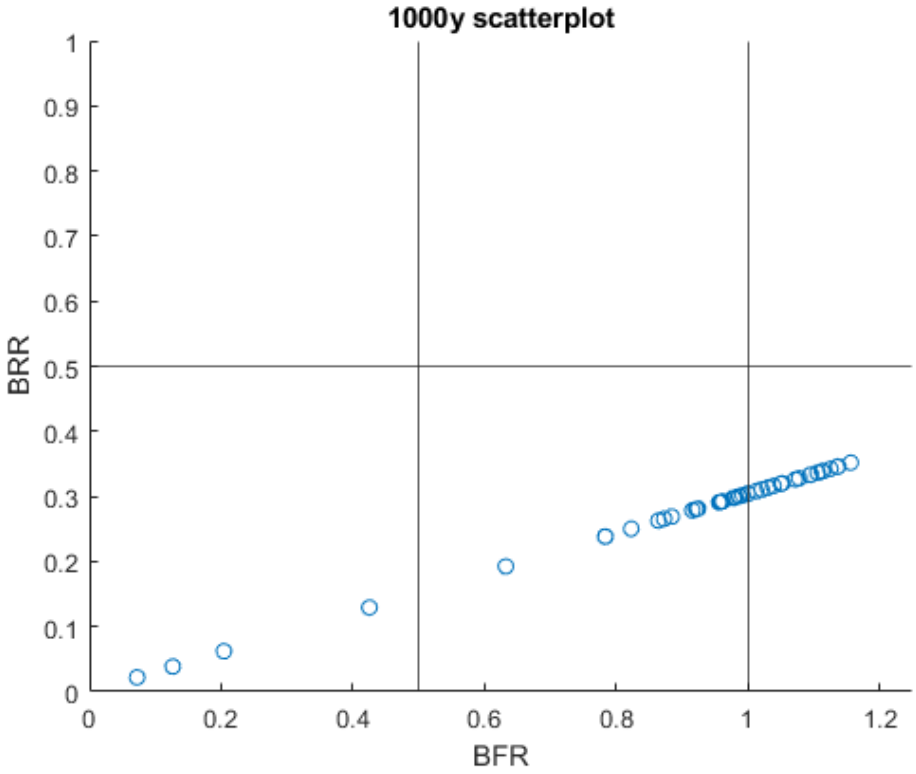

Figure 4.20: 2km floodplain width setup for 1000y return period with extension.

4.3.4 Influence of floodplain depth

For these variation the ground level of the cells in the floodplain were reduced. For the first setup the reduction was $1\,m$. As the water depth remains below the $1\,m$ level for most of the floodplain it is reasonable to start with a small increase in depth. Due to settlement of the surrounding area these kind of height differences are commonly found. The second setup had a reduction of $5\,m$. This large step was to study of a larger difference would lead to a significantly larger impact. And whether the influence is limited by the previously found water depths or if a larger depth increases this influence. The depth of the breach was left unchanged at the winterbed level.

The initial hypothesis is that the reduce height will lead to a increase of the breaching volume. Simultaneously the storage volume will increase strongly. In summary the BRR will increase while the BFR will be reduced. The increase of storage volume will be significantly larger than the increase of breaching volume.

The different maps for the wet feet chance are presented in Figure B.9. The total areas that are inundated with the specified water depth do not change significantly. This could mean that the discharge volume does not change as much as initially expected. The overall probabilities increase along the second half of the floodplain near the levees. This can be seen in Figure 4.21. The change does not affect the complete width of the floodplain. The difference between B.9b and B.9c is very small. It seems that the extra depth after the first meter has very minor influence on the probability of exceeding certain water depths.

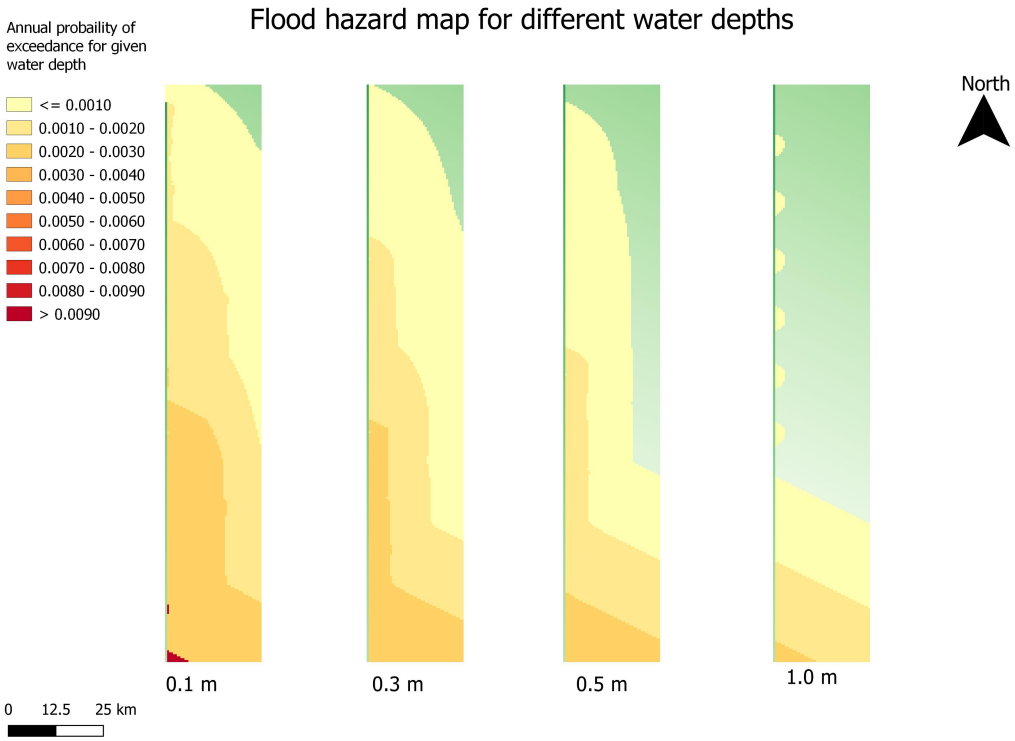

Figure 4.21: $Z_f = -5$ setup wet feet map.

The plots over the west-east cross sections are presented in Figure B.10. The influence on the 0.1 % exceedance water levels in minimal at $X = 150$ (B.10adg). In plots at $X = 240$ and $X = 300$ a small increase is seen compared to the base setup. The difference between the $1\,m$ reduction and the $5\,m$ reduction is minimal. As also seen in the wet feet maps of B.9, the additional depth has minimal impact.

The plots over the north-south cross sections are presented in Figure B.11. These plots are very similar to the plots of the base setup. The only difference is that there is a 0.1 % exceedance level found for further upstream along the river. This can be seen in Figure 4.22.

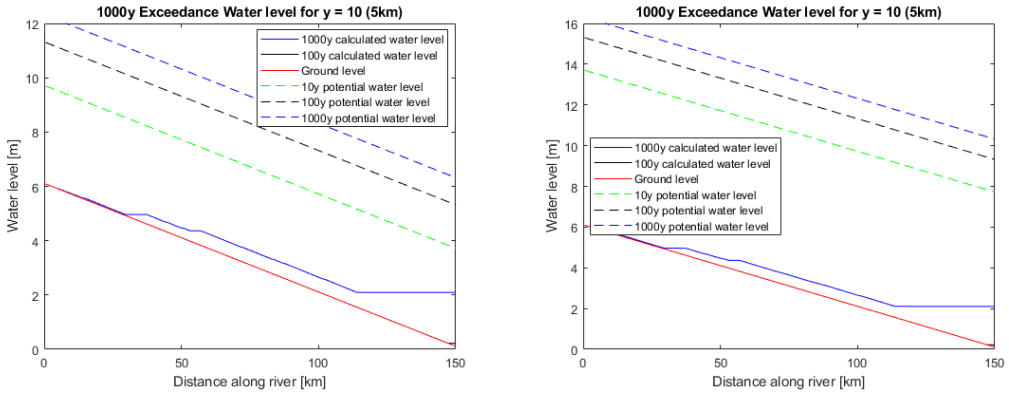

(a) $Z_f = -1$ setup at Y = 10 **(b)** $Z_f = -5$ setup at Y = 10

Figure 4.22: Plots of 100 year and 1000 year return period exceedance water levels along the north-south cross sections at 5km from the river for the reduced floodplain width setups.

The maps of the 1000 year return period inundation depth are presented in Figure 4.23. There is little influence on the inundation depth or extent.

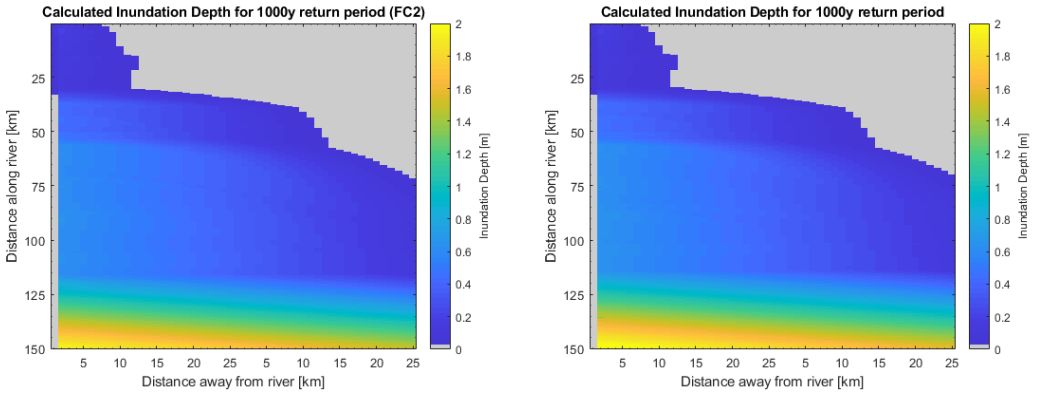

(a) 1000y return period exceedance depth for the base setup

(b) 1000y return period exceedance depth for the $Z_f = -1$ setup

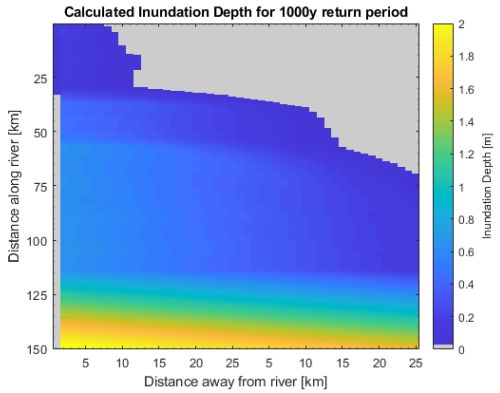

(c) 1000y return period exceedance depth for the $Z_f = -5$ setup

Figure 4.23: 1000y return period exceedance depths for increased floodplain depth setups.

4.3.5 Influence of split floodplains

In this variation the influence of wall-like obstacle in the floodplain is studied. This can be a road, railway or even an other channel like the Dunav-Tisa-Dunav channel. The location of the wall was set at row 165 of the 2D grid. This is close to the halfway point of the river. But at this point breach locations 5 is found. The wall was therefore moved stream downward by $7.5\,km$. This is halfway between breach location 5 and 6. Initially the height of the cells in row 165 was increased by $1\,m$. This height represents a road through the flood plain. In the second setup the height of the cells was increased by $5\,m$. This height represents the levees along a channel through the floodplain. The direct influence of the channel on the 1D model of the river is not included.

The initial hypothesis is that the $1\,m$ wall will lead to some redistribution of the water levels. But this will not lead to a large increase of a water levels over $1\,m$ just before the wall. The water will flow over the wall into the southern half of the floodplain. The $5\,m$ wall will most block the water from reaching the southern half of the flood plain and will lead to two areas where the water will accumulate.

The wet feet maps are presented in Figures B.13 and 4.24. The split in the floodplain caused by

the raise of height in that row is clearly visible. The chance in inundation area between the base setup and the $1\,m$ wall is relatively minor. Only at the northeastern corner of the lower part of the floodplain the area is reduced. A larger effect is the increased probabilities of higher water depth just upstream of the obstacle.

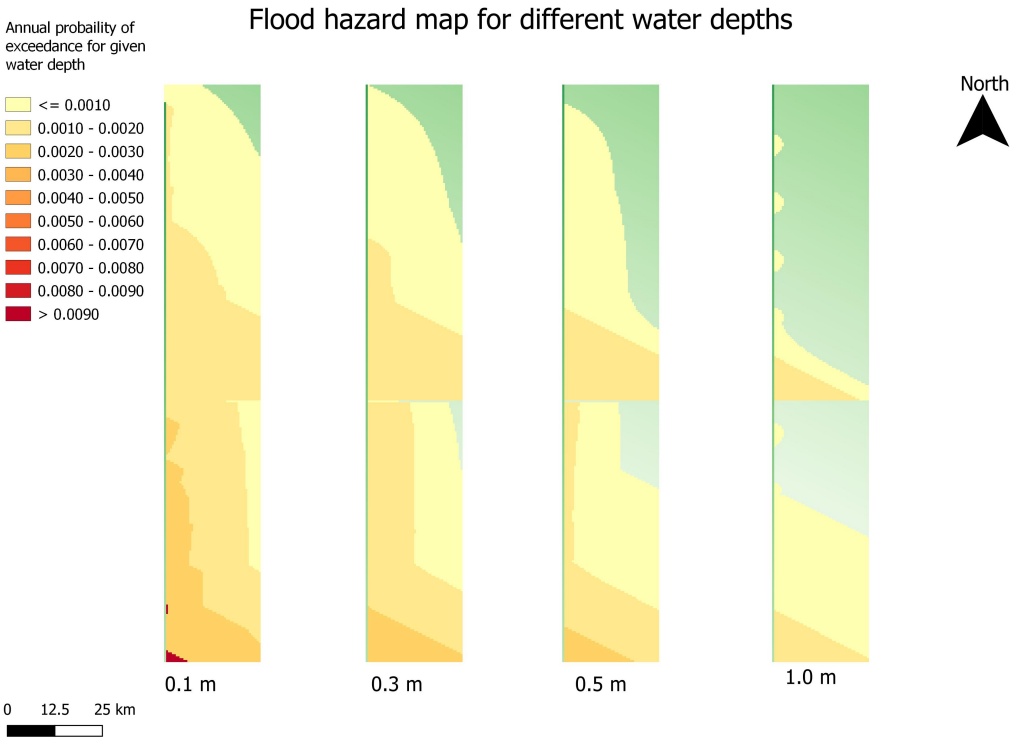

(a) $h_w = 1m$ setup wet feet map.

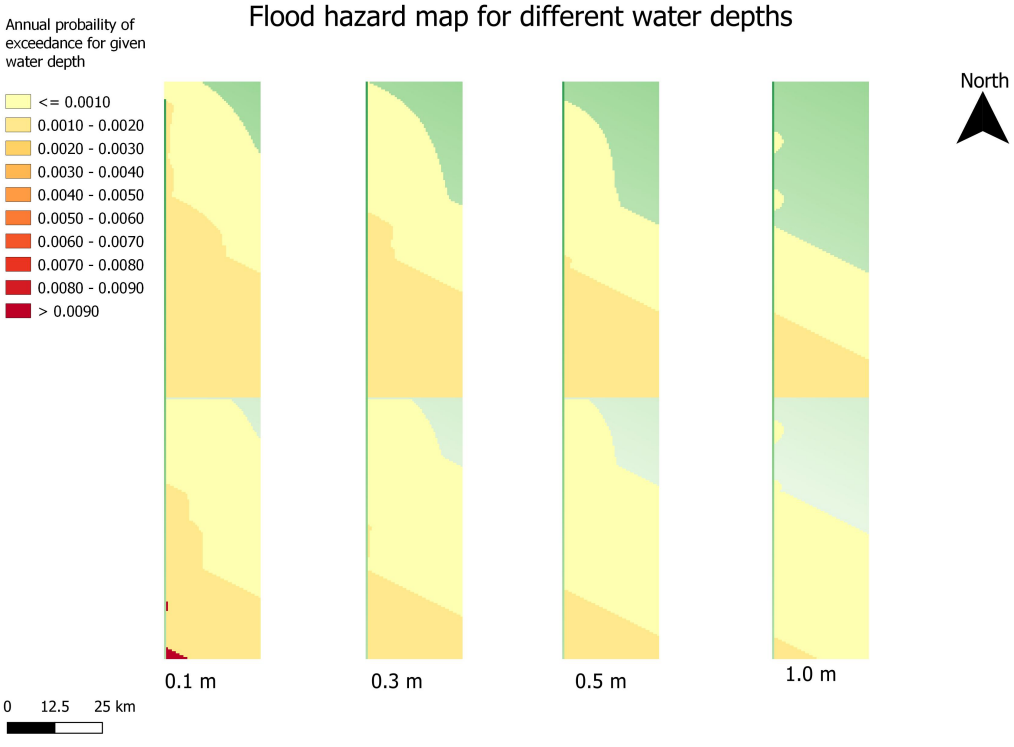

(b) $h_w = 5m$ setup wet feet map.

Figure 4.24: Wet feet maps for the $1m$ and $5m$ wall in the floodplain.

The impact of the $5m$ obstacle is significantly stronger. The probabilities at the southern edge of the floodplain have been reduced while the probabilities upstream of the obstacle have remain the same.

The plots over the west-east cross sections are presented in Figure B.14. The influence of the obstacles can be seen as a redistribution of the inundation volume. Just before the obstacle at $X = 164$ the water levels are increased while at $X = 240$ the water levels have dropped significantly. At $X = 150$ the increase is also visible. At the southern edge the water level has decreased slightly for the $1\,m$ obstacle but the effect of the $5\,m$ obstacle is far larger. The influence of the wall on the peak water level in both parts of the floodplain can be seen in figure 4.25.

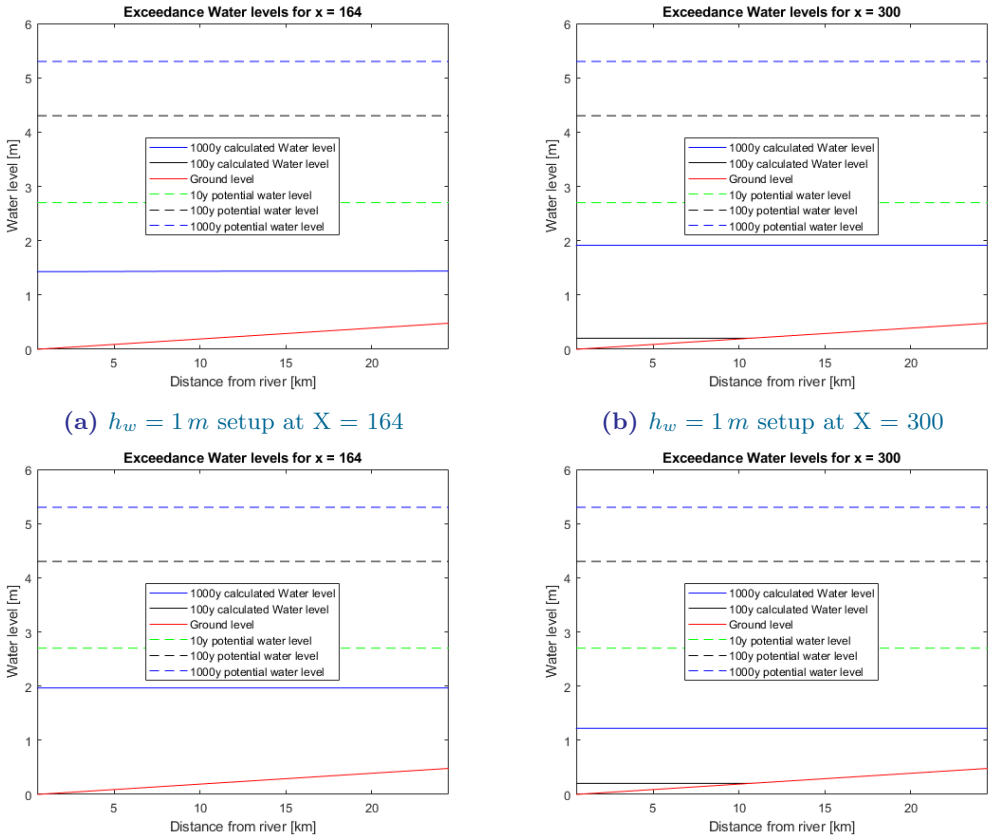

(a) $h_w = 1\,m$ setup at X = 164

(b) $h_w = 1\,m$ setup at X = 300

(c) $h_w = 5\,m$ setup at X = 240

(d) $h_w = 5\,m$ setup at X = 300

Figure 4.25: Plots of 100 year and 1000 year return period exceedance water levels along the west-east cross section directly in front of the wall and the southern edge of the floodplain.

The plots over the north-south cross sections are presented in Figure B.15. The influence of the obstacles is clearly visible. The water level just before the obstacle is higher than the obstacle in B.15def. The higher $5\,m$ obstacle completely blocks any water from moving between the 2 parts of the floodplain.

The maps of the 1000 year return period inundation depth are presented in Figure 4.26.

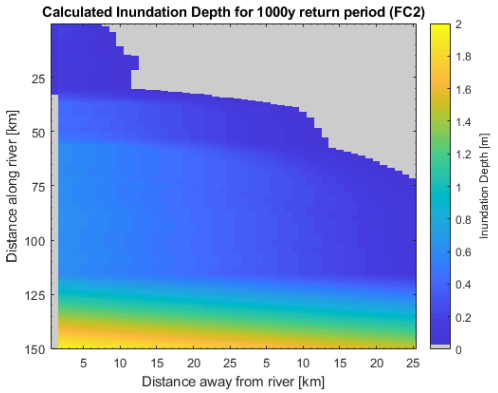

(a) 1000-year return period exceedance depth for the base setup

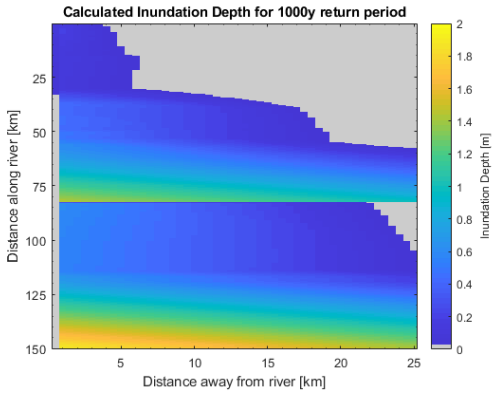

(b) 1000-year return period exceedance depth for the $h_w = 1\,m$ setup

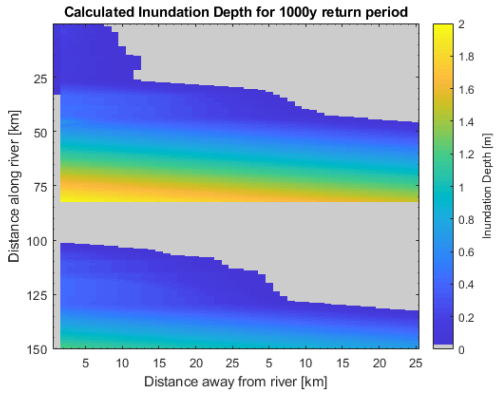

(c) 1000-year return period exceedance depth for the $h_w = 5\,m$ setup

Figure 4.26: 1000-year return period exceedance depths for split floodplain setups.

The scatter plots of the BRR and BFR are presented in Figure B.16. These are calculated based on the storage volume of the whole floodplain. Determining the BFR per breach location is complicated by overflow over the wall and combinations that have breaches in both parts. Very little difference can be seen between the different setups. This can be explained by the fact that the stream upward breaches are not affected by the increased water levels down stream.

4.3.6 Influence of breaching start time

In this final variation the influence of changing the start time of the breach is studied. In the base setup the breach starts halfway trough the run time. When the discharge peak enters the river. This is at $T_b = 26 days$. For these setups the start time is pulled forward by 5 days and 10 days. This means the breach will occur at a lower water level. This can happen in real world scenarios as well. The breach does not wait for the largest load to appear to fail.

As an initial hypothesis, the earlier breach will lead to a reduced discharge through the breach. This means that the breach will remain smaller. The discharge will be present for a larger time. The total discharge volume should therefore remain similar to the base setup.

The wet feet maps can be found in figure B.17. The total inundation area remains very similar to the base setup. The probabilities have increased near the levee comparable to the floodplain depth setup.

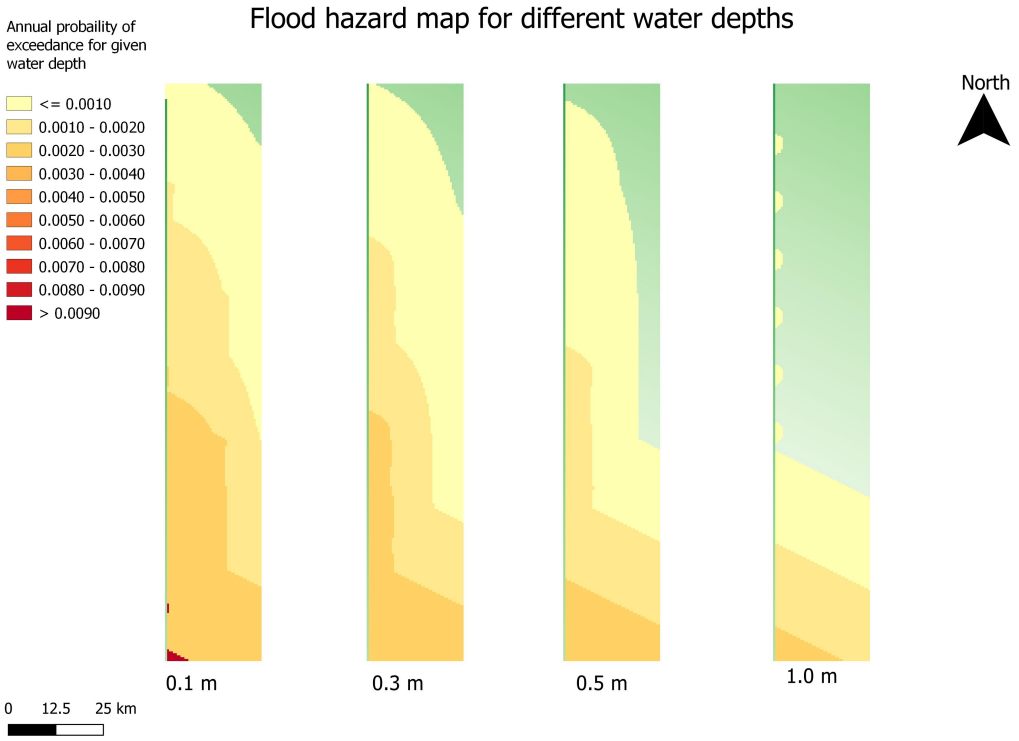

Figure 4.27: $T_b = 21$ setup wet feet map.

The 0.1% exceedance levels in the west-east cross sections are presented in Figure B.18. The water levels have increased by around 10 % implying an equal increase in breach volume. The difference between the two setups is minimal.

The 0.1 % exceedance levels in the north-south cross sections are presented in Figure B.19. Water levels have increased slightly but more noticeable there is a presence further upstream. This additional part of the plot is very minor however. Both of these sets of plots are very similar to the floodplain depth setup.

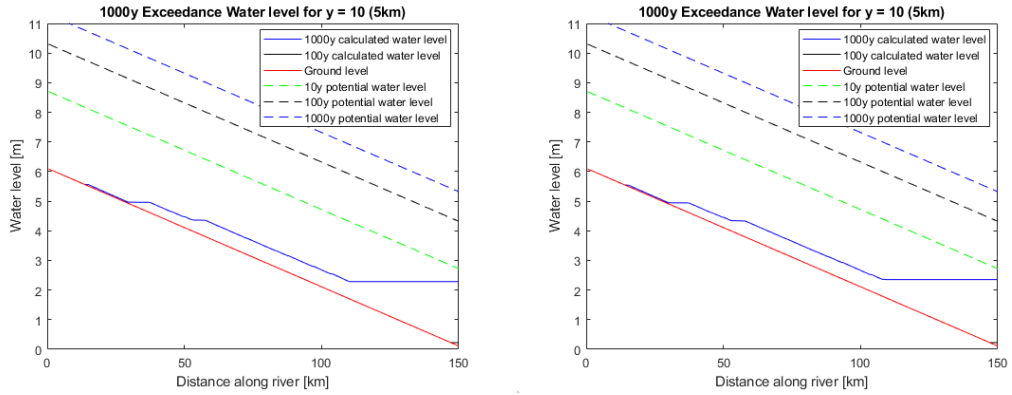

(a) $T_b = 21$ setup at Y = 10

(b) $T_b = 16$ setup at Y = 10

Figure 4.28: Plots of 100 year and 1000 year return period exceedance water levels along the north-south cross sections at 5km from the river for the earlier breach start setups.

The maps of the 1000 year return period inundation depth are presented in Figure 4.29. A slight increase in inundation depths is visible at the stream downward end of the floodplain. The inundation caused by the stream upward breach locations is reduced which leads to a slight reduction in inundation extent. Also the slight amount of overflow is prevented at the stream upwards side of the floodplain.

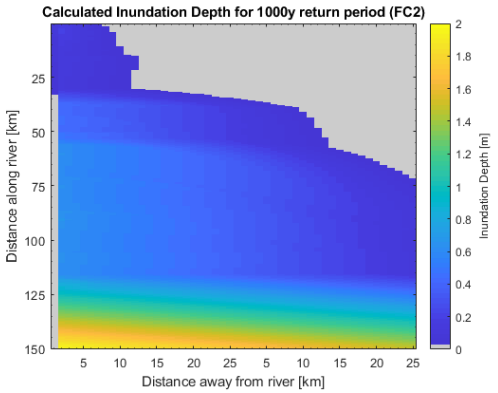

(a) 1000-year return period exceedance depth for the base setup

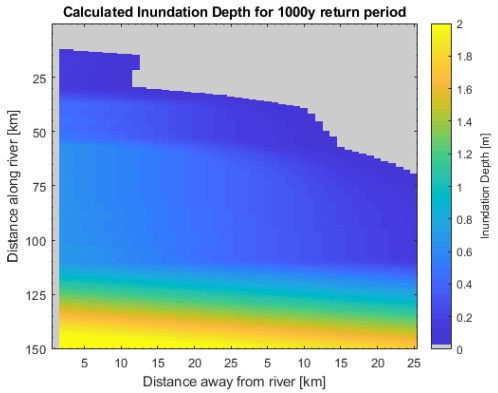

(b) 1000-year return period exceedance depth for the $T_b = 21$ setup

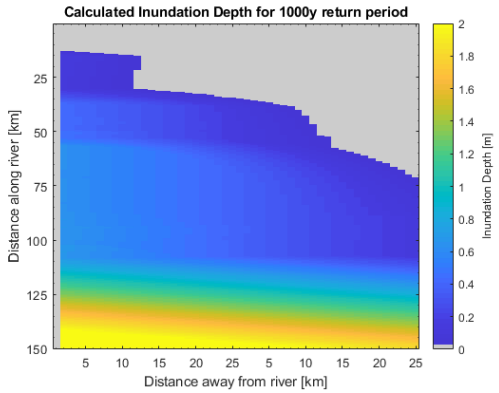

(c) 1000y return period exceedance depth for the $T_b = 16$ setup

Figure 4.29: 1000-year return period exceedance depths for earlier breach start setups.

The scatter plots of the BRR and the BFR are found in Figure B.20. The BRR increases to around 0.4 for both setup with the $T_b = 16$ setup being slightly larger. The BFR increases also slightly. This is the opposite of the BFR development of the floodplain depth setups. It can be seen that total discharge volume has increased based on the ratios.

4.4 Discussion

The results presented in this chapter are based on an idealized model of the Tisa river. In this model, the occurrence and consequences of levee breaching were explicitly included. Based on this model the probabilities of certain inundation depths have been calculated throughout the entire area protected with the embankments. These were presented as inundation probability maps. The water levels in the floodplain for certain annual exceedance probabilities have also been determined. These were plotted on a selection of different cross sections. There are many input parameters involved with the running of this model. These are related to the forcing of the model, the geometry of the river and the floodplain and to the forming of the breaches.

The variations were made by changing a single parameter in the model. The parameters were kept within reasonable values for a real world scenario. The levee along the Tisa river is designed for a $100y$ return period event. The resulting inundation probabilities remain significantly smaller than the 0.01 annual probability for most of the floodplain. Only in the lowest point, this annual probability is reached, as this is where the water naturally flows towards. The 0.001 annual probability is reached for a large part of the floodplain. The variations change how much of the area reaches this return period. The water levels found for the exceedance probability plots mirror these results. Only by limiting the width of the floodplain to an almost unreasonable $2km$ the water level reaches the crest height of the levee. And this only occurs at the lowest point. In all other setups the water level remain low compared to the water levels within the levees.

In Figure 4.30 the different scatter plots of the BRR and BFR were combined into a single plot. The 1000yr return period plots have been used as these provide more data points since the cases with two simultaneous breaches are included. The limited water levels can be explained by the scatter plot. Even though the BRR increases for several of the variations the total amount of water that can be discharged remains far smaller than the storage volume. A line was added for each of the setups. By extrapolating this line, the effect of a larger BRR value can be estimated. If the BRR would reach a value of 1, this implies that all of the water that flows above the winterbed would enter the floodplain. The corresponding BFR values would still be far smaller than 1. This means that the river volume is too small compared to the storage volume. It is also unreasonable to assume that a breach would allow so much of the discharge to exit the river channel. And only if the storage volume is relatively small, it is possible to reach a high BFR value. This only occurs in the reduced floodplain width setups.

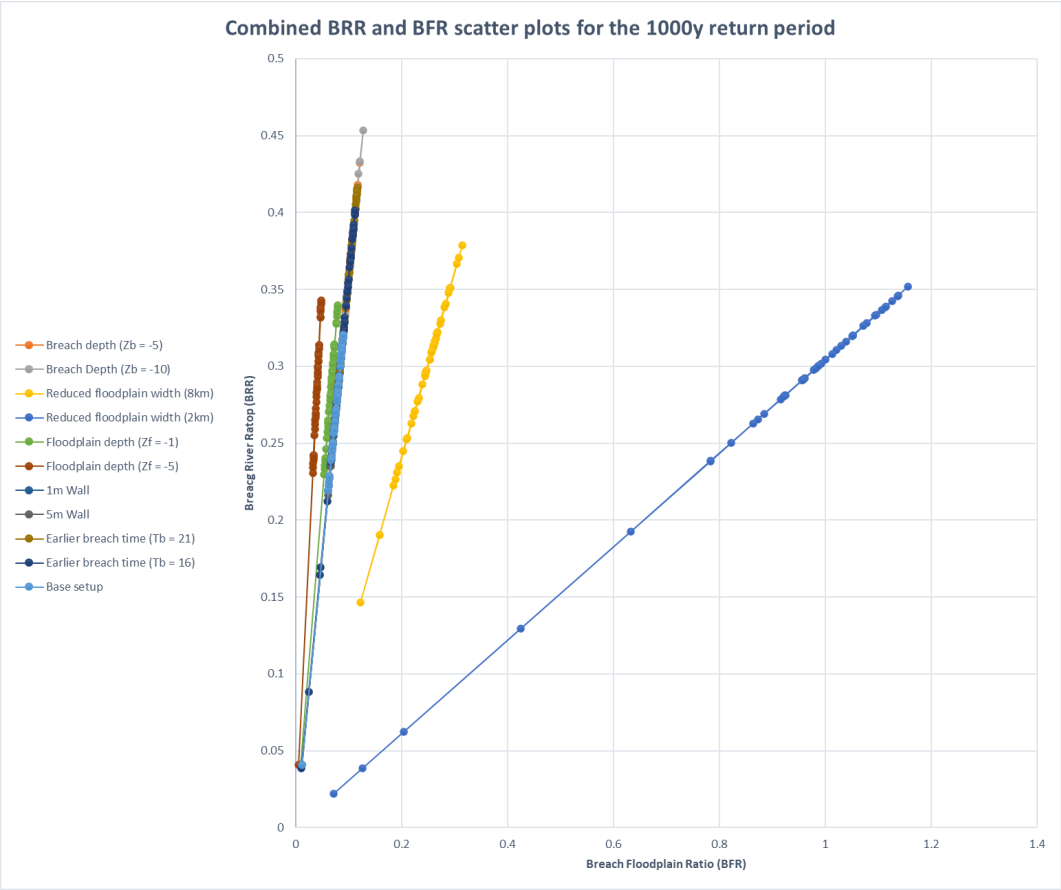

Figure 4.30: Combined scatter plot of the 1000-year return period values of the BRR and BFR

The bathtub approximation is used in the current flood maps of the Tisa and many other rivers over the world. In the current flood maps for the Tisa River (see (COWI 2019)), the potential inundation is determined by extrapolating horizontally the water levels found in the river over the floodplain. If this would be applied to the wet-feet map the result would be as seen in Figure 4.32. The results of this model show that this approximation should be used with great care in large floodplains. The behaviour of the inundation in the floodplain is very likely different that is assumed. The shape of the water levels does not follow the water levels inside of the river and the approximation is extremely conservative in most of the Tisa River area.

There may exist situations in other rivers, however, were this approximation will underestimate the potential inundation level. A breach at a 100yr return period water level can lead to a larger water level in the floodplain downstream of the breach. For example in the breach 6 case of the 2km floodplain width setup, the largest water depth found in $4.95\,m$. This is significant larger than the $4.30\,m$ in the river for this return period. The development of the depth can be seen in figure 4.31.

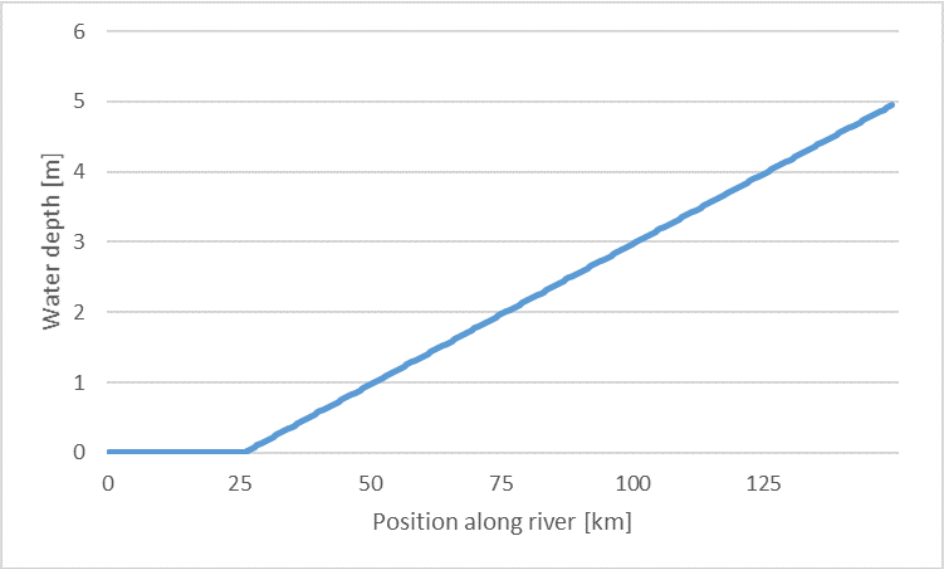

Figure 4.31: Water depth directly outside of the levee for a breach at location 6 for the 2km floodplain width setup.

All of this is based on an idealized model of the Tisa river. Only a very limited amount of detail could be included. Many of the parameters that were assumed constant in this model are actually vary greatly. Local changes in geometry of the river and the floodplain will change the inundation behaviour. Therefore it is of great interest to apply the method to a more detailed and realistic model of the Tisa river. The setup and results of this model in HEC-RAS will be presented in chapter 5.

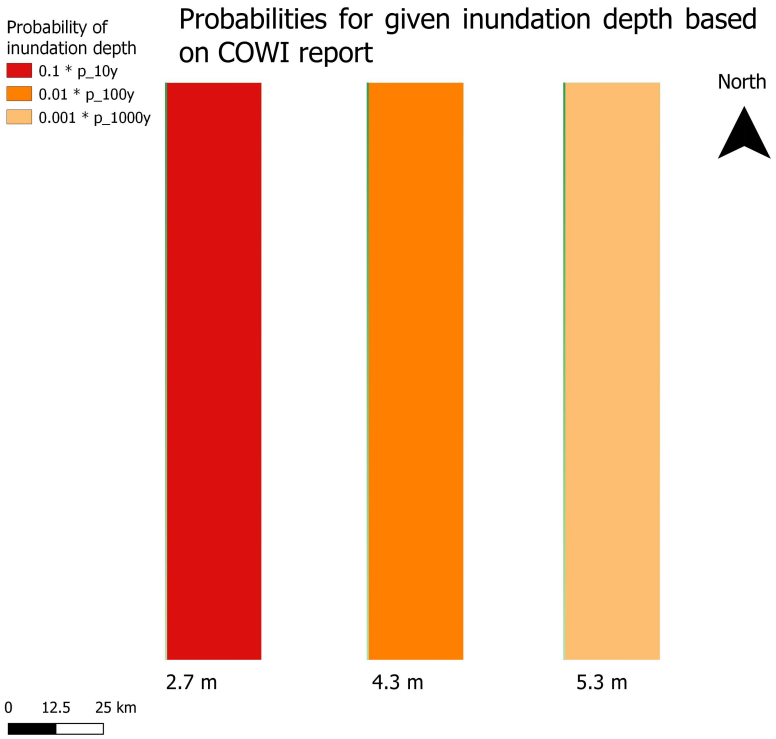

Figure 4.32: Wet feet chance map of the potential inundation based on the water surface elevations outside of the embankments. Actual annual inundation probabilities are undefined.

Chapter 5

Setup of a more detailed model of the Tisa River

5.1 Introduction

Previously, an idealized model was made to include probabilistic failure of flood defences to flood mapping in Chapters 3 and 4. It was found that the commonly used bathtub method may lead to some overestimation of the actual inundations. This holds especially in areas with large flood plains.

In this chapter, the method to include explicit failure of levees in flood mapping is applied to the Tisa River in a more realistic way. For this purpose, a model schematization is made in HEC-RAS (Hydrologic Engineering Center's River Analysis System). This software is freely available for the study of rivers and flooding and is provided by the US Army Corps of Engineers. A description of the studied case is presented in Section 5.2.

The model consist out of the same parts as were discussed in Chapter 3. First, the one-dimensional model has been setup with the realistic cross-sections and the levees added to this model. In HEC-RAS the levees are lateral structures which connect the one-dimensional model with the two dimensional grid used to model the floodplains. Levee failure probabilities are used to determine how likely a breach occurs. These are than combined with the resulting inundation to provide flood hazard maps.

The model schematization in HEC-RAS is made based using two primary data sets. A DTM of the area has been applied which has been created with LiDAR survey and this DTM has a resolution of one meter (COWI 2019). This data is used for the setup of the 2D grids after resampling. The 1D river is made with data used in (Kolaković *et al.* 2016). From this data the cross-sections of the river as well as the height of the surrounding levees is taken.

In Section 5.3 the schematization of the model is described. In Section 5.4 the results from the model are presented with several maps. Finally the result are discussed in Section 5.5.

5.2 Case description

The Tisa is a major river that originates in the Ukraine. It flows westward from this point and follows the border between the Ukraine with Romania and Hungary. Further downstream, it follows the border between Slovakia and Hungary before entering Hungary completely. Finally, it continues into Serbia where it flows into the Danube near Slankamen about 45 kilometers upstream of Serbia's capital city Belgrade.

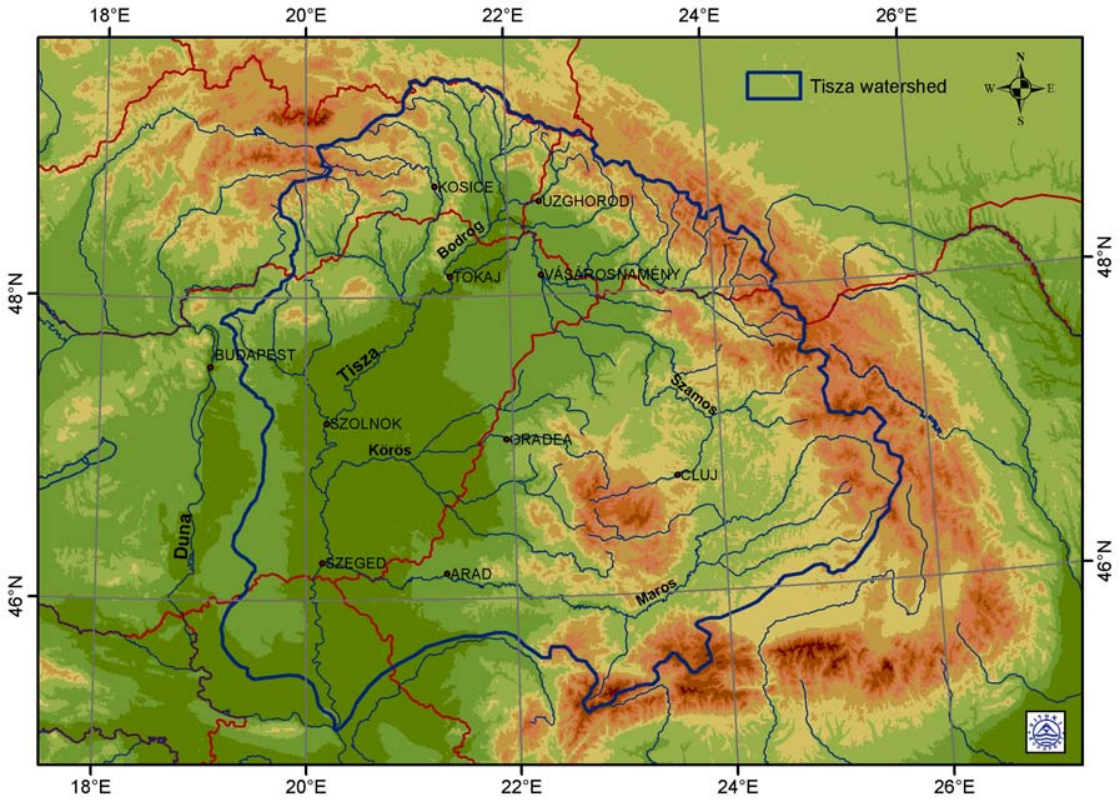

Figure 5.1: The complete Tisa watershed. (Gauzer 2009)

In Serbia, the area surrounding the Tisa river mainly comprises plains and the topography therefore is very flat. This makes the region sensitive to large floods. In previous centuries, the Tisa was known for large and devastating floods. In the 19th century the river was straightened and its length was strongly reduced. Its original entire length was 1420 km and after the regulation it was reduced to 962 km. As a result the water level drop over the river was increased from 3.7 cm to 6.0 cm per kilometer. The current levees were build along the Tisa after the 1965 floods to protect the hinterlands from further flooding. The plans were amended after the 1970 floods. The influence of the old meandering bends can still be seen in the terrain model.

5.3 Schematization

In the first part of this chapter the setup of the model is described. The model is split into three different parts. The river along with the cross sections, the floodplains with a DTM and the breaching of the levee. In the first subsection the implementation of the river with its cross sections is discussed. The implementation of the levees is also described here. In the second subsection the floodplains surrounding the river are discussed. The third part discussed the breaching of the levees.

5.3.1 Schematization of the river

The data for the main reach of the Tisa River and the cross sections were kindly provided by Ir. Slobodan Kolaković from the University of Novi Sad as used in (Kolaković *et al.* 2016). As the data was used for an one-dimensional model before it was not warped to a specific projection. Several horizontal projections were tried to find one were this data fits closely to the map. Eventually EPSG:8682 was found to be a reasonable fit. This is a projection of Serbia including Vojvodinja. The river was manually positioned and rotated to fit with minor further adjustments. The final fit can be seen in Figure 5.2.

Figure 5.2: The studied stretch of the Tisa River overlaid on satellite images from ArcGIS.

The profiles from the cross sections in the one-dimensional model resemble the profiles found from the DTM. However, the profiles of the river were increased by one meter to fit more closely to the DTM heights. In the Figures of 5.3 the two profiles are presented for several cross sections. The differences are in part caused by the manual positioning of the cross sections. The cross sections are not exactly in the correct locations along the river and do not correspond exactly to the DTM. The DTM can also be used to generate the cross sections but this does not provide data for the profile below the water level.

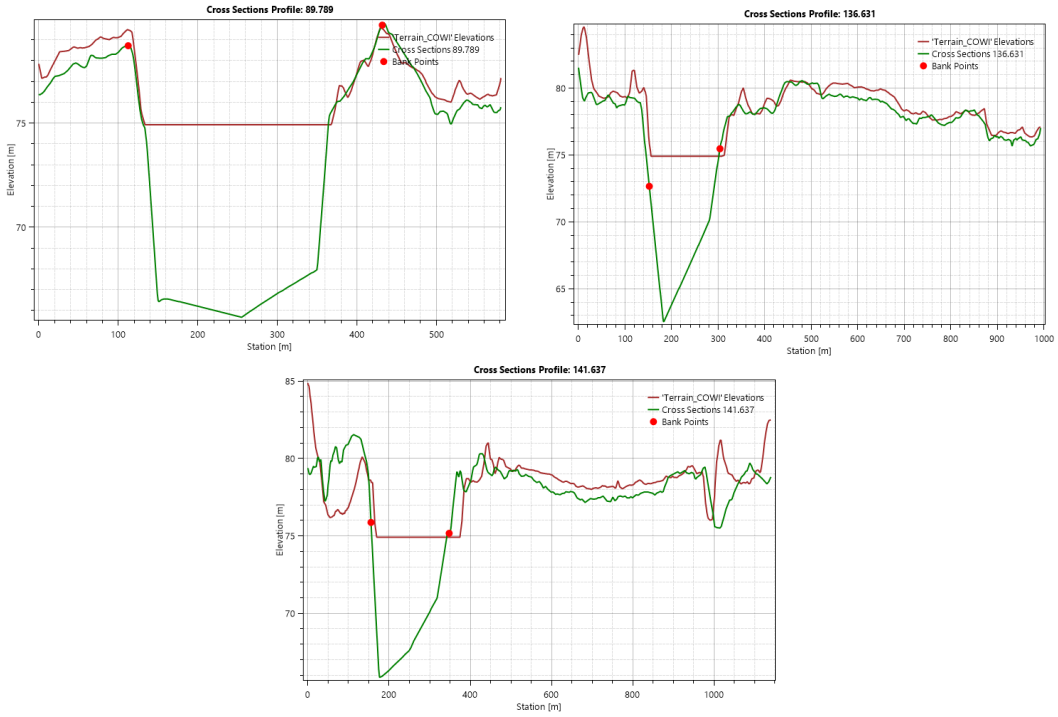

Figure 5.3: Cross sections of the 1D river in combination with the 2D DTM.

After the main reach of the river was positioned, the different cross sections were similarly placed by hand. The cross section included a larger area than just the area between the embankments and had to be manually be cut to the right size. Several bridges are found that cross the Tisa in the studied area. These could not be automatically be imported from the original model. The bridges have been left out of the model as their influence on the river flow is restricted to being relatively local. There is also a gated dam used to control the water levels in the river. This is named the Tisa dam (Brana Na Tisi). The structure can be seen in Figure 5.5. This structure was copied by hand and is assumed to be opened fully during the modelling period. The dam is used to control the water levels in the Danube-Tisa-Danube canal. The cross section of the dam can be seen in figure 5.4.

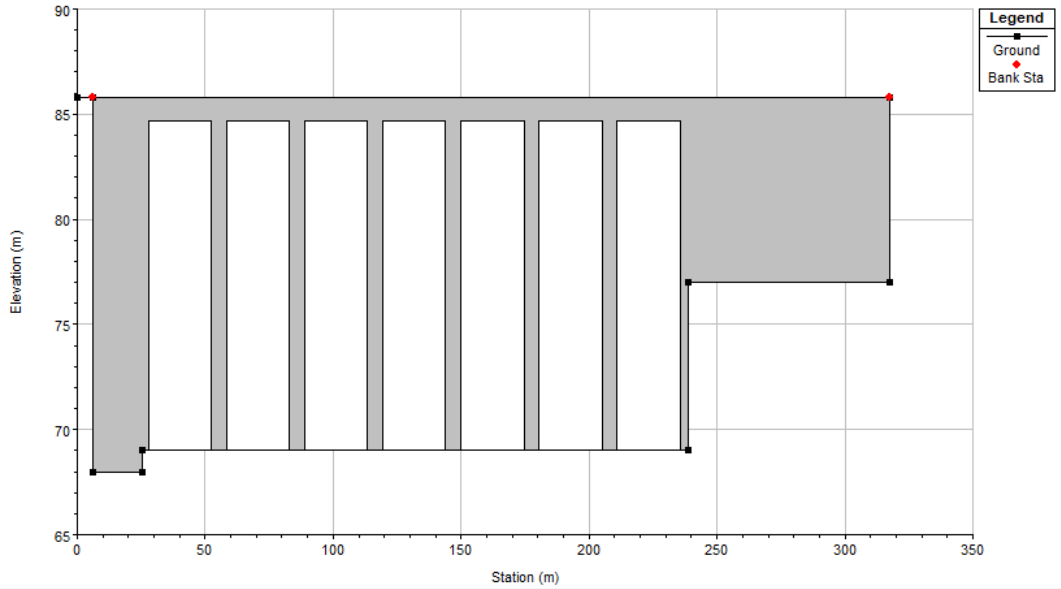

Figure 5.4: Inline structure in the model for the Tisa dam.

Figure 5.5: Tisa dam seen from the air. URL:https://mapio.net/pic/p-17965790/

The levees surrounding the river have been added as lateral structures. The levees that were added in the river data were removed and included as lateral structures. These form the connection between the one-dimensional river and the floodplains beyond the levees. The levee is treated as a broad-crested weir with a standard weir coefficient of 1.1 and a width of 50 meters.

5.3.2 Schematization of the floodplain

The floodplains have been schematized with a DTM to provide the surface height of each pixel and a roughness to represent the use of the land. A standard Nikuradse value of 0.045 was used for the roughness. For the height data Lidar data collected has been used which has a resolution of 1 meter (COWI 2019). To reduce the computation time and to reduce to required RAM needed for the use of large grids, the data was re-sampled to a resolution of 5 meter. This was done with the QGIS software simultaneously to the re-projection of the data. The selected method of re-sampling was taking the average of the pixels. This can reduce the highest point in the cell but all objects of interest like levees or roads are wide enough for this to not be of influence. For the friction a manning roughness of $0.045 s/m^{1/3}$ was used for the whole floodplain. This is a reasonable estimate for land being used for agriculture which is the dominant land use in the Tisa River basin.

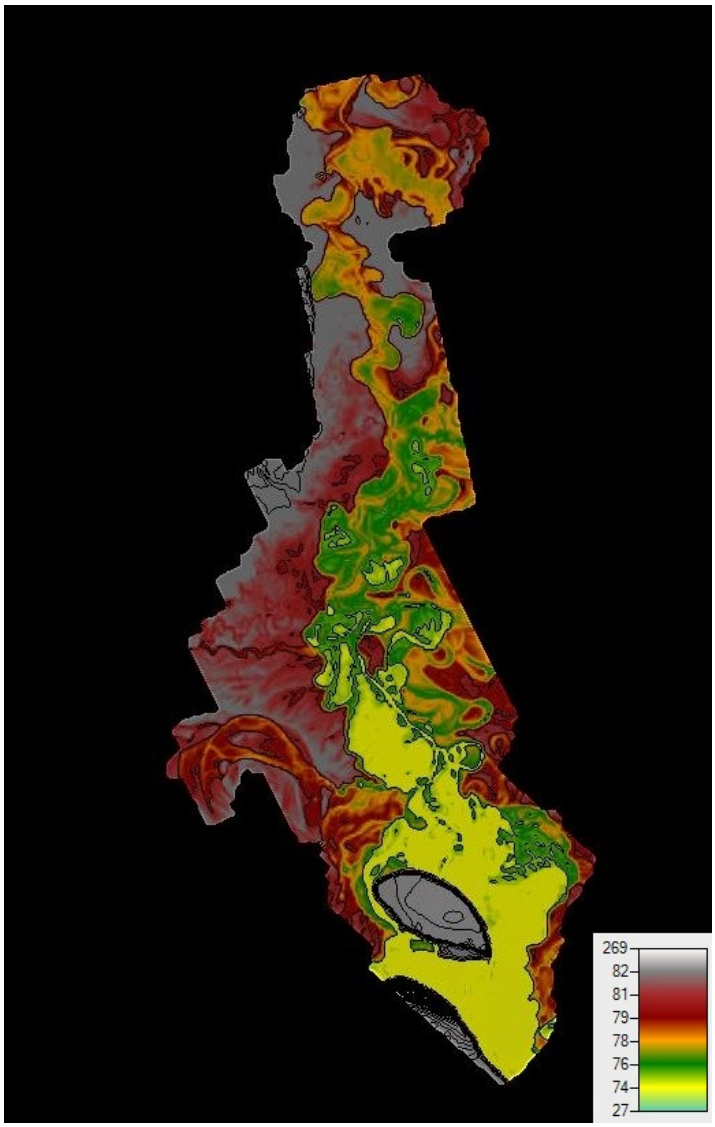

Figure 5.6: DTM of the Tisa River basin based on the COWI rapport data.

For the 2D grids used in the model, a cell size of 100 meters by 100 meters was selected. Each cell will on average contain 400 pixels of 5 by 5 meters. The 2D-flow was calculated with the default diffuse wave equations. The exact shape and size of the cells can depend on break lines and the edges of the grid. The selection of a cell size is a balancing act between accuracy and computation speed. By halving the size of the cells the amount of cells is roughly quadrupled. This will directly increase the computation times. Secondly the smaller cells will require smaller time steps to prevent instability further increasing the computation time. There are two grids used for this model. One for the eastern floodplain and one for the western floodplain. The two grids can be seen in Figure 5.7.

To model the presence of levees around smaller side streams of the Tisa and raised roads, several break lines were added to the 2D grids. Not all of the potential line elements were added as break lines. Some of the roads have multiple viaducts which reduce their capacity to slow down the development of the inundation. In other cases, the break lines end up too close to each other leading to leakage due to oddly shaped cells. This issue can be solved by reducing the cell size but the increased computation times make this undesirable. In practice if the two break lines are very close to each other only the higher of the two has meaningful influence on the inundation development. A map with the break lines added is presented in Figure 5.7.

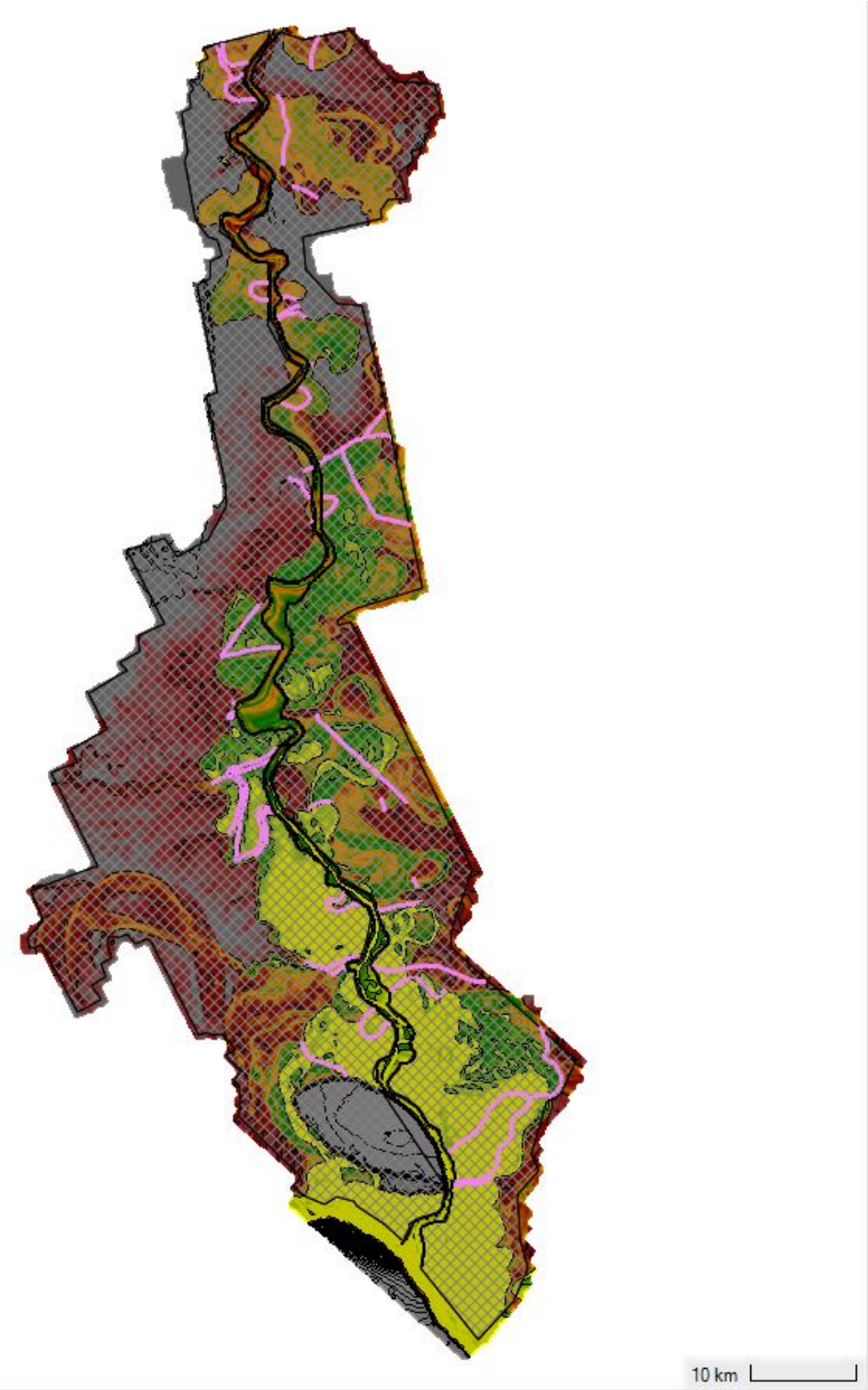

Figure 5.7: 2D grids with break lines. Levees are included in black. The breaklines are shown in pink.

5.3.3 Levee breaching

The levees are breached at several points based on the consequences of the following inundation. The different locations were selected at roughly 15 kilometer distances of each other and based on the presence of break lines in the grids. At some locations a higher region in the DTM would lead to no or little inundation and therefore no breaches are made there. In Figure 5.8 the breach locations for the flood plains are shown.

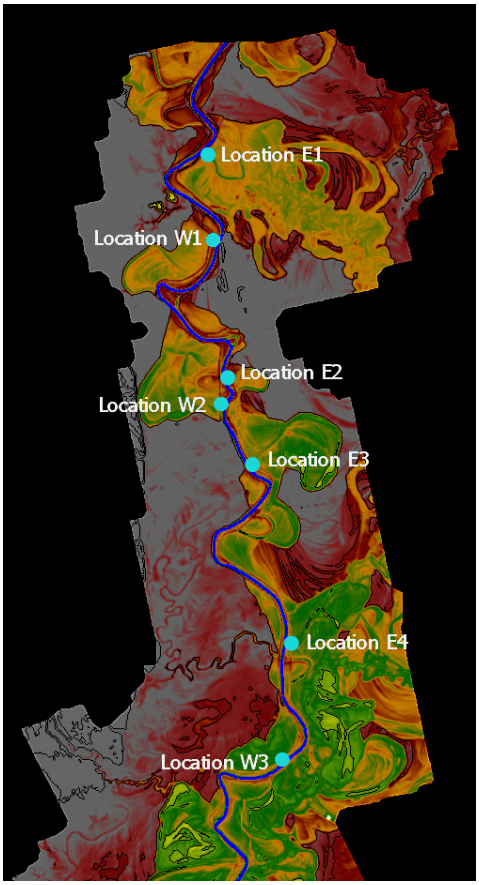

(a) Breaches for the northern half of the studied area.

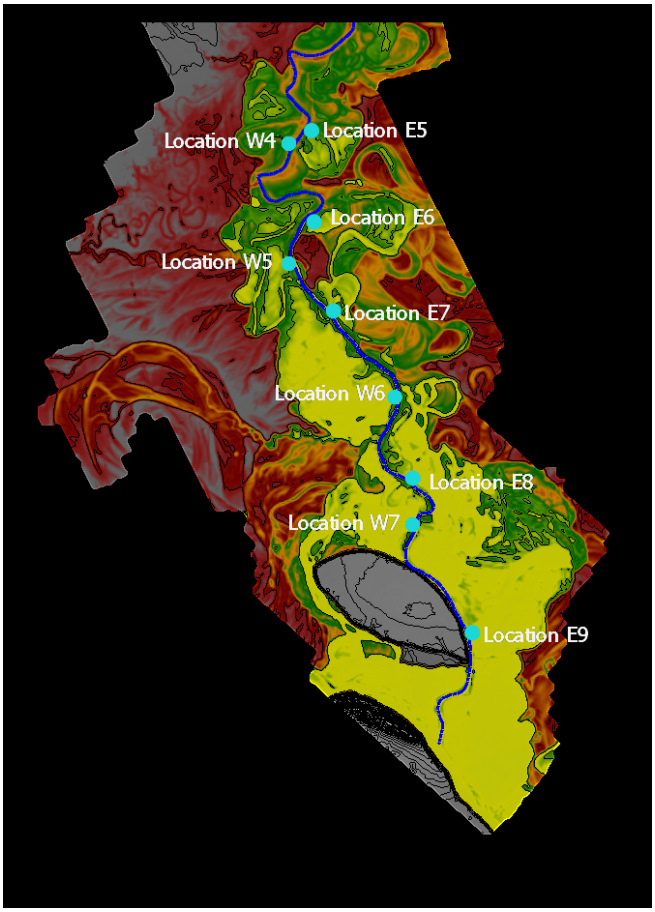

(b) Breaches for the southern half of the studied area.

Figure 5.8: Breach locations for the eastern floodplain.

For the breaching of the levees, the mass wasting failure feature of HEC-RAS is used. This feature allows for a spontaneous levee breach without a specific cause. The initial width of the breach is 10 meters and develops in 12 hours starting at the time the discharge peak enters the system. With limited available data, it is difficult to determine the exact conditions surrounding a levee. For this reason modeling of piping or overtopping as a failure mode is not used.

For the initial failure, the same development as in Chapter 3 is used. A initial stretch of 10 meters wide will decrease in crest height in a time span of 12 hours. The final crest height will be slightly below the ground level. As was seen in the result of the variation with lower breaching depths with the idealized model, additional depth has a very minor effect on the total inundation (see Section 4.3.2).

The maximum width of the breach is limited again to 200 meters based on (Verheij & Van der Knaap 2002).

For the further development of the breach, HEC-RAS has two different methods. A simplified physical method and a more advanced physical method. The advanced method requires a large amount of very specific data for the levee. For this reason, the simplified method was used. This method only requires a down-cutting rate and a widening rate based on the flow velocity through the breach. For this model an estimate was used based on the Verheij-vdKnaap formula used in Chapter 3.

5.3.4 Probability for levee breaching

To determine the breaching probability several steps are used:

1. The levee will be divided in several stretches with similar consequences.
2. Each stretch will be assign a probability P_{loc} for the chance a breach will occur in that stretch based on the relative length of the stretches.
3. An estimate for the failure probability P_f of a single segment is made.
4. The number of segments per stretch is determined.
5. The probabilities $P_{b,e}$ of a breach occurring in the each of the locations for each return period, can be determined based on the P_{loc}, P_f and the return period.

The western levee has a length of around 139 km and the eastern levee a length of around 150 km. The difference is caused by the presence of a higher area near the end of the studied stretch of the river. This area can be seen in Figure 5.7 as the larger grey area near the bottom of the image.

Each of the locations needs a probability of a breach occurring in that specific stretch of the levees. In the idealized model of Chapter 3, this was one in nine as there were nine stretches with identical length. In this model, this is dependent on the length of the levee stretch represented. This length varies between the different locations. The variation in length is based on the selection of the breach locations based on breaklines and higher areas in the floodplain.

The total studied length of the eastern levee is 114.5 km. The total studied length of the western side is 102.5 km for a combined 217 km. Based on the total length, the probability of a breach at each location can be determined with the following equation. The probability of a breach occurring at a specific location, provided that a breach occurs, can be found in Table 5.1. Here f is the probability of a breach occurring.

$$P_{loc|f} = L_{stretch}/Ltot$$

Breach location	Length of stretch	P_{loc}
East side		
Location E1	12.1 km	0.056
Location E2	4.3 km	0.020
Location E3	18.7 km	0.086
Location E4	9.5 km	0.044
Location E5	17.5 km	0.081
Location E6	7.5 km	0.035
Location E7	11.9 km	0.055
Location E8	14.5 km	0.067
Location E9	18.5 km	0.085
West side		
Location W1	8.8 km	0.040
Location W2	9.8 km	0.045
Location W3	19.0 km	0.088
Location W4	14.0 km	0.064
Location W5	15.6 km	0.072
Location W6	20.4 km	0.094
Location W7	14.9 km	0.069

Table 5.1: Caption

Based on these values the probability of failure in a specific location can be calculated based on the same estimates found in Section 3.3.1. Combined with a slightly different implementation of the binomial distribution to account for the different number of the levee segments represented in the locations. Due to the running time of this model, it has become impossible to test a large number of combinations. While the 10 year and 100 year flood levels can be represented with a single breach, the 1000 year flood level cannot. The chances found based on the binomial distribution are collected in Table 5.2. It is clear that only accounting for a single breach does not suffice for the 1000 year return period.

For this reason, the probability for at least one breach is used. This means that the probabilities related to the 1000 year return period are not underestimated too much. The only questions is whether or not this leads to a underestimation of the inundation extent for the 1000 year cases. And an overestimation of the inundation depth for 1000 year cases. It is assumed due to limited space in the floodplains that the inundation depth will lead to significant values even when less water enters the floodplain. In this way this assumption should end up with similar results for inundation probability compared to making multiple breach cases. To account for the increased probability of a breach occurring at a specific location, a correction needs to be added. For two breach cases the chance of a breach occurring at a specific location is twice as large than with one breach cases. By the same logic the combined probability for three breach cases is thrice as big as for a single breach.

$$p_b = \binom{N}{k} P_f^k (1 - P_f)^{N-k}$$

With N being the total amount of segments and k the number of simultaneous breaches. P_f is the

assumed probability of a breach occurring during a certain return period.

Number of breaches	$P_{b,10y}$	$P_{b,100y}$	$P_{b,1000y}$
1	0.0212	0.1747	0.2477
2	0.0002	0.0189	0.2691
3	0.0000	0.0014	0.1947
4	0.0000	0.0001	0.1055
5	0.0000	0.0000	0.0457

Table 5.2: Annual probabilities of occurrence of different amount of breaches based on the binomial distribution.

$$P_{b,e} = P_e * \sum_{n=1}^{5} (\binom{N}{n} n * P_{f|e}^{n_b} (1 - P_f)^{N-n_b}) * P_{loc|f}$$

$P_{b,e}$ is that annual probability that a breach occurs for a given location. Here P_e is annual probability related to the return period. N is the number of 200m segments in the whole studied levee. There are $217 * 5 = 1085$ segments. P_f is the chance of a segment breaching. And N_b is that amount of simultaneous breaches. The different probabilities are collected in Table 5.3. The sum of all the annual probabilities combined with the annual probability of no breaches is 0.1. Event with an annual probability of larger than 0.1 are assumed to be unlikely to cause breaching and are not included.

Breach Location	$P_{b,10y}$	$P_{b,100y}$	$P_{b,1000y}$
No Breach	$8.8068 * 10^{-2}$	7.244210^{-3}	1.139310^{-4}
Location E1	$1.089 * 10^{-4}$	$1.089 * 10^{-4}$	$1.127 * 10^{-4}$
Location E2	$3.870 * 10^{-5}$	$3.870 * 10^{-5}$	$4.004 * 10^{-5}$
Location E3	$1.683 * 10^{-4}$	$1.683 * 10^{-4}$	$1.741 * 10^{-4}$
Location E4	$8.550 * 10^{-5}$	$8.550 * 10^{-5}$	$8.846 * 10^{-5}$
Location E5	$1.575 * 10^{-4}$	$1.575 * 10^{-4}$	$1.629 * 10^{-4}$
Location E6	$6.750 * 10^{-5}$	$6.750 * 10^{-5}$	$6.983 * 10^{-5}$
Location E7	$1.071 * 10^{-4}$	$1.071 * 10^{-4}$	$1.108 * 10^{-4}$
Location E8	$1.305 * 10^{-4}$	$1.305 * 10^{-4}$	$1.350 * 10^{-4}$
Location E9	$1.665 * 10^{-4}$	$1.665 * 10^{-4}$	$1.723 * 10^{-4}$
Location W1	$7.920 * 10^{-5}$	$7.920 * 10^{-5}$	$8.194 * 10^{-5}$
Location W2	$8.820 * 10^{-5}$	$8.820 * 10^{-5}$	$9.125 * 10^{-5}$
Location W3	$1.710 * 10^{-4}$	$1.710 * 10^{-4}$	$1.769 * 10^{-4}$
Location W4	$1.260 * 10^{-4}$	$1.260 * 10^{-4}$	$1.304 * 10^{-4}$
Location W5	$1.404 * 10^{-4}$	$1.404 * 10^{-4}$	$1.453 * 10^{-4}$
Location W6	$1.836 * 10^{-4}$	$1.836 * 10^{-4}$	$1.899 * 10^{-4}$
Location W7	$1.341 * 10^{-4}$	$1.341 * 10^{-4}$	$1.387 * 10^{-4}$

Table 5.3: Annual probabilities for each breach location.

5.4 Results

Based on the probabilities in Table 5.3 a series of maps were made. These maps are shown in Figures 5.9 and 5.10. Each of the maps is made with a logarithmic scale. The main interest is how the probabilities of inundation are distributed over the flood plain.

The resulting water depths and water levels for all of the different cases can be found in Appendix C. The relevant sections of the water depth maps are presented in this section to provide more insight in the development of the inundation probabilities. Only the maps for the 1000 year return period have been included here.

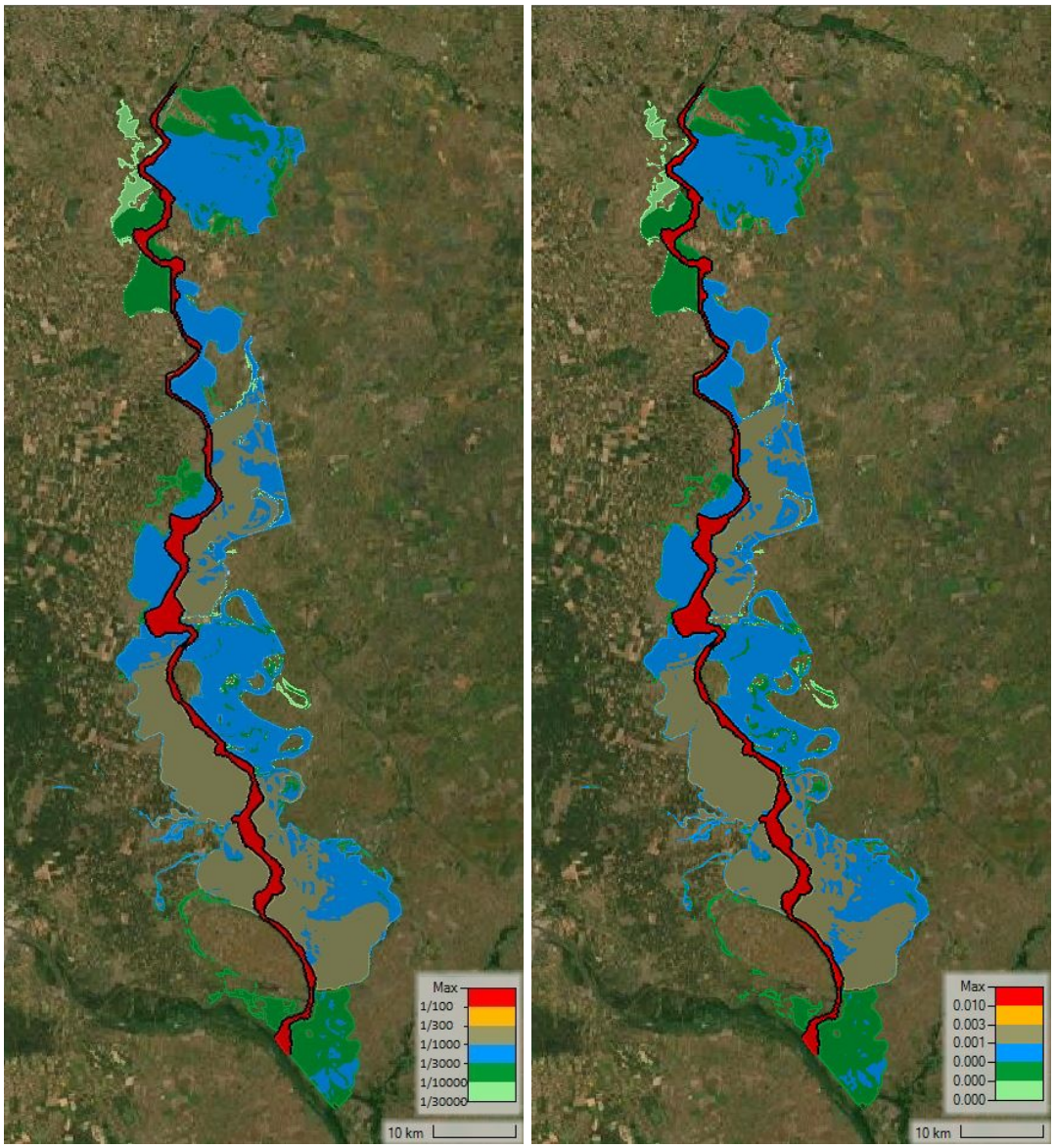

(a) Inundation of 0.1 meter. **(b)** Inundation of 0.3 meter.

Figure 5.9: Annual probability of inundation above a certain meter water depth.

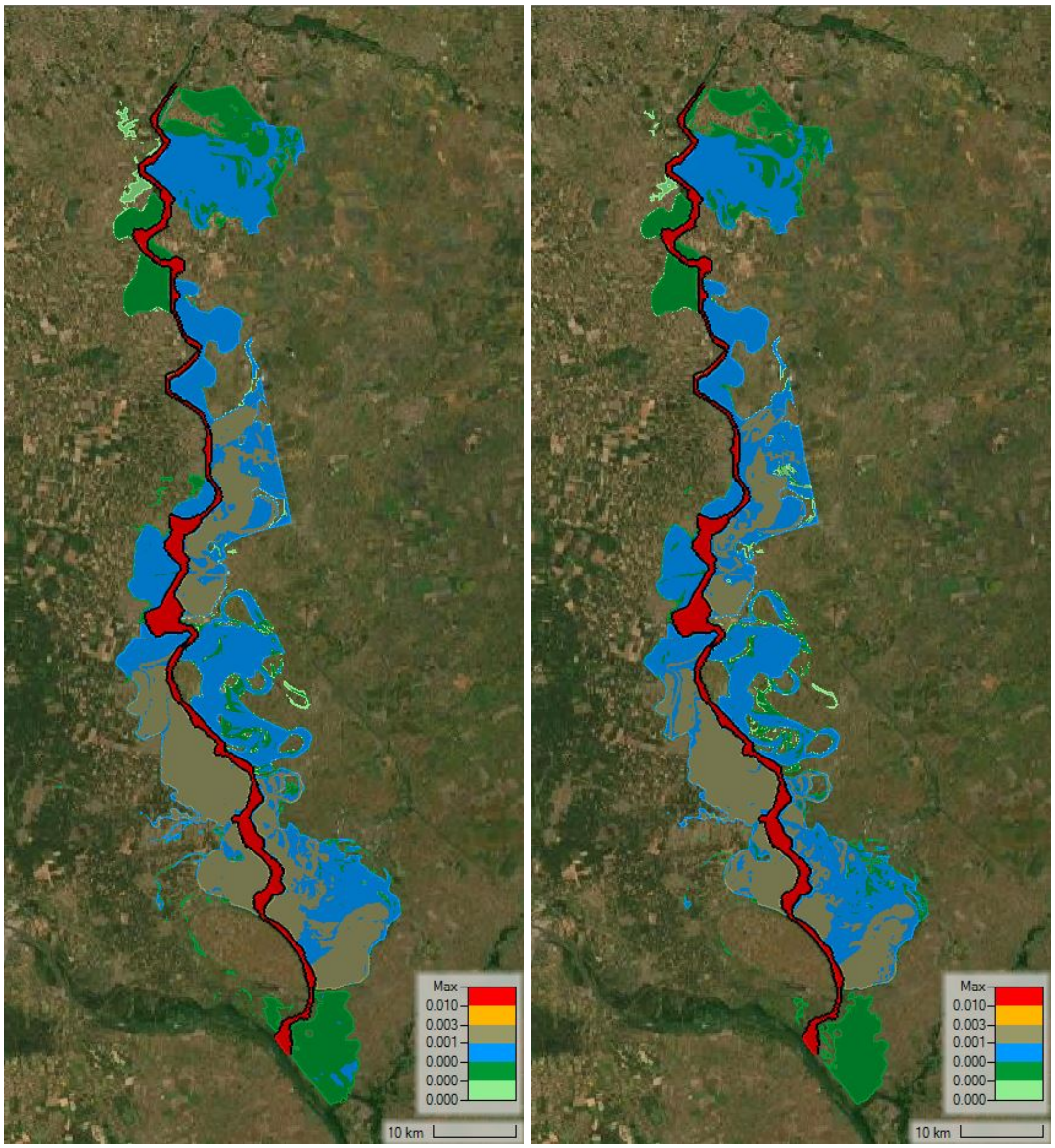

(a) Inundation of 0.5 meter. **(b)** Inundation of 1.0 meter.

Figure 5.10: Annual probability of inundation above a certain water depth.

Several observations can be made based on the different maps.

- The maps are very similar to each other. At the edges of the inundation areas the chance reduce slightly for higher depths. The inundation areas are also slightly smaller for the higher depths. The similarity between the different maps show that the inundation is relatively large in the areas where the probability is high. Outside of the levees the probabilities remain below 0.01 annually. The 0.001 annual probability is exceeded in the beige areas.

Looking at the different zones in more detail can explain why certain areas show a larger risk for inundation than others. By combining the DTM as shown in Figure 5.6 with the details of the model,

an explanation can be provided. Starting with the most upstream part of the map around breach locations E1 and W1. A close-up of the map is presented in Figure 5.11.

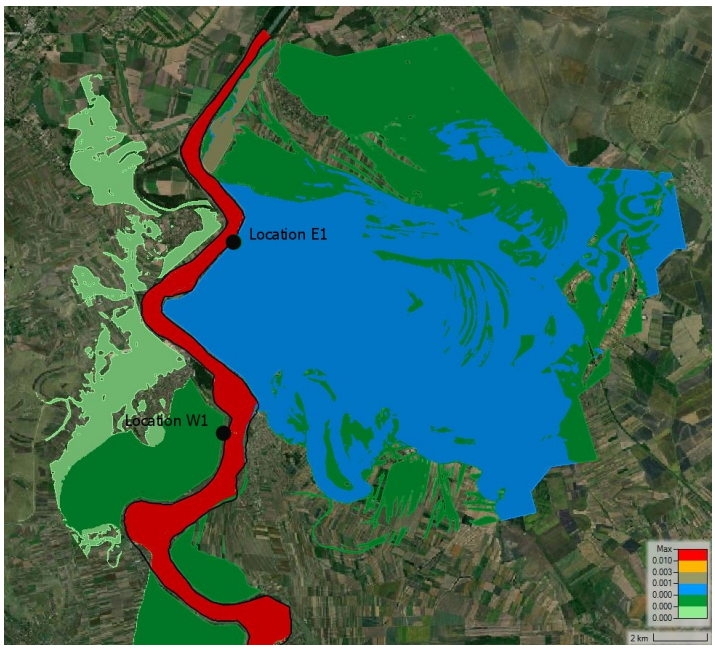

Figure 5.11: Close up of the map for breach locations E1 and W1.

- On the east side of the river, the inundation caused by breach E1 is clearly visible. The northern border of the area is the edge of the 2D grid which does not let the water flow out of the area. The southern edge of the blue area is caused by a local raise in height. The water level in this area is similar to the water level over the river.
- The inundation caused by a breach at location 10 is also visible as the small blue area left of the river. The surrounding area is higher which leads to a natural limit to the inundated area. The difference in water level is around 0.3 meter for the 1000 year return period for most of the area. The northern most third section of the inundation area has a water level roughly three meters below the level over the river.
- A small area of inundation at the eastern side of the river is caused by overflow. This is most likely caused by some modelling error of the levee at the edge of the system or some minor instability.

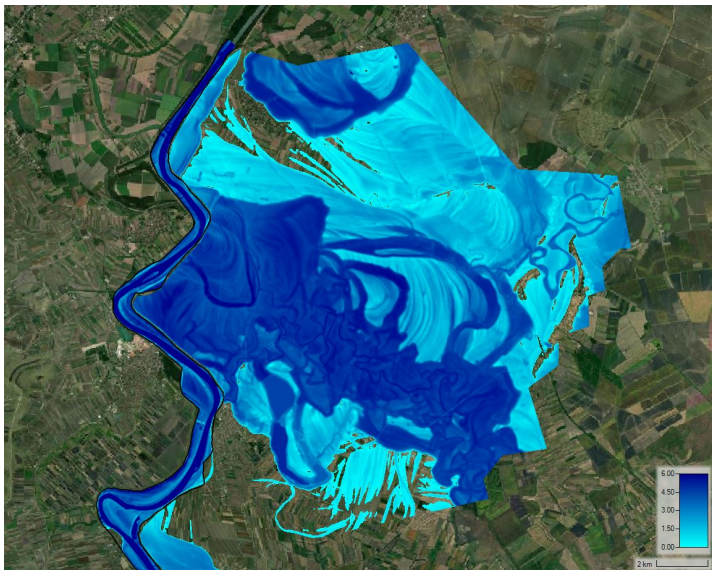

(a) 1000 year return period maximum depth for breach location E1.

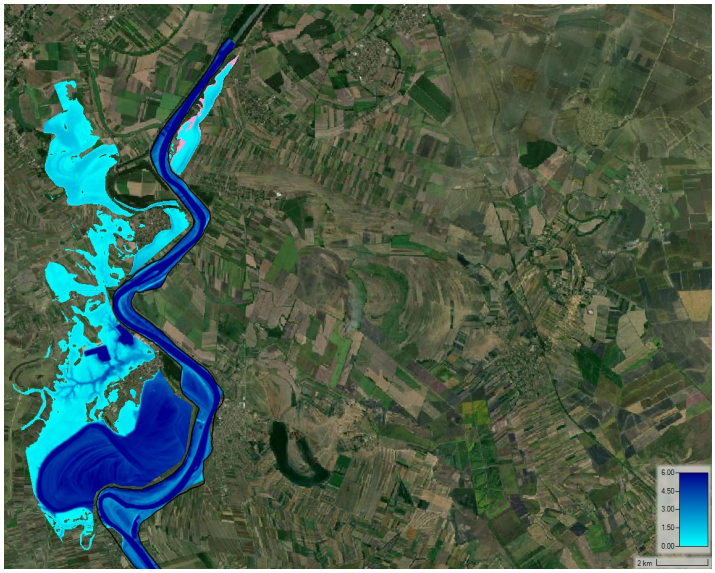

(b) 1000 year return period maximum depth for breach location W1.

Figure 5.12: Close-ups to the inundation depth maps of breach locations E1 and W1.

The next area stream downward is affected by the breaches at locations E2 till E5,W2 and W3. This area is presented in Figure 5.13. Individual inundation depths are presented in Figures 5.14, 5.15 and 5.16.

- The right edge of the DTM is visible in the part of the map. This also means that the water depth in the area might be higher than expected during a real flooding event. On the left side of the river the inundation is limited by higher areas.

- On the eastern side a difference in the probabilities is visible. Due to local differences in the terrain the inundation reaches certain areas during all of the different cases. The blue area is only reached by cases with a larger return period.
- The maximum water level difference near breach location W2 is roughly 0.6 meters. This area is limited by local higher areas in the DTM.
- The difference in water level near location W3 is almost zero near the breach. The smaller blue area to the south-west of the green area is caused by a small channel that is found in this area. The water surface level here is almost 6 meters below the water level over the river.
- The breaches at locations E2 and E3 lead to an inundation of roughly the same area. The water level is similar to the water level over the river for the northern part of the inundation area. The presence of a road leads to a difference in water level between the northern half and southern half of over 1.0 meter. The presence of a road between these breach locations has little influence of the final inundation map.
- The breaches at locations E4 and E5 also result in very similar inundation areas. But the water surface levels are different. For the E4 case the difference is roughly 1.5 meters. While the E5 case leads to a difference of roughly 0.9 meter.

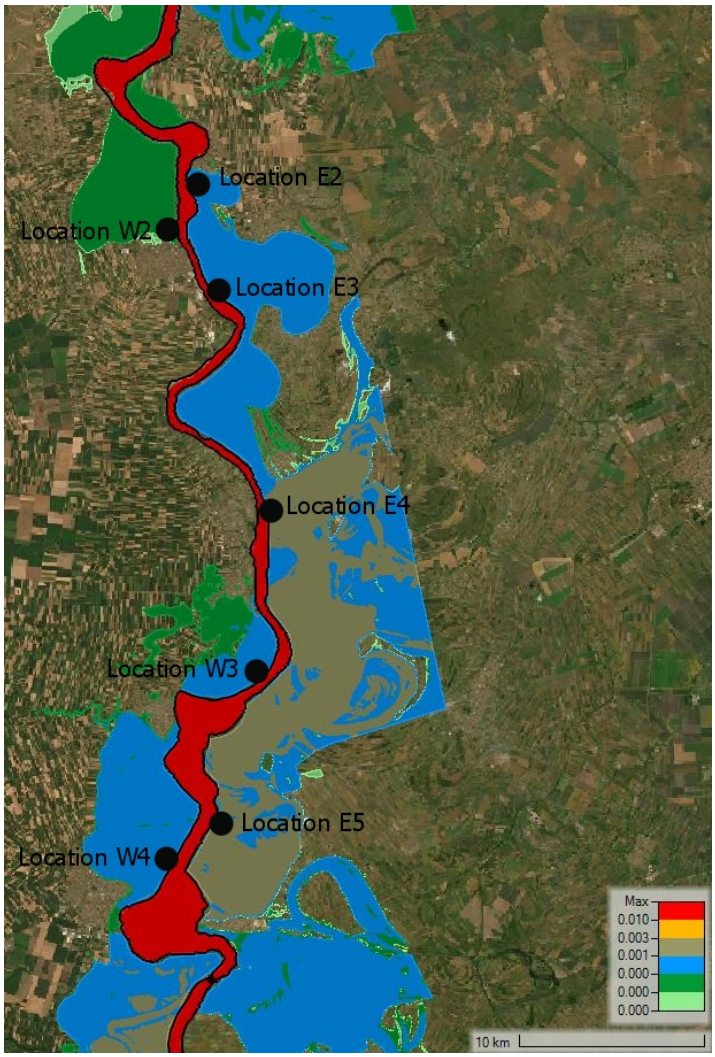

Figure 5.13: Close up of the map for breach locations E2 till E5, W2 till W4.

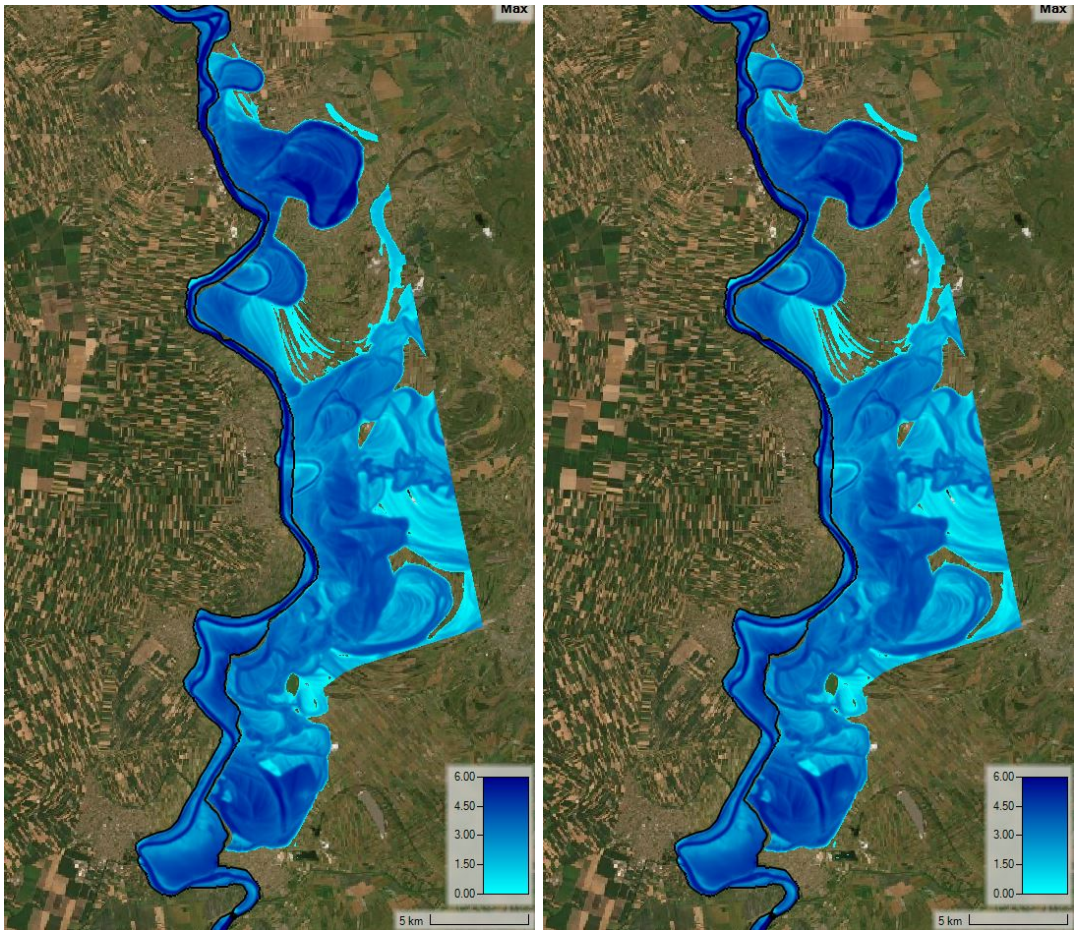

(a) 1000 year return period maximum depth for breach location E2.

(b) 1000 year return period maximum depth for breach location E3.

Figure 5.14: Close-ups to the inundation depth maps of breach locations E2 and E3.

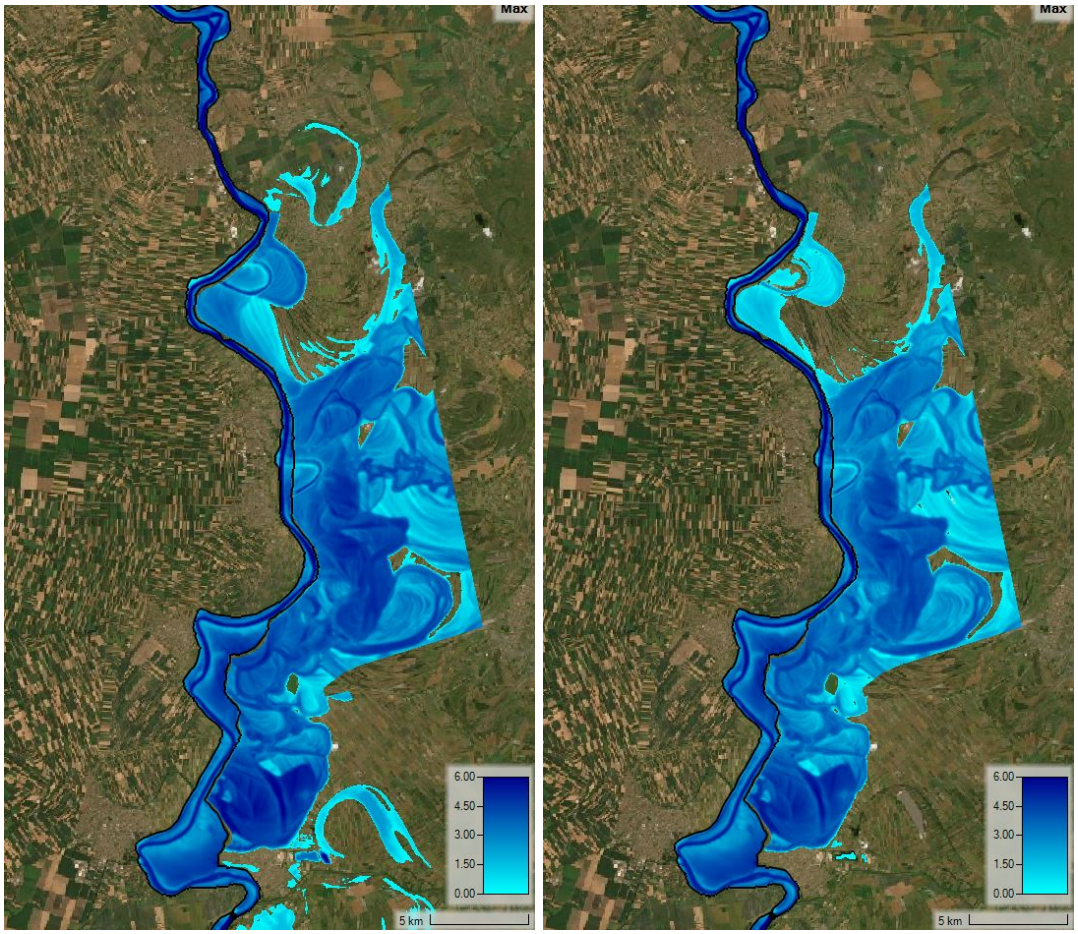

(a) 1000 year return period maximum depth for breach location E4.

(b) 1000 year return period maximum depth for breach location E5.

Figure 5.15: Caption

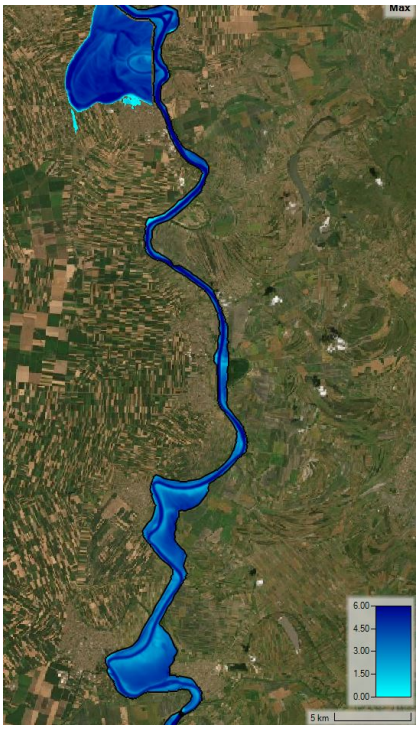

(a) 1000 year return period maximum depth for breach location W2.

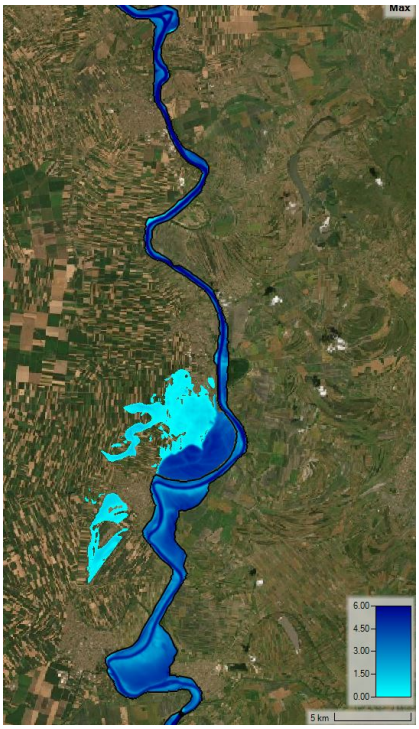

(b) 1000 year return period maximum depth for breach location W3.

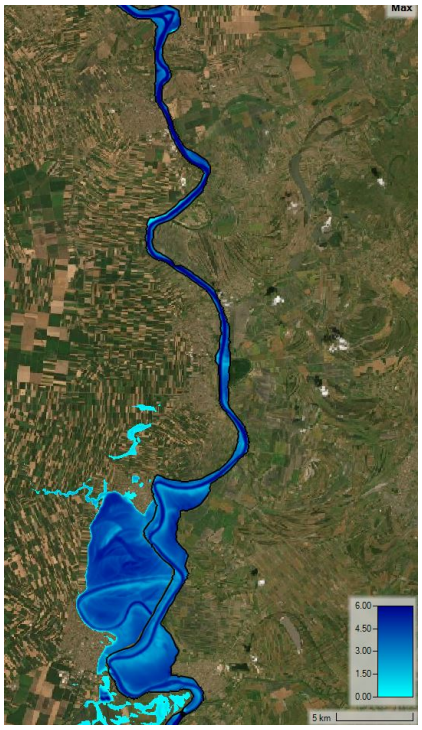

(c) 1000 year return period maximum depth for breach location W4.

Figure 5.16: Close-ups to the inundation depth maps of breach locations W2, W3 and W4.

The next area studied is the area downstream from the Tisa dam to the large raised area in the DTM. The inundation probability map of this area is visualized in Figure 5.17. The inundation maps of the different breach cases are found in Figures 5.18 and 5.19.

- The inundation probability is roughly similar on the western side. Of note is the influence of some smaller channels on the western side. These allow for some smaller inundation areas relatively far from the river. The beige parts surrounding the channels are in part cause by inundation from location W7 south of this map. The area north of W5 can only be reached by inundation from location W5 and therefore has a lower probability of inundation.
- The inundation caused by breaches at locations E6 and E7 lead to similar inundation extents. The water surface levels are also similar although E6 leads to slightly higher values. The northern most half of the area has a surface level of roughly 1.6 meter below the river at the breach location. There is a break line roughly in the middle of the area. Below the break line the water surface is 2 meters lower that the area north of there.
- The inundation caused by a breach at location E8 is more limited in this area. Due to overlap with the inundation caused by E6 and E7 there is an area with a larger probability. The water surface level is the floodplain is almost 2 meters below the level in the river at the breach location.
- On the western side the breaches at location W5 and W6 lead to similar inundation extents. The water surface levels are also similar to each other. The W5 case has a slightly higher surface level in the northern third of the area. The water surface level is here just over 1 meter below the river. The rest of the area is 0.5 meter below this. For case W6 the whole area has roughly the same water surface level about 1.5 meter below the river at the breach location.

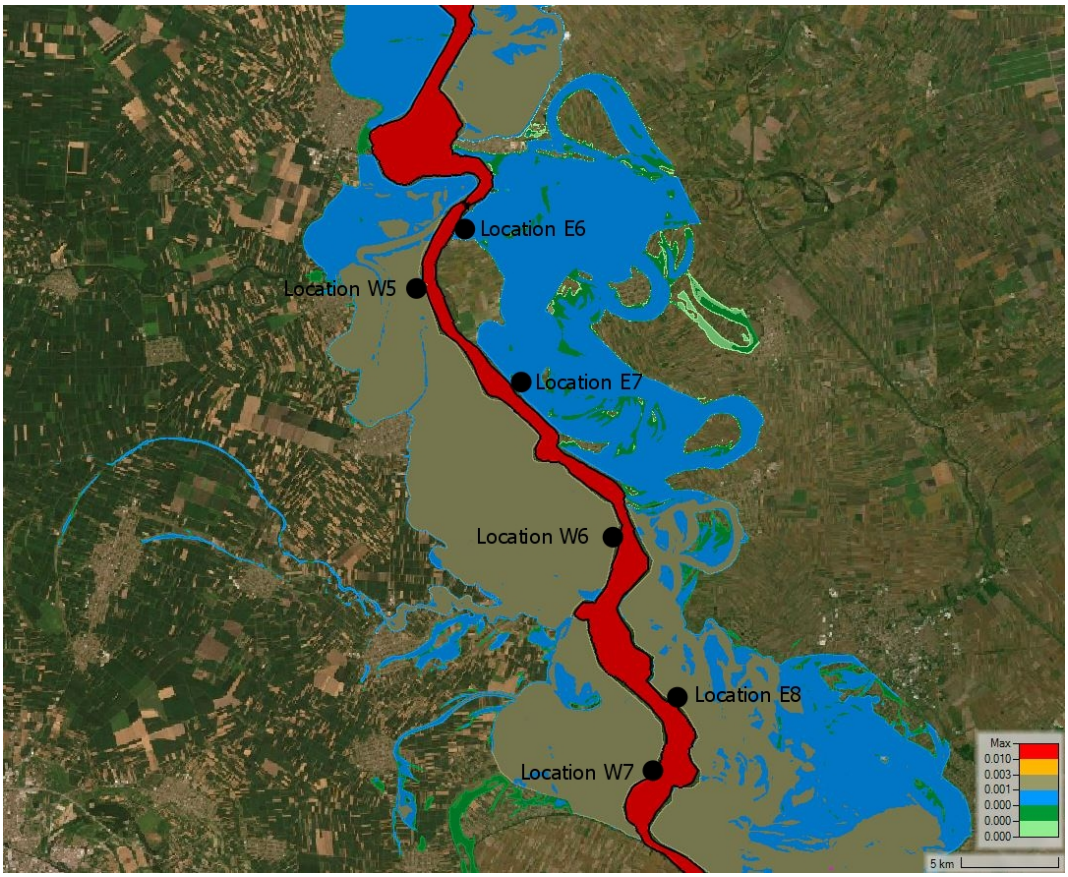

Figure 5.17: Close up of the map for breach locations E6 till E8 and W5 and W6.

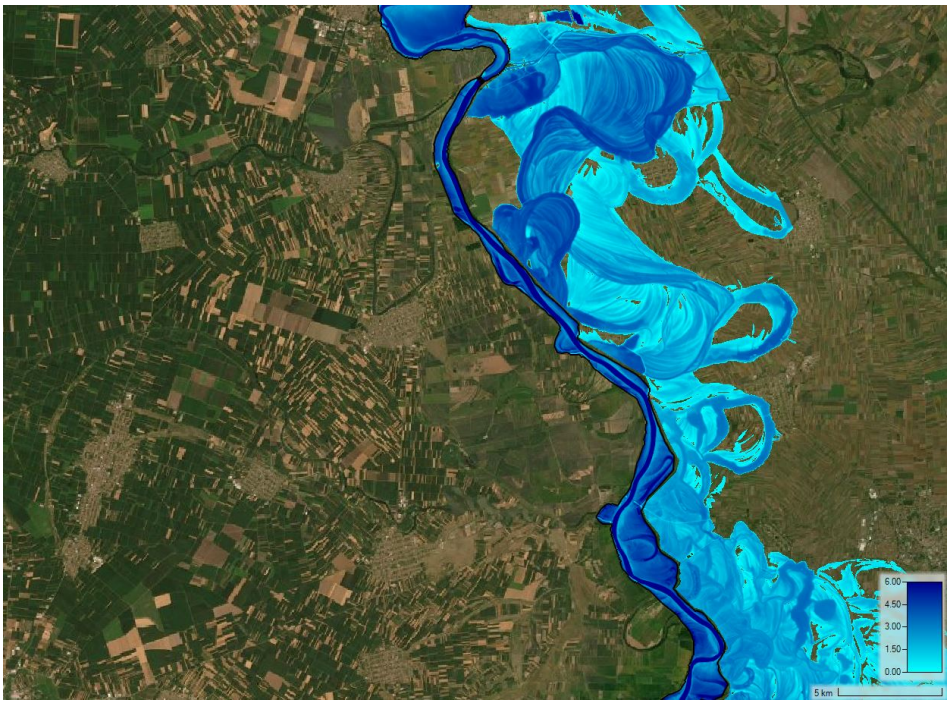

(a) 1000 year return period maximum depth for breach location E6.

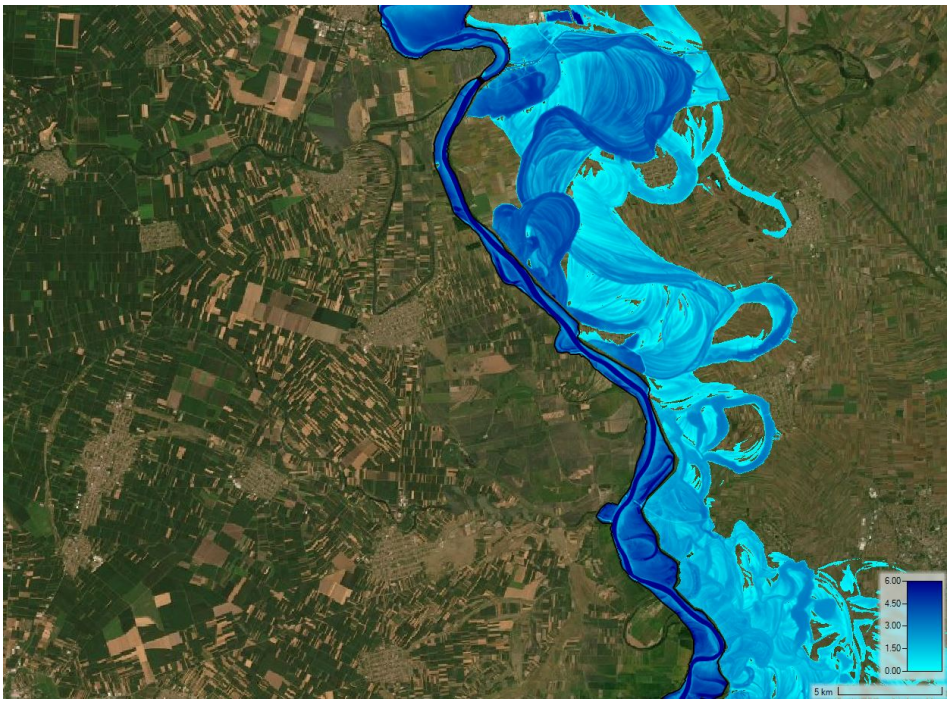

(b) 1000 year return period maximum depth for breach location E7.

Figure 5.18: Close-ups to the inundation depth maps of breach locations E6 and E7.

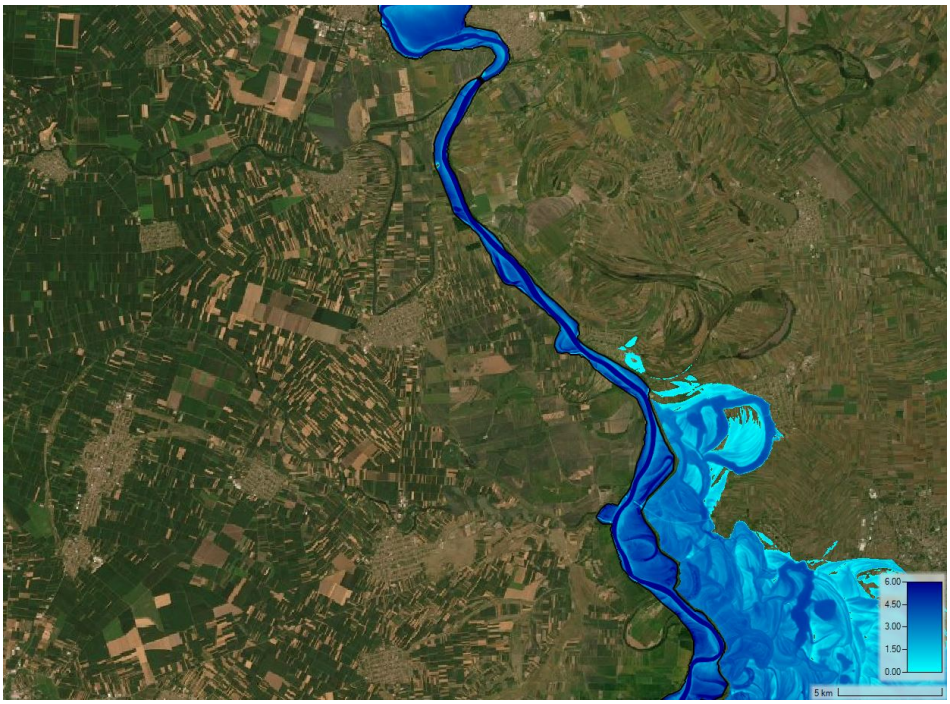

(a) 1000 year return period maximum depth for breach location E8.

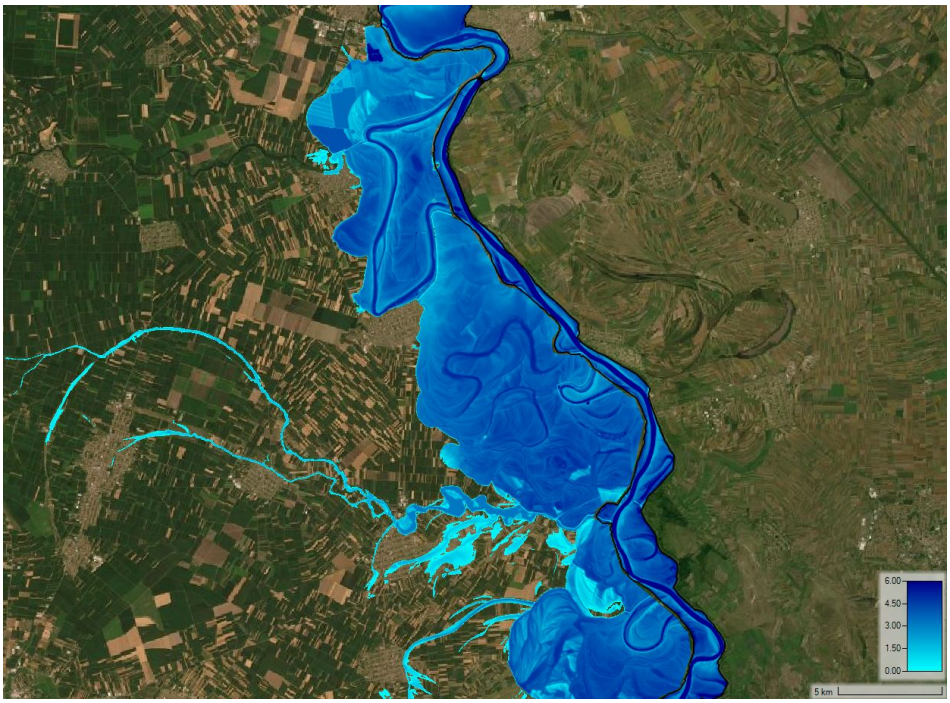

(b) 1000 year return period maximum depth for breach location W5.

Figure 5.19: Close-ups to the inundation depth maps of breach locations E8 and W5.

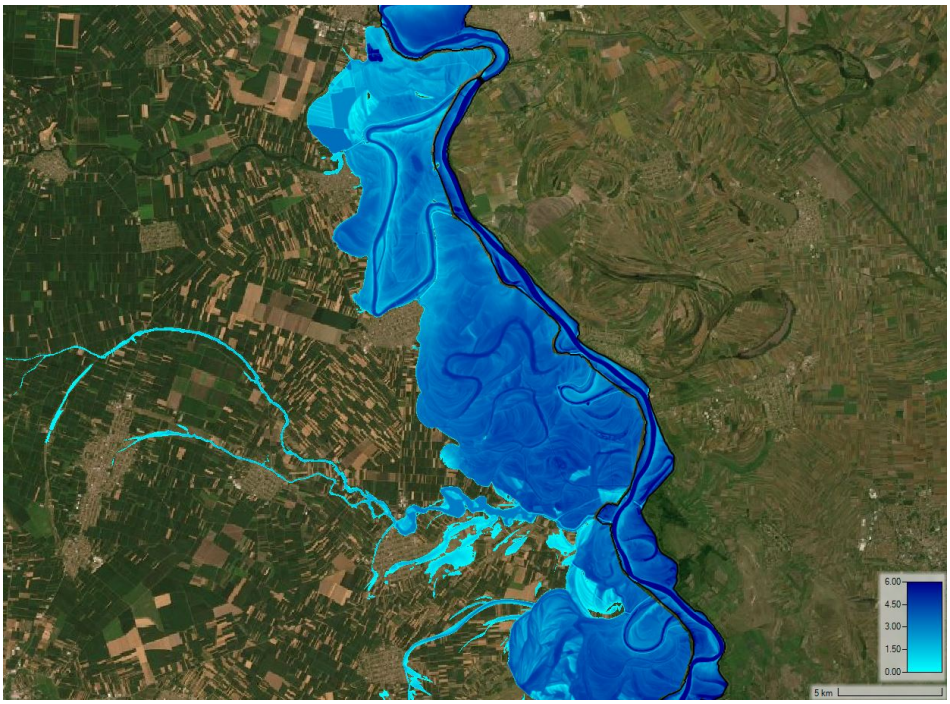

Figure 5.20: 1000 year return period maximum depth for breach location W6.

In the most downstream part of the map several things are noticeable. The inundation probability map of this area is depicted in Figure 5.21. The inundation maps of the different breach cases are found in figure 5.22.

- In this map some of the inundation caused by breaches at locations W5 and W6 can be seen. These are the cause of the beige area on the eastern side. These cause some inundation up to the edge of the beige area as here a break line exists.
- For location W7 the inundation leads to the area on the western side a overflow the break line leading to the green area south of this area. The total inundation area is similar to that of locations W5 and W6. Only the southern third has a higher water surface level compared to those cases. The water level is roughly 1 meter below the river at the breach. The green area that has flown over the break line has a very low surface level almost 7 meters below the river water level.
- For location E9 the inundation leads to the area on the eastern side. The beige area is formed by inundation from location E6 till E9. The breaklines do not prevent inundation to reach this area during the thousand year return period cases. The water surface level is roughly 2 meters lower than the level in the river. Just south of the breach location a break line exists. South of this area the water level is more than 4 meters lower than the rest of the area.

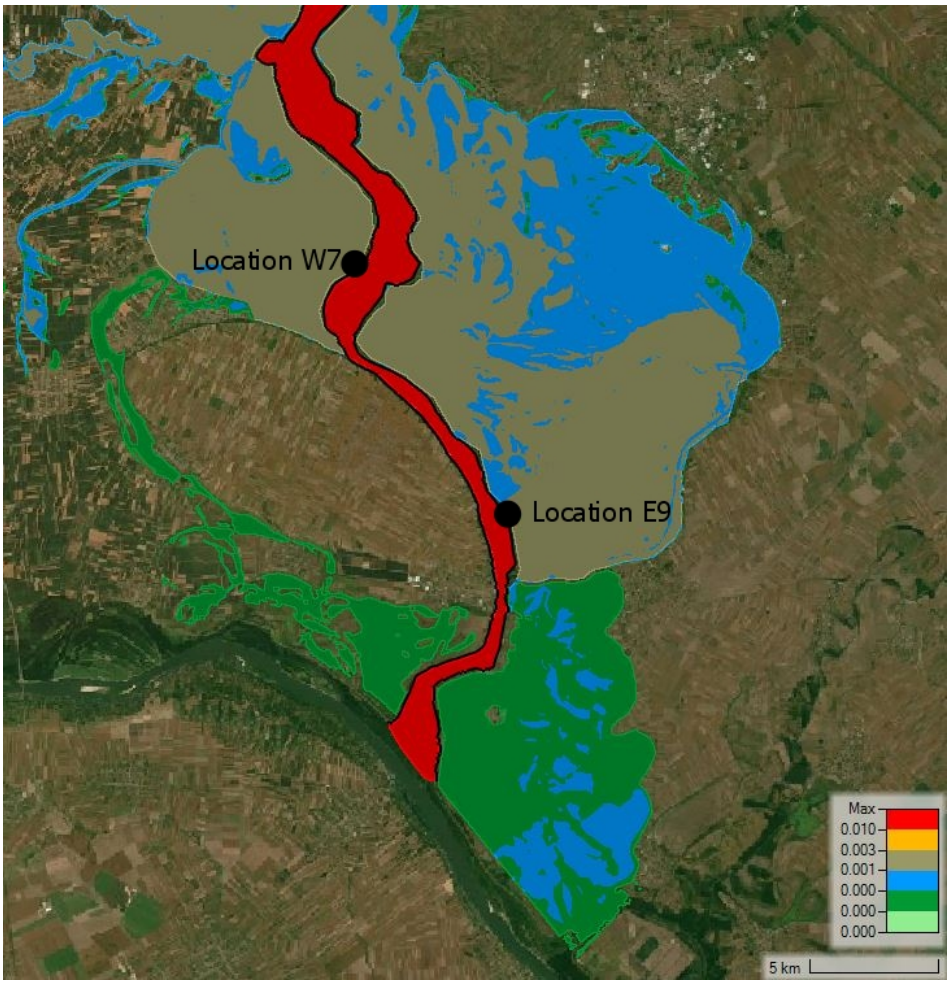

Figure 5.21: Close up of the map for breach locations E9 and W7.

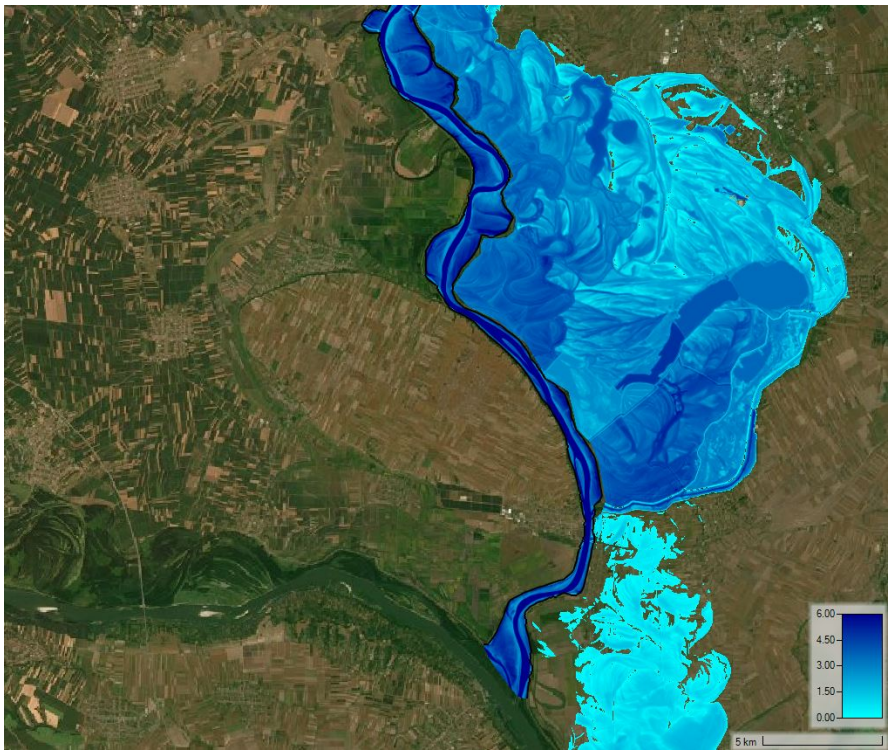

(a) 1000 year return period maximum depth for breach location E9.

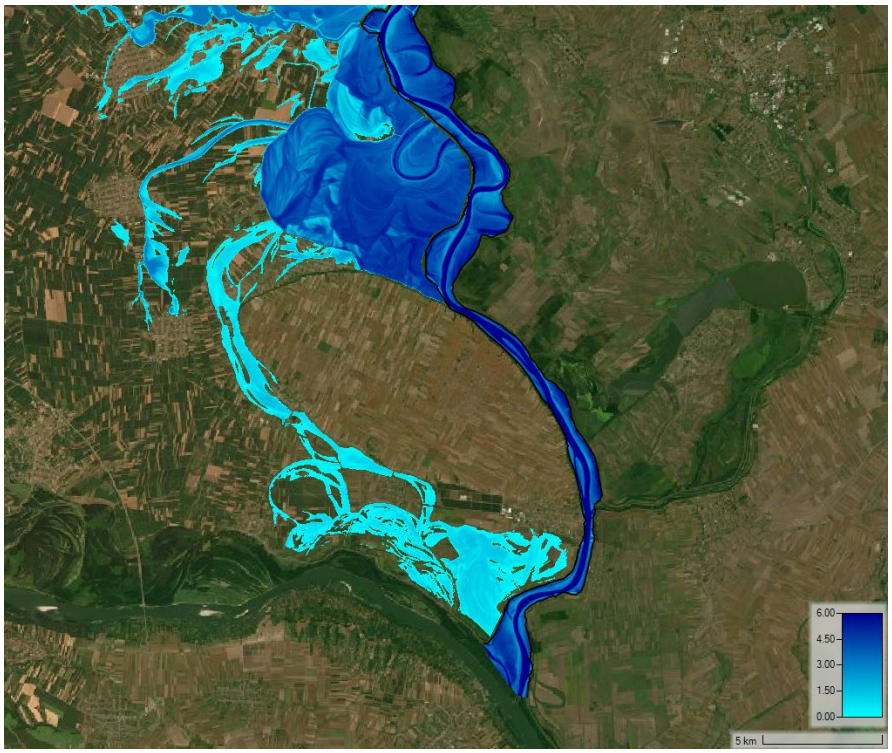

(b) 1000 year return period maximum depth for breach location W7.

Figure 5.22: Close-ups to the inundation depth maps of breach locations E9 and W7.

The previous maps show that several areas were found with a probability above 0.001 annually. An important bit of information is the expected inundation depth that corresponds with this probability. The inundation depth can be used to predict what and how much damage would be caused. This can be used to determine appropriate prevention measures.

With the help of MATLAB the inundation depth were calculated based on the results of the different relevant cases. Due to computational limitations not the whole map could be made as a single image. As only in the brown areas on the map the 0.001 annual probability is exceeded. Only these parts of the map are studied.

In Figure 5.23 the beige area seen in Figure 5.13 is studied. This is the area caused by breaches at locations E2, E3, E4 and E5. For most of the area the depth remains below a depth of 2.5 meters. Only in the lowest areas the depth increases to 4 meters. There are ditches around the farmland were the depths are larger but these are of lesser interest. Inside the river the location of the Tisa dam can be seen by the jump in depth. The potential inundation depth based on the water surface level outside of the levees is shown in Figure 5.24 and 5.25. In the potential inundation depth maps of both the studied return periods the inundation area is far larger. The depth is similarly larger.

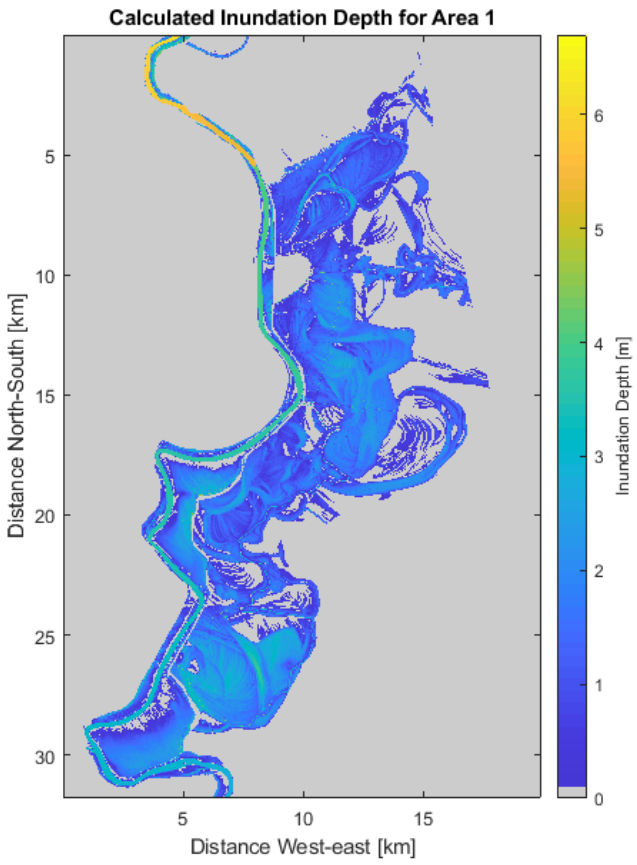

Figure 5.23: Water depths with a return period of 1000 years in the area around breach locations E2 till E5.

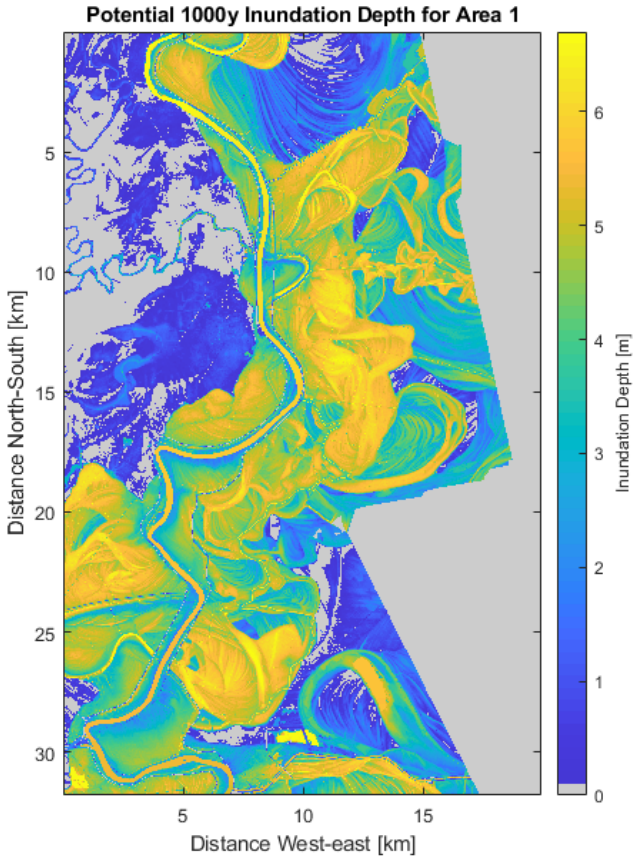

Figure 5.24: Water depths based on the 1000 year water surface elevation of the river in the area around breach locations E2 till E5.

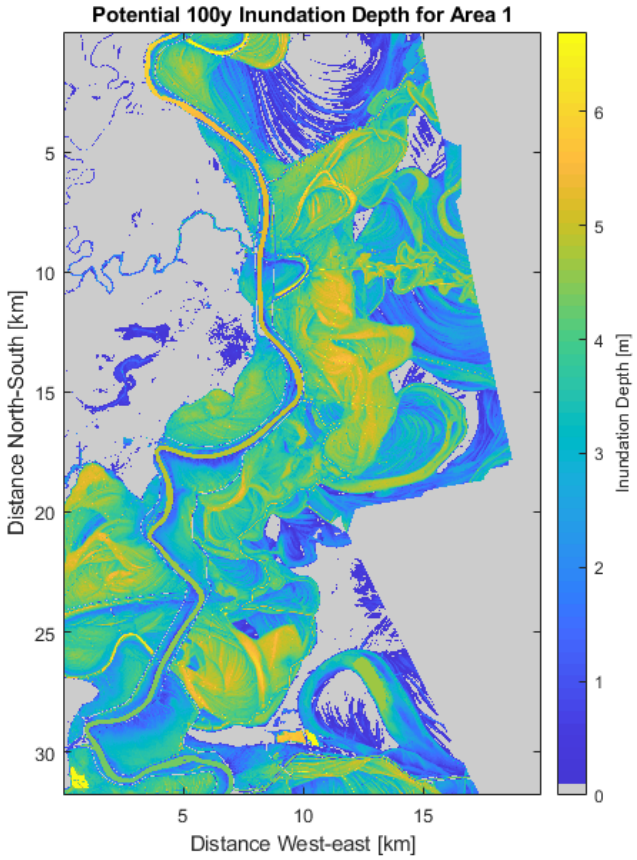

Figure 5.25: Water depths based on the 100 year water surface elevation of the river in the area around breach locations E2 till E5.

In figure 5.26 the beige area seen in figure 5.17 is studied. This is the area on the western side caused by breaches at locations W5, W6 and W7. The inundation depth varies over the floodplain but reaches a maximum of around 3 meters. Local ditches and channels lead to larger depths but these are of lesser importance. The potential inundation depth based on the water surface level outside of the levees is shown in Figure 5.27 and 5.28. The inundation extent is increased at some areas but to a smaller degree as in area 1. The inundation depths are larger over the whole inundation extent.

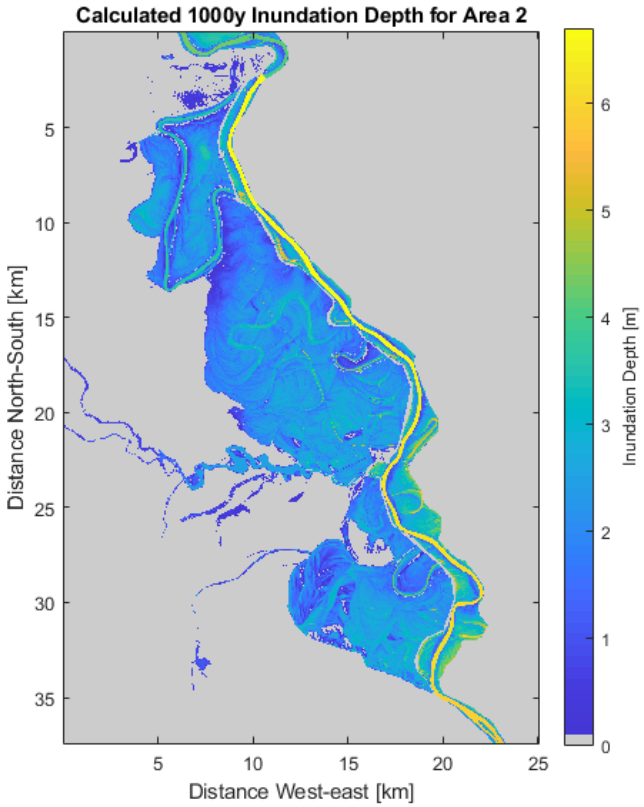

Figure 5.26: Water depths with a return period of 1000 years in the area around breach locations W4 till W6.

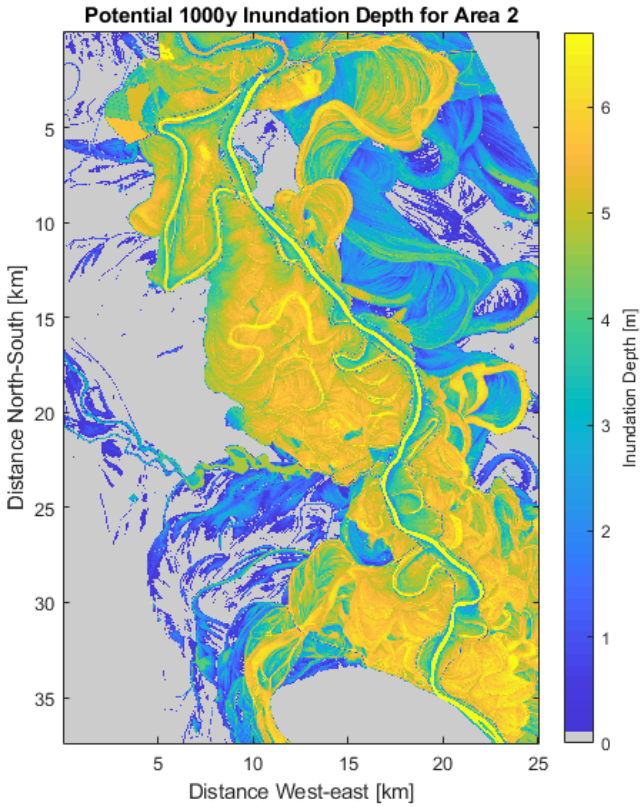

Figure 5.27: Water depths based on the 1000 year water surface elevation of the river in the area around breach locations W4 till W6.

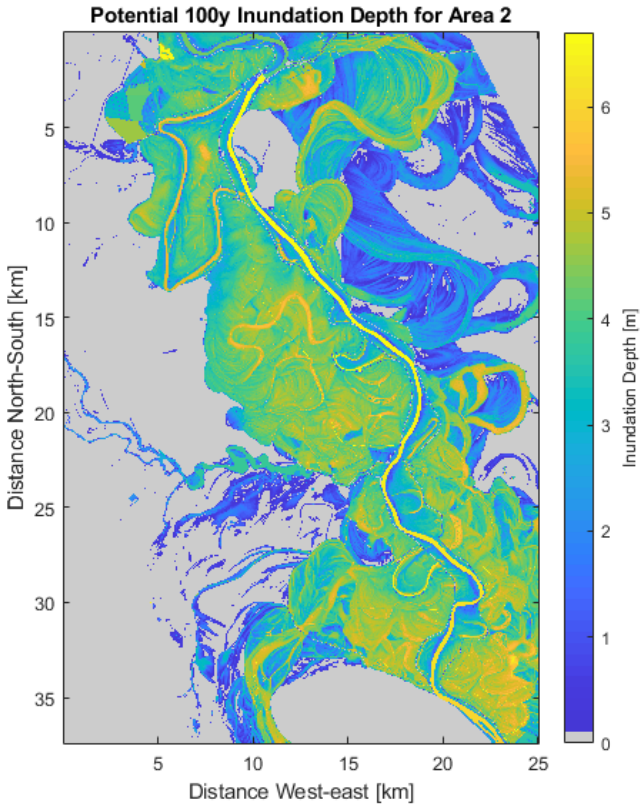

Figure 5.28: Water depths based on the 100 year water surface elevation of the river in the area around breach locations W4 till W6.

In Figure 5.29 the beige area on the eastern side of the river as seen in Figures 5.17 and 5.21 is studied. This area is caused by breaches at locations E6, E7, E8 and E9. This map shows two areas with different depths. The northern area has a maximum depth of around 2 meters and the southern area has a maximum depth of 3 meters. The presence of a break line leads to this differences. The potential inundation depth based on the water surface level outside of the levees is shown in Figure 5.30 and 5.31. The inundation extent is roughly the same as for the calculated map but the inundation depths are larger.

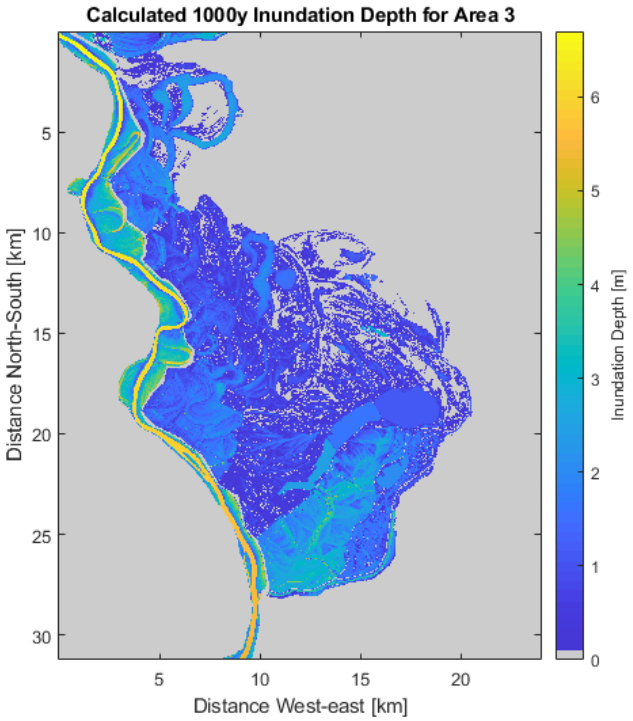

Figure 5.29: Water depths with a return period of 1000 years in the area around breach locations E6 till 9.

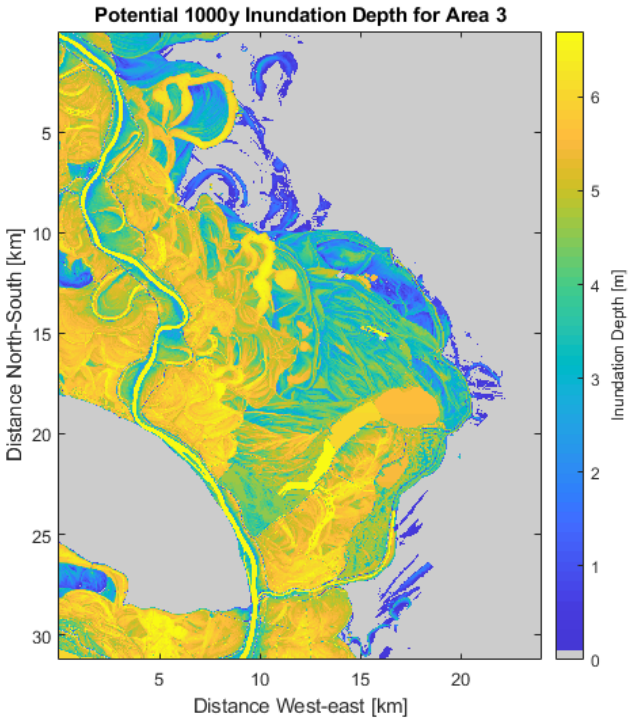

Figure 5.30: Water depths based on the 1000 year water surface elevation of the river in the area around breach locations E6 till 9..

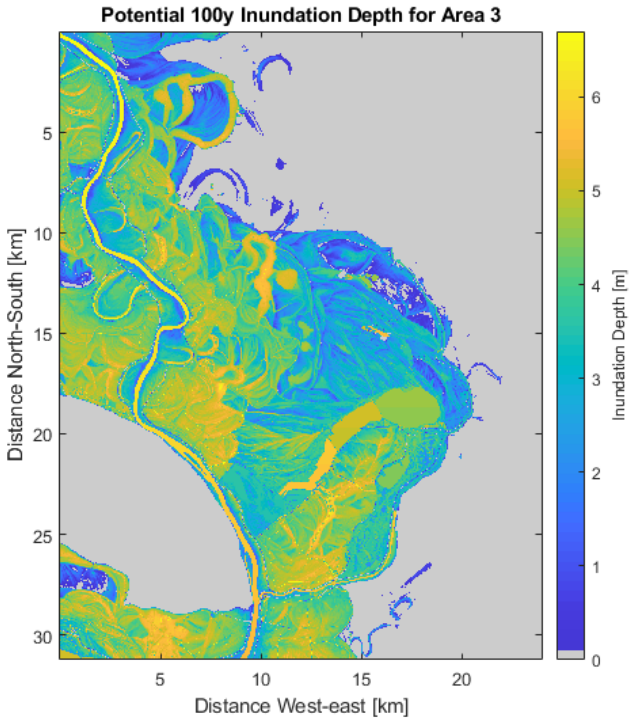

Figure 5.31: Water depths based on the 100 year water surface elevation of the river in the area around breach locations E6 till 9.

A technique commonly used in the creation of inundation maps is applying the water surface elevation from within the river to the area protected by the embankments. This can then be used to determine the potential inundation depth. Based on this technique the water surface elevation of the case with no breaches for a return period of thousand years was used to create two maps. The first map presented in Figure 5.35 shows the values based on the 1000 year return period water levels. The second map in Figure 5.36 is based on the 100 year return period. This map is very similar to the currently used maps as seen in Figure 2.7.

The difference in inundation depths is quite noticeable. Where in the previous maps the depth only reached above 3 meters at ditches or due to breaklines leading to contained areas, this map shows depths reaching above 6 meters in many different areas. The difference can be seen in Figures 5.32, 5.33 and 5.34. In the rest of the map depths of more than 4 meters are common. Another difference is that a far larger area is found to be inundated with a 0.001 annual probability.

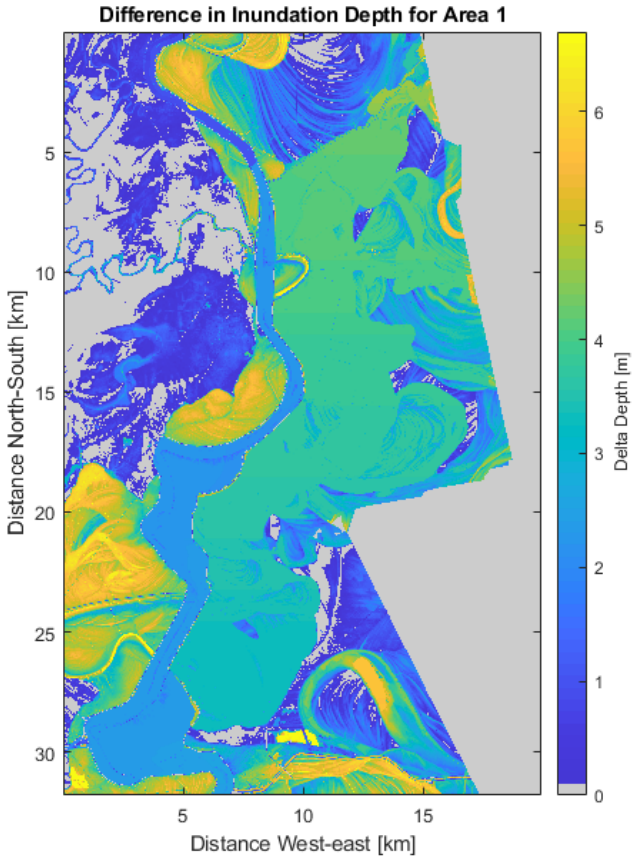

Figure 5.32: Difference inundation depth found by subtracting the calculated depths from the 1000-year potential depths for area A1.

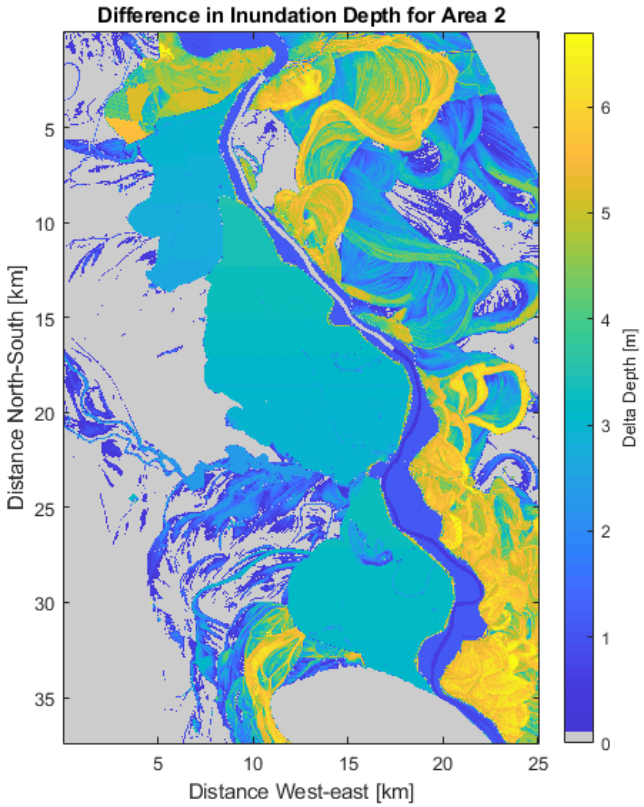

Figure 5.33: Difference inundation depth found by subtracting the calculated depths from the 1000-year potential depths for area A2.

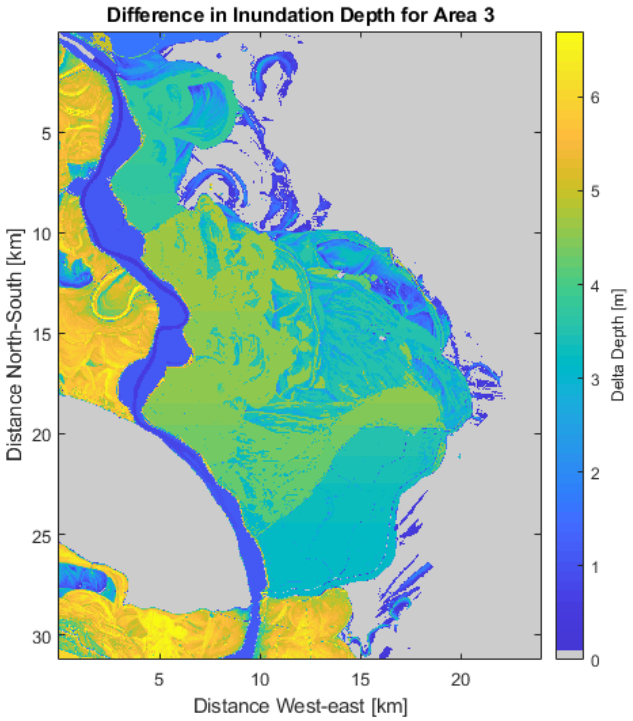

Figure 5.34: Difference inundation depth found by subtracting the calculated depths from the 1000-year potential depths for area A3.

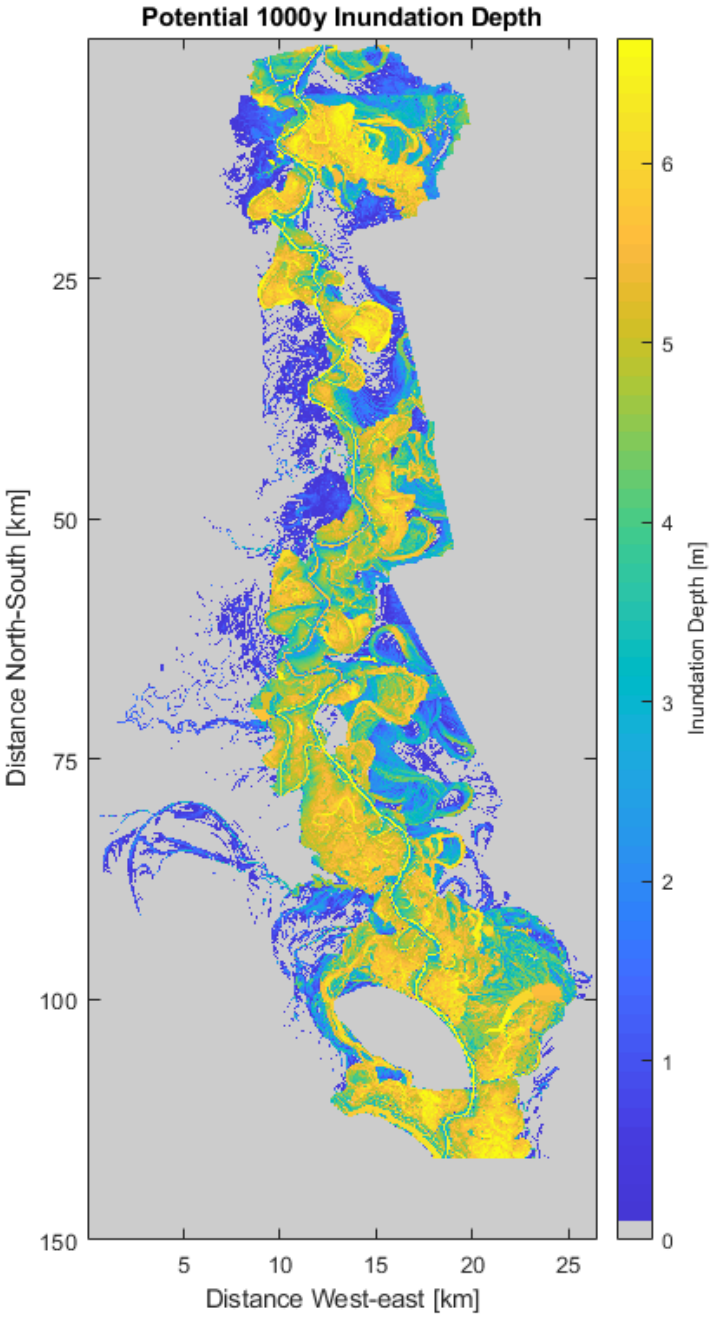

Figure 5.35: Water depths with a return period of 1000 years as found by applying the water surface elevation from outside the defences to the terrain map. With the same legend as the calculated maps.

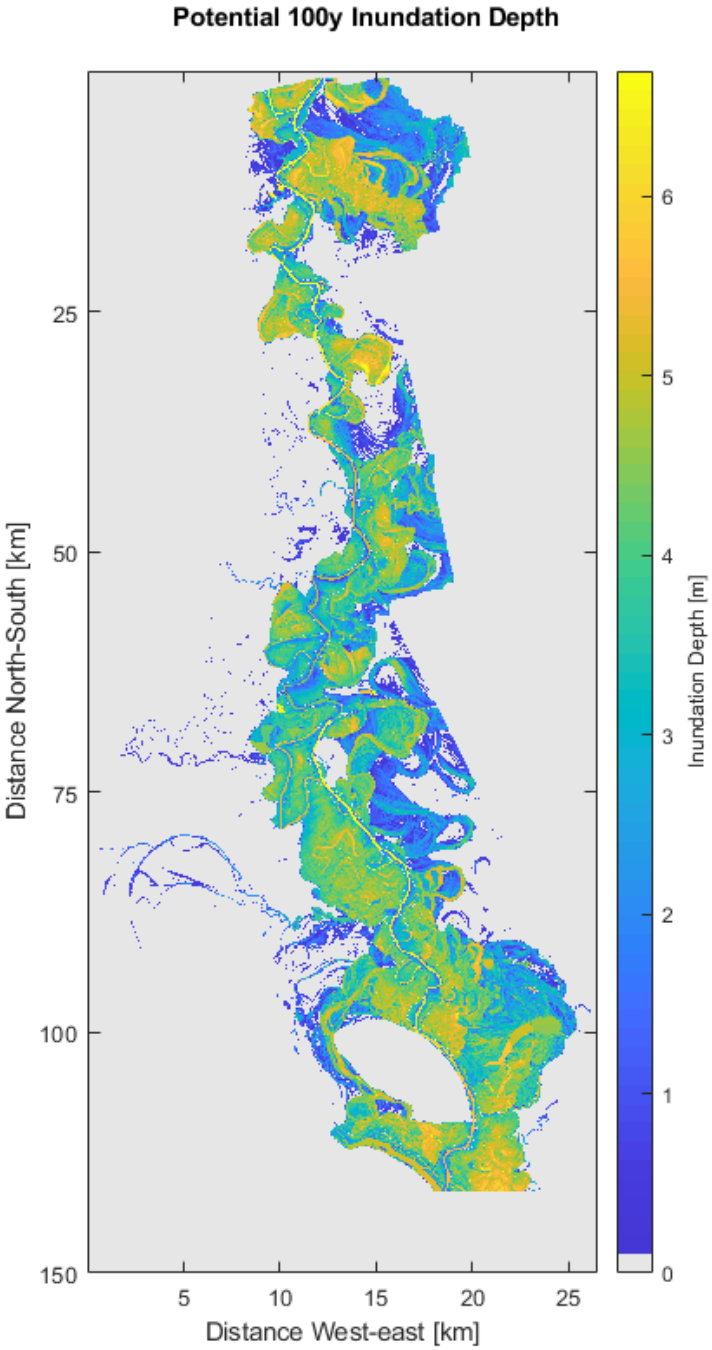

Figure 5.36: Water depths with a return period of 100-years as found by applying the water surface elevation from outside the defences to the terrain map. With the same legend as the calculated maps.

5.5 Discussion

In this section the results presented in the previous section are discussed and related to the purpose of this study. The original study question associated with this chapter was:

How could this method be applied in practice to a real-world situation and what can be learned from this for application to other riverine areas around the world?

First the focus is on the application of the method to the real-world case in this chapter. The inundation probabilities could be calculated with a similar method as in the more idealized model. The estimation of the failure rate of the flood defences is the most important part of this step. This can be based on historical data but this can be difficult to acquire due to lack of information. Conservative estimates based on comparable riverine area can be used to provide a realistic but conservative value for the failure probabilities.

The setup of the one-dimensional and two dimensional models turns out to be relatively easy in HEC-RAS. The schematization of the river was made more difficult due to data compatibility. For more accurate results the different data sets should be based on the same projection. The resolution of the DTM is of interest as the presence of line elements does affect the size of the inundated area in several cases. It is possible that satellite data with a coarse resolution will lead to an overestimation of the inundation area. Local obstacles such as line elements will not be visible in the data. These could be added manually but great care should be used to account for viaducts and local dips in roads as these provide opportunity for the water to pass the obstacle. The presence of local obstacles can lead to larger inundation depths is some areas. In other areas the obstacles lead to a smaller inundation depth as of a limited amount of water can reach these areas. These influences on the results make line elements very valuable for the prediction of inundation depths and extents.

The limited data makes it difficult to reliable calculate the exact probabilities of inundation in an area. But a lot can be learned from differences between areas. On the logarithmic inundation probability maps it can be seen that the differences are limited. This can be expected if the levee failure probability is the same for each part. If more historical and design data was available, it could be possible to assign different failure probabilities to the different sections of the levee.

The water surface levels do show that the bathtub approach leads to some degree of overestimation in large areas of the floodplain. In turn the lower water surface levels cause the inundation to be limited by local line element or raised areas. Based on these results the bathtub method should be used with care in large floodplains.

5.5.1 Application to other riverine area

To apply this method to other riverine areas several key points can be identified. For the initial schematization of the one-dimensional river model two sets of data are required. River cross sections and some data on the roughness in the channel. The presence of line structures such as dams or bridges can also be important if these lead to a change in the flow behaviour. For the two dimensional grids of the floodplain, a DEM or DTM of reasonable (1-5m) resolution is needed. For the levees a estimation of the failure probability is needed in combination with data on the levee height. The development of a breaching probability from this data is not very difficult. The reliability of these prediction can be low. Historical data is not always a good indication of the current strength of the flood defences. Maintenance and climate change can lead to different real failure probabilities than could be expected from historical records.

Another aspect is the inundation depth and extent that is predicted by this method. The bathtub method provides an easily achieved but often very conservative prediction. By modeling the river with more detail and including levee height and some form of breaching simulation more realistic values can be found. The presence of an obstacle can limit the inundation area a lot as was seen in the results of this method. The simulation can also show that the total inundation volume is far smaller that the bathtub approximation assumes. The question is whether the extra effort in using this method over the bathtub method is worth it for all riverine areas.

If the potential floodplains near the river are very small as for example in a valley, the bathtub approximation may hold quite well. Especially if the floodplain is split by line element such as roads. If the area is large enough, the water surface level over the floodplain is lower than the water surface level over the river. It depends on the actual water level over the floodplain whether the difference matter. The difference in damages between one or two meters of inundation depth is not always very relevant. It depends on the local terrain and intentions of the study.

Chapter 6

Conclusion

The overarching objective of this scientific study has been to explore the development of a method to integrate probabilistic failure of flood defenses into flood maps based on limited data. The Tisa River in Serbia has been used as a case study. This chapter presents the findings of the study by answering the research question provided in section 1.3. Also several recommendations for further study are provided.

The main findings of this rapport are related to the difference in results between including the flood defences explicitly, but with some uncertainties, or not including them. Not including flood defenses results in a good prediction of the worst case scenario. Based on conservative estimates for the reliability of the levees and modeling of breaches, a more realistic prediction of the consequences of a breach can be presented. Both reducing the inundation area and depth with a noticeable amount and providing more insight for policy makers.

6.1 Research questions

1. What are the current methods of including the effects of levees and the possible failure of these structures in flood inundation maps?

- On a global scale, flood hazard mapping does not make use of explicit probabilistic modeling for flood defenses. The effects of flood defences are included either, as a fully deterministic effect or not included at all. The low resolution of the maps also makes it difficult to model the effects of local changes in the terrain. This often results in very conservative estimates of flood hazards.
- The resolution of flood hazard maps on a regional scale are often higher, allowing for better insight into flood characteristics such as extent and depth. The probabilistic modelling of flood defenses is not used commonly due to lack of data. The exact parameters of the defenses as well of the underground are often unknown.
- There exist flood mapping efforts in which the flood defenses are included with a probabilistic approach. From two of these projects, it becomes clear that a large amount of data and knowledge is required. This would not be available in all riverine areas around the world.

2. What is the structure of a simplified method to include the likelihood of levee failure into flood inundation maps considering an environment with limited available field data?

- The first component of the flood hazard mapping strategy is the breaching of the levees. By using historical data of a comparable defense system as a basis, a breaching probability can be estimated. With use of the binomial distribution, it is possible to use the breaching probability of a single segment to determine the failure probability of a larger section of the defenses.

- The breaching of the levee itself also needs to be modeled. For the idealized model this was done based on conservative estimates of the material parameters. The development of the breach was assumed to complete in 25 hours and reach a theoretical maximum.
- The second component is the modeling of the river and flood plains. A normative estimation of the discharge and the river geometry is required to model a reasonable flood wave. The floodplain can be modeled with an assumed roughness.
- To determine a probabilistic value for the inundation hazard in a floodplain a multiple different scenarios need to be ran. Were other methods only need a single run per return period, for this method a large number of runs was needed.

3. What can be learned from applying this method to various idealized cases about the importance of taking into account levee failure in flood inundation mapping?

This idealized model was based on the Tisa river basin in Serbia. By taking a comparable length, slope and geometry the the real river a 1D model for the river was made. The discharges were based on measurements preformed near Senta, roughly halfway the studied stretch of the real river. The floodplains were designed with a similar slope alongside the river and a slight slope increasing the surface level further away from the river. To represent the size of the real floodplains a width of $20km$ was used.

The results were studied by creating maps of inundation probability for specific inundation depths. And maps and graphs of inundation depth for specific return periods. These can than be compared to the results of bathtub approximation results for this idealized model.

- The idealized model was based on the characteristics of the Tisa river in Serbia. As the floodplain also follows the slope of the river to some extent this was added in this model. With this the viability of the bathtub approximation can be studied for a large floodplain.
- The influence of different parameters were tested by changing them one-by-one in the idealized model. To study the influence of the variations the results were presented as inundation areas and inundation maps. These can be compared to potential areas and depths based created by removing the flood defenses from the model.
- In addition to this the ratios between the volume that is available for flooding, the volume that can flow trough the breach and the volume required to fill the flood plain are studied. Based on the ratio between the available volume and the breaching volume the limiting factor can be predicted. By studying the ratio between the breaching volume and the potential volume required to fill the floodplain, the potential overestimation of the bathtub approximation be estimated.
- Based on the ratios it was found that the total amount of water that could be stored was far larger that the volume that could enter the floodplain. Only by reducing the size of the floodplain significantly this volume could be reached. The other variations did lead to an increase in breaching volume but not to such extents.
- In most of the currently used methods studied in Chapter 2, a bathtub approximation is applied. Hereby it is assumed that the water surface level inside of the defenses will be the same as outside the defenses. This is then used to determine the potential inundation area and depth. Based on the maps created from the idealized model these methods lead to very conservative predictions for the Tisa River parameter settings. It is recognized that the introduction of the failure probability of flood defenses comes with uncertainties. However, the difference is so large that the bathtub approximation should be used with care. Only in specific circumstance with relatively small floodplains, the bathtub approximation hold well according to this analysis.

4. How could this method be applied in practice to a real-world situation and what can be learned from this for application to other riverine areas around the world?

For this application to a real-world riverine area, a case study was made of the Tisa river basin in Serbia. Based on river geometry and a DTM generated with LIDAR technology a model of this area was developed in HEC-RAS.

- The application of the strategy to a real-world scenario requires various input data. Historic records for the river discharge and geometric data on the river are required to model the case study area. The defenses have been simplified to a height and a breaching probability. This probability can be determined based on comparable food defense systems. The geometry of the floodplains has been set with a terrain model. The presences of obstacles in this terrain are of noticeable influence in the resulting inundation.
- The limited data leads to a degree of uncertainty in the resulting flood hazard maps. But the magnitude and distribution of the inundation probabilities provide insight in the behaviour of the flooding. The annual inundation probabilities are found below one in thousand for a large part of the floodplain. Even the parts most at risk, the annual probabilities remain below 0.01. The inundation depth reaches significant values of over a meter in almost all affected areas but only for with a return period of a thousand years.
- The currently used flood maps have been created using a bathtub approximation and the flooded protected areas have been indicated "potential flood zones". In comparison to these maps, the results of the modeling exercise in this study show a far smaller inundation area. It remains important to take into account the uncertainty of these results. The potential inundation approach of the existing flood maps do provide an upper limit scenario. The modeling results herein suggest that these maps are very conservative mainly due to the very large and flat floodplains surrounding the Tisa.

In most currently used strategies the defenses are not explicitly included. This new modeling strategy does not replace these methods completely but provide the ability to differentiate the inundation hazards in different parts of the floodplain. The Tisa River has been used solely as case study area to test this new modeling strategy. By providing more reasonable predictions of inundation extent and depth, policy makers are better informed to develop preventive measures. The findings of this study can serve as good grounds for further methodological considerations in the improvement of flood hazard mapping assessments in similar river basins in the future.

6.2 Recommendations

Based on the results of the study and the lessons learned during the study, several recommendations are made:

- The failure probabilities were estimated based on historical failure rates of a comparable flood defence system. It would be of interest to collect this data for a far larger amount of defence systems from all over the world to provide a basis for more accurate estimates.
- The use of historical data on breaching of flood defenses could be replaced with actual probabilistic modeling based on the parameters of the levees. The data required for this is often not available or unreliable. It would be very interesting and useful, if a method to survey this data in a cost-effective and reliable way could be found.

- In the strategy presented in this study the breaching of the defenses were to a great extent idealized. A more in-depth implementation on the exact development of breaches could reduce the uncertainty of the modeling results.
- This study focused on low-land rivers with large floodplains. The results indicate that the bathtub approximation might hold better for rivers in mountainous or hilly regions. Further study would be required to confirm this hypothesis.
- This study focuses on flooding caused by rivers. For the application to coastal flooding several aspects of the strategy would require changing. The probability is not only depended on storm surge and breaching probabilities but also on tides. Coastal flooding is also more likely to cause multiple simultaneous failures.

Bibliography

1. Hohenbichler, M. & Rackwitz, R. First-order concepts in system reliability. *Structural safety* **1,** 177–188 (1982).
2. Vrouwenvelder, A., Steenbergen, H. & Slijkhuis, K. *Theoriehandleiding PC-Ring Deel A: Mechanismebeschrijvingen* (1999).
3. Vrouwenvelder, A., Steenbergen, H. & Slijkhuis, K. *Theoriehandleiding PC-Ring Deel B: statistische modellen* (1999).
4. Verheij, H. & Van der Knaap, F. Modification breach growth model in HIS-OM. *WL— Delft Hydraulics Q* **3299,** 2002 (2002).
5. Witteveen+Bos. *Decimeringshoogten TMR2006* (2006).
6. Irish, J. L., Resio, D. T. & Ratcliff, J. J. The influence of storm size on hurricane surge. *Journal of Physical Oceanography* **38,** 2003–2013 (2008).
7. Waterdienst, R. Decimeringshoogten TMR2006. *RW1708-1/zeir/006, Witteveen+ Bos, Deventer, Netherlands* (2008).
8. Alphen, J. V., Martini, F., Loat, R., Slomp, R. & Passchier, R. Flood risk mapping in Europe, experiences and best practices. *Journal of Flood Risk Management* **2,** 285–292 (2009).
9. Gauzer, B. Scenario Analysis-The Impact of Extreme Precipitation Patterns. *T22-07-03* (2009).
10. IPET. *Performance Evaluation of the New Orleans and Southeast Louisiana Hurricane Protection System;Volume VIII – Engineering and Operational Risk and Reliability Analysis* (2009).
11. Masutomi, Y., Inui, Y., Takahashi, K. & Matsuoka, Y. Development of highly accurate global polygonal drainage basin data. *Hydrological Processes: An International Journal* **23,** 572–584 (2009).
12. *Onzekerheden in overstromingsrisico's* (2009).
13. Yamazaki, D., Kanae, S., Kim, H. & Oki, T. A physically based description of floodplain inundation dynamics in a global river routing model. *Water Resources Research* **47** (2011).
14. Pappenberger, F., Dutra, E., Wetterhall, F. & Cloke, H. L. Deriving global flood hazard maps of fluvial floods through a physical model cascade. *Hydrology and Earth System Sciences* **16,** 4143–4156 (2012).
15. VNK2 project office. *Flood risk in the Netherlands VNK2: The method in brief* (2012).
16. Ward, P. J. *et al.* Assessing flood risk at the global scale: model setup, results, and sensitivity. *Environmental research letters* **8,** 044019 (2013).
17. Vergouwe, R. *The National Flood Risk Analysis for the Netherlands* (2014).
18. Rudari, R. *et al. Improvement of the global flood model for the GAR 2015* (2015). `https://www.preventionweb.net/english/hyogo/gar/2015/en/bgdocs/risk-section/CIMAFoundation,%20ImprovementoftheGlobalFloodModelfortheGAR15.pdf`.
19. Sampson, C. C. *et al.* A high-resolution global flood hazard model. *Water resources research* **51,** 7358–7381 (2015).
20. Dottori, F. *et al.* Development and evaluation of a framework for global flood hazard mapping. *Advances in water resources* **94,** 87–102 (2016).

21. Kolaković, S., Fabian, J., Kovács, S., Budinski, L. & Stipić, M. Exploitation of documented historical floods for achieving better flood defense. *Advances in Meteorology* **2016** (2016).

22. Pakoksung, K. & Takagi, M. Digital elevation models on accuracy validation and bias correction in vertical. *Modeling Earth Systems and Environment* **2,** 11 (2016).

23. Scussolini, P. *et al.* FLOPROS: an evolving global database of flood protection standards. *Natural Hazards and Earth System Sciences* **16,** 1049–1061 (2016).

24. Betsholtz, A. & Nordlöf, B. *Potentials and limitations of 1D, 2D and coupled 1D-2D flood modelling in HEC-RAS A case study on Höje river* (Division of Water Resources Engineering Department of Building & Environmental Technology Lund University, 2017).

25. Yamazaki, D., Ikeshima, D., *et al. MERIT DEM: A new high-accuracy global digital elevation model and its merit to global hydrodynamic modeling* in *AGU fall meeting abstracts* **2017** (2017), H12C–04.

26. Bernhofen, M. V. *et al.* A first collective validation of global fluvial flood models for major floods in Nigeria and Mozambique. *Environmental Research Letters* **13,** 104007 (2018).

27. Deltaris. *SOBEK user manual* (2018).

28. Eptisa Servicios de Ingeniería S.L. *Flood Risk Management Plan for the Sava River Basin - Draft* (2018).

29. Kumbier, K., Carvalho, R. C., Vafeidis, A. T. & Woodroffe, C. D. Investigating compound flooding in an estuary using hydrodynamic modelling: a case study from the Shoalhaven River, Australia. *Natural Hazards and Earth System Sciences* **18,** 463–477 (2018).

30. *Syllabus River Dynamics 1* (2018).

31. Wallemacq, P. & House, R. *Economic losses, poverty & disasters: 1998-2017* (2018).

32. Almukhtar, S., Migliozzi, B., Schwartz, J. & Williams, J. *The great flood of 2019: A complete picture of a slow motion disaster* `https://www.nytimes.com/interactive/2019/09/11/us/midwest-flooding.html` (2021).

33. Barnard, P. L. *et al.* Dynamic flood modeling essential to assess the coastal impacts of climate change. *Scientific reports* **9,** 1–13 (2019).

34. COWI. *Reports and maps: flood hazard and risk Priority area 1 - Tisa river basin* (2019).

35. Didier, D. *et al.* Multihazard simulation for coastal flood mapping: Bathtub versus numerical modelling in an open estuary, Eastern Canada. *Journal of Flood Risk Management* **12,** e12505 (2019).

36. OSHA. *Eastern Africa Region: Regional Flood Snapshot (November 2019)* (2019). `https://reliefweb.int/report/south-sudan/eastern-africa-region-regional-flood-snapshot-november-2019`.

37. Paprotny, D., Morales-Nápoles, O., Vousdoukas, M. I., Jonkman, S. & Nikulin, G. Accuracy of pan-European coastal flood mapping. *Journal of Flood Risk Management* **12,** e12459 (2019).

38. Aerts, J. P., Uhlemann-Elmer, S., Eilander, D. & Ward, P. J. Comparison of estimates of global flood models for flood hazard and exposed gross domestic product: a China case study. *Natural Hazards and Earth System Sciences* **20,** 3245–3260 (2020).

39. Kool, J. J., Kanning, W. & Jonkman, S. N. The influence of deviating conditions on levee failure rates. *Journal of Flood Risk Management,* e12784 (2022).

40. WMO, W. M. O. *Global Runoff Data Centre* `https://www.bafg.de/GRDC/EN/Home/homepage_node.html` (2021).

Appendix A

Tables of BRR and BFR values

In this appendix the values for the discharge volume for the different breach combinations are summarized. The resulting BRR and BFR are also presented here. These tables are presented for the sake of completion and to show the underlaying results that are used to create the scatter plots in figure 4.5.

Breach	10y	100y	1000y	Breach	1000y	Breach	1000y
1	$3.3311 * 10^{-8}$	$3.3311 * 10^{-8}$	$1.6153 * 10^{-9}$	123	$1.0228 * 10^{-9}$	269	$1.4326 * 10^{-9}$
2	$3.3762 * 10^{-8}$	$3.3762 * 10^{-8}$	$1.6346 * 10^{-9}$	124	$1.0514 * 10^{-9}$	278	$1.4632 * 10^{-9}$
3	$3.4085 * 10^{-8}$	$3.4085 * 10^{-8}$	$1.6492 * 10^{-9}$	125	$1.0724 * 10^{-9}$	279	$1.4828 * 10^{-9}$
4	$3.4256 * 10^{-8}$	$3.4256 * 10^{-8}$	$1.6597 * 10^{-9}$	126	$1.0880 * 10^{-9}$	289	$1.5305 * 10^{-9}$
5	$3.4331 * 10^{-8}$	$3.4331 * 10^{-8}$	$1.6673 * 10^{-9}$	127	$1.1026 * 10^{-9}$	345	$1.0556 * 10^{-9}$
6	$3.4232 * 10^{-8}$	$3.4232 * 10^{-8}$	$1.6699 * 10^{-9}$	128	$1.1200 * 10^{-9}$	346	$1.0864 * 10^{-9}$
7	$6.0483 * 10^{-7}$	$6.0483 * 10^{-7}$	$2.1353 * 10^{-8}$	129	$1.1375 * 10^{-9}$	347	$1.1191 * 10^{-9}$
8	$3.1321 * 10^{-8}$	$3.1321 * 10^{-8}$	$1.4666 * 10^{-9}$	134	$1.1772 * 10^{-9}$	348	$1.1547 * 10^{-9}$
9	$2.7267 * 10^{-8}$	$2.7267 * 10^{-8}$	$1.2801 * 10^{-9}$	135	$1.1960 * 10^{-9}$	349	$1.1857 * 10^{-9}$
12		$6.9680 * 10^{-8}$	$1.1425 * 10^{-9}$	136	$1.2099 * 10^{-9}$	356	$1.2159 * 10^{-9}$
13		$7.5864 * 10^{-8}$	$1.2558 * 10^{-9}$	137	$1.2231 * 10^{-9}$	357	$1.2469 * 10^{-9}$
14		$8.0519 * 10^{-8}$	$1.3376 * 10^{-9}$	138	$1.2391 * 10^{-9}$	358	$1.2807 * 10^{-9}$
15		$8.4072 * 10^{-8}$	$1.3984 * 10^{-9}$	139	$1.2551 * 10^{-9}$	359	$1.3095 * 10^{-9}$
16		$8.6821 * 10^{-8}$	$1.4447 * 10^{-9}$	145	$1.2832 * 10^{-9}$	367	$1.3368 * 10^{-9}$
17		$8.8973 * 10^{-8}$	$1.4833 * 10^{-9}$	146	$1.2964 * 10^{-9}$	368	$1.3698 * 10^{-9}$
18		$9.0854 * 10^{-8}$	$1.5237 * 10^{-9}$	147	$1.3090 * 10^{-9}$	369	$1.3978 * 10^{-9}$
19		$9.3109 * 10^{-8}$	$1.5637 * 10^{-9}$	148	$1.3243 * 10^{-9}$	378	$1.4406 * 10^{-9}$
23		$7.0848 * 10^{-8}$	$1.1600 * 10^{-9}$	149	$1.3394 * 10^{-9}$	379	$1.4657 * 10^{-9}$
24		$7.7181 * 10^{-8}$	$1.2755 * 10^{-9}$	156	$1.3593 * 10^{-9}$	389	$1.5303 * 10^{-9}$
25		$8.1929 * 10^{-8}$	$1.3585 * 10^{-9}$	157	$1.3719 * 10^{-9}$	456	$1.0692 * 10^{-9}$
26		$8.5542 * 10^{-8}$	$1.4203 * 10^{-9}$	158	$1.3875 * 10^{-9}$	457	$1.1189 * 10^{-9}$
27		$8.8340 * 10^{-8}$	$1.4735 * 10^{-9}$	159	$1.4024 * 10^{-9}$	458	$1.1699 * 10^{-9}$
28		$9.0950 * 10^{-8}$	$1.5294 * 10^{-9}$	167	$1.4189 * 10^{-9}$	459	$1.2113 * 10^{-9}$
29		$9.4011 * 10^{-8}$	$1.5810 * 10^{-9}$	168	$1.4358 * 10^{-9}$	467	$1.2519 * 10^{-9}$
34		$7.1697 * 10^{-8}$	$1.1725 * 10^{-9}$	169	$1.4514 * 10^{-9}$	468	$1.3004 * 10^{-9}$
35		$7.8180 * 10^{-8}$	$1.2903 * 10^{-9}$	178	$1.4724 * 10^{-9}$	469	$1.3394 * 10^{-9}$
36		$8.3024 * 10^{-8}$	$1.3754 * 10^{-9}$	179	$1.4898 * 10^{-9}$	478	$1.4014 * 10^{-9}$
37		$8.6741 * 10^{-8}$	$1.4506 * 10^{-9}$	189	$1.5238 * 10^{-9}$	479	$1.4344 * 10^{-9}$
38		$9.0462 * 10^{-8}$	$1.5278 * 10^{-9}$	234	$1.0419 * 10^{-9}$	489	$1.5235 * 10^{-9}$
39		$9.4653 * 10^{-8}$	$1.5949 * 10^{-9}$	235	$1.0709 * 10^{-9}$	567	$1.1131 * 10^{-9}$
45		$7.2353 * 10^{-8}$	$1.1823 * 10^{-9}$	236	$1.0925 * 10^{-9}$	568	$1.1859 * 10^{-9}$
46		$7.8980 * 10^{-8}$	$1.3038 * 10^{-9}$	237	$1.1141 * 10^{-9}$	569	$1.2418 * 10^{-9}$
47		$8.4034 * 10^{-8}$	$1.4118 * 10^{-9}$	238	$1.1390 * 10^{-9}$	578	$1.3365 * 10^{-9}$
48		$8.9375 * 10^{-8}$	$1.5187 * 10^{-9}$	239	$1.1622 * 10^{-9}$	579	$1.3812 * 10^{-9}$
49		$9.5096 * 10^{-8}$	$1.6074 * 10^{-9}$	245	$1.1985 * 10^{-9}$	589	$1.5077 * 10^{-9}$
56		$7.2817 * 10^{-8}$	$1.1922 * 10^{-9}$	246	$1.2180 * 10^{-9}$	678	$1.2218 * 10^{-9}$
57		$7.9840 * 10^{-8}$	$1.3495 * 10^{-9}$	247	$1.2381 * 10^{-9}$	679	$1.2880 * 10^{-9}$
58		$8.7458 * 10^{-8}$	$1.4990 * 10^{-9}$	248	$1.2613 * 10^{-9}$	689	$1.4751 * 10^{-9}$
59		$9.5272 * 10^{-8}$	$1.6189 * 10^{-9}$	249	$1.2827 * 10^{-9}$	789	$1.3833 * 10^{-9}$
67		$7.3520 * 10^{-8}$	$1.2456 * 10^{-9}$	256	$1.3061 * 10^{-9}$		
68		$8.4295 * 10^{-8}$	$1.4607 * 10^{-9}$	257	$1.3256 * 10^{-9}$		
69		$9.5010 * 10^{-8}$	$1.6279 * 10^{-9}$	258	$1.3481 * 10^{-9}$		
78		$7.8725 * 10^{-8}$	$1.3510 * 10^{-9}$	259	$1.3687 * 10^{-9}$		
79		$9.3882 * 10^{-8}$	$1.6142 * 10^{-9}$	267	$1.3893 * 10^{-9}$		
89		$8.6943 * 10^{-8}$	$1.4614 * 10^{-9}$	268	$1.4120 * 10^{-9}$		

Table A.1: Breaching volumes in $[m^3]$ for the different model scenarios

Breach	10y	100y	1000y	Breach	1000y	Breach	1000y
1	0.2096	0.2794	0.3100	123	0.1963	269	0.2749
2	0.2124	0.2833	0.3137	124	0.2017	278	0.2808
3	0.2145	0.2863	0.3165	125	0.2058	279	0.2845
4	0.2155	0.2884	0.3185	126	0.2088	289	0.2937
5	0.2160	0.2899	0.3199	127	0.2116	345	0.2025
6	0.2154	0.2904	0.3204	128	0.2149	346	0.2085
7	0.0381	0.0408	0.0410	129	0.2183	347	0.2147
8	0.1971	0.2619	0.2814	134	0.2259	348	0.2216
9	0.1716	0.2200	0.2456	135	0.2295	349	0.2275
12		0.2002	0.2192	136	0.2322	356	0.2333
13		0.2180	0.2410	137	0.2347	357	0.2393
14		0.2314	0.2567	138	0.2378	358	0.2457
15		0.2416	0.2683	139	0.2408	359	0.2513
16		0.2495	0.2772	145	0.2462	367	0.2565
17		0.2557	0.2846	146	0.2488	368	0.2628
18		0.2611	0.2924	147	0.2512	369	0.2682
19		0.2676	0.3001	148	0.2541	378	0.2764
23		0.2036	0.2226	149	0.2570	379	0.2812
24		0.2218	0.2447	156	0.2608	389	0.2936
25		0.2354	0.2607	157	0.2633	456	0.2052
26		0.2458	0.2725	158	0.2662	457	0.2147
27		0.2539	0.2827	159	0.2691	458	0.2245
28		0.2614	0.2935	167	0.2723	459	0.2324
29		0.2702	0.3034	168	0.2755	467	0.2402
34		0.2060	0.2250	169	0.2785	468	0.2495
35		0.2247	0.2476	178	0.2825	469	0.2570
36		0.2386	0.2639	179	0.2859	478	0.2689
37		0.2493	0.2784	189	0.2924	479	0.2752
38		0.2600	0.2932	234	0.1999	489	0.2923
39		0.2720	0.3060	235	0.2055	567	0.2136
45		0.2079	0.2269	236	0.2096	568	0.2276
46		0.2270	0.2502	237	0.2138	569	0.2383
47		0.2415	0.2709	238	0.2186	578	0.2564
48		0.2568	0.2914	239	0.2230	579	0.2650
49		0.2733	0.3084	245	0.2300	589	0.2893
56		0.2093	0.2288	246	0.2337	678	0.2344
57		0.2294	0.2590	247	0.2376	679	0.2471
58		0.2513	0.2876	248	0.2420	689	0.2831
59		0.2738	0.3106	249	0.2461	789	0.2654
67		0.2113	0.2390	256	0.2506		
68		0.2422	0.2803	257	0.2544		
69		0.2730	0.3124	258	0.2587		
78		0.2262	0.2592	259	0.2626		
79		0.2698	0.3097	267	0.2666		
89		0.2499	0.2804	268	0.2709		

Table A.2: BRR ratios for the different model scenarios

Breach	10y	100y	1000y	Breach	1000y	Breach	1000y
1	0.0369	0.0652	0.0869	123	0.0550	269	0.0771
2	0.0374	0.0661	0.0880	124	0.0566	278	0.0787
3	0.0378	0.0668	0.0887	125	0.0577	279	0.0798
4	0.0379	0.0673	0.0893	126	0.0585	289	0.0824
5	0.0380	0.0677	0.0897	127	0.0593	345	0.0568
6	0.0379	0.0678	0.0899	128	0.0603	346	0.0585
7	0.0067	0.0095	0.0115	129	0.0612	347	0.0602
8	0.0347	0.0611	0.0789	134	0.0633	348	0.0621
9	0.0302	0.0514	0.0689	135	0.0644	349	0.0638
12		0.0467	0.0615	136	0.0651	356	0.0654
13		0.0509	0.0676	137	0.0658	357	0.0671
14		0.0540	0.0720	138	0.0667	358	0.0689
15		0.0564	0.0752	139	0.0675	359	0.0705
16		0.0582	0.0777	145	0.0690	367	0.0719
17		0.0597	0.0798	146	0.0698	368	0.0737
18		0.0609	0.0820	147	0.0704	369	0.0752
19		0.0625	0.0841	148	0.0713	378	0.0775
23		0.0475	0.0624	149	0.0721	379	0.0789
24		0.0518	0.0686	156	0.0731	389	0.0823
25		0.0550	0.0731	157	0.0738	456	0.0575
26		0.0574	0.0764	158	0.0747	457	0.0602
27		0.0593	0.0793	159	0.0755	458	0.0630
28		0.0610	0.0823	167	0.0764	459	0.0652
29		0.0631	0.0851	168	0.0773	467	0.0674
34		0.0481	0.0631	169	0.0781	468	0.0700
35		0.0524	0.0694	178	0.0792	469	0.0721
36		0.0557	0.0740	179	0.0802	478	0.0754
37		0.0582	0.0781	189	0.0820	479	0.0772
38		0.0607	0.0822	234	0.0561	489	0.0820
39		0.0635	0.0858	235	0.0576	567	0.0599
45		0.0485	0.0636	236	0.0588	568	0.0638
46		0.0530	0.0702	237	0.0599	569	0.0668
47		0.0564	0.0760	238	0.0613	578	0.0719
48		0.0600	0.0817	239	0.0625	579	0.0743
49		0.0638	0.0865	245	0.0645	589	0.0811
56		0.0488	0.0642	246	0.0655	678	0.0657
57		0.0536	0.0726	247	0.0666	679	0.0693
58		0.0587	0.0807	248	0.0679	689	0.0794
59		0.0639	0.0871	249	0.0690	789	0.0744
67		0.0493	0.0670	256	0.0703		
68		0.0565	0.0786	257	0.0713		
69		0.0637	0.0876	258	0.0725		
78		0.0528	0.0727	259	0.0737		
79		0.0630	0.0869	267	0.0748		
89		0.0583	0.0786	268	0.0760		

Table A.3: BFR ratios for the different model scenarios

Appendix B

Detailed model outputs for evaluation

In this appendix the result are collected of the different variations used in chapter 4. For each of the variations the wet feet maps, the plots of the exceedance water levels of the various cross section and the scatter plots of the BRR and BFR are presented. The base setup for fragility curve 2 is included for comparison.

B.1 Breach depth outputs

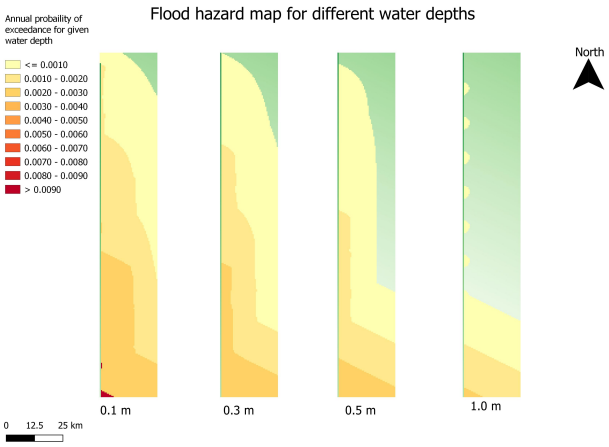

(a) Base setup for FC2

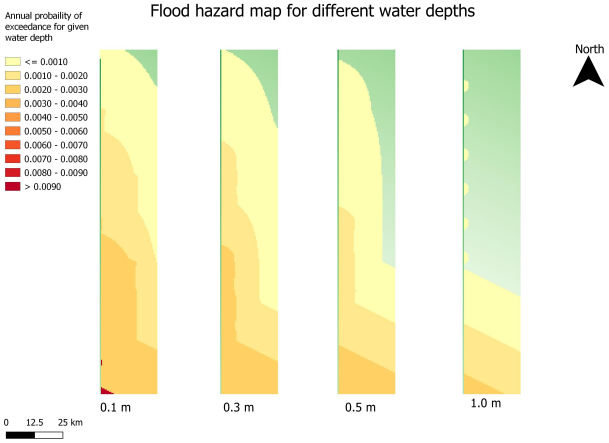

(b) $Z_b = -5m$ setup

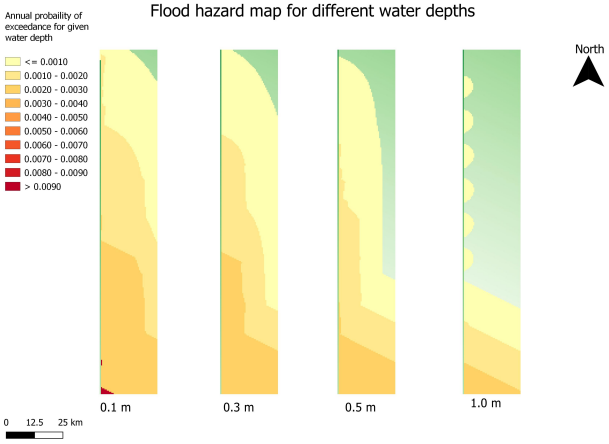

(c) $Z_b = -10m$ setup

Figure B.1: Wet feet maps for the base setup and the setups with a increased breaching depth.

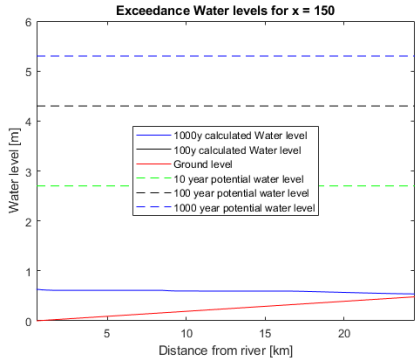

(a) Base setup at X = 150

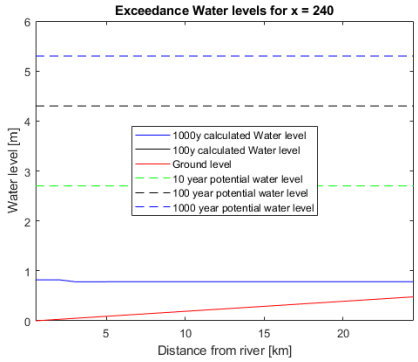

(b) Base setup at X = 240

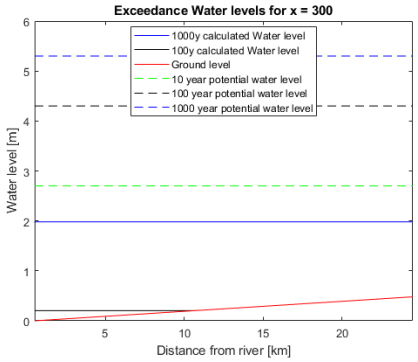

(c) Base setup at X = 300

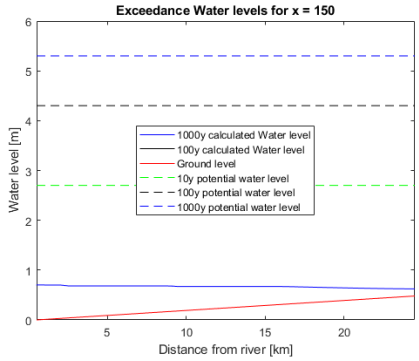

(d) $Z_b = -5m$ setup at X = 150

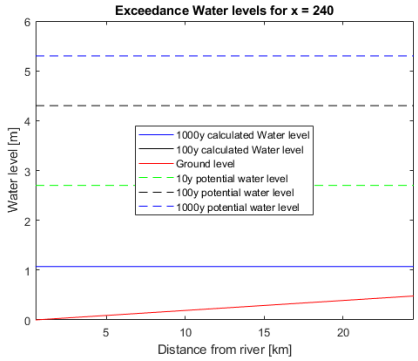

(e) $Z_b = -5m$ setup at X = 240

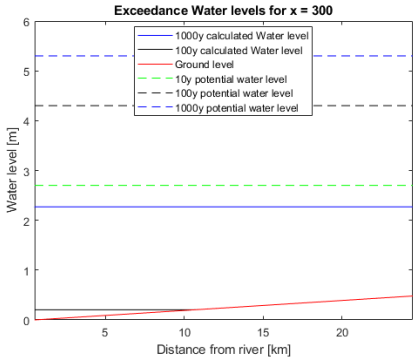

(f) $Z_b = -5m$ setup at X = 300

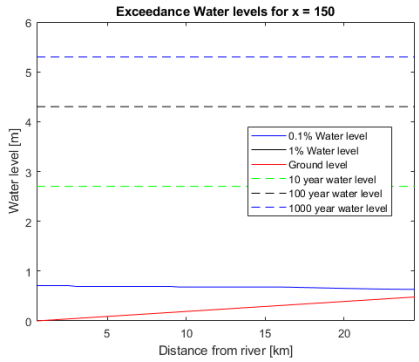

(g) $Z_b = -10m$ setup at X = 150

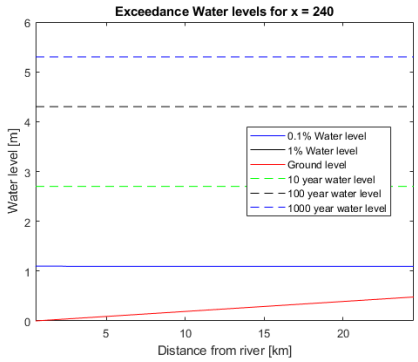

(h) $Z_b = -10m$ setup at X = 240

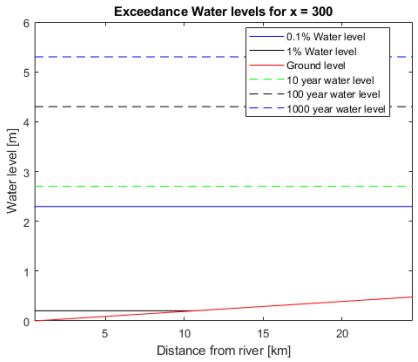

(i) $Z_b = -10m$ setup at X = 300

Figure B.2: Plots of 1000 year and 100 year return period exceedance water levels for the increased breach depth setups, along the west-east cross sections at 75km, 120km and 150km downstream from the begin point

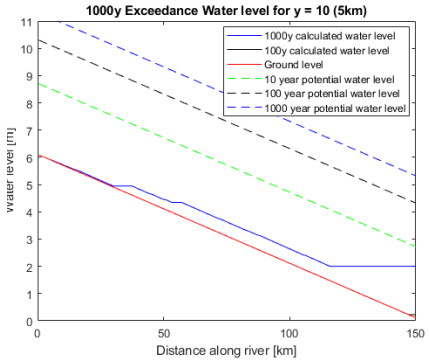

(a) Base setup at Y = 10

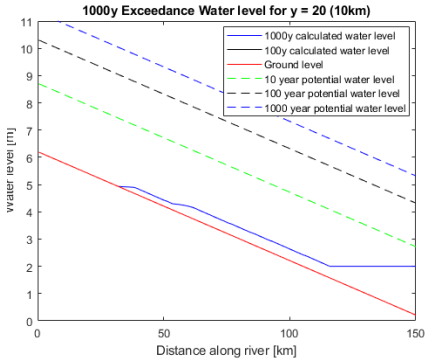

(b) Base setup at Y = 20

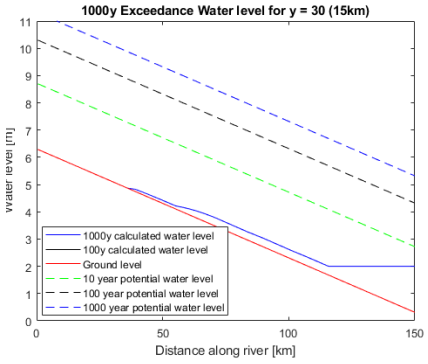

(c) Base setup at Y = 30

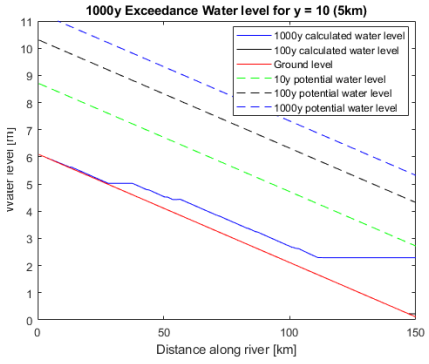

(d) $Z_b = -5m$ setup at Y = 10

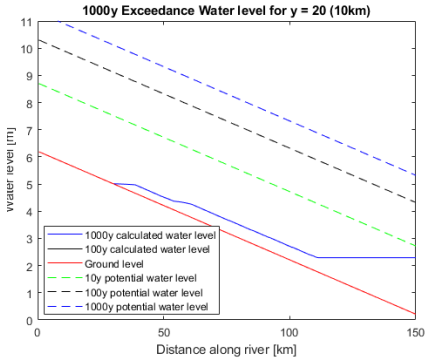

(e) $Z_b = -5m$ setup at Y = 20

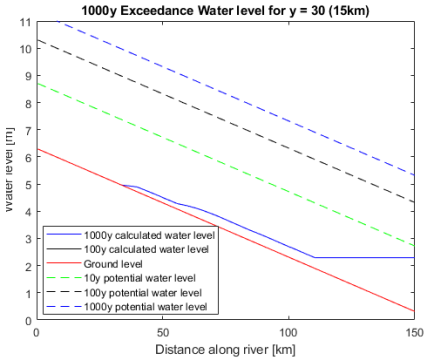

(f) $Z_b = -5m$ setup at Y = 30

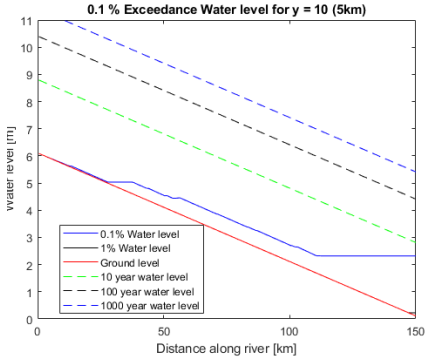

(g) $Z_b = -10m$ setup at Y = 10

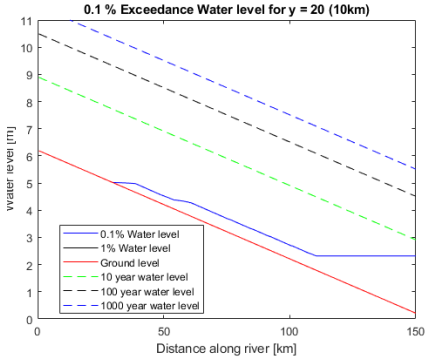

(h) $Z_b = -10m$ setup at Y = 20

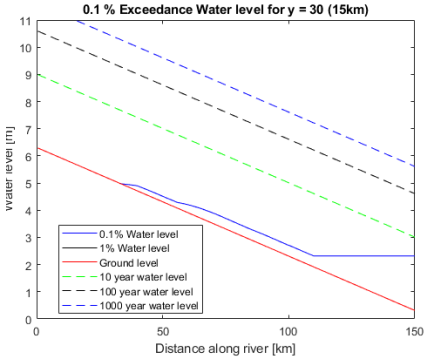

(i) $Z_b = -10m$ setup at Y = 30

Figure B.3: Plots of 1000 year and 100 year return period exceedance water levels for the breach depth setups, along the North-South cross sections for 5km, 10km and 15km away from the river

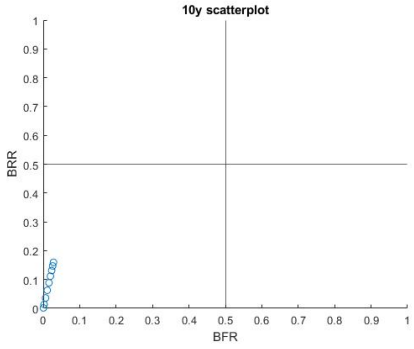

(a) Base setup scatter plot for 10y return period

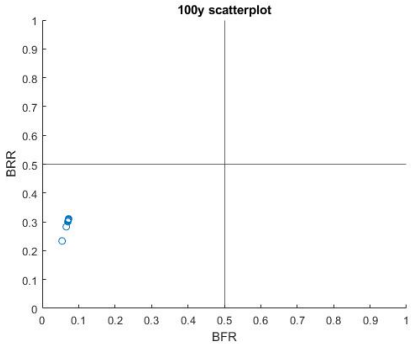

(b) Base setup scatter plot for 100y return period

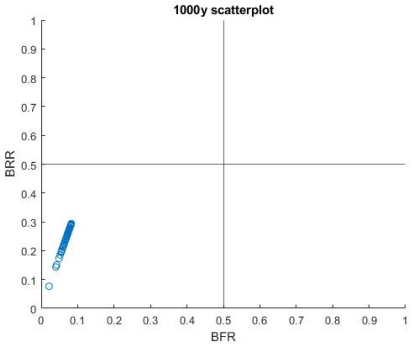

(c) Base setup scatter plot for 1000y return period

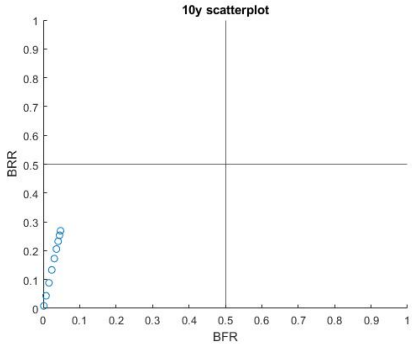

(d) $Z_b = -5m$ setup for 10y return period

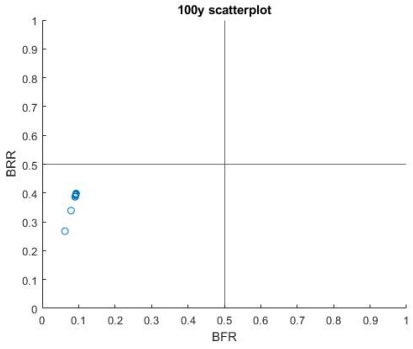

(e) $Z_b = -5m$ setup for 100y return period

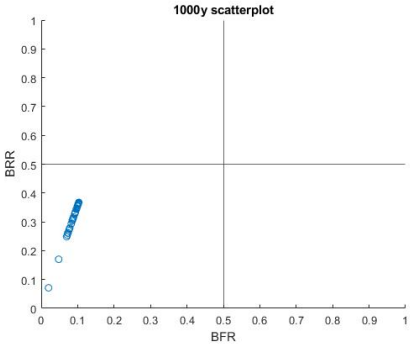

(f) $Z_b = -5m$ setup for 1000y return period

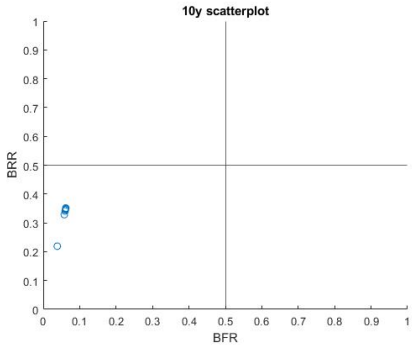

(g) $Z_b = -10m$ setup for 10y return period

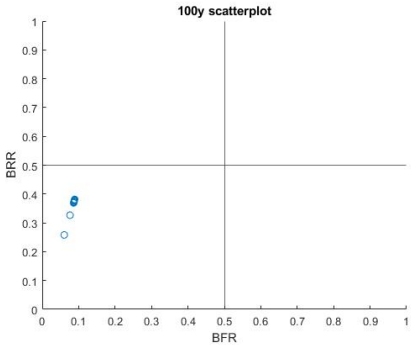

(h) $Z_b = -10m$ setup for 100y return period

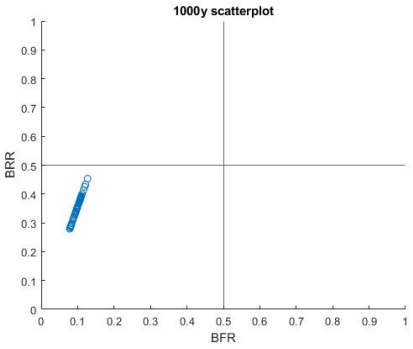

(i) $Z_b = -10m$ setup for 1000y return period

Figure B.4: Scatter plots of the BFR and BRR ratios for the Base setup and the setups for a breach depth increased by $5m$ and $10m$.

B.2 Floodplain width outputs

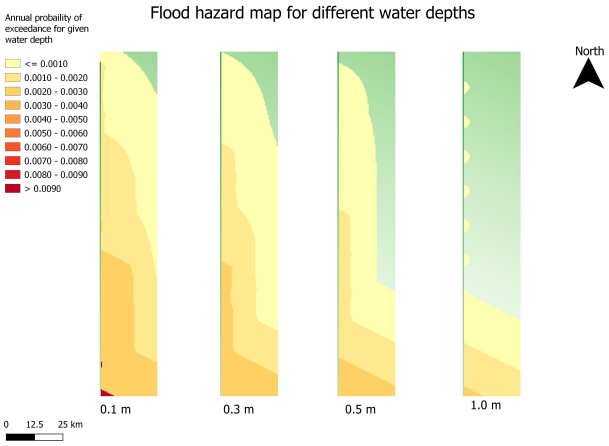

(a) Base setup for FC2

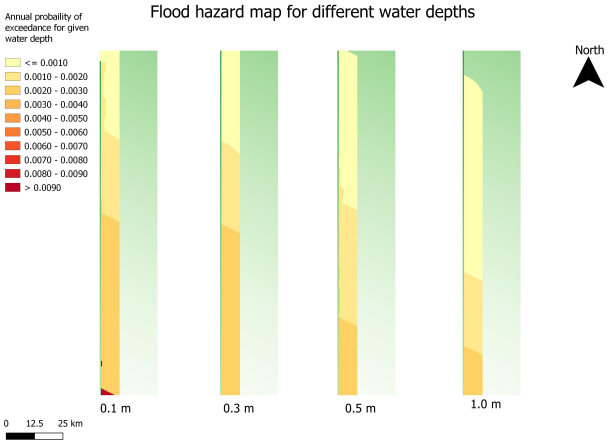

(b) 8km floodplain width setup for FC2

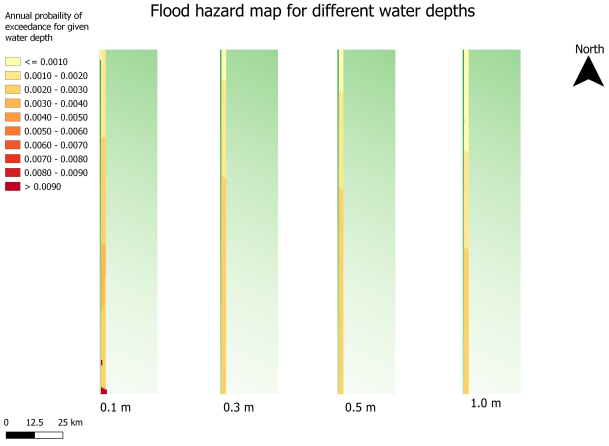

(c) 2km floodplain width setup for FC2

Figure B.5: Wet feet maps for the base setup and the setups with reduced width of the flood plain.

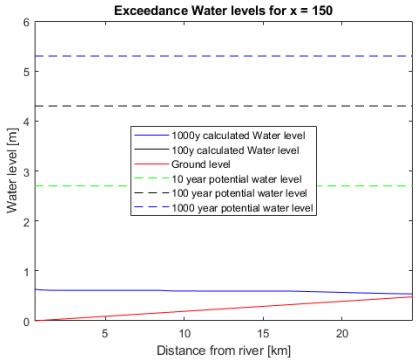

(a) Base setup at X = 150

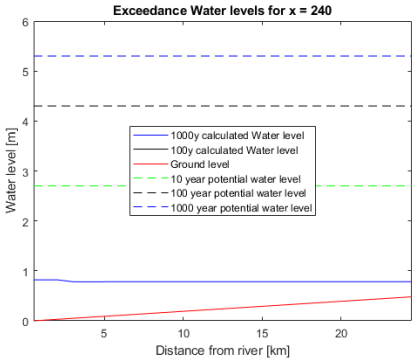

(b) Base setup at X = 240

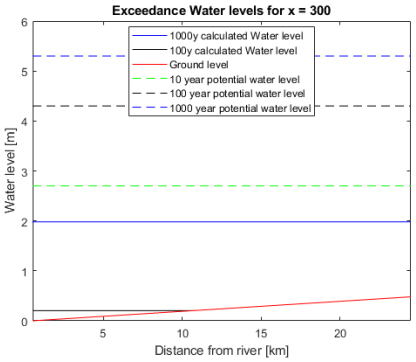

(c) Base setup at X = 300

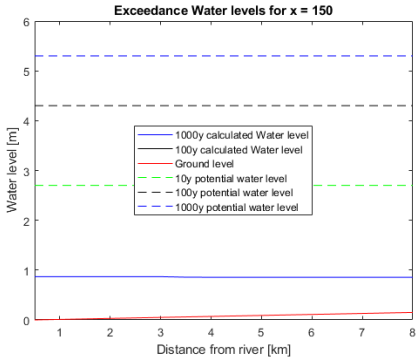

(d) 8km floodplain width setup at X = 150

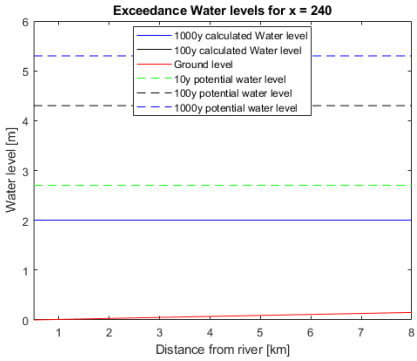

(e) 8km floodplain width setup at X = 240

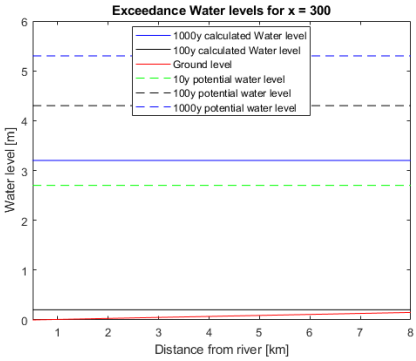

(f) 8km floodplain width setup at X = 300

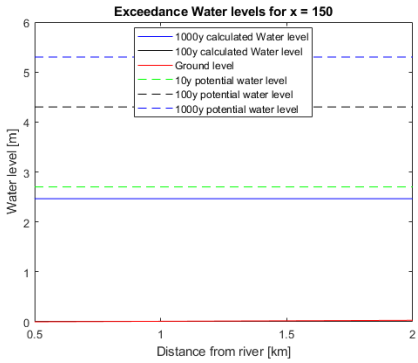

(g) 2km floodplain width setup at X = 150

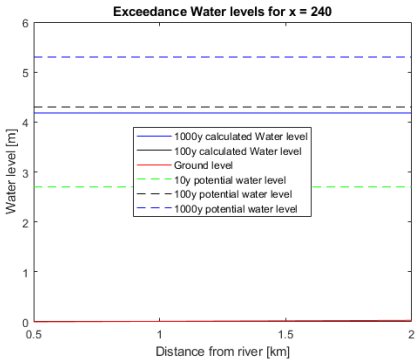

(h) 2km floodplain width setup at X = 240

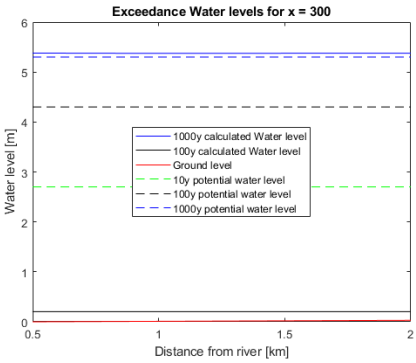

(i) 2km floodplain width setup at X = 300

Figure B.6: Plots of 1000 year return period exceedance water levels along the West-East Axis for 75km, 120km and 150km away from the northern boundary.

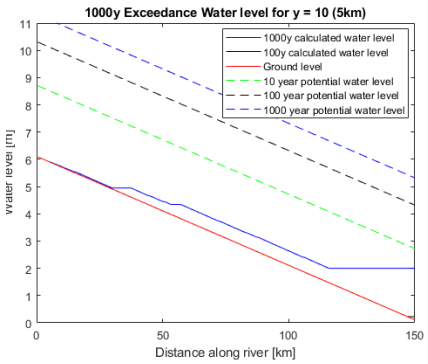

(a) Base setup at Y = 10

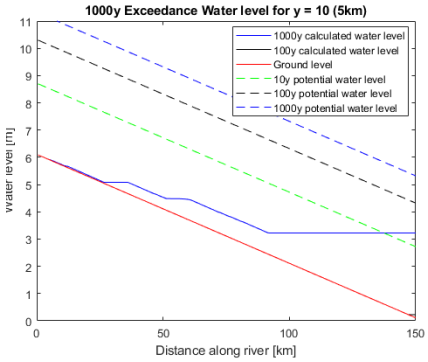

(b) 8km floodplain width setup at Y = 10

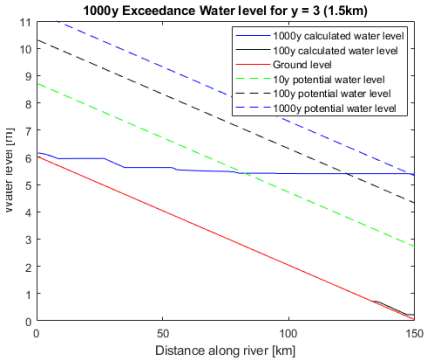

(c) 2km floodplain width setup at Y = 3

Figure B.7: Plots of 1000 year and 100 year return period exceedance water levels for the floodplain width setups, along the west-east cross sections for 5km and 1.5km away from the river

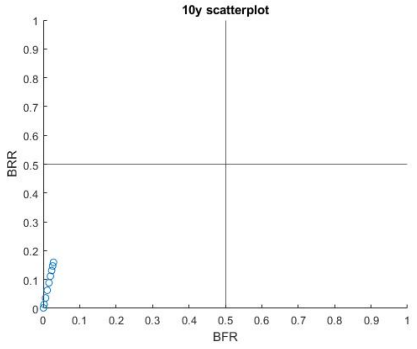

(a) Base setup scatter plot for 10y return period

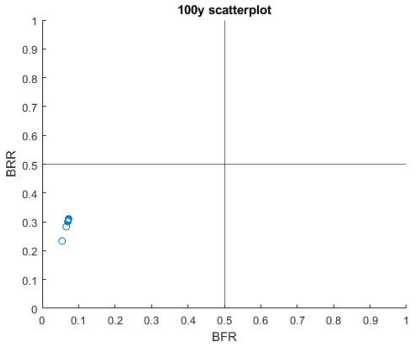

(b) Base setup scatter plot for 100y return period

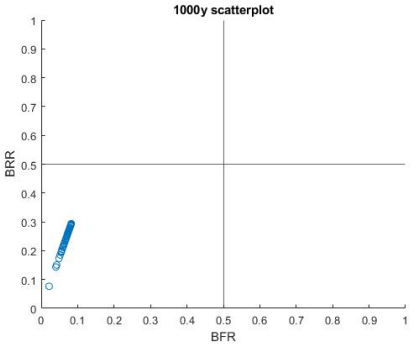

(c) Base setup scatter plot for 1000y return period

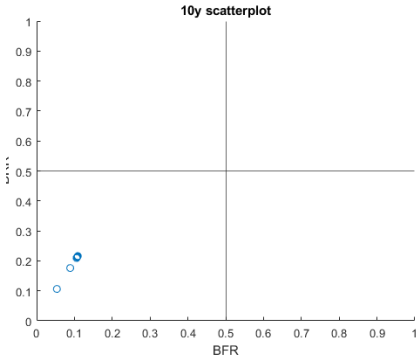

(d) 8km floodplain width setup for 10y return period

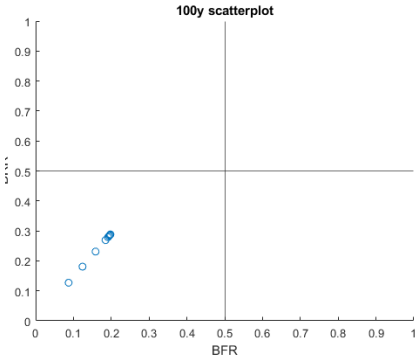

(e) 8km floodplain width setup for 100y return period

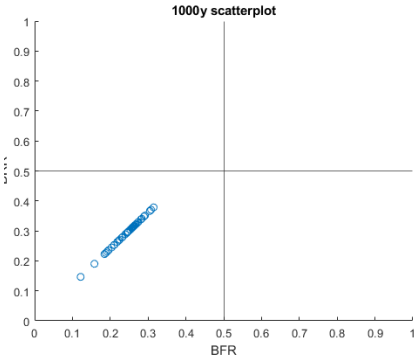

(f) 8km floodplain width setup for 1000y return period

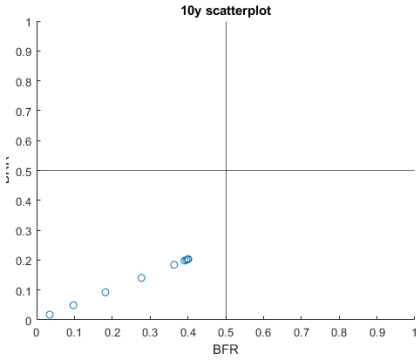

(g) 2km floodplain width setup for 10y return period

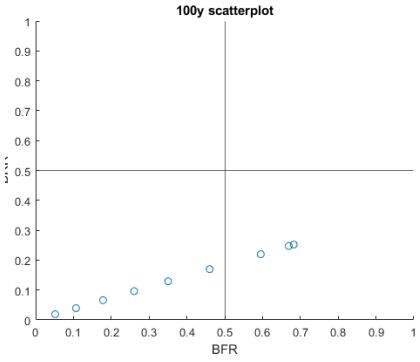

(h) 2km floodplain width setup for 100y return period

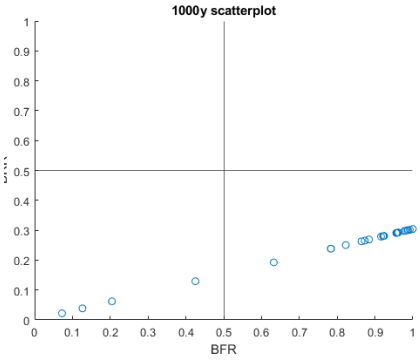

(i) 2km floodplain width setup for 1000y return period

Figure B.8: Scatter plots of the BFR and BRR ratios for the Base setup and the setups for a floodplain depth increased by $1m$ and $5m$.

B.3 Floodplain depth output

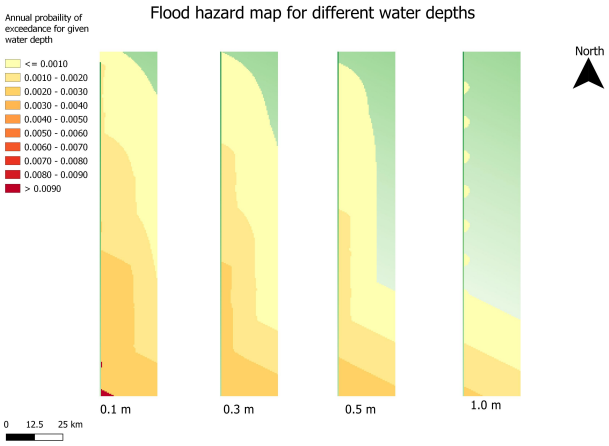

(a) Base setup for FC2

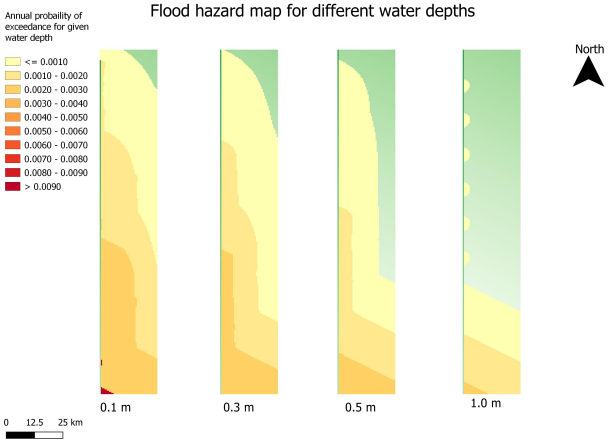

(b) $Z_f = -1$ setup for FC2

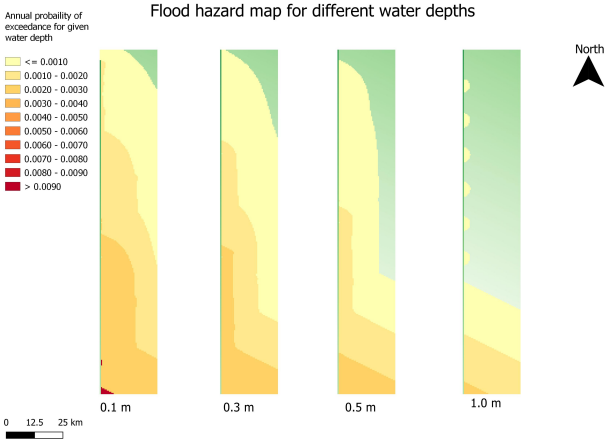

(c) $Z_f = -5$ setup for FC2

Figure B.9: Wet feet maps for the base setup and the setups with a increased breaching depth.

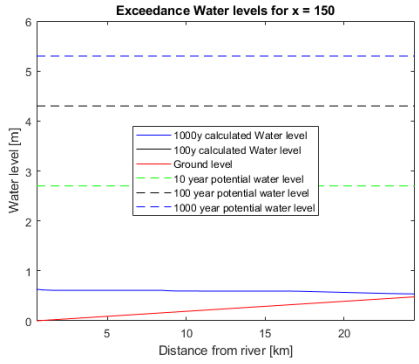

(a) Base setup at X = 150

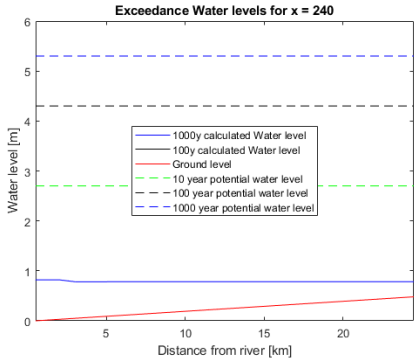

(b) Base setup at X = 240

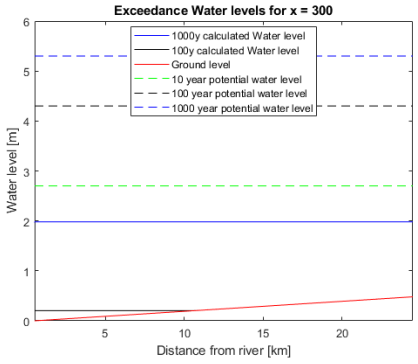

(c) Base setup at X = 300

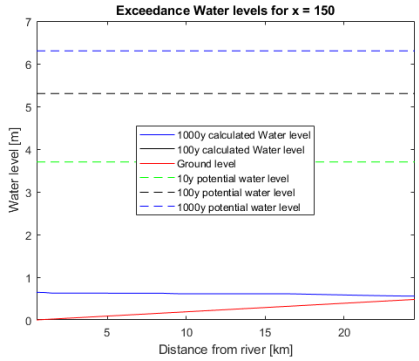

(d) $Z_f = -1$ setup at X = 150

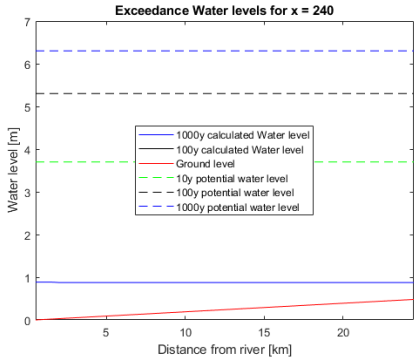

(e) $Z_f = -1$ setup at X = 240

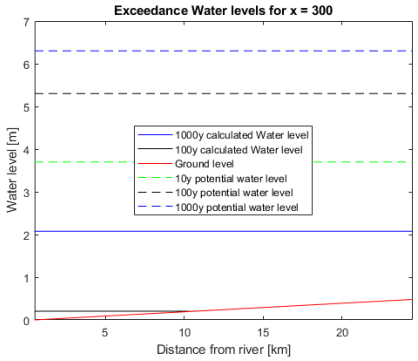

(f) $Z_f = -1$ setup at X = 300

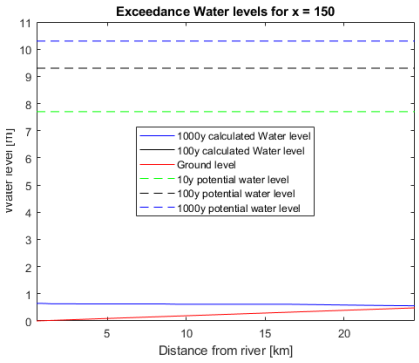

(g) $Z_f = -5$ setup at X = 150

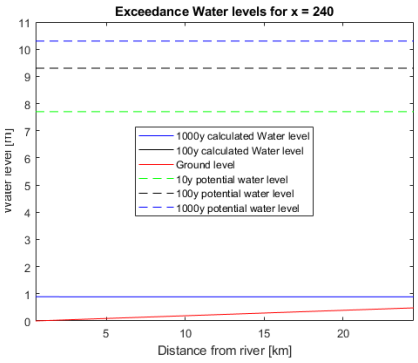

(h) $Z_f = -5$ setup at X = 240

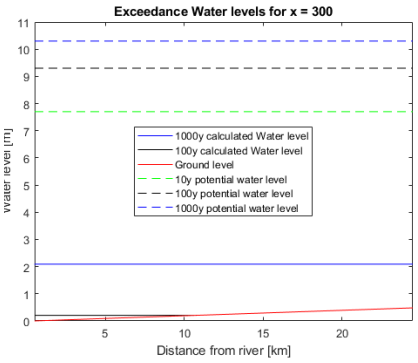

(i) $Z_f = -5$ setup at X = 300

Figure B.10: Plots of 1000 year and 100 year return period exceedance water levels for the increased floodplain depth setups, along the west-east cross sections at 75km, 120km and 150km downstream from the begin point

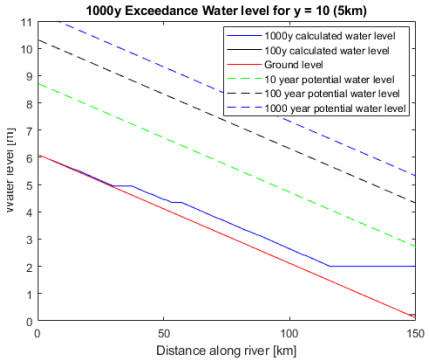

(a) Base setup at Y = 10

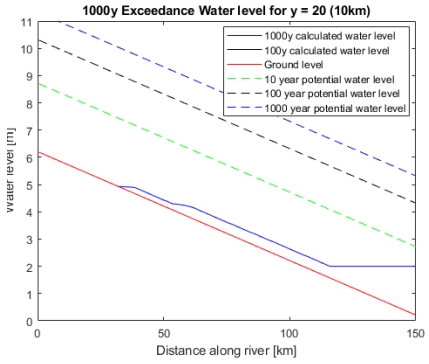

(b) Base setup at Y = 20

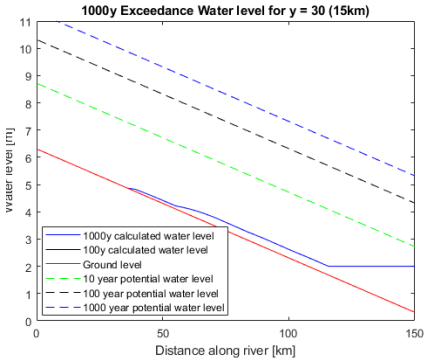

(c) Base setup at Y = 30

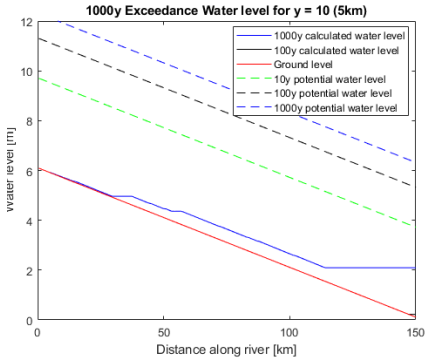

(d) $Z_f = -1$ setup at Y = 10

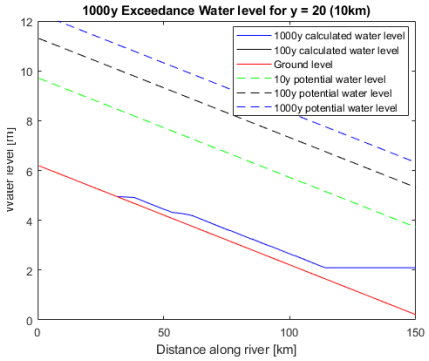

(e) $Z_f = -1$ setup at Y = 20

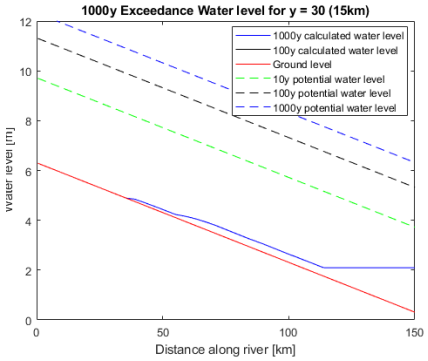

(f) $Z_f = -1$ setup at Y = 30

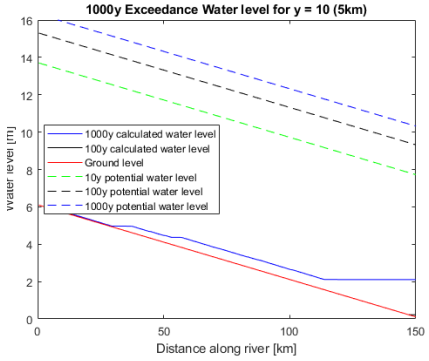

(g) $Z_f = -5$ setup at Y = 10

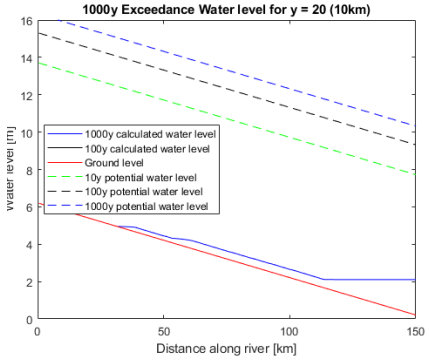

(h) $Z_f = -5$ setup at Y = 20

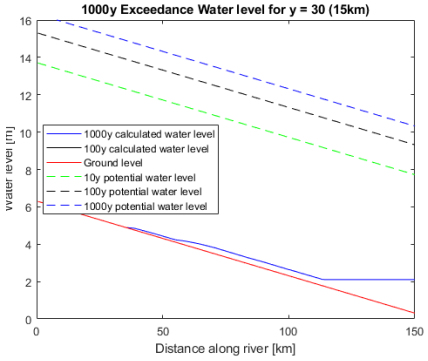

(i) $Z_f = -5$ setup at Y = 30

Figure B.11: Plots of 1000 year return period exceedance water levels along the North-South Axis for 5km, 10km and 15km away from the river.

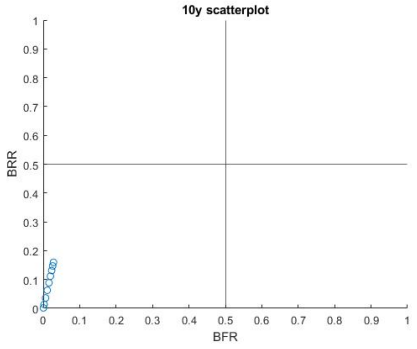

(a) Base setup scatter plot for 10y return period

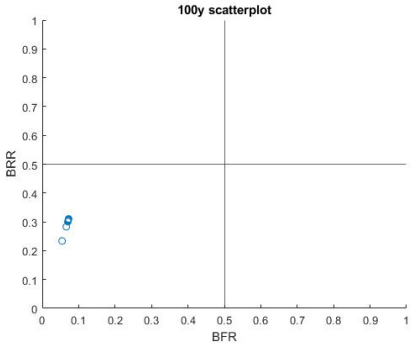

(b) Base setup scatter plot for 100y return period

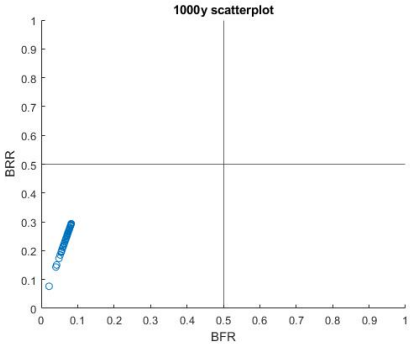

(c) Base setup scatter plot for 1000y return period

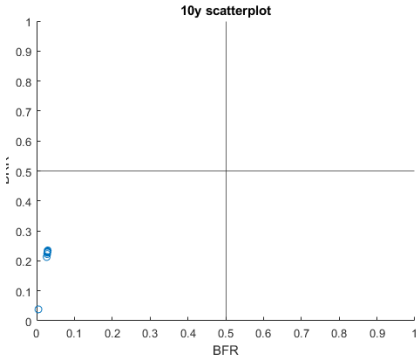

(d) $Z_f = -1$ setup for 10y return period

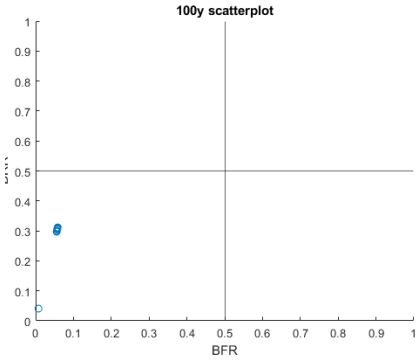

(e) $Z_f = -1$ setup for 100y return period

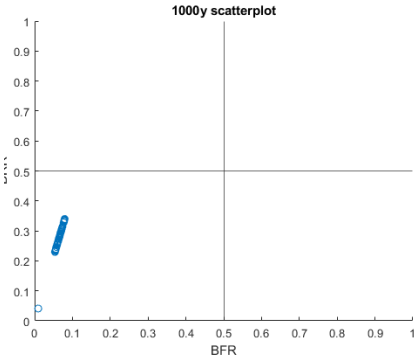

(f) $Z_f = -1$ setup for 1000y return period

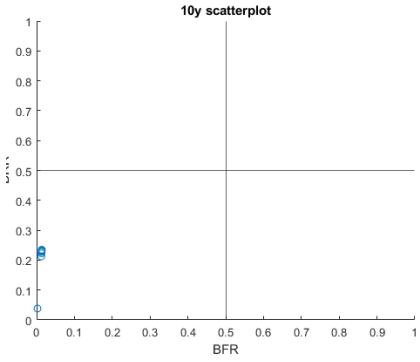

(g) $Z_f = -5$ setup for 10y return period

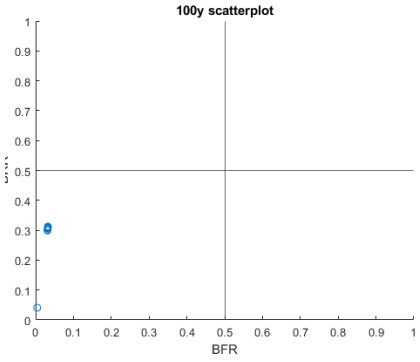

(h) $Z_f = -5$ setup for 100y return period

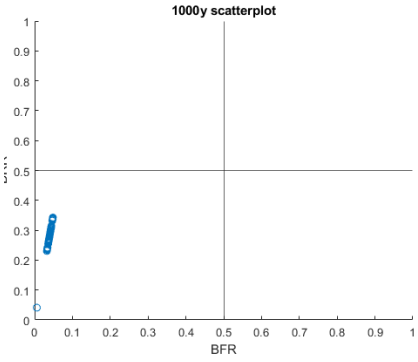

(i) $Z_f = -5$ setup for 1000y return period

Figure B.12: Scatter plots of the BFR and BRR ratios for the base setup and the setups for a floodplain with a wall of $1m$ and $5m$.

B.4 Split floodplain outputs

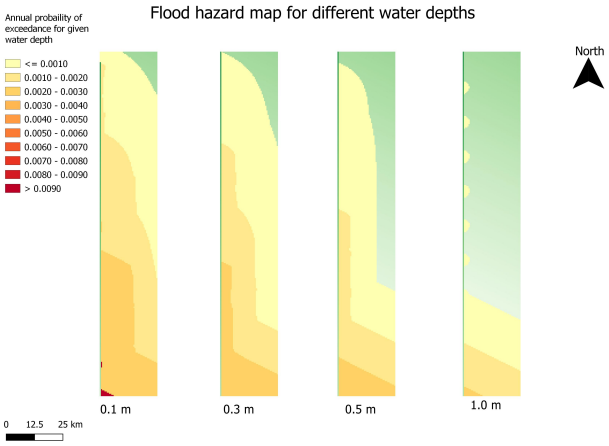

(a) Base setup for FC2

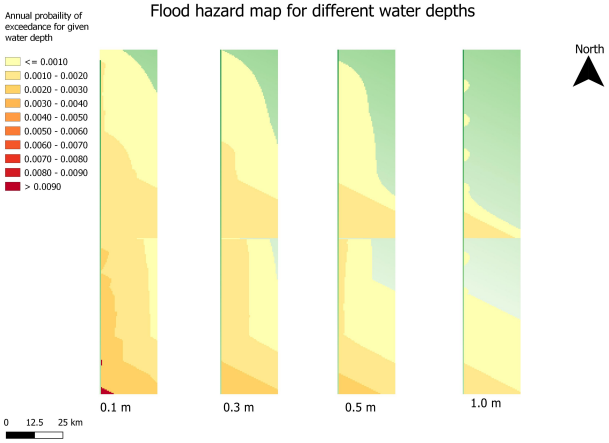

(b) $h_w = 1m$ setup for FC2

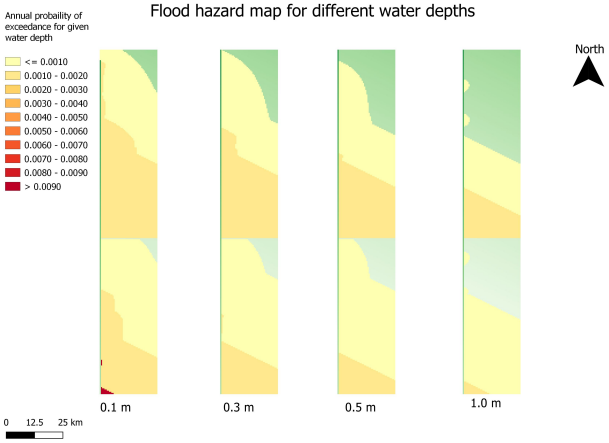

(c) $h_w = 5m$ setup for FC2

Figure B.13: Wet feet maps for the base setup the setups for a wall of $1m$ and $5m$.

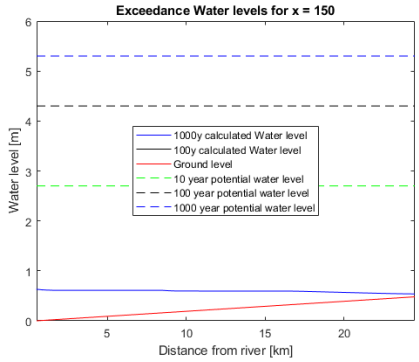

(a) Base setup at X = 150

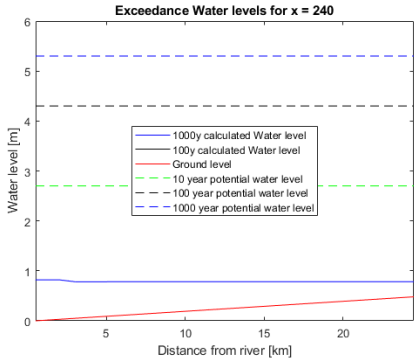

(b) Base setup at X = 240

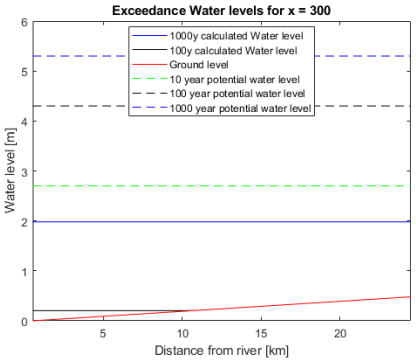

(c) Base setup at X = 300

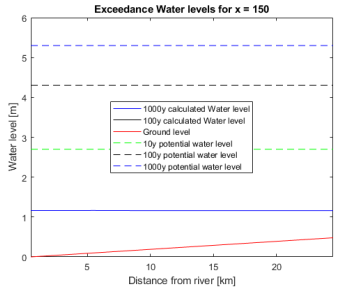

(d) $h_w = 1m$ setup at X = 150

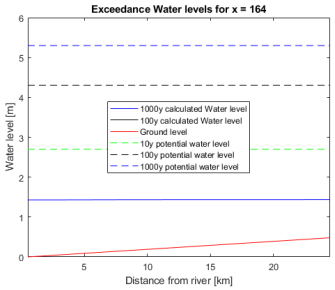

(e) $h_w = 1m$ setup at X = 164

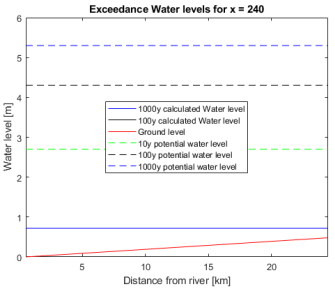

(f) $h_w = 1m$ setup at X = 240

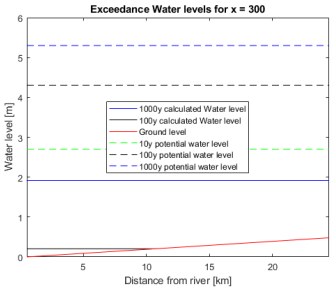

(g) $h_w = 5m$ setup at X = 300

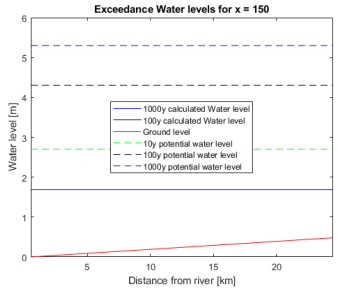

(h) $h_w = 5m$ setup at X = 150

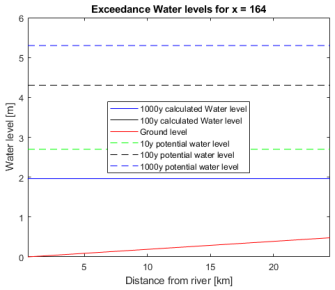

(i) $h_w = 5m$ setup at X = 240

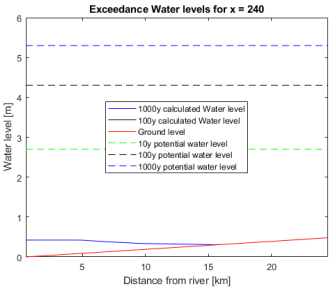

(j) $h_w = 5m$ setup atl X = 240

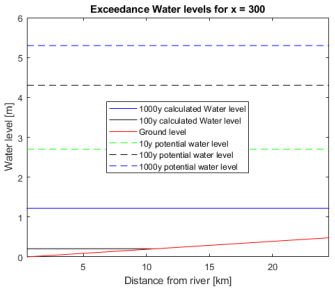

(k) $h_w = 5m$ setup at X = 300

Figure B.14: Plots of 1000 year return period exceedance water levels along the west-east Axis for 5km, 10km and 15km away from the river.

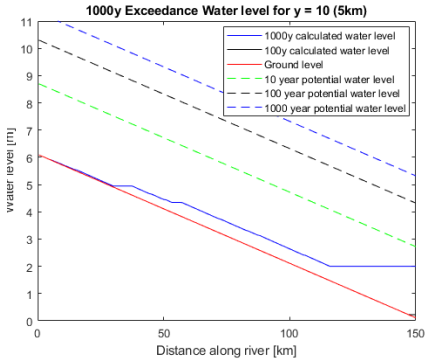

(a) Base setup at Y = 10

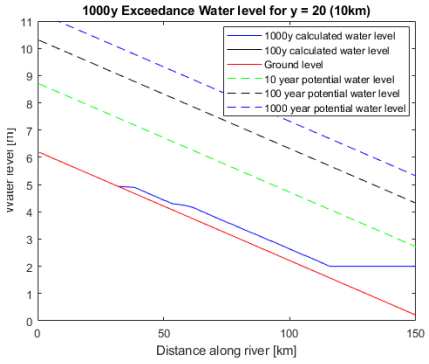

(b) Base setup at Y = 20

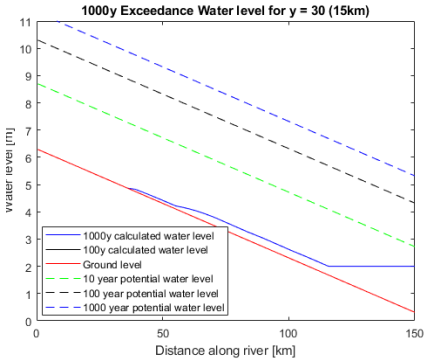

(c) Base setup at Y = 30

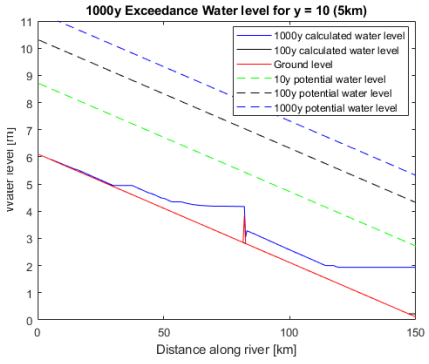

(d) $h_w = 1m$ setup at Y = 10

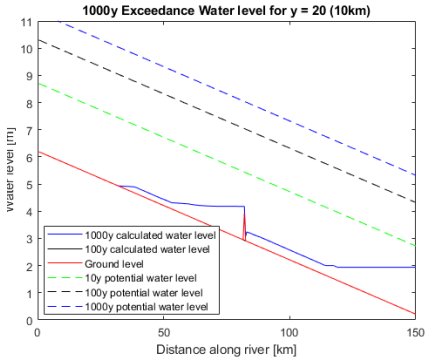

(e) $h_w = 1m$ setup at Y = 20

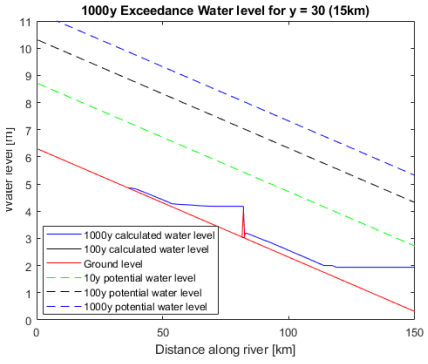

(f) $h_w = 1m$ setup at Y = 30

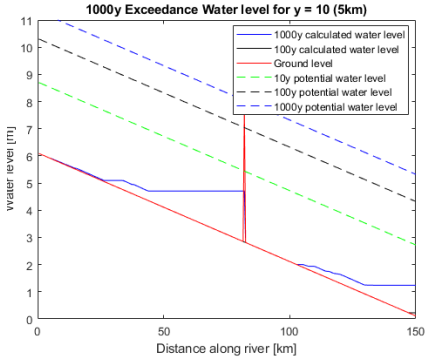

(g) $h_w = 5m$ setup at Y = 10

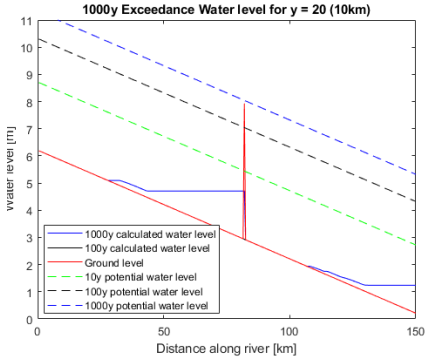

(h) $h_w = 5m$ setup at Y = 20

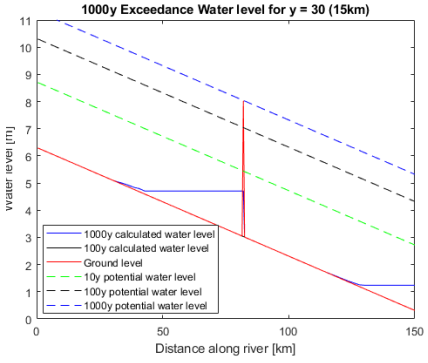

(i) $h_w = 5m$ setup at Y = 30

Figure B.15: Plots of 1000 year return period exceedance water levels along the north-south Axis for 5km, 10km and 15km away from the river.

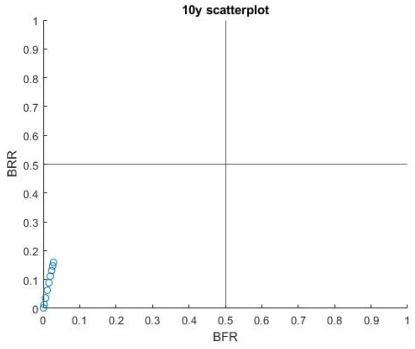

(a) Base setup scatter plot for 10y return period

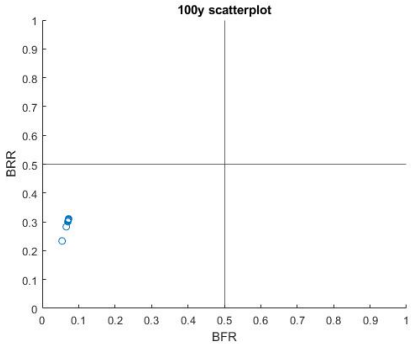

(b) Base setup scatter plot for 100y return period

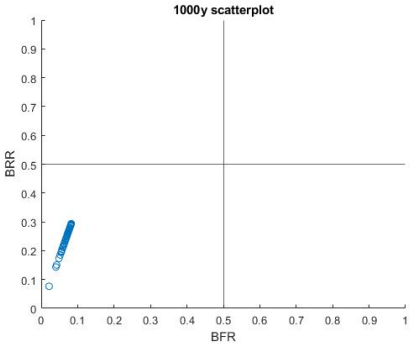

(c) Base setup scatter plot for 1000y return period

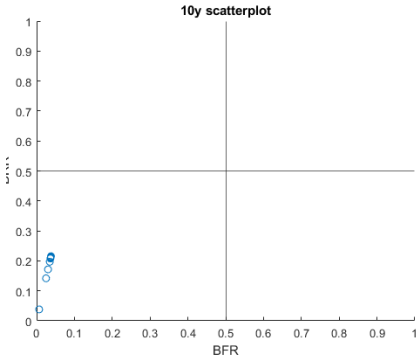

(d) $h_w = 1m$ setup for 10y return period

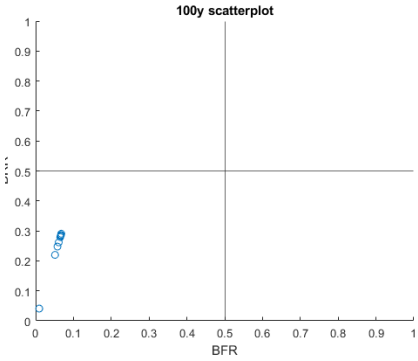

(e) $h_w = 1m$ setup for 100y return period

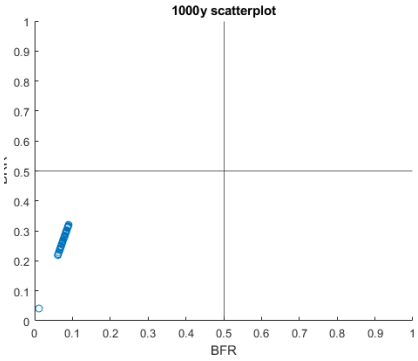

(f) $h_w = 1m$ setup for 1000y return period

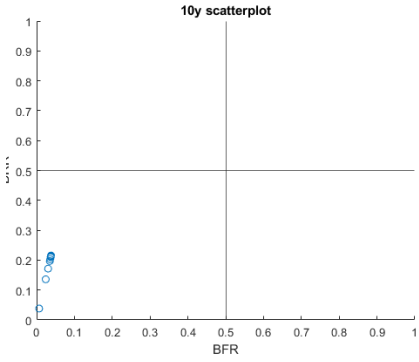

(g) $h_w = 5m$ setup for 10y return period

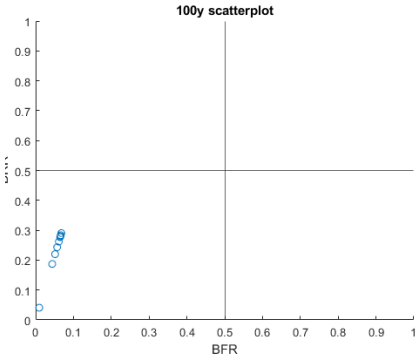

(h) $h_w = 5m$ setup for 100y return period

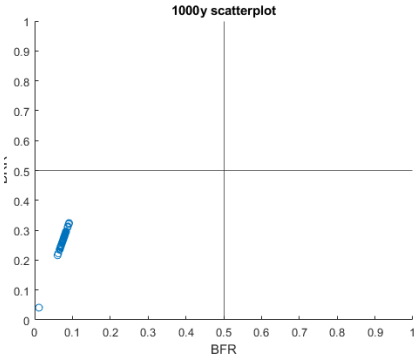

(i) $h_w = 5m$ setup for 1000y return period

Figure B.16: Scatter plots of the BFR and BRR ratios for the Base setup and the setups for a wall of $1m$ and $5m$.

B.5 Breaching time outputs

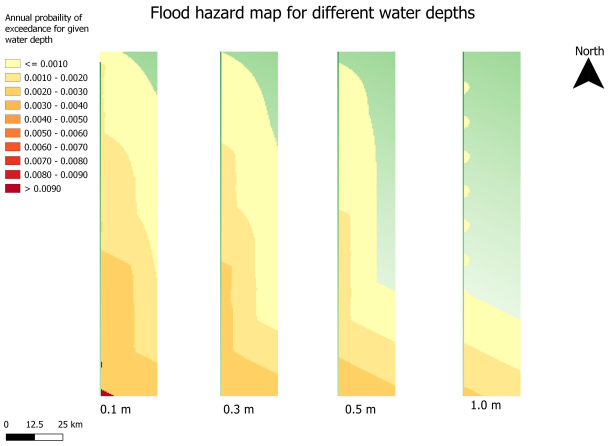

(a) Base setup for FC2

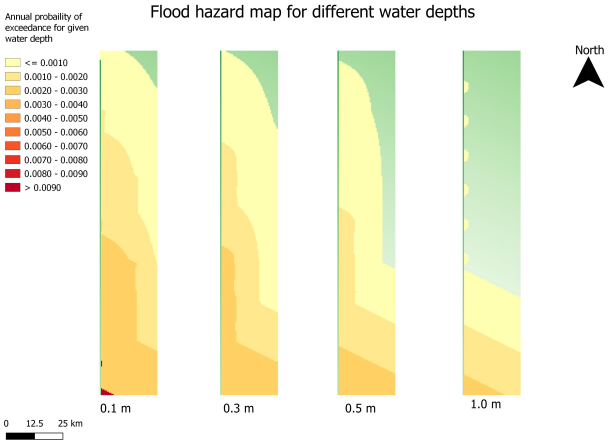

(b) $T_b = 20$ setup for FC2

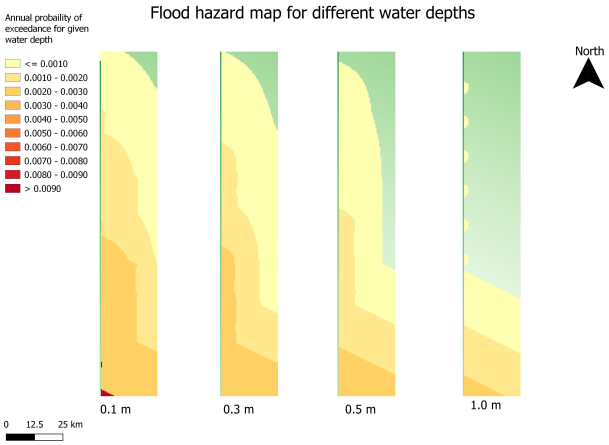

(c) $T_b = 15$ setup for FC2

Figure B.17: Wet feet maps for the base case and the cases with an earlier breach start time.

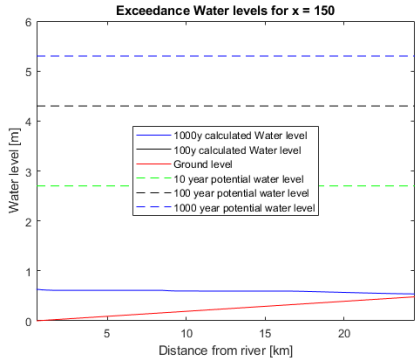

(a) Base setup at X = 150

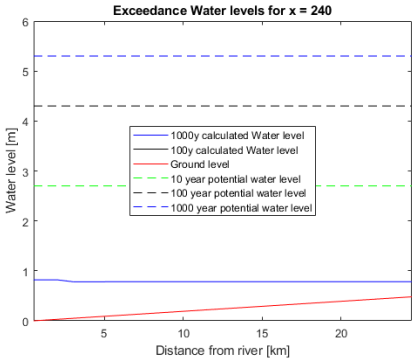

(b) Base setup at X = 240

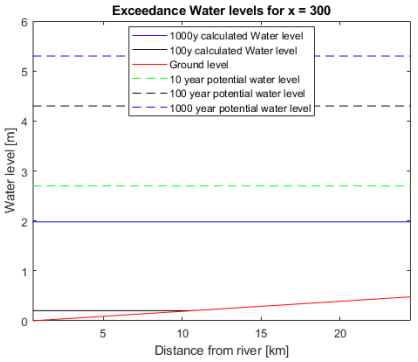

(c) Base setup at X = 300

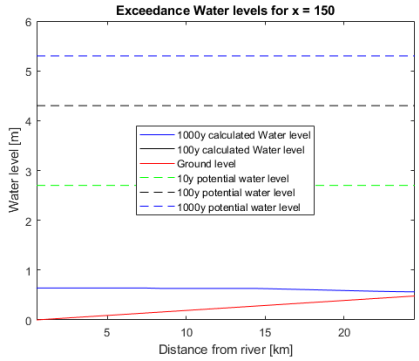

(d) $T_b = 20$ setup at X = 150

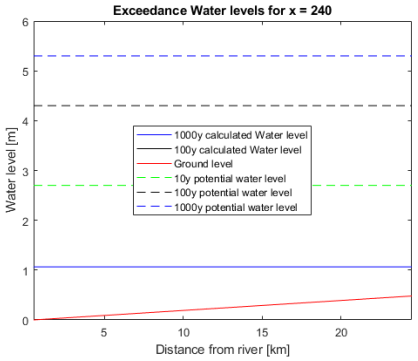

(e) $T_b = 20$ setup at X = 240

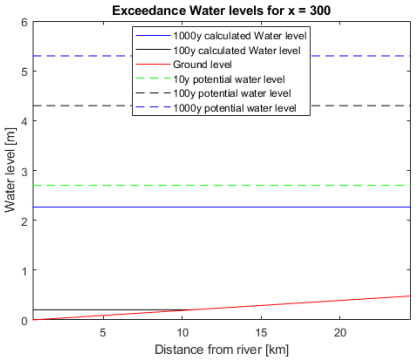

(f) $T_b = 20$ setup at X = 300

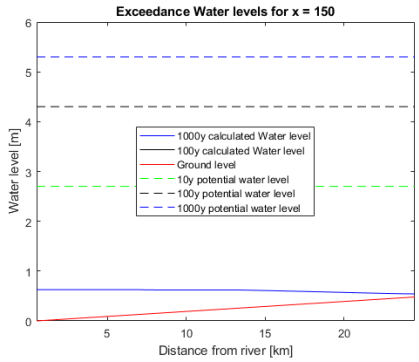

(g) $T_b = 15$ setup at X = 150

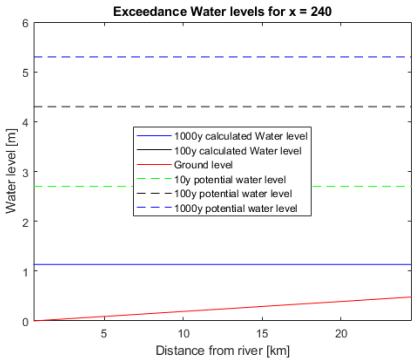

(h) $T_b = 15$ setup at X = 240

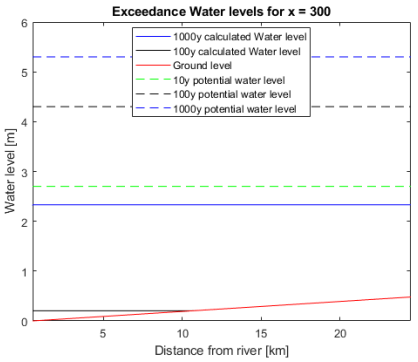

(i) $T_b = 15$ setup at X = 300

Figure B.18: Plots of 1000 year and 100 year return period exceedance water levels for the earlier breach start time setups, along the west-east cross sections at 75km, 120km and 150km downstream from the begin point.

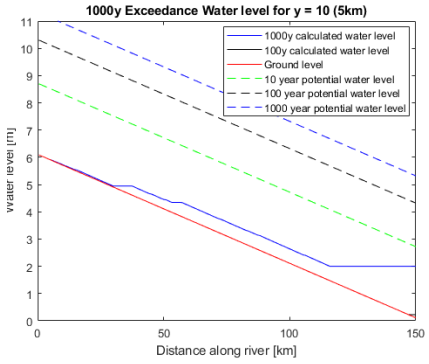

(a) Base setup at Y = 10

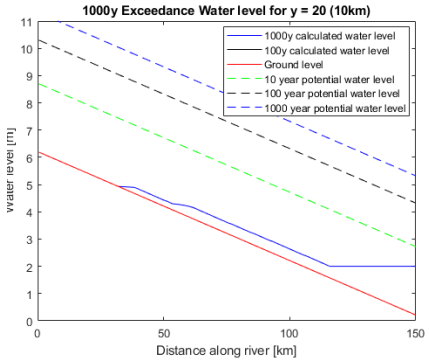

(b) Base setup at Y = 20

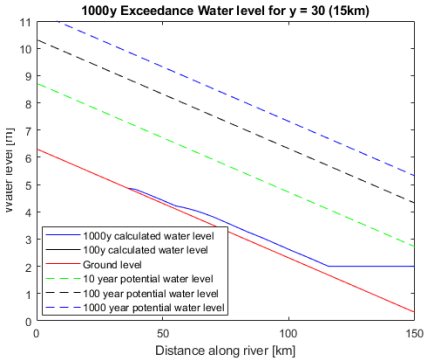

(c) Base setup at Y = 30

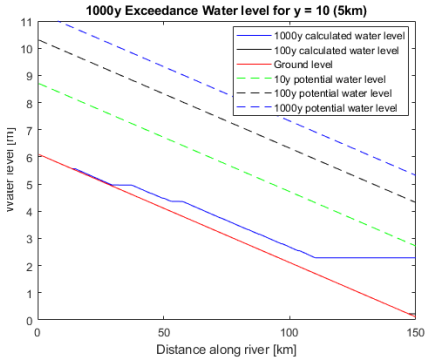

(d) $T_b = 20$ setup at Y = 10

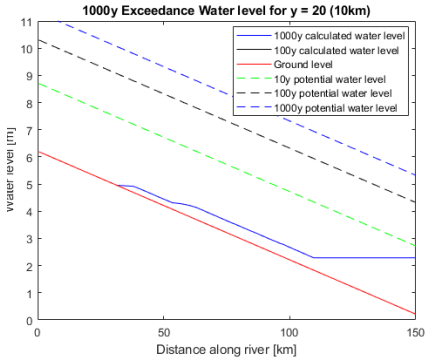

(e) $T_b = 20$ setup at Y = 20

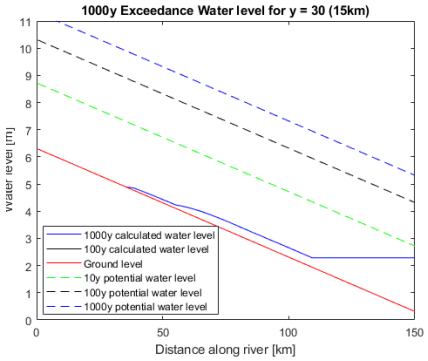

(f) $T_b = 20$ setup at Y = 30

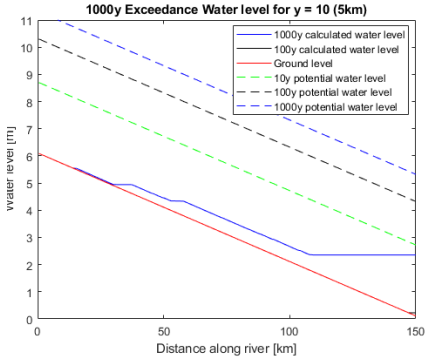

(g) $T_b = 15$ setup at Y = 10

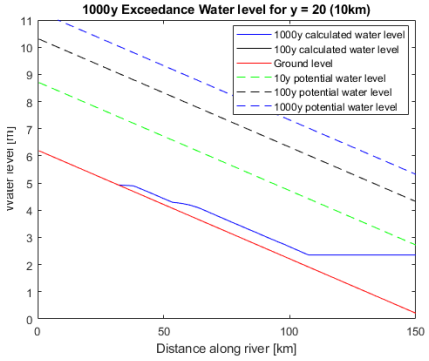

(h) $T_b = 15$ setup at Y = 20

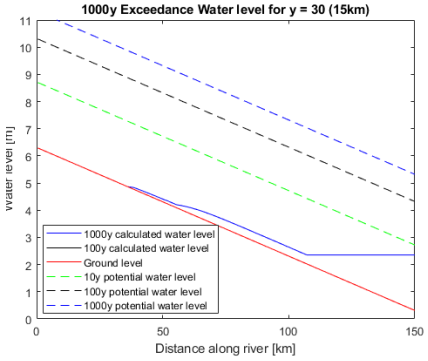

(i) $T_b = 15$ setup at Y = 30

Figure B.19: Plots of 1000 year and 100 year return period exceedance water levels for the earlier breach start time setups, along the North-South Axis for 5km, 10km and 15km away from the river.

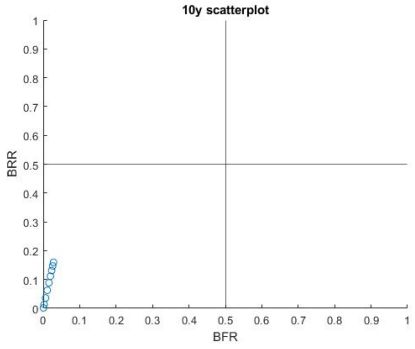

(a) Base setup at 10y return period

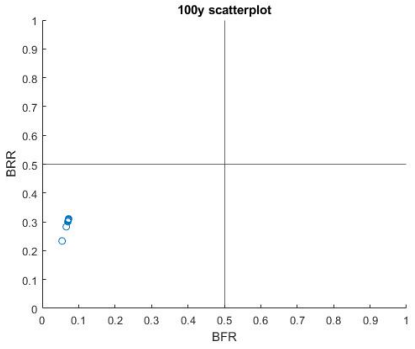

(b) Base setup at 100y return period

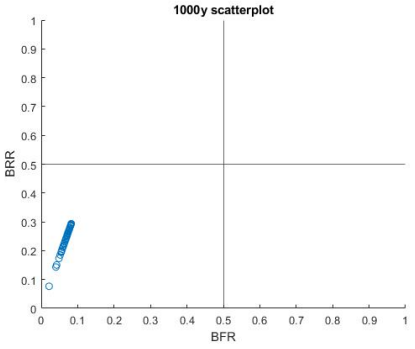

(c) Base setup at 1000y return period

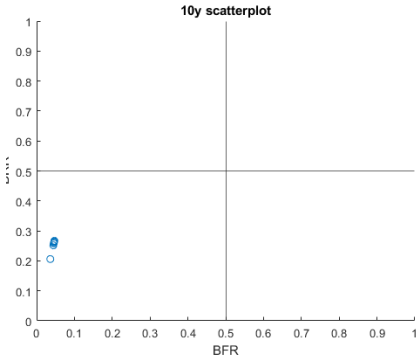

(d) $T_b = 20$ setup for 10y return period

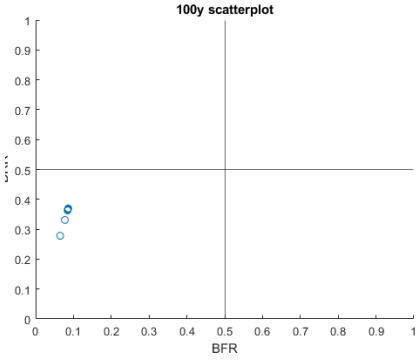

(e) $T_b = 20$ setup for 100y return period

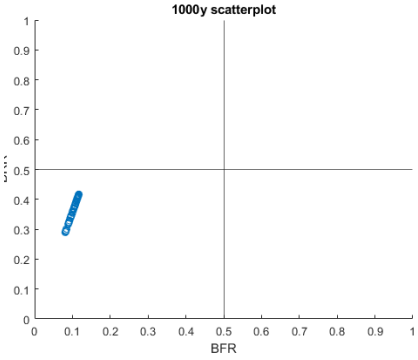

(f) $T_b = 20$ setup for 1000y return period

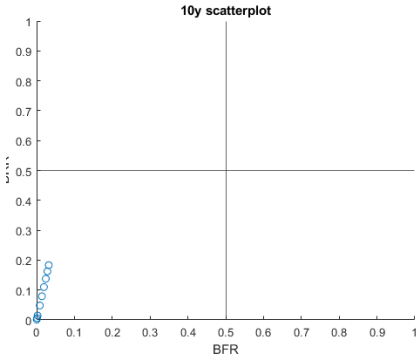

(g) $T_b = 15$ setup for 10y return period

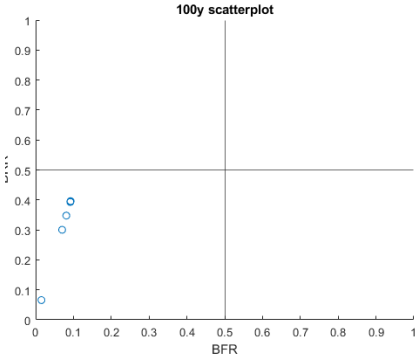

(h) $T_b = 15$ setup for 100y return period

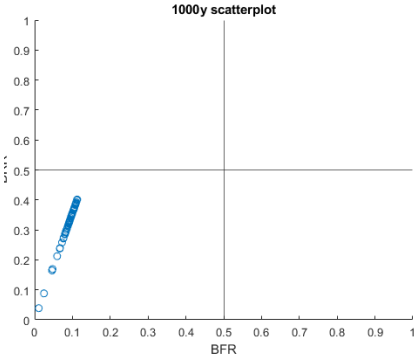

(i) $T_b = 15$ setup for 1000y return period

Figure B.20: Scatter plots of the BFR and BRR ratios for the Base setup and the setups for a earlier breach start time

Appendix C

Detailed results maps from HEC-RAS model

In this appendix are the inundation depths and the water surface levels maps found for each breaching location during the case study.

C.1 Location E1

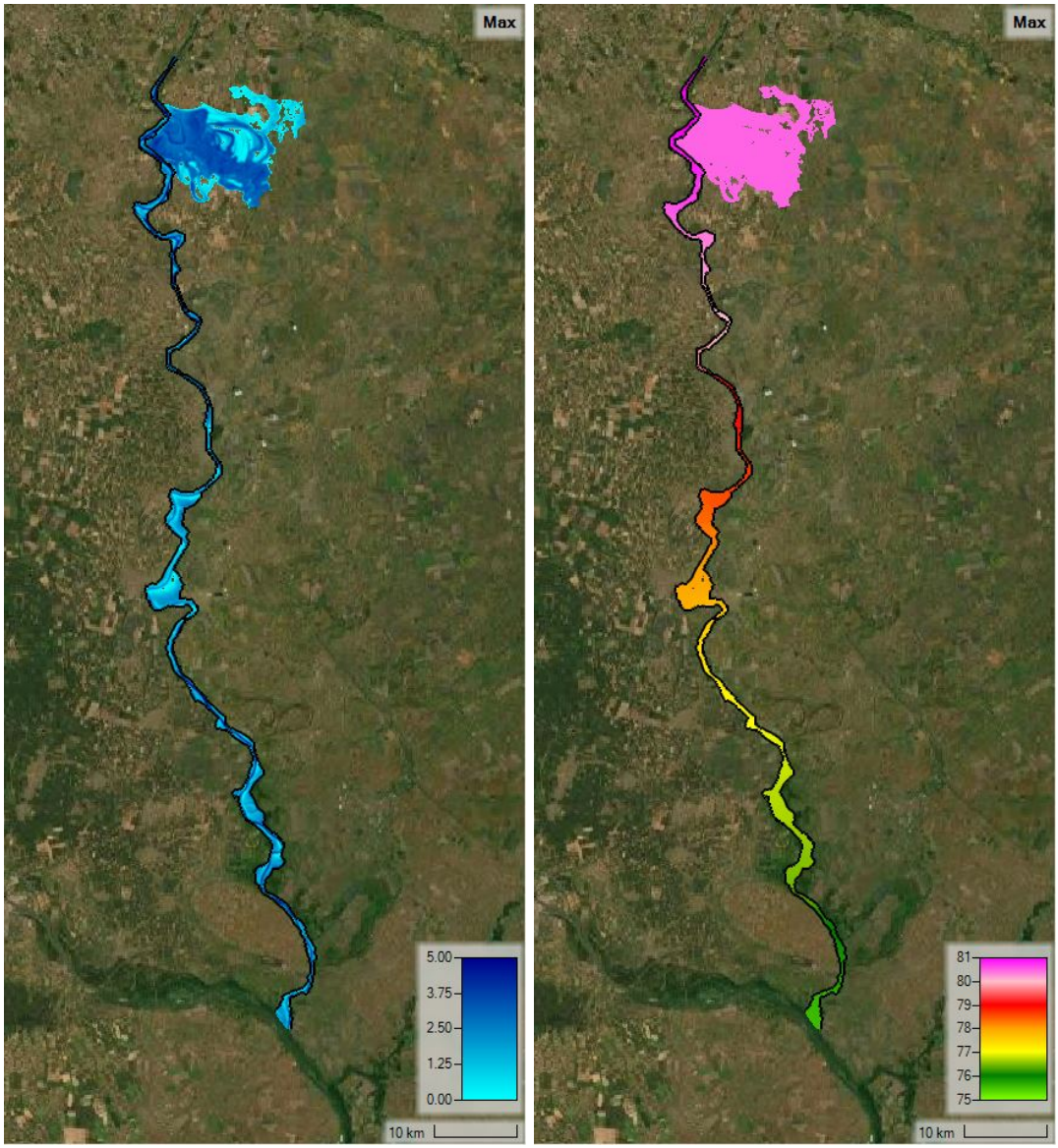

Figure C.1: Inundation depth and water surface level maps for location E1 with a return period of 10 years.

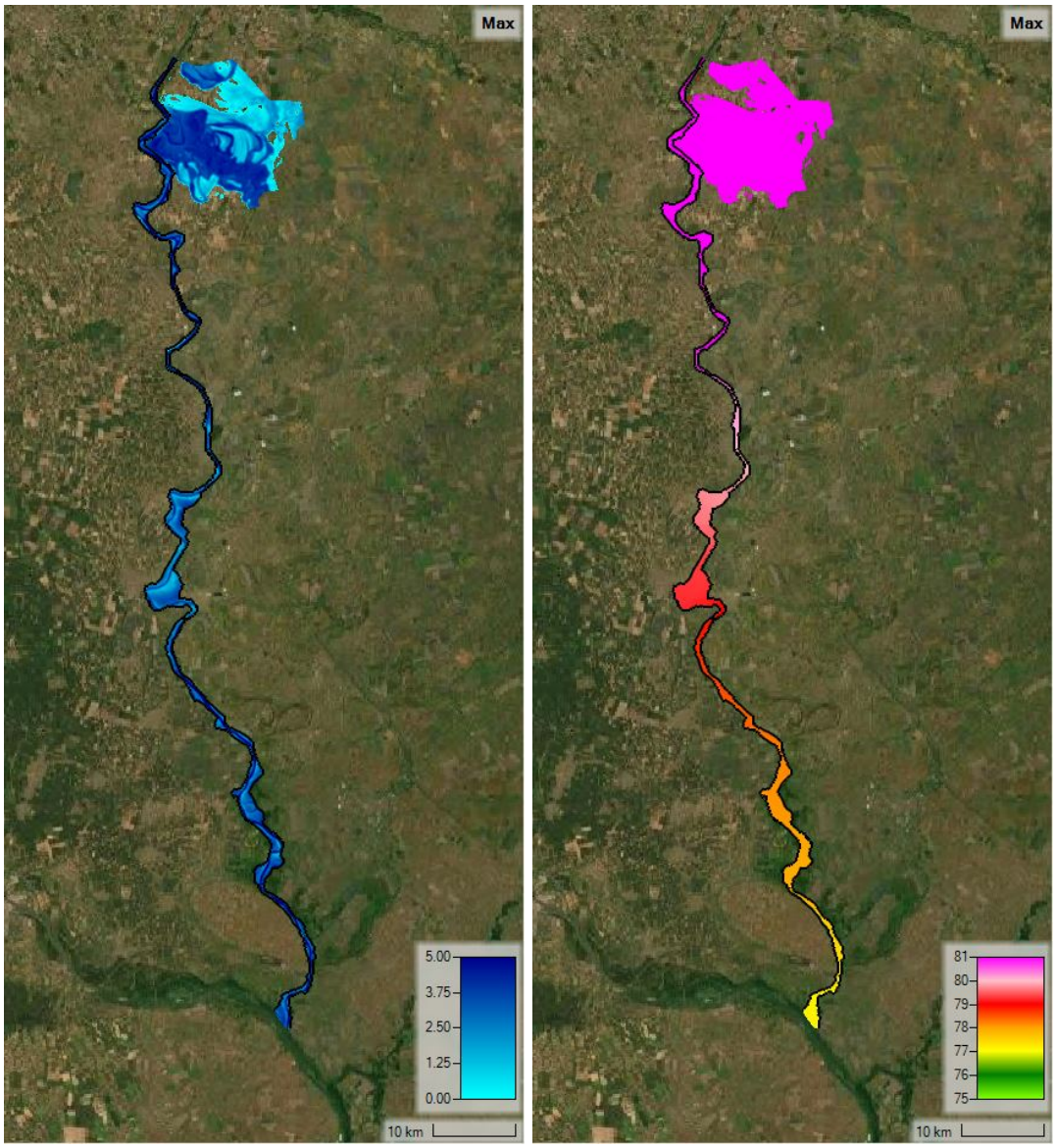

Figure C.2: Inundation depth and water surface level maps for location E1 with a return period of 100 years.

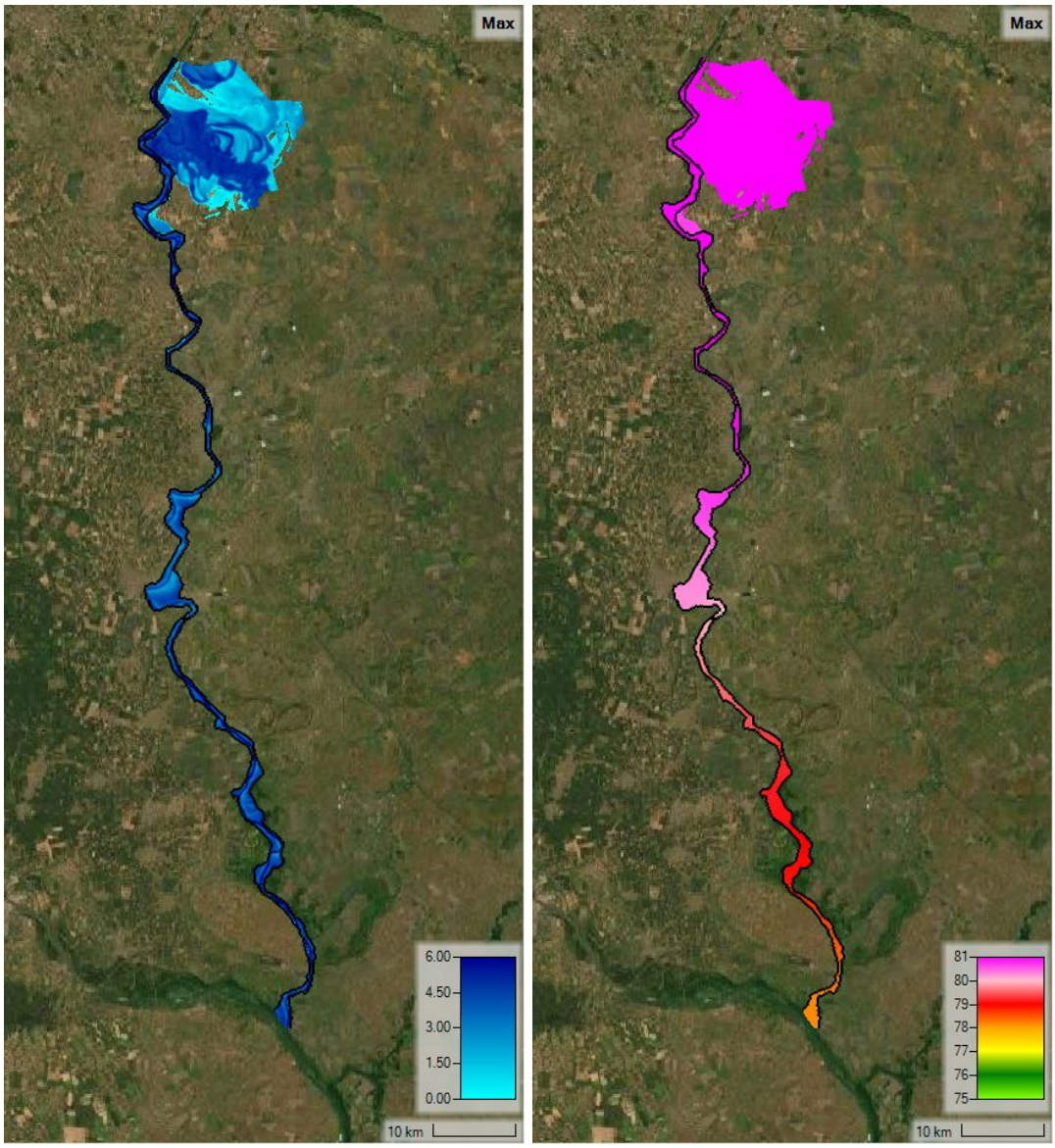

Figure C.3: Inundation depth and water surface level maps for location E1 with a return period of 1000 years.

C.2 Location E2

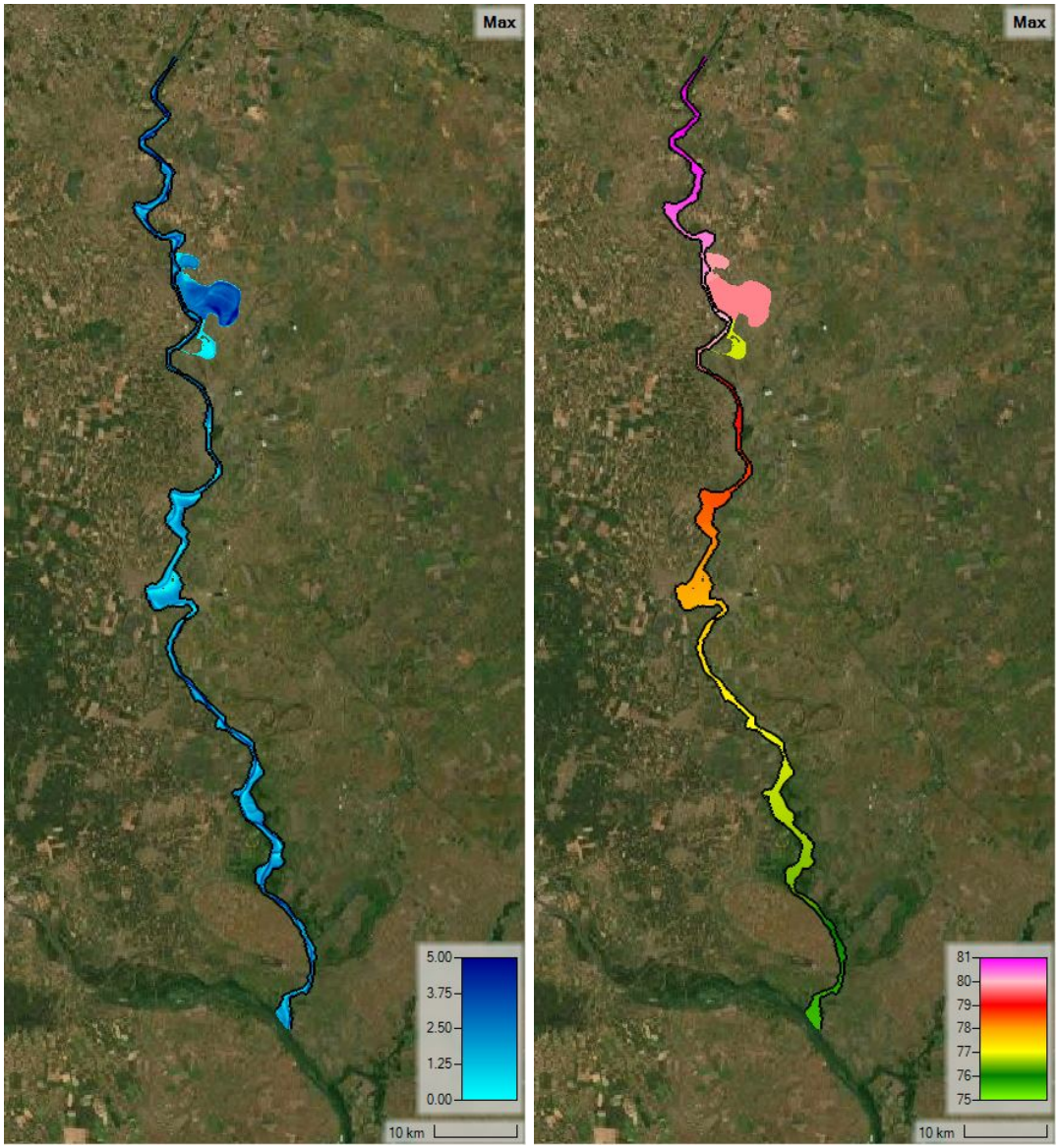

Figure C.4: Inundation depth and water surface level maps for location E2 with a return period of 10 years.

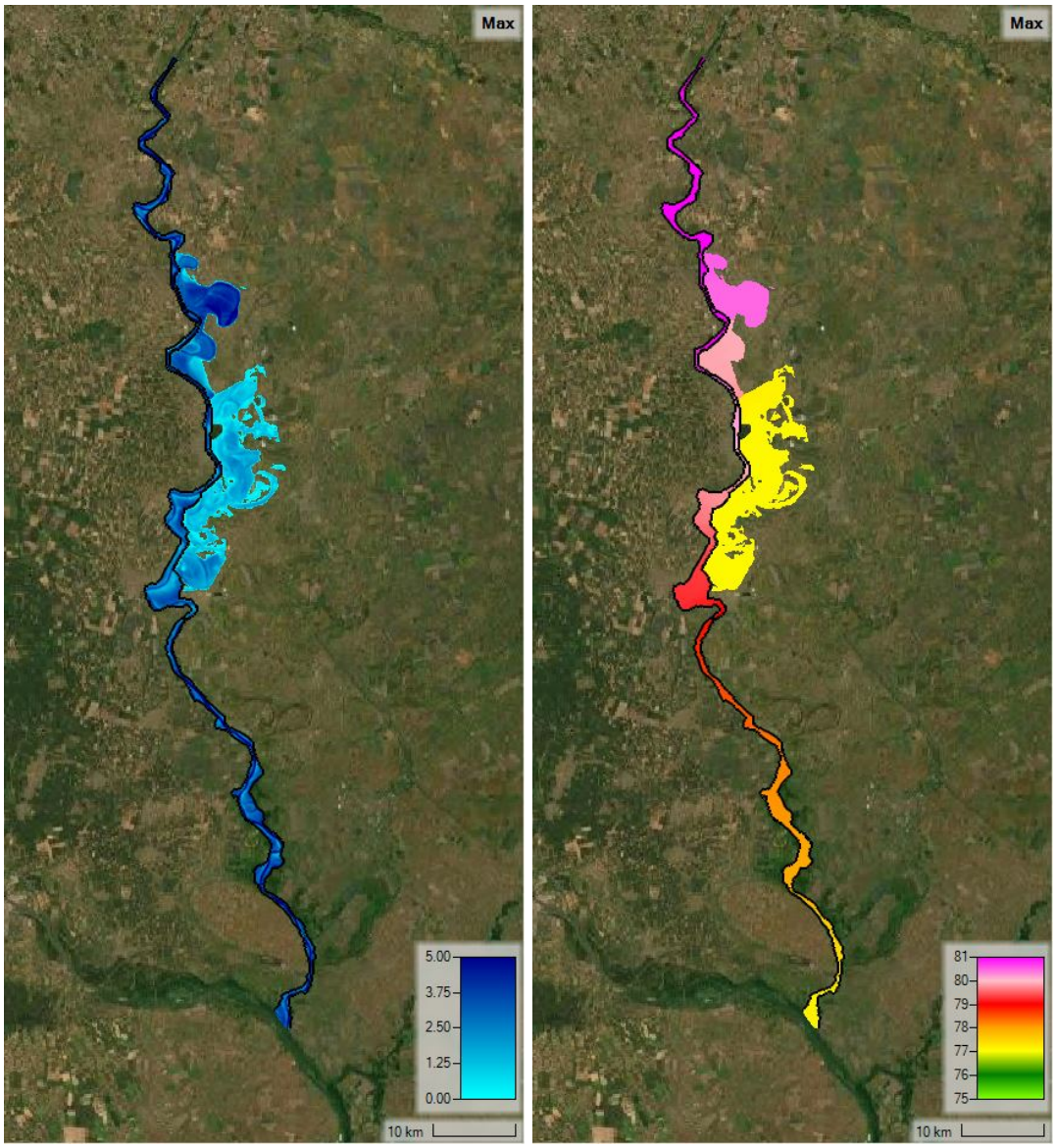

Figure C.5: Inundation depth and water surface level maps for location E2 with a return period of 100 years.

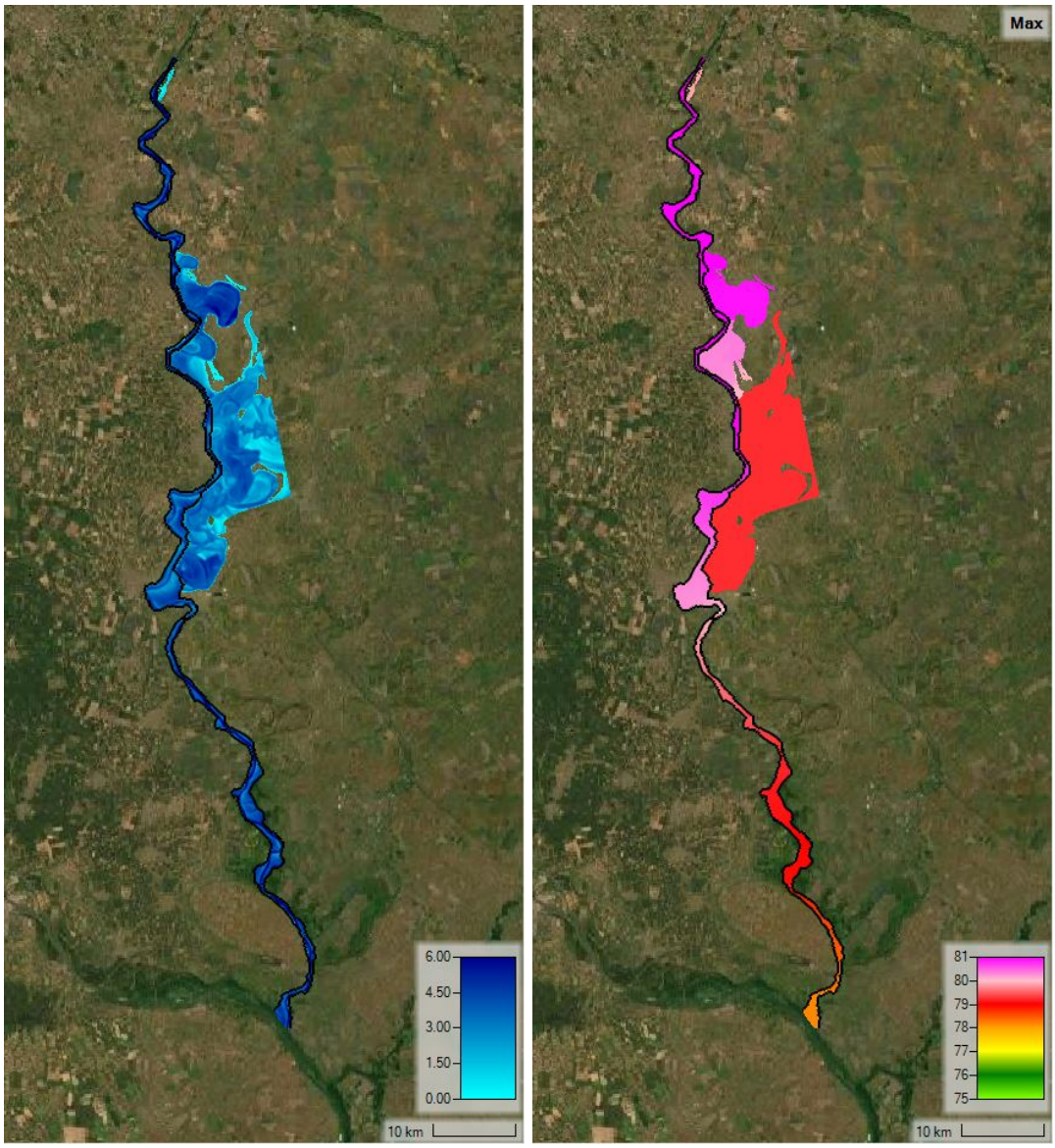

Figure C.6: Inundation depth and water surface level maps for location E2 with a return period of 1000 years.

C.3 Location E3

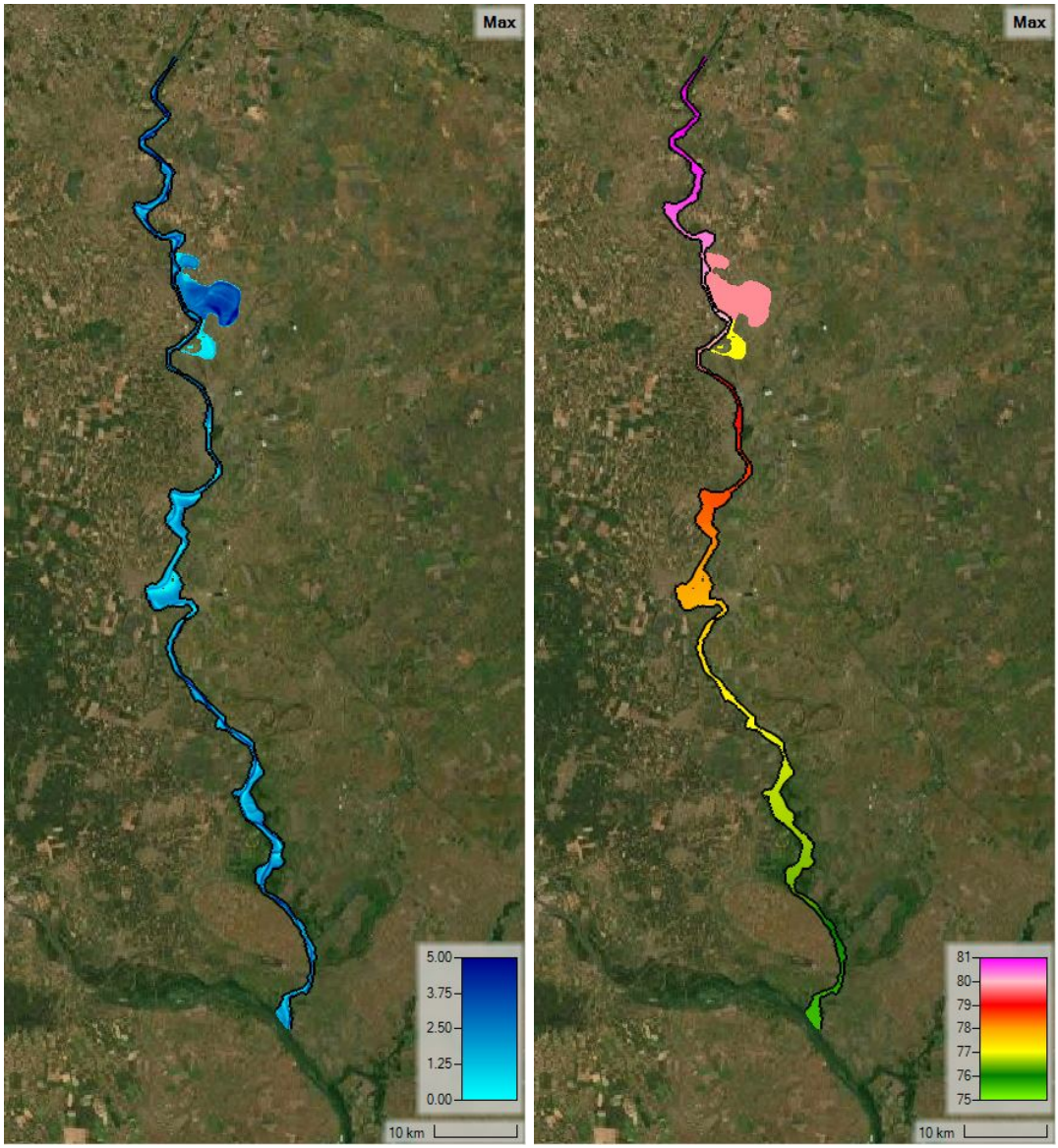

Figure C.7: Inundation depth and water surface level maps for location E3 with a return period of 10 years.

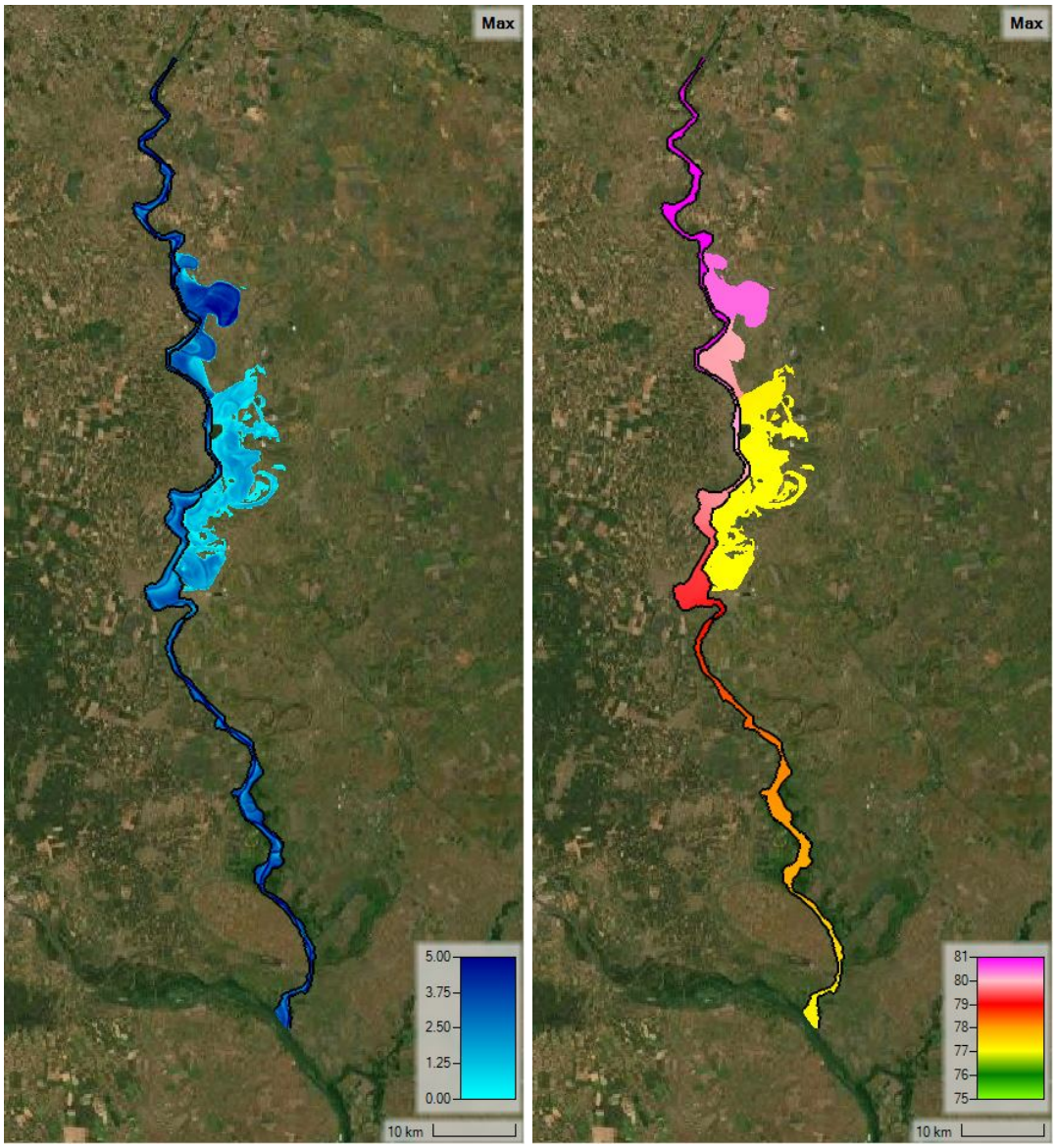

Figure C.8: Inundation depth and water surface level maps for location E3 with a return period of 100 years.

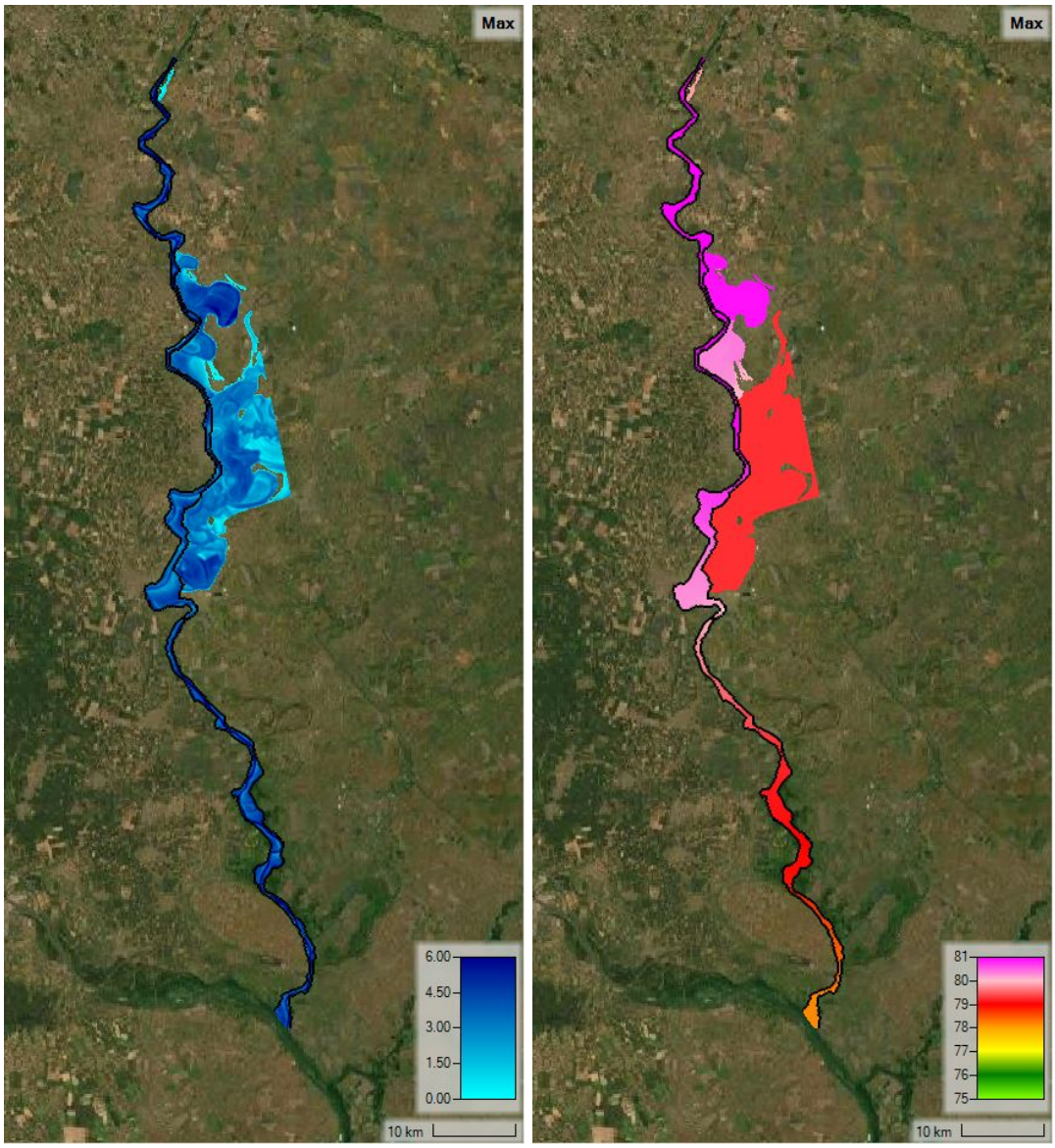

Figure C.9: Inundation depth and water surface level maps for location E3 with a return period of 1000 years.

C.4 Location E4

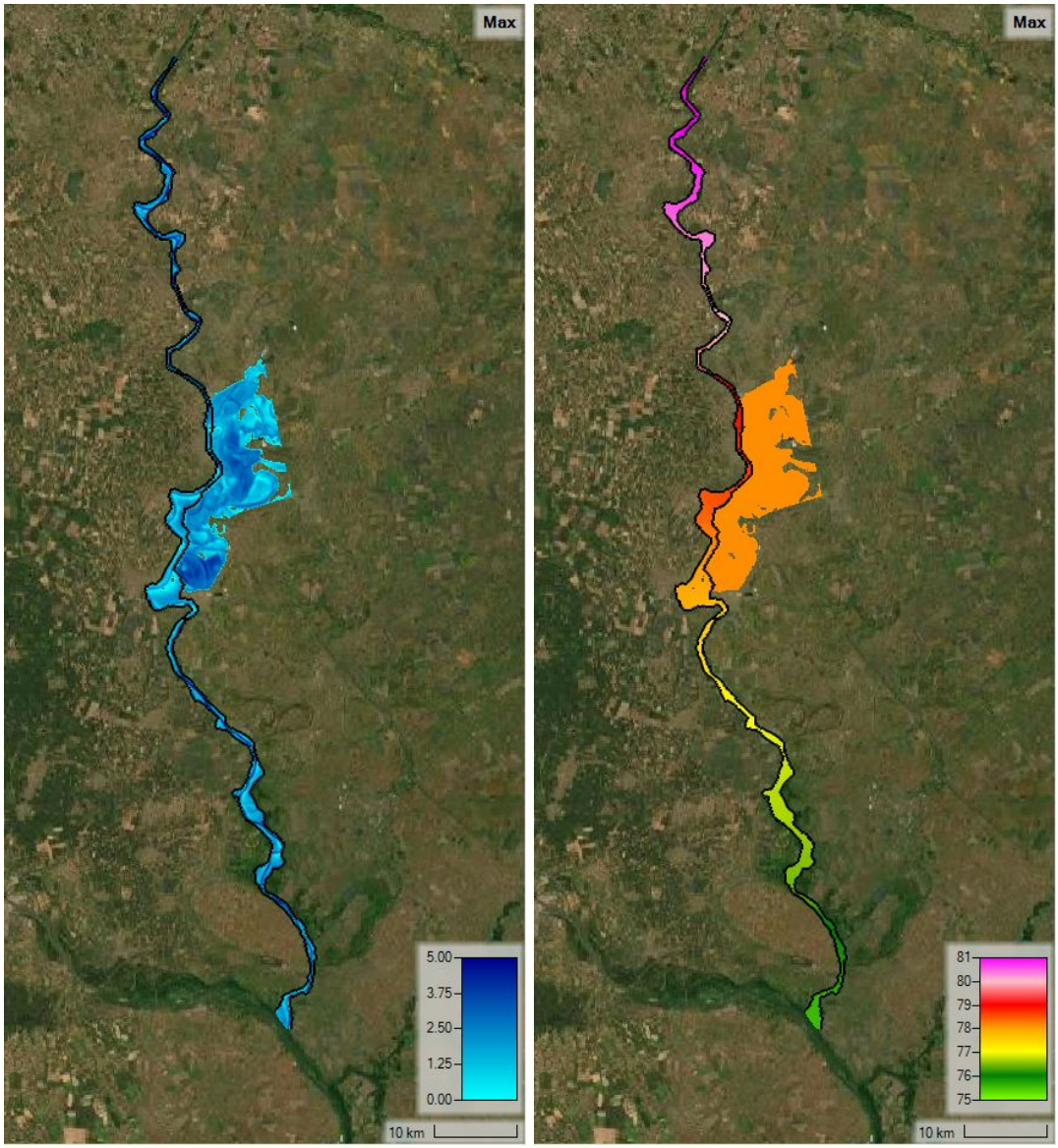

Figure C.10: Inundation depth and water surface level maps for location E4 with a return period of 10 years.

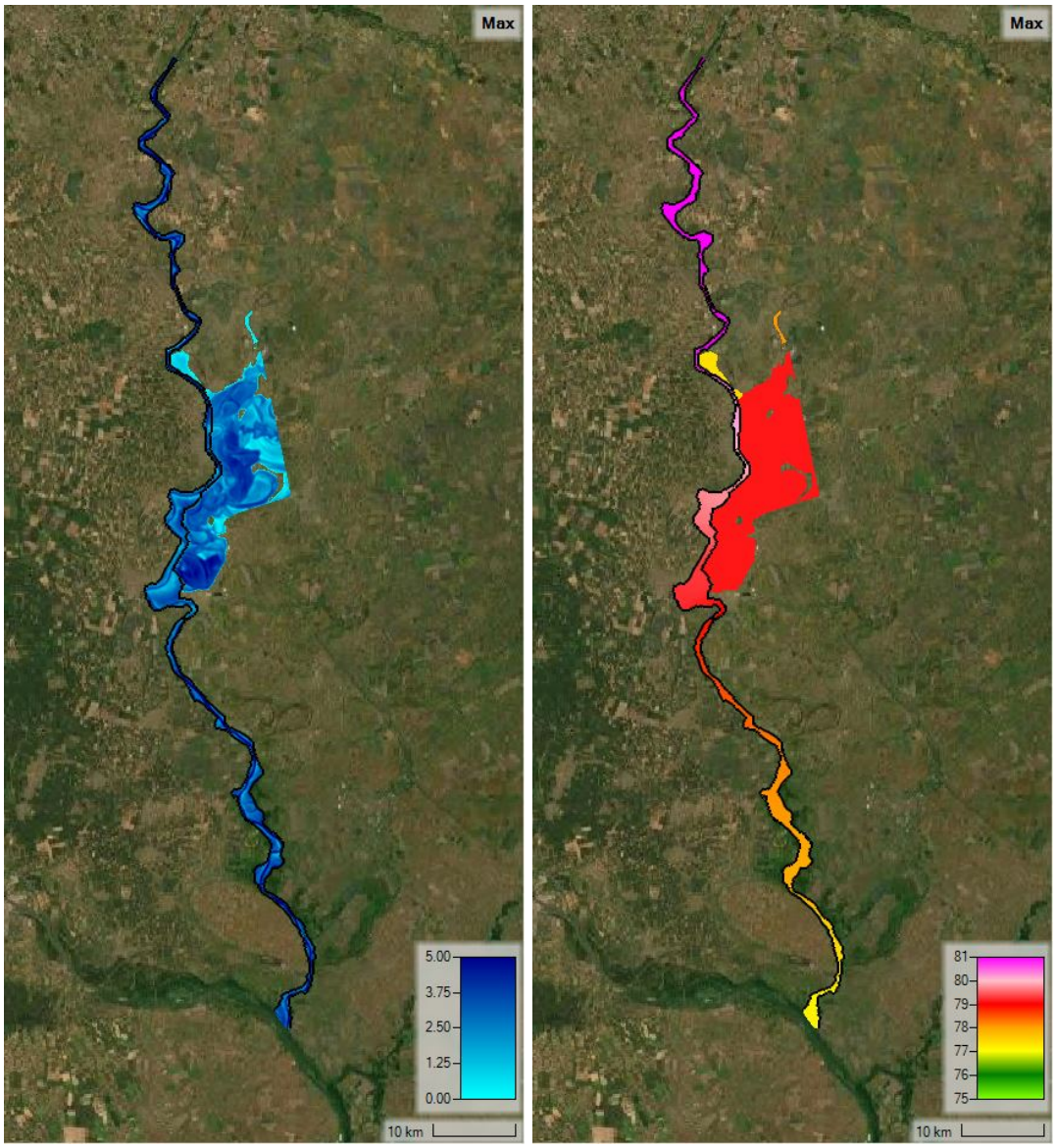

Figure C.11: Inundation depth and water surface level maps for location E4 with a return period of 100 years.

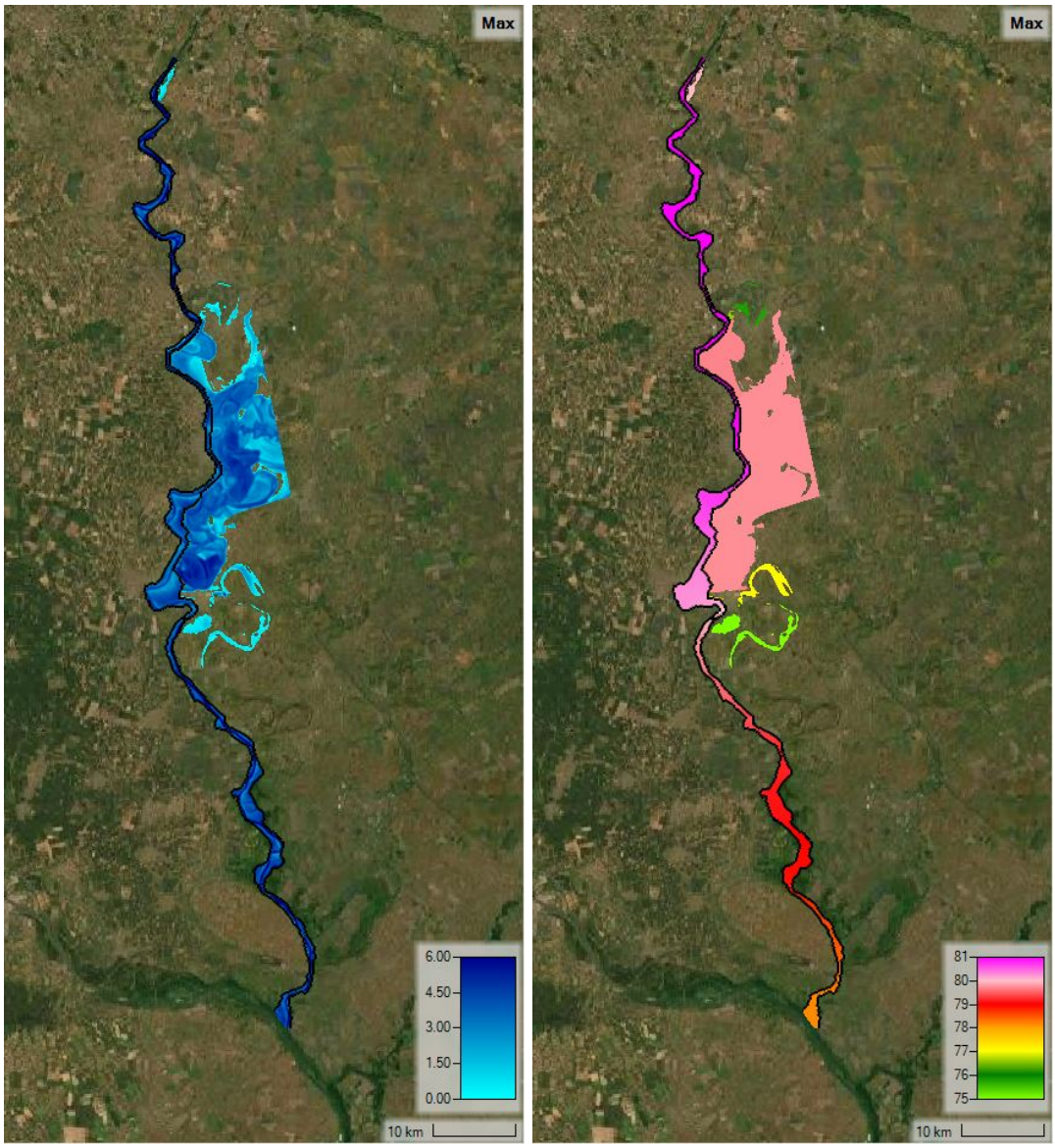

Figure C.12: Inundation depth and water surface level maps for location E4 with a return period of 1000 years.

C.5 Location E5

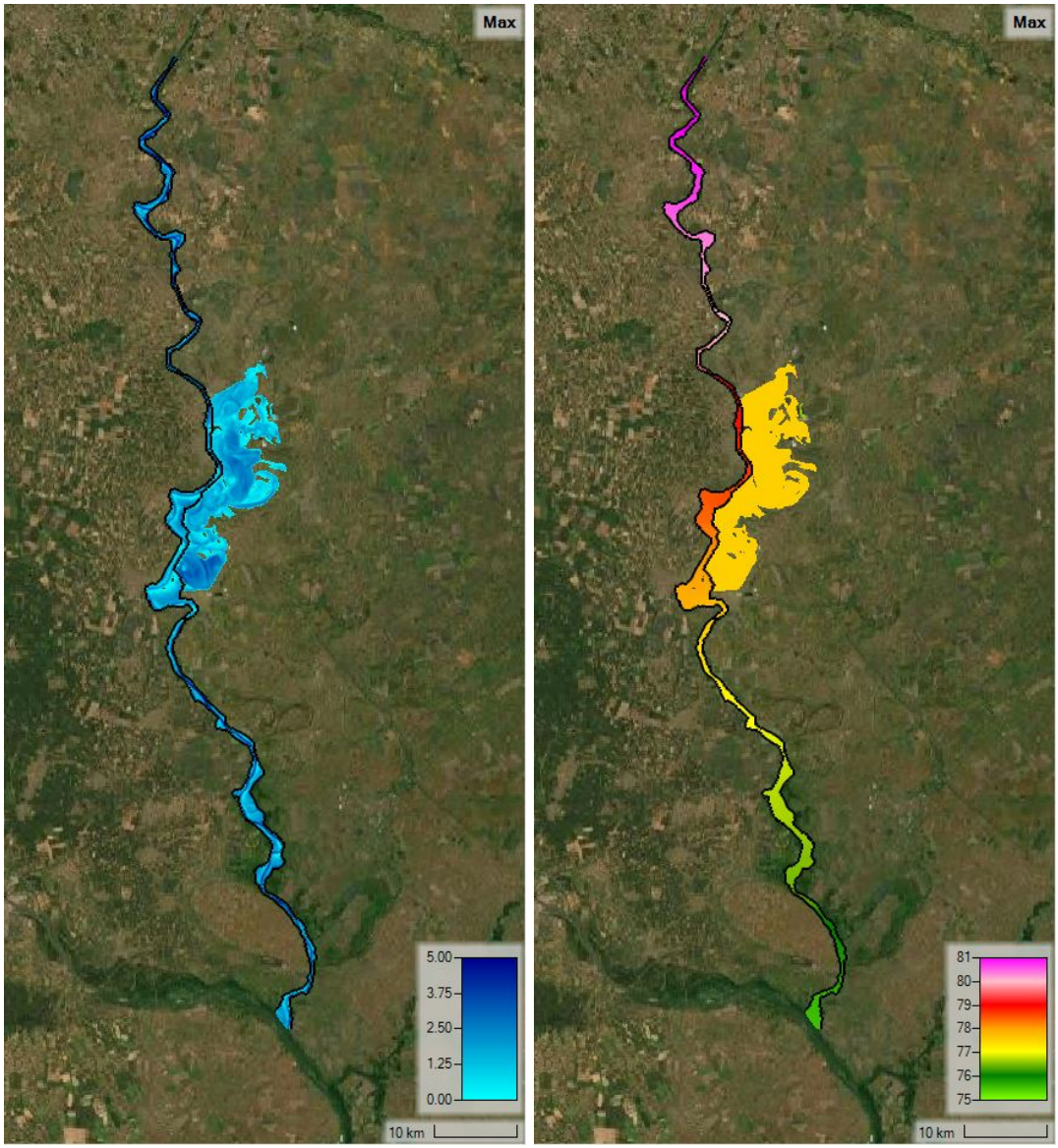

Figure C.13: Inundation depth and water surface level maps for location E5 with a return period of 10 years.

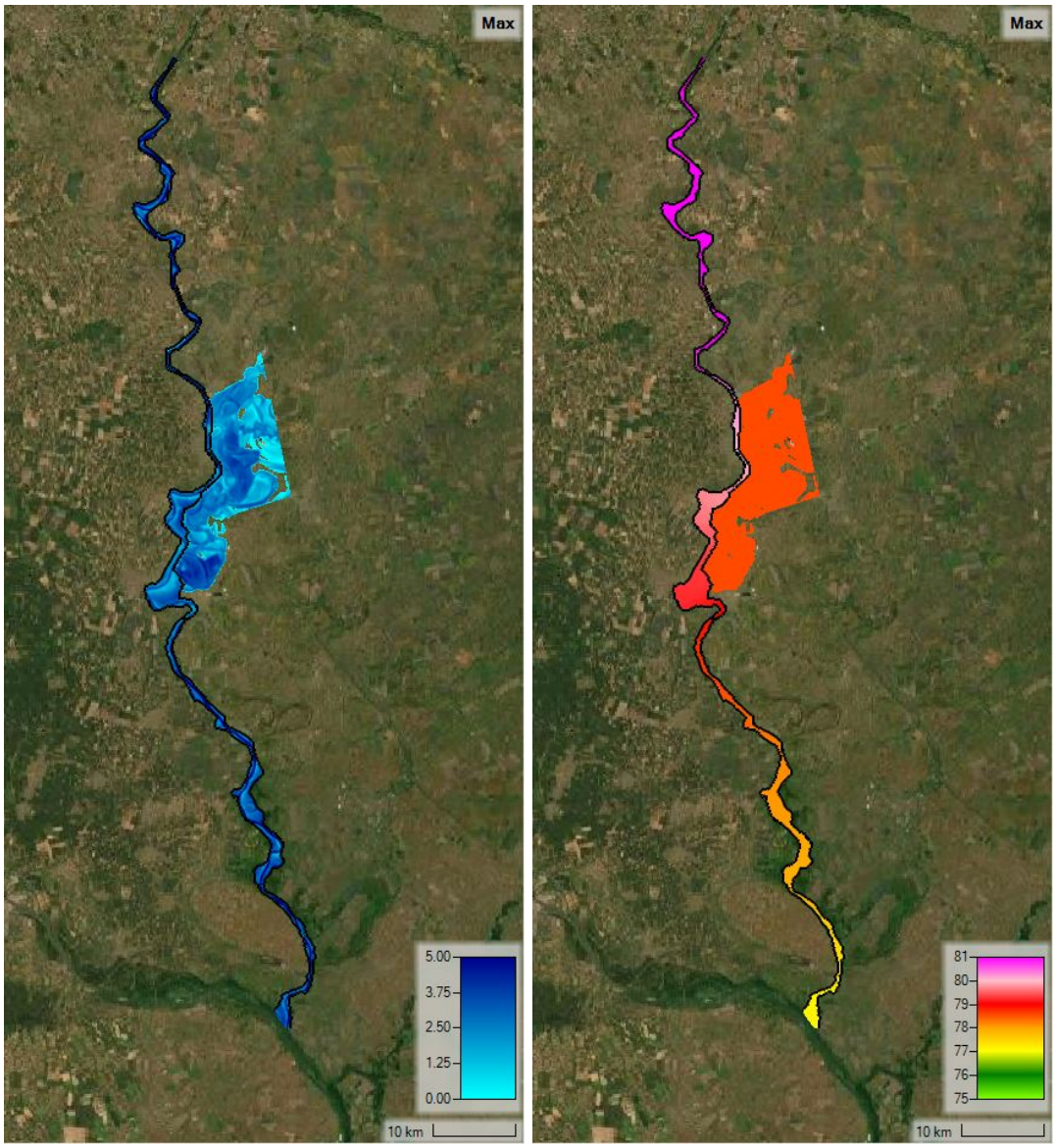

Figure C.14: Inundation depth and water surface level maps for location E5 with a return period of 100 years.

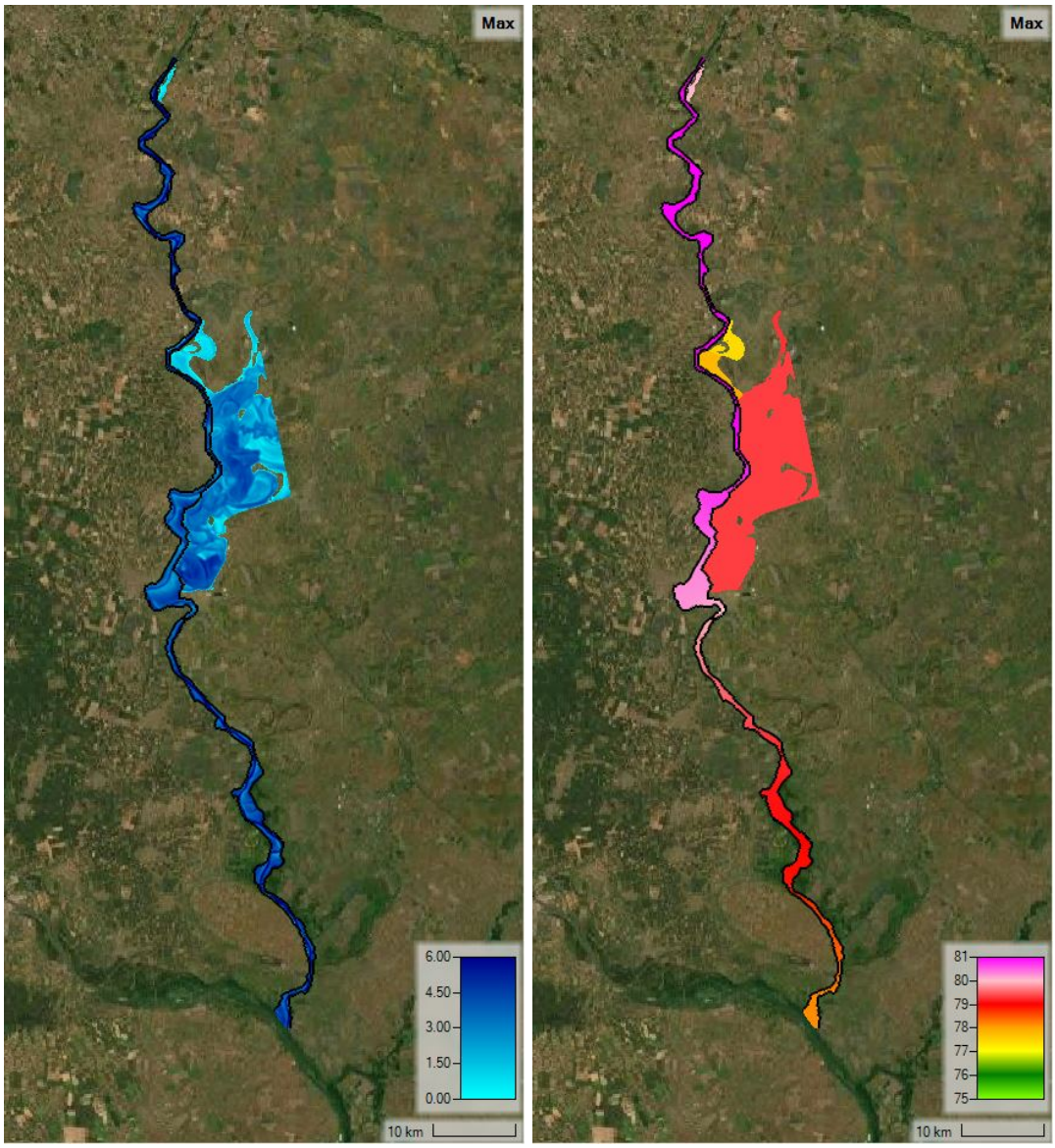

Figure C.15: Inundation depth and water surface level maps for location E5 with a return period of 1000 years.

C.6 Location E6

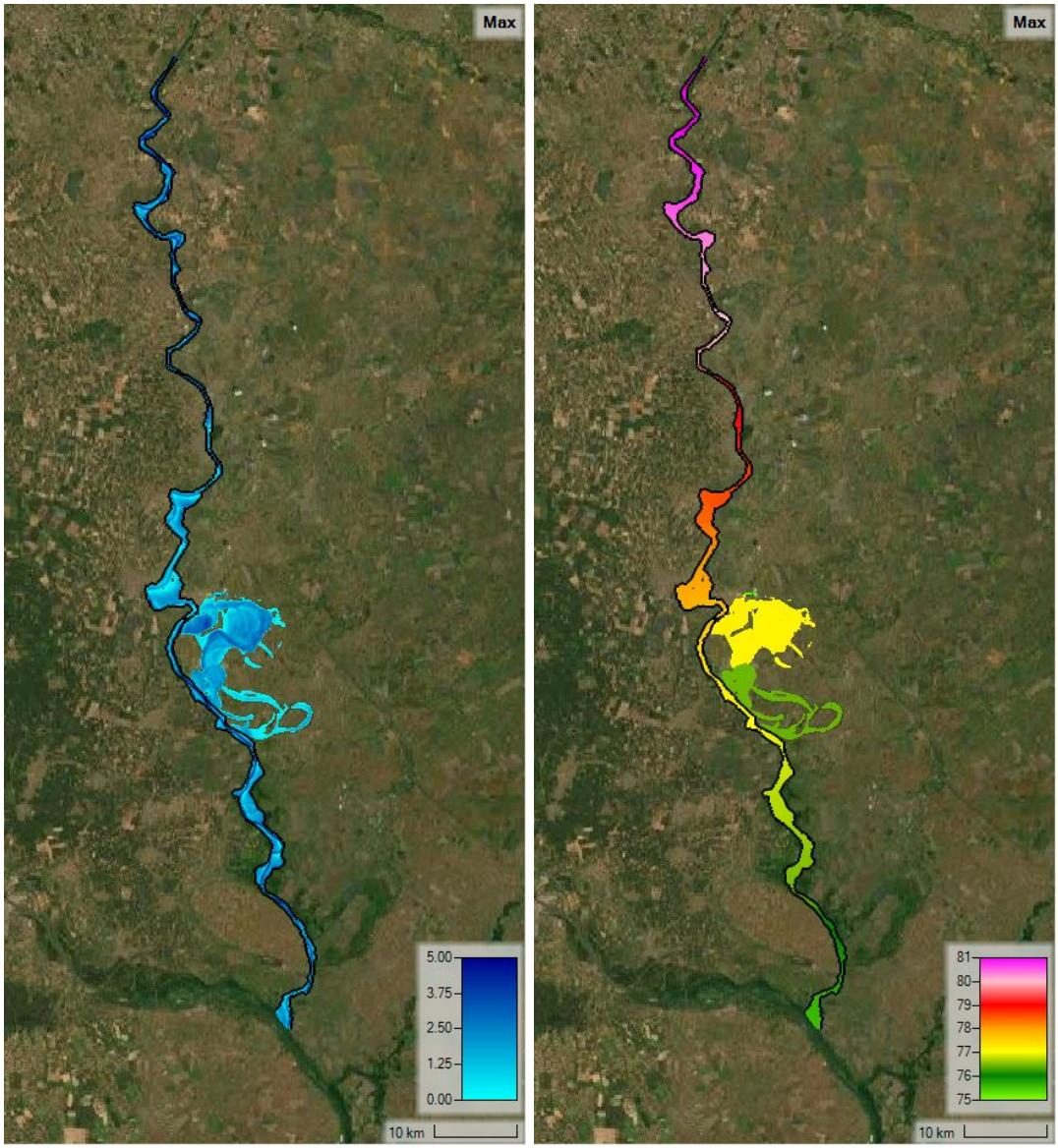

Figure C.16: Inundation depth and water surface level maps for location E6 with a return period of 10 years.

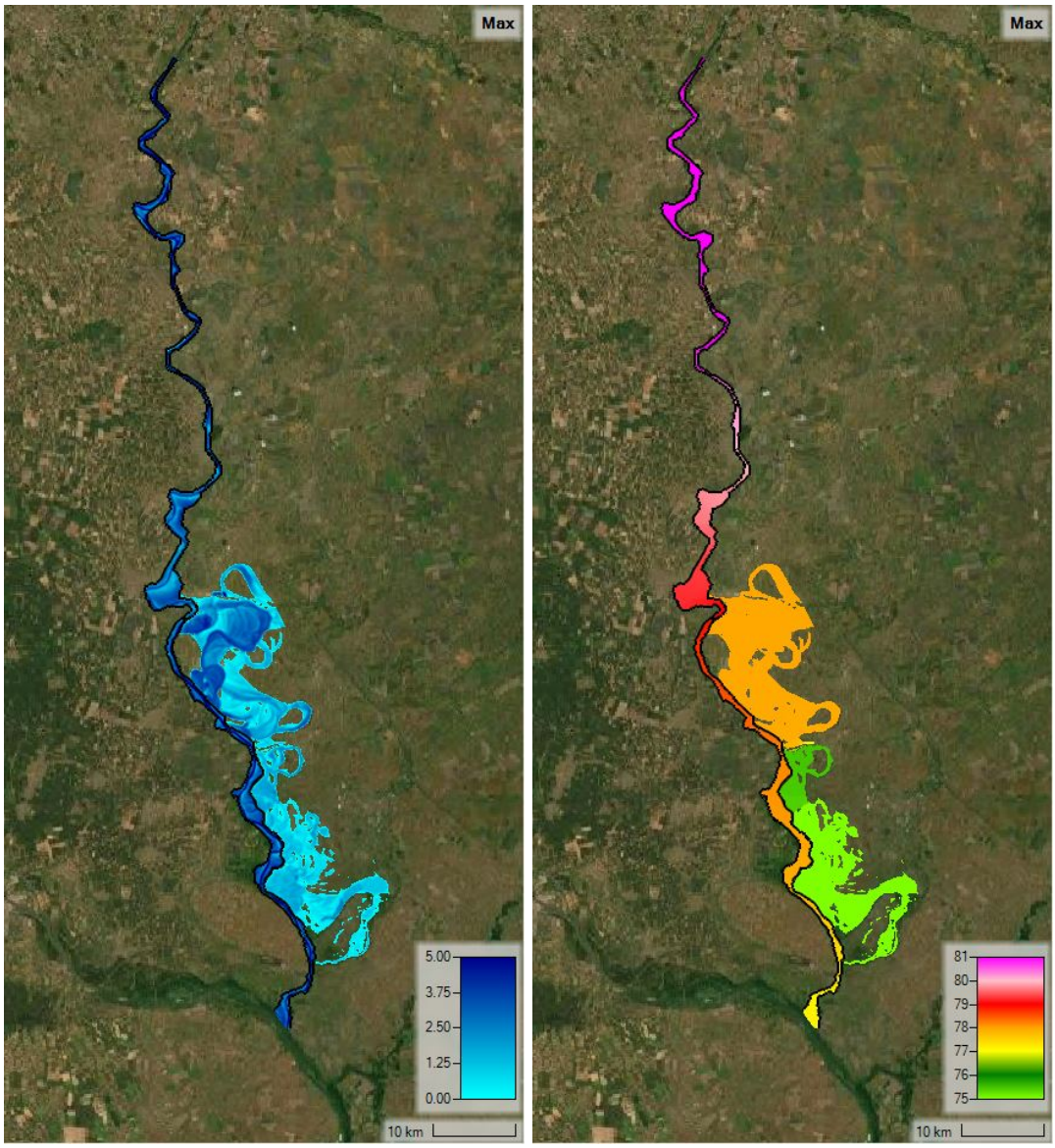

Figure C.17: Inundation depth and water surface level maps for location E6 with a return period of 100 years.

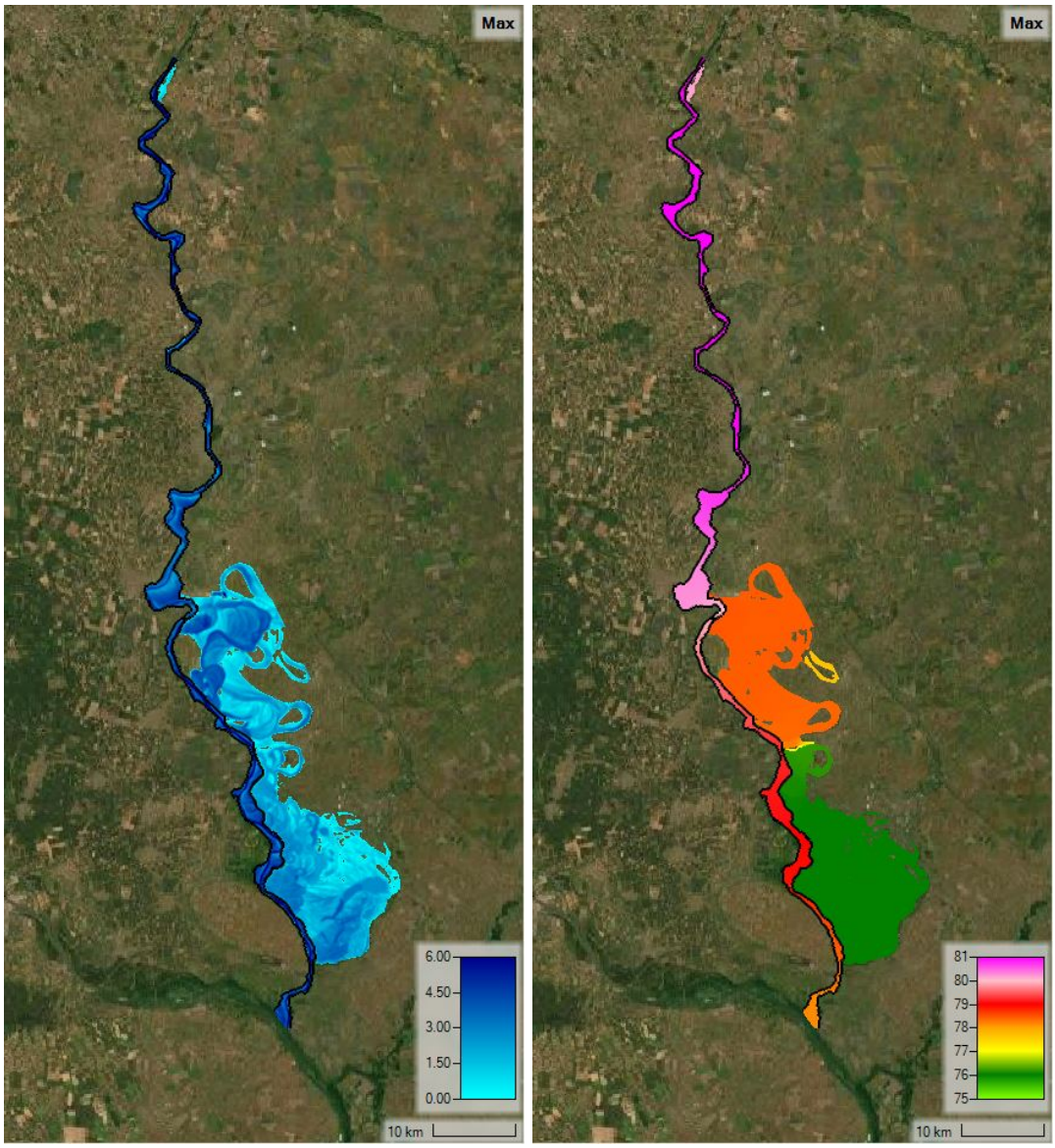

Figure C.18: Inundation depth and water surface level maps for location E6 with a return period of 1000 years.

C.7 Location E7

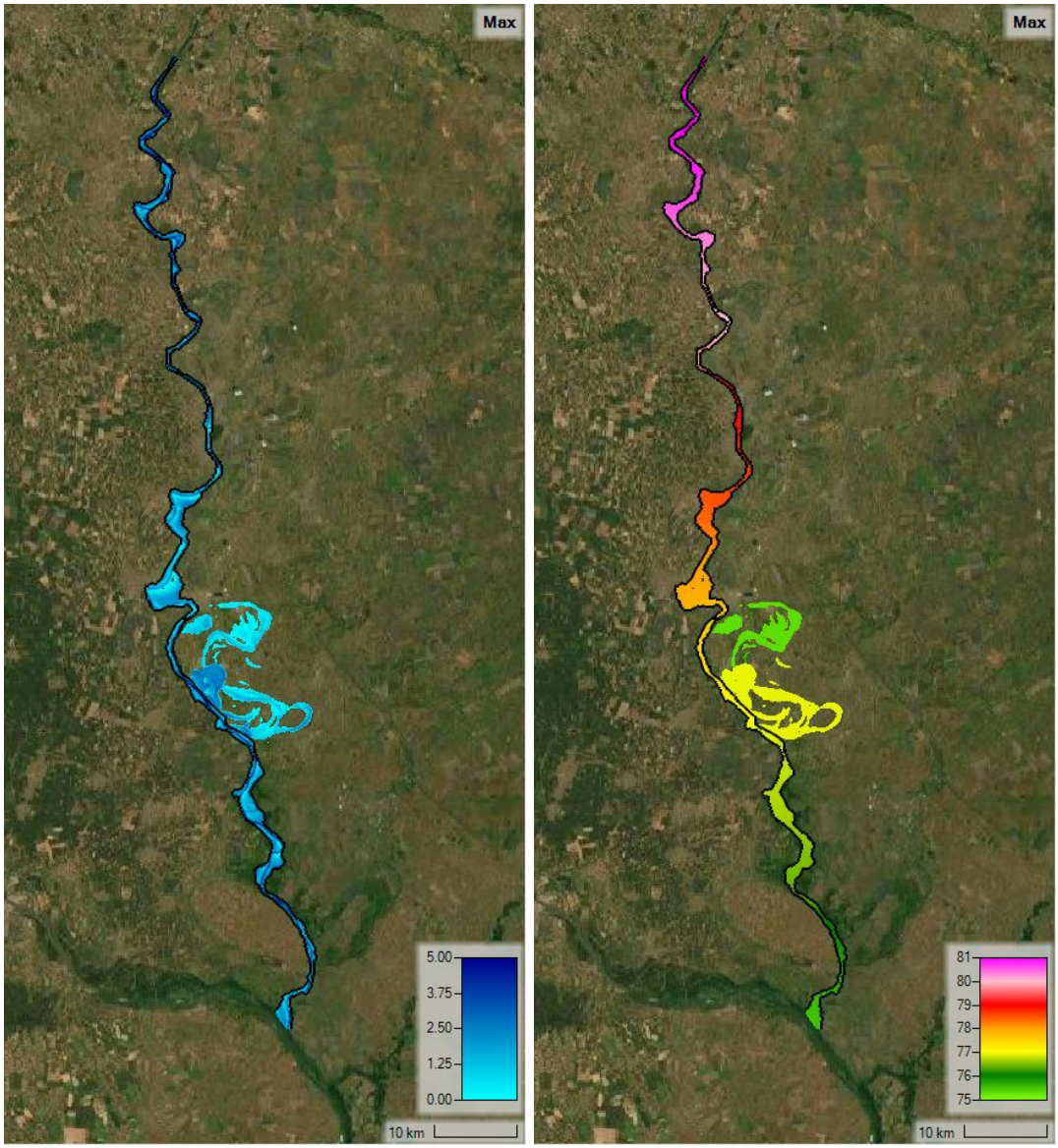

Figure C.19: Inundation depth and water surface level maps for location E7 with a return period of 10 years.

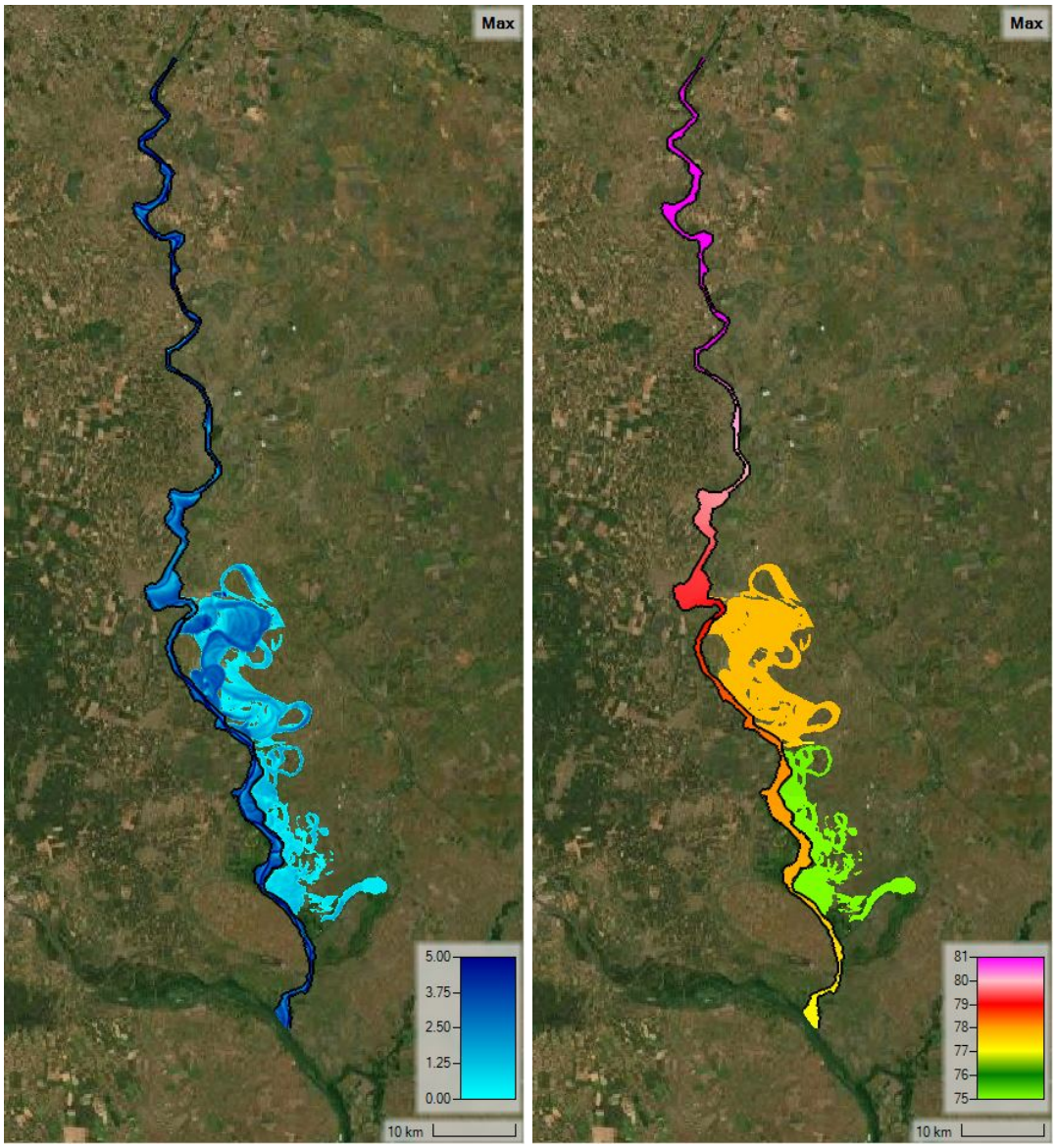

Figure C.20: Inundation depth and water surface level maps for location E7 with a return period of 100 years.

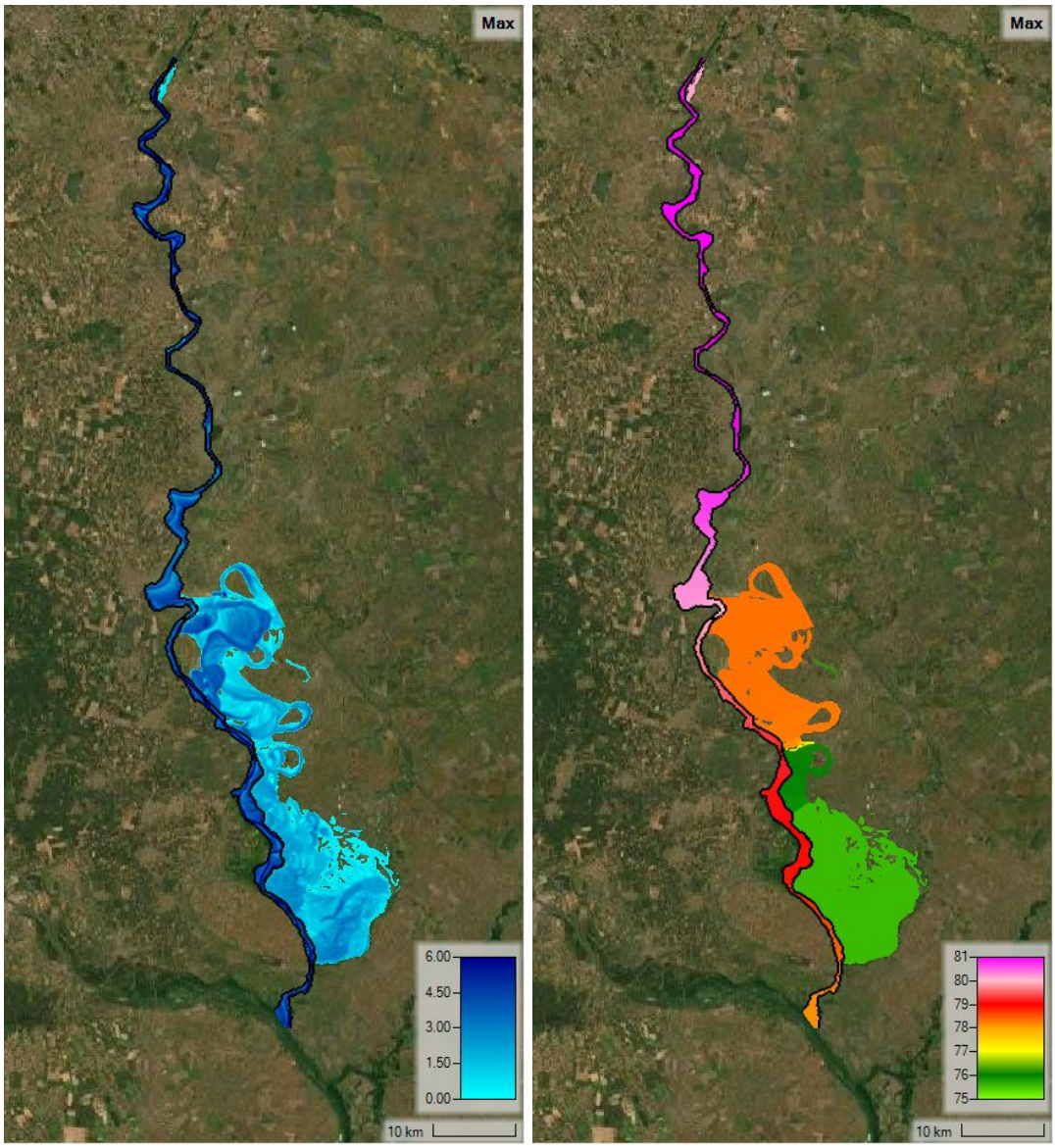

Figure C.21: Inundation depth and water surface level maps for location E7 with a return period of 1000 years.

C.8 Location E8

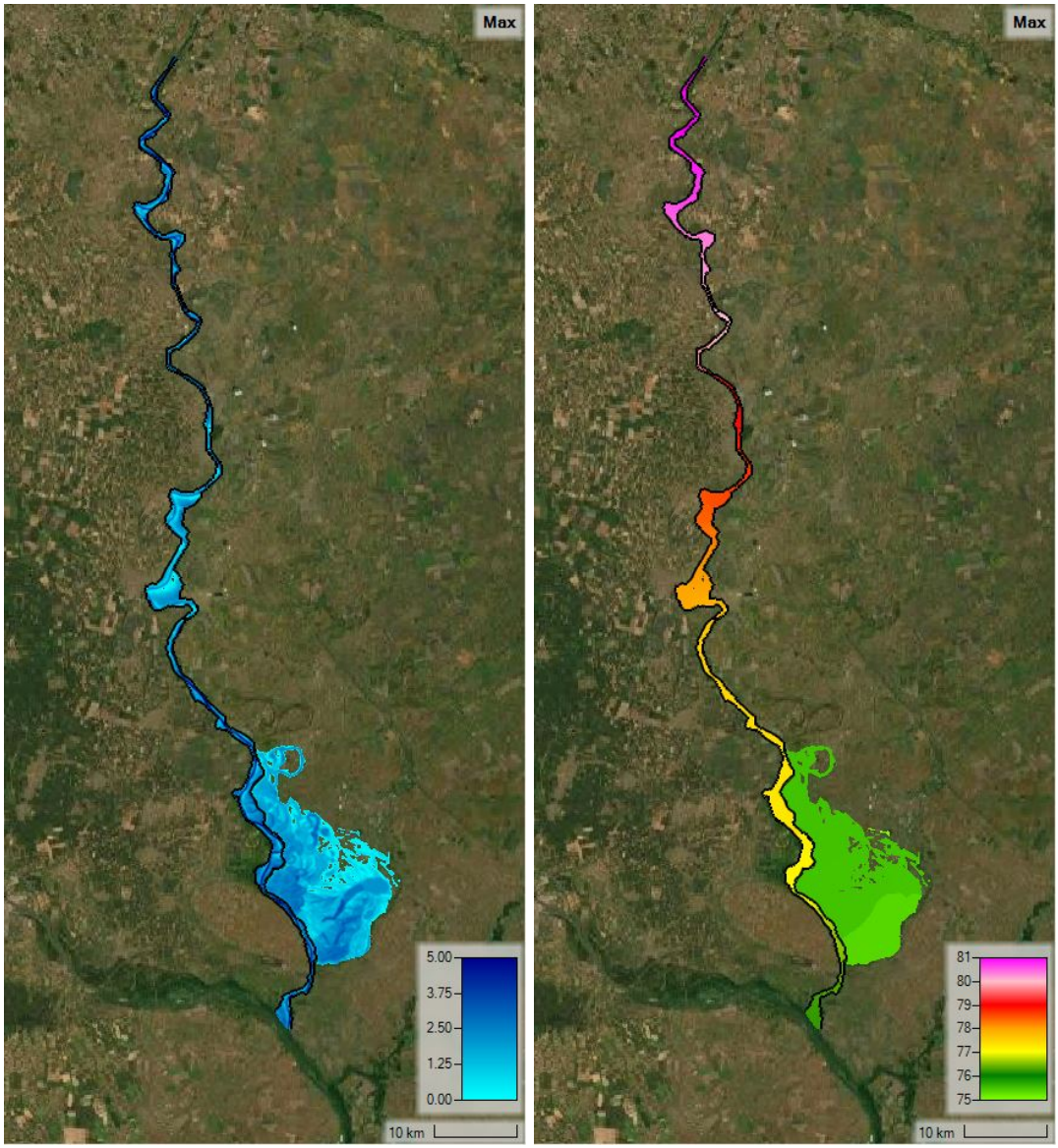

Figure C.22: Inundation depth and water surface level maps for location E8 with a return period of 10 years.

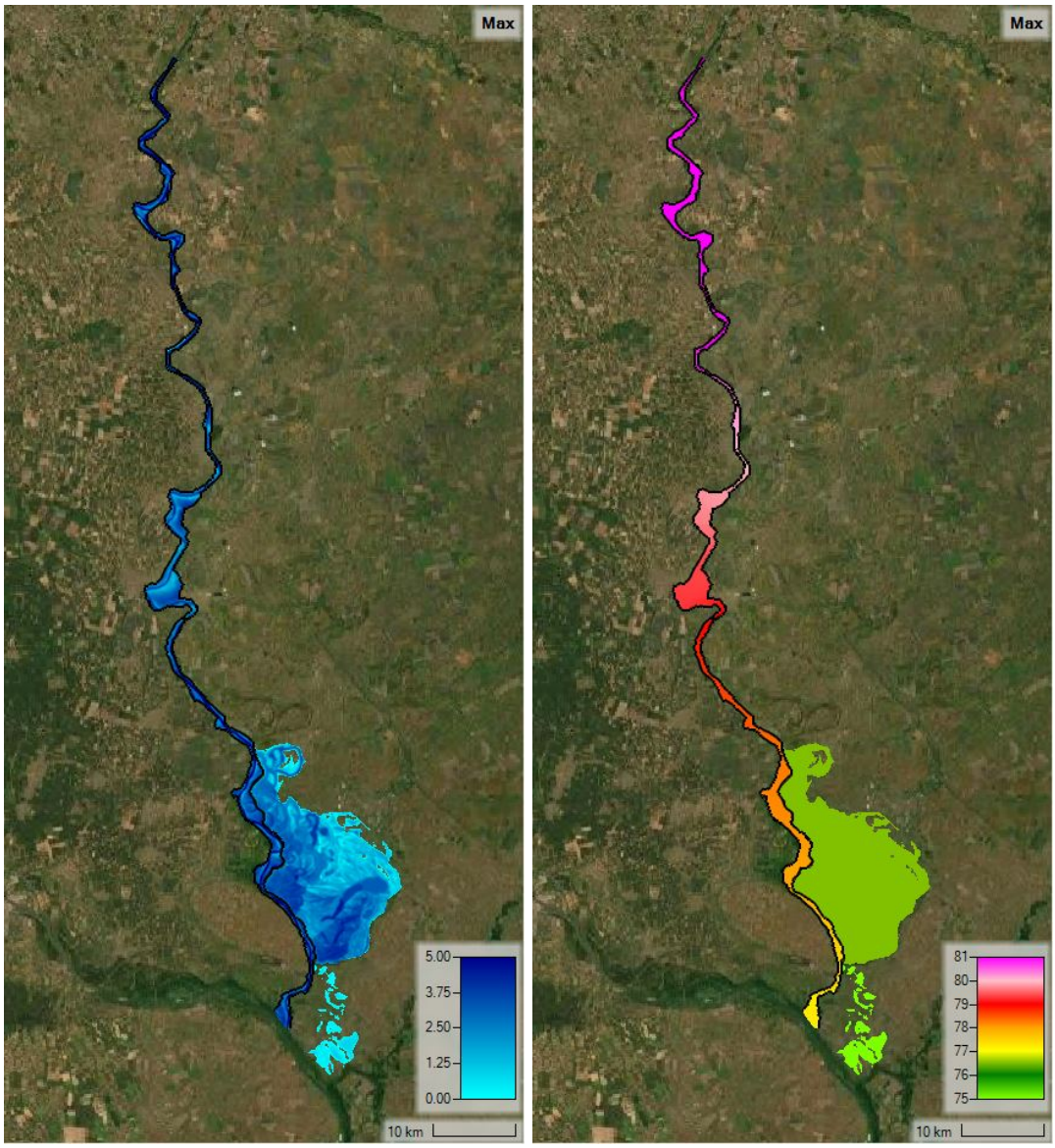

Figure C.23: Inundation depth and water surface level maps for location E8 with a return period of 100 years.

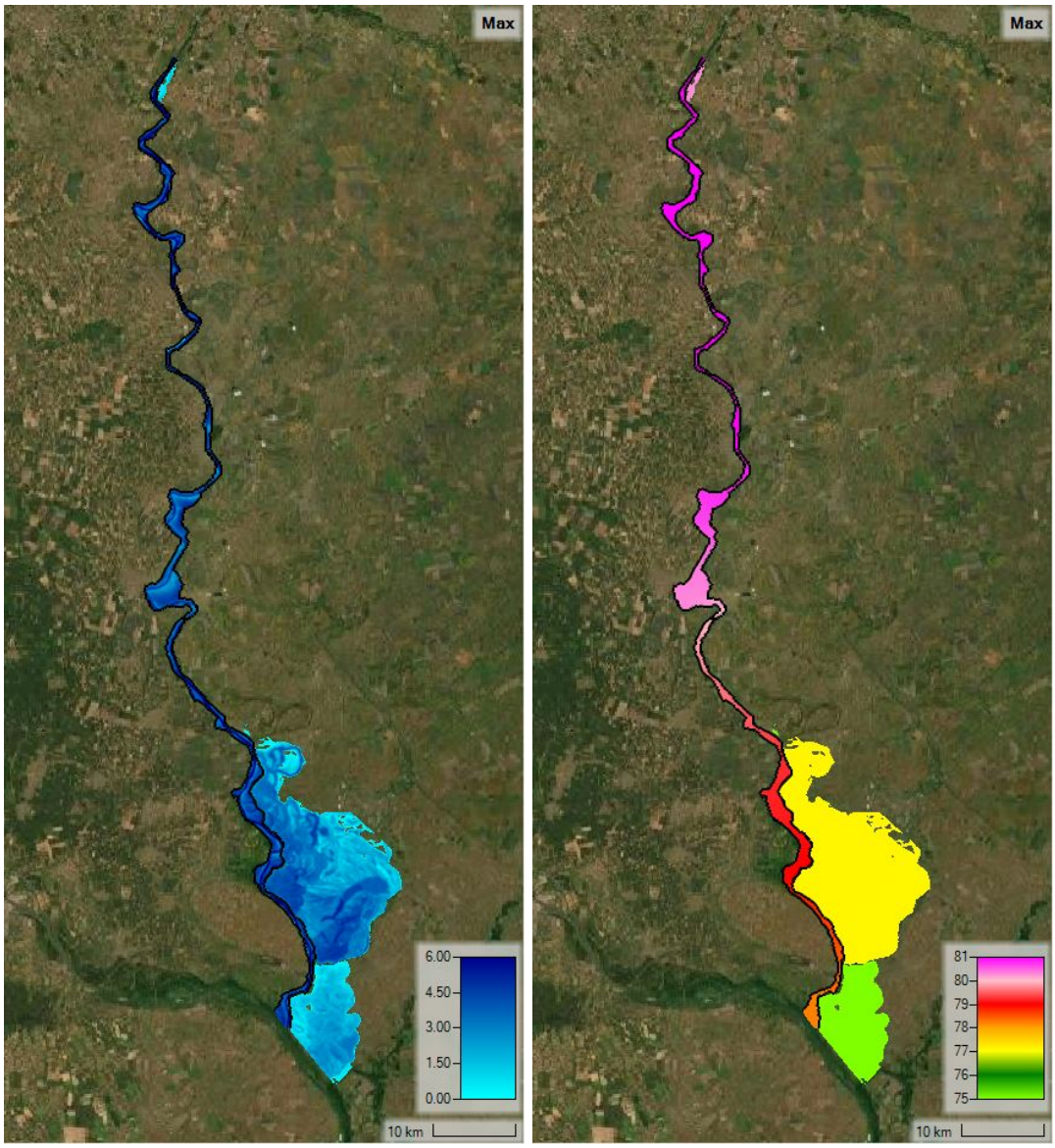

Figure C.24: Inundation depth and water surface level maps for location E8 with a return period of 1000 years.

C.9 Location E9

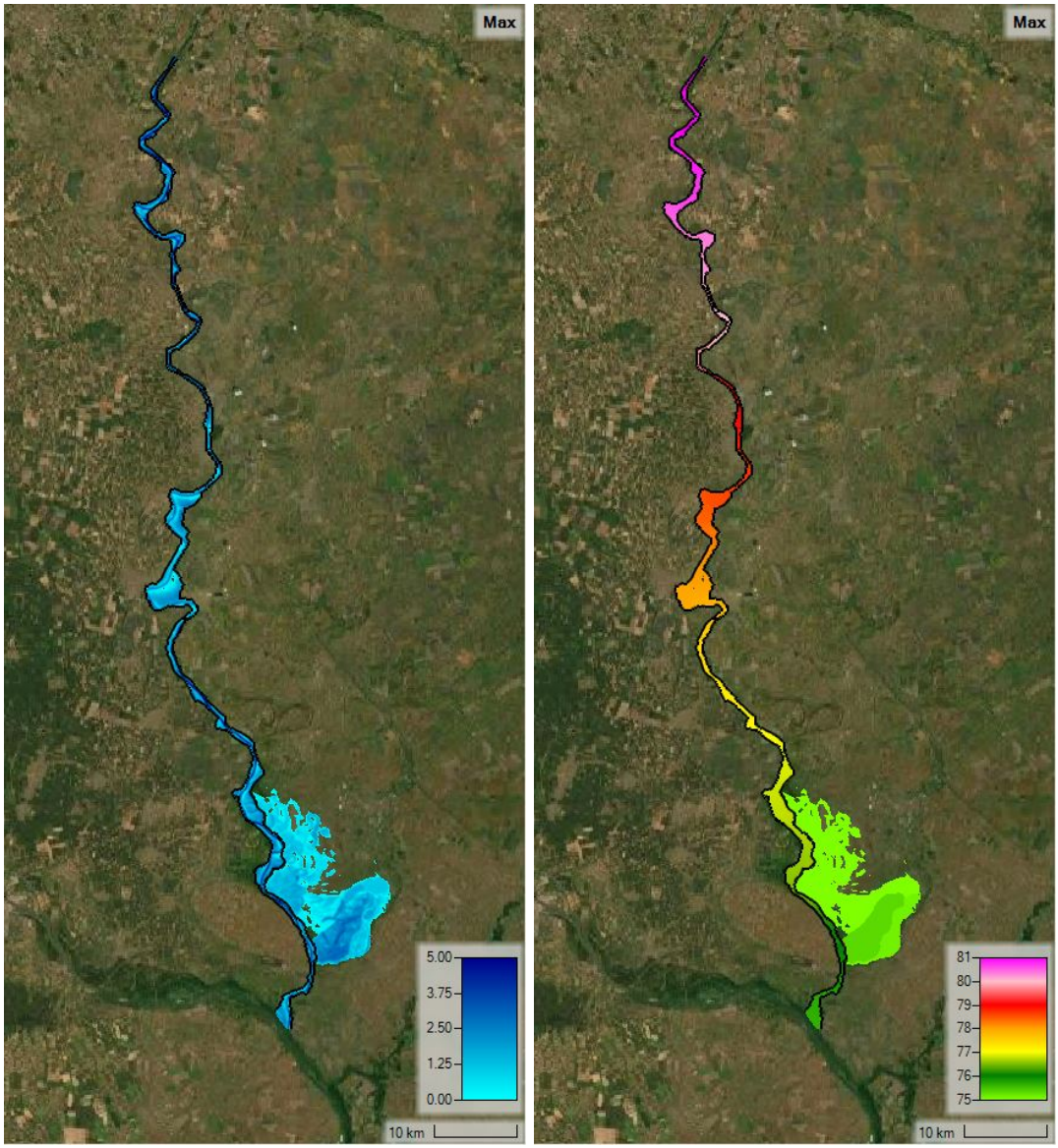

Figure C.25: Inundation depth and water surface level maps for location E9 with a return period of 10 years.

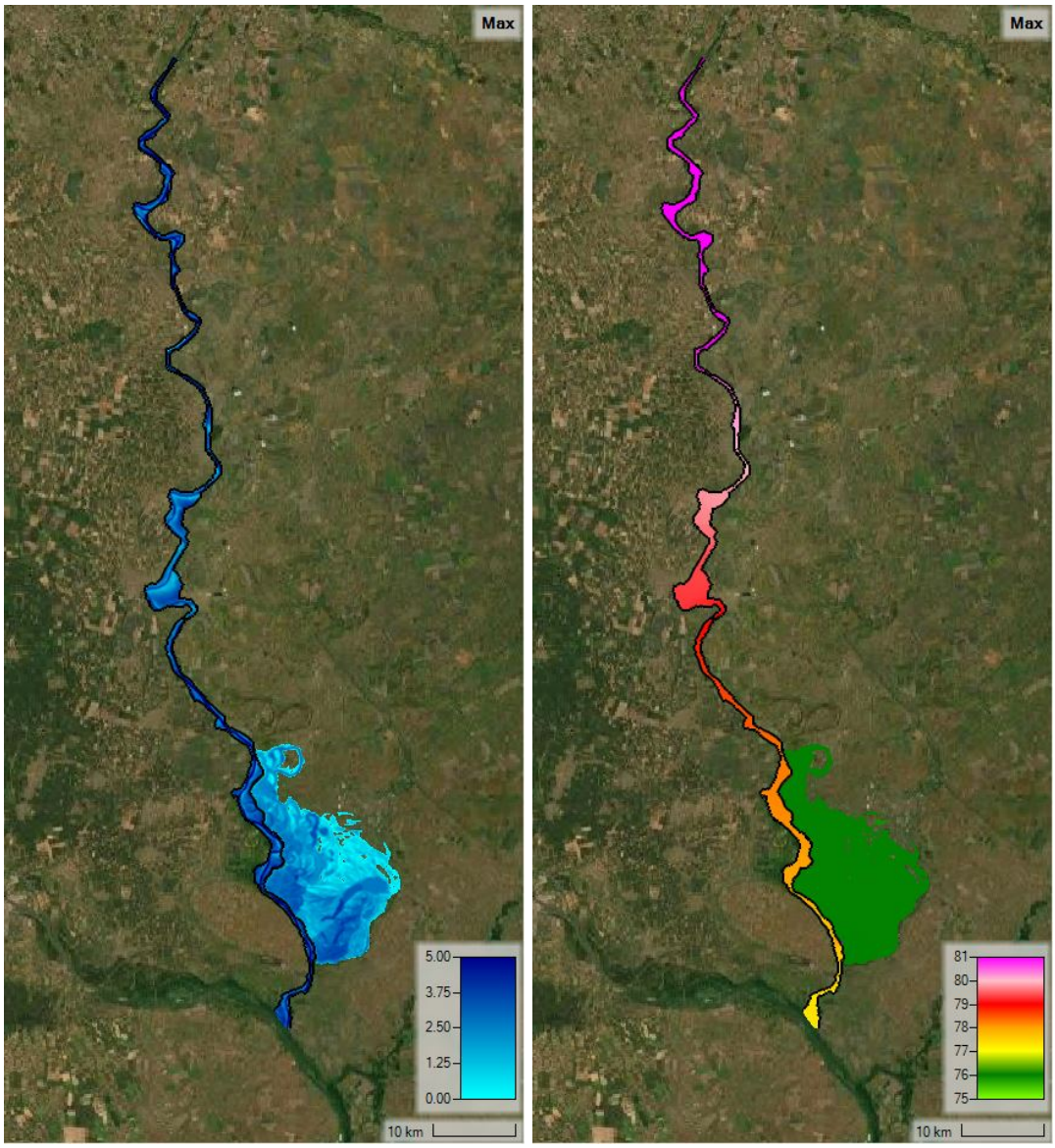

Figure C.26: Inundation depth and water surface level maps for location E9 with a return period of 100 years.

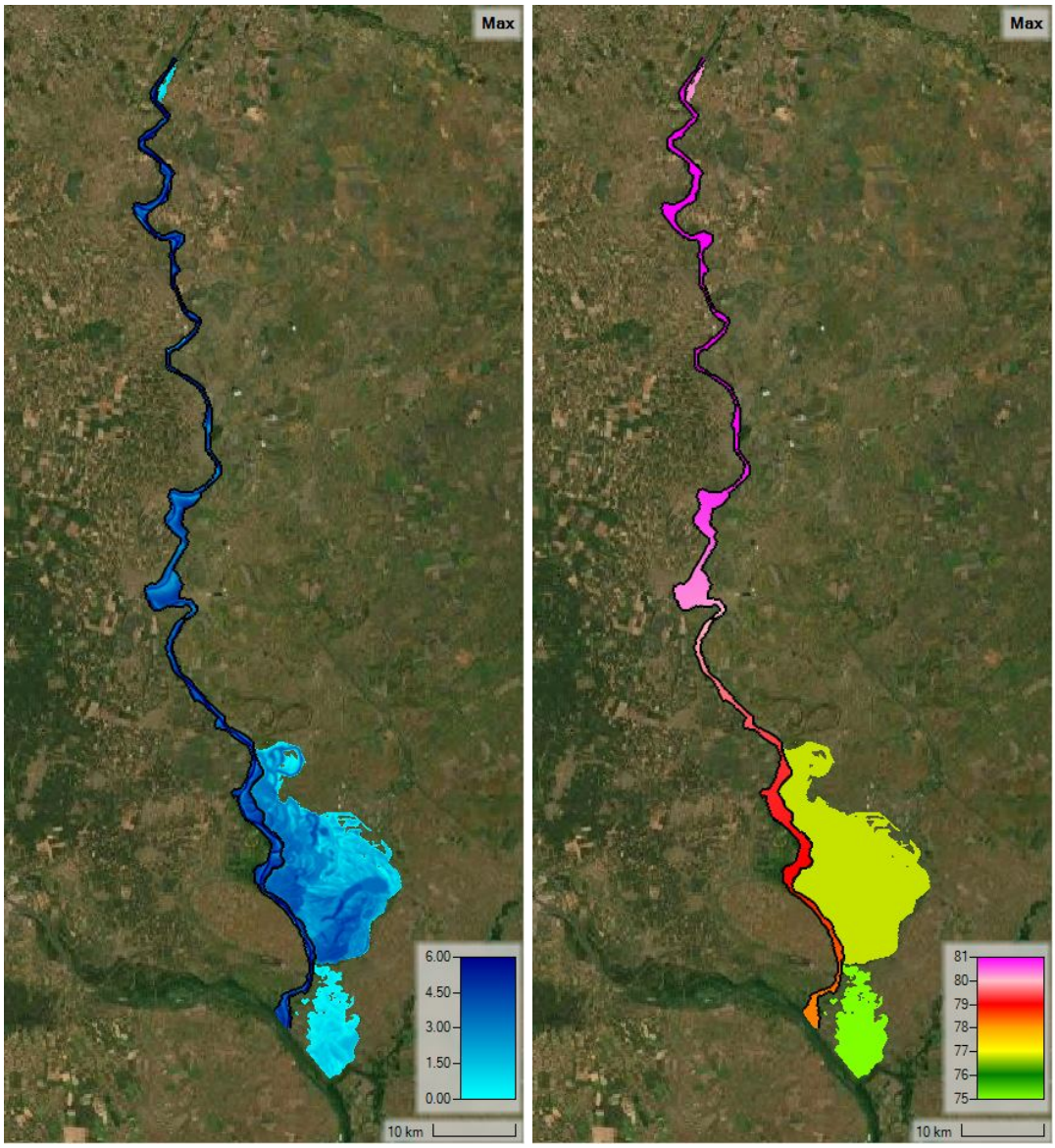

Figure C.27: Inundation depth and water surface level maps for location E9 with a return period of 1000 years.

C.10 Location W1

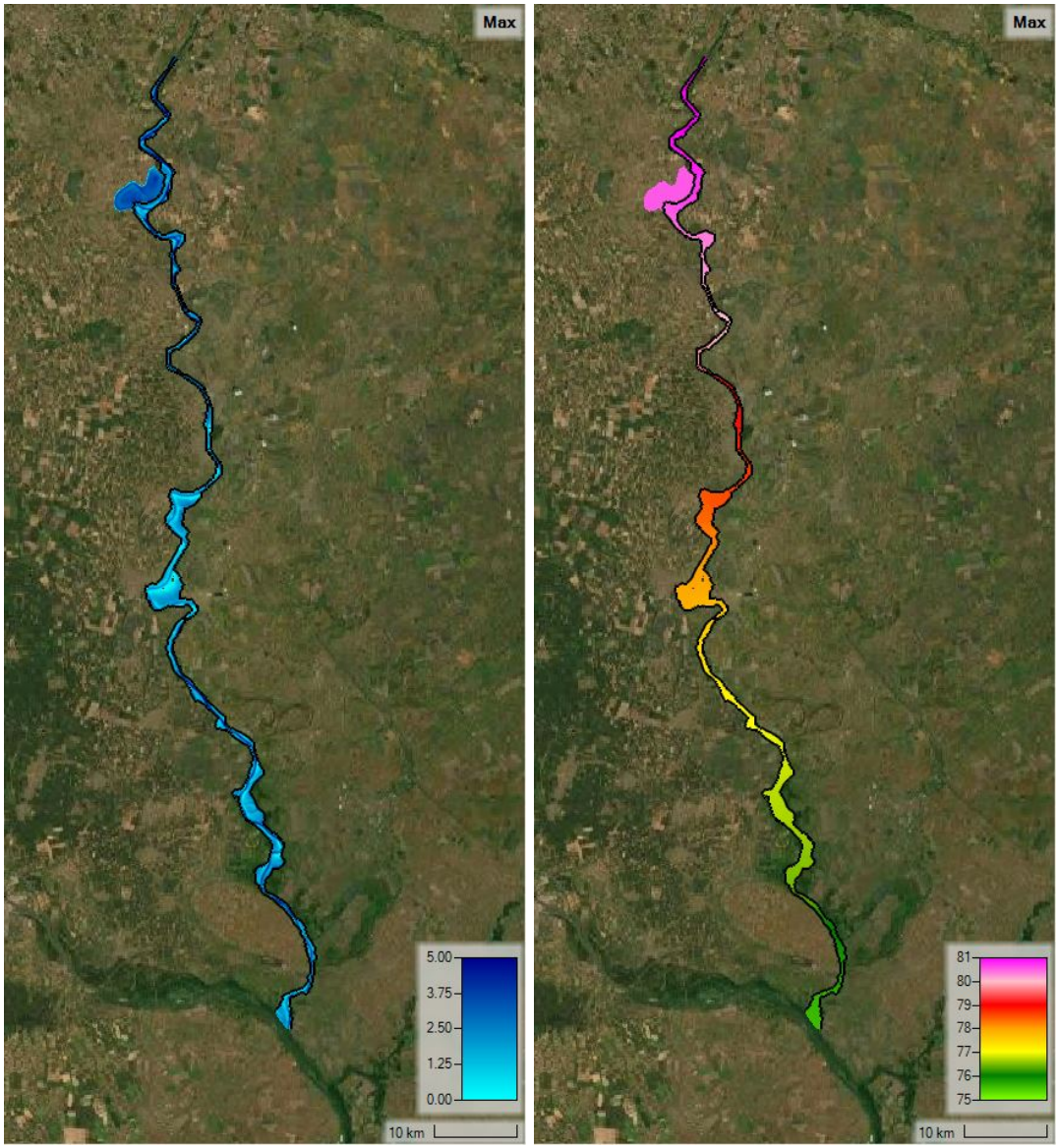

Figure C.28: Inundation depth and water surface level maps for location W1 with a return period of 10 years.

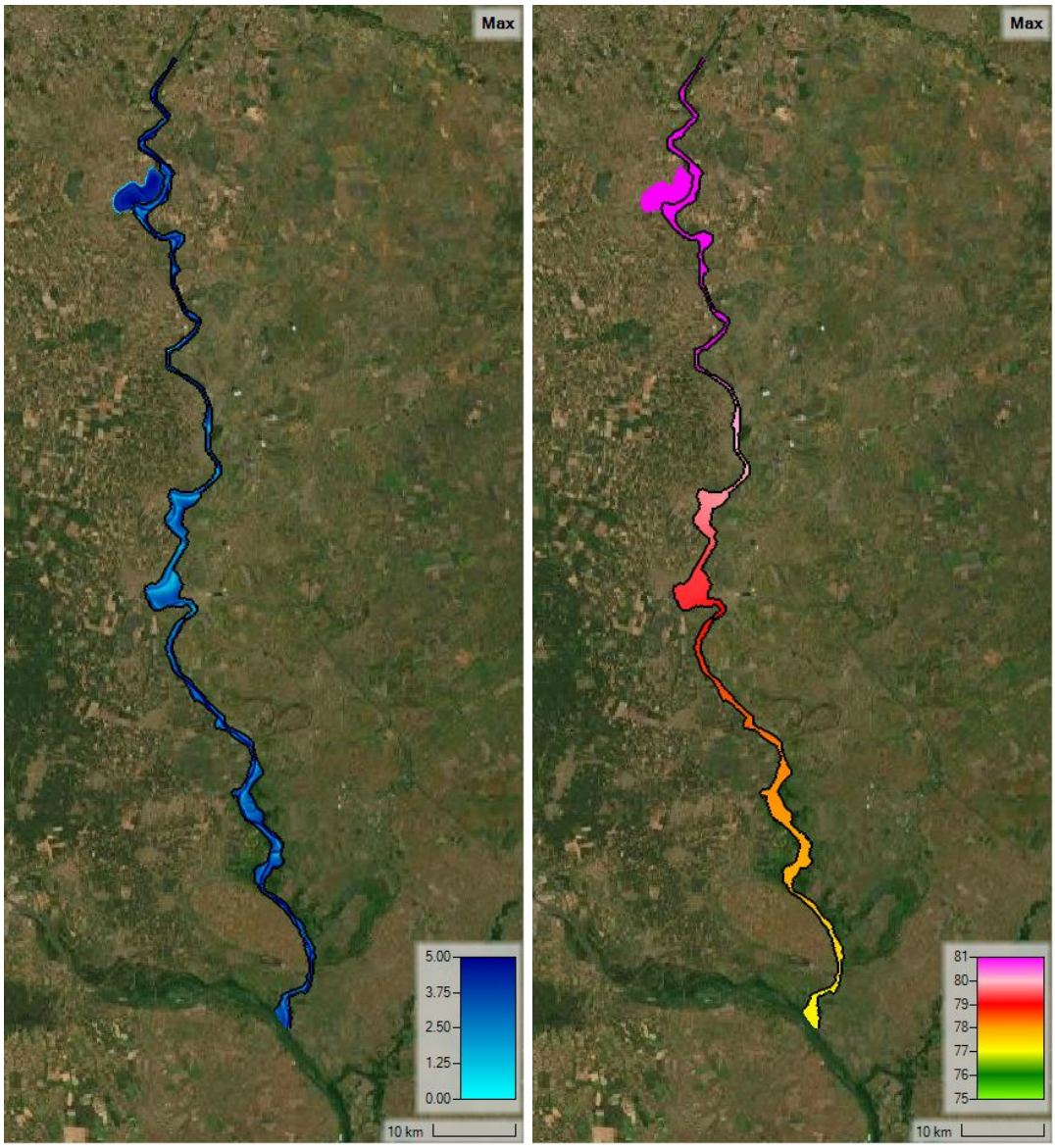

Figure C.29: Inundation depth and water surface level maps for location W1 with a return period of 100 years.

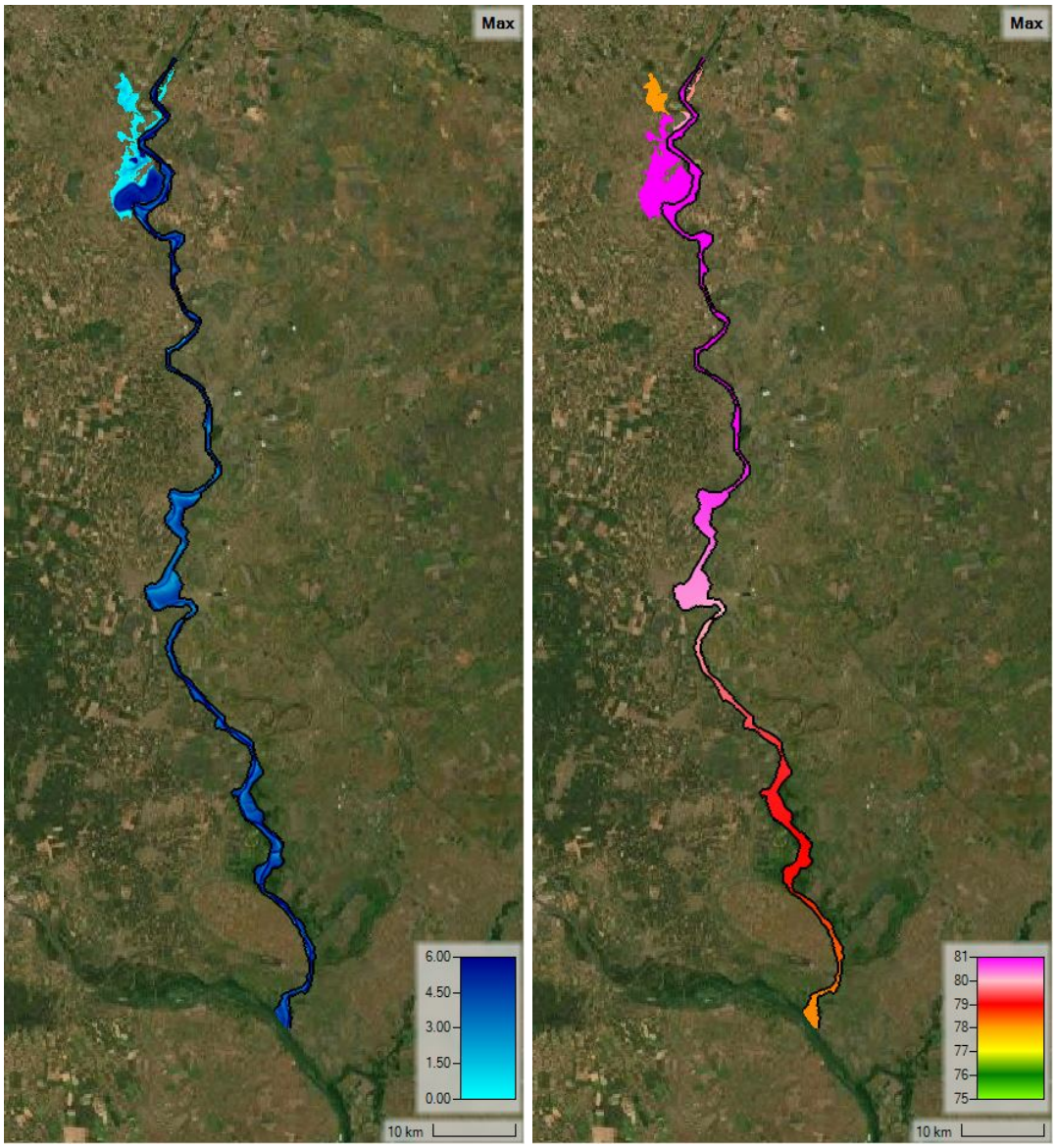

Figure C.30: Inundation depth and water surface level maps for location W1 with a return period of 1000 years.

C.11 Location W2

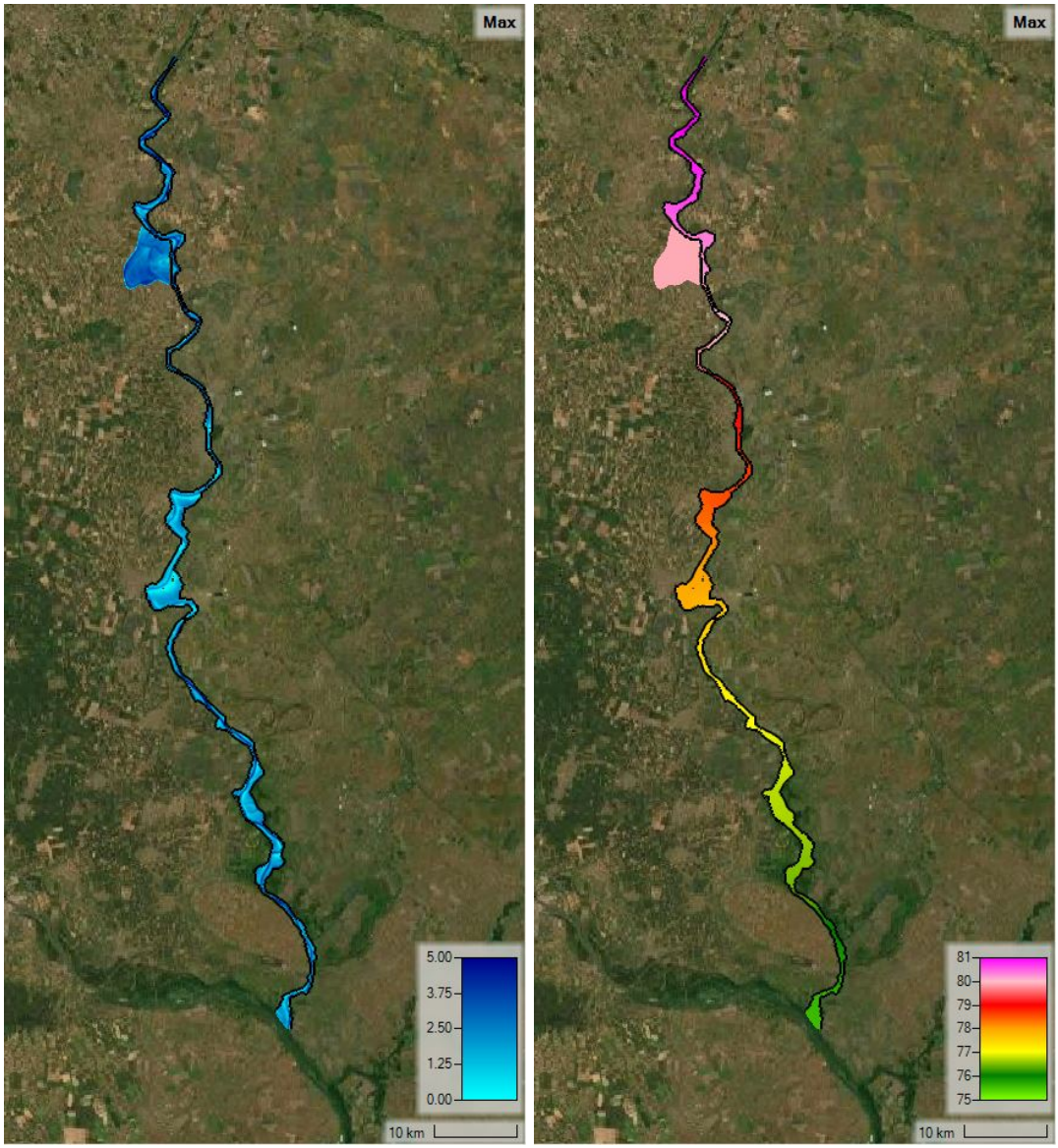

Figure C.31: Inundation depth and water surface level maps for location W2 with a return period of 10 years.

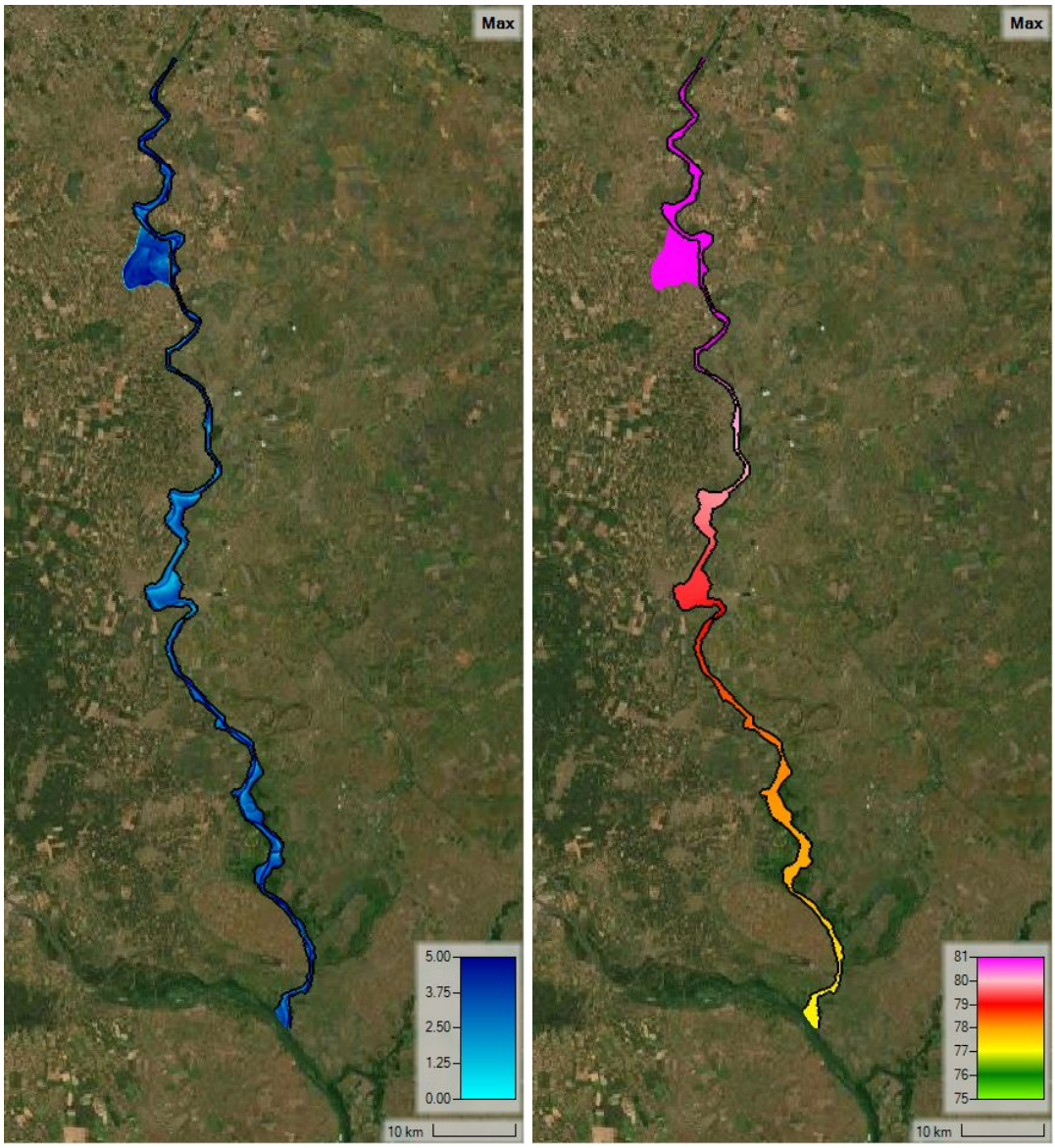

Figure C.32: Inundation depth and water surface level maps for location W2 with a return period of 100 years.

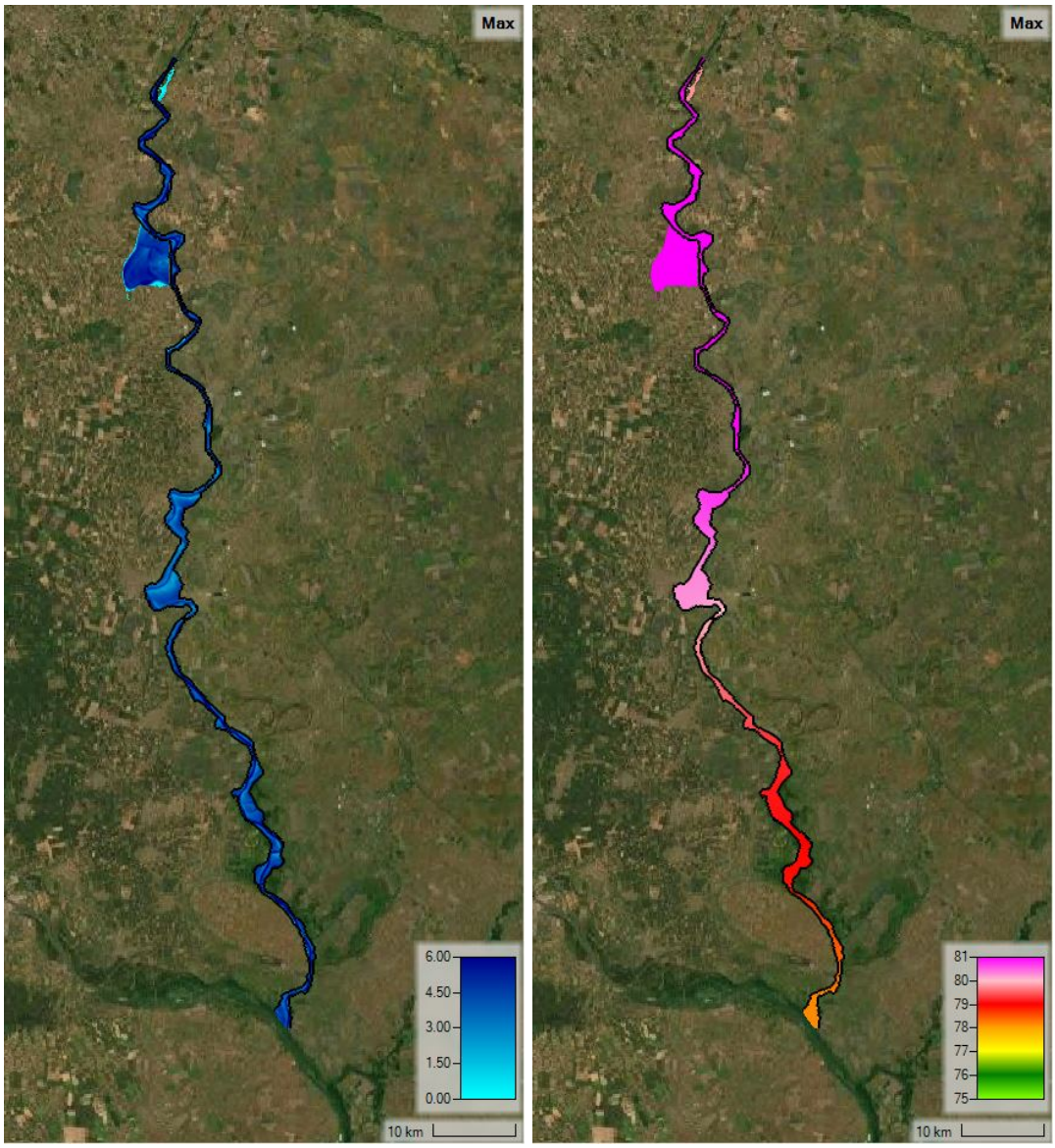

Figure C.33: Inundation depth and water surface level maps for location W2 with a return period of 1000 years.

C.12 Location W3

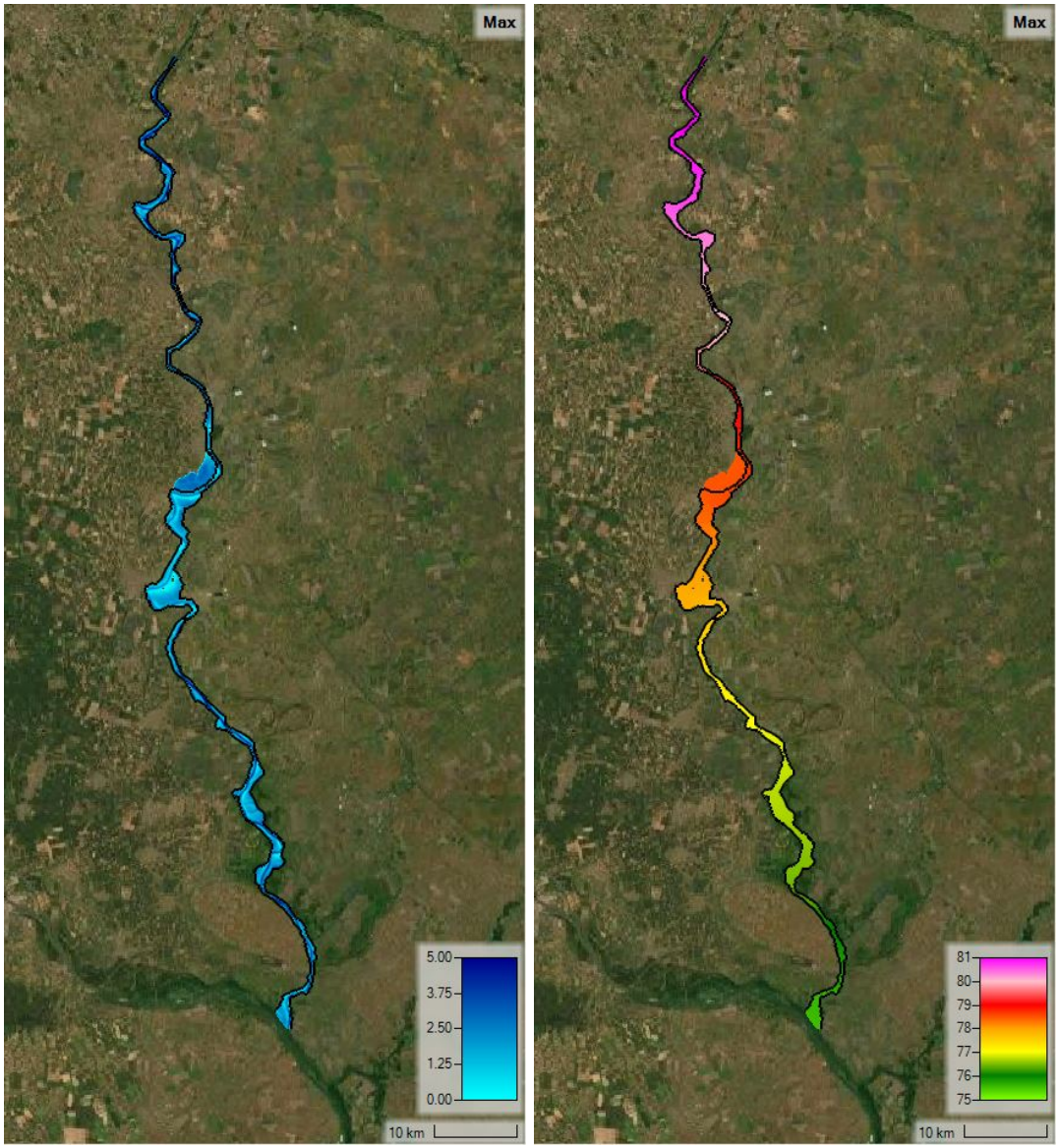

Figure C.34: Inundation depth and water surface level maps for location W3 with a return period of 10 years.

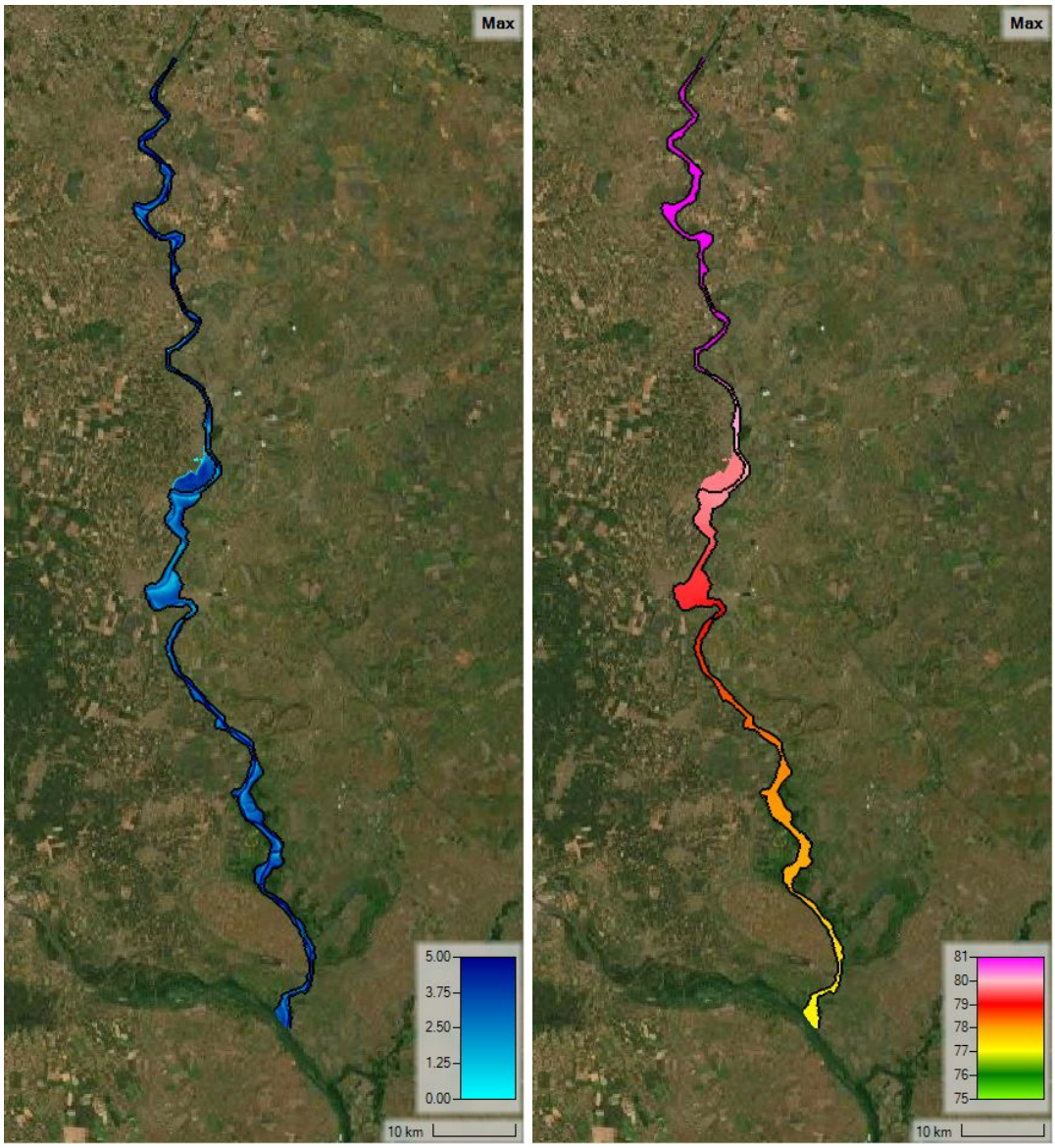

Figure C.35: Inundation depth and water surface level maps for location W3 with a return period of 100 years.

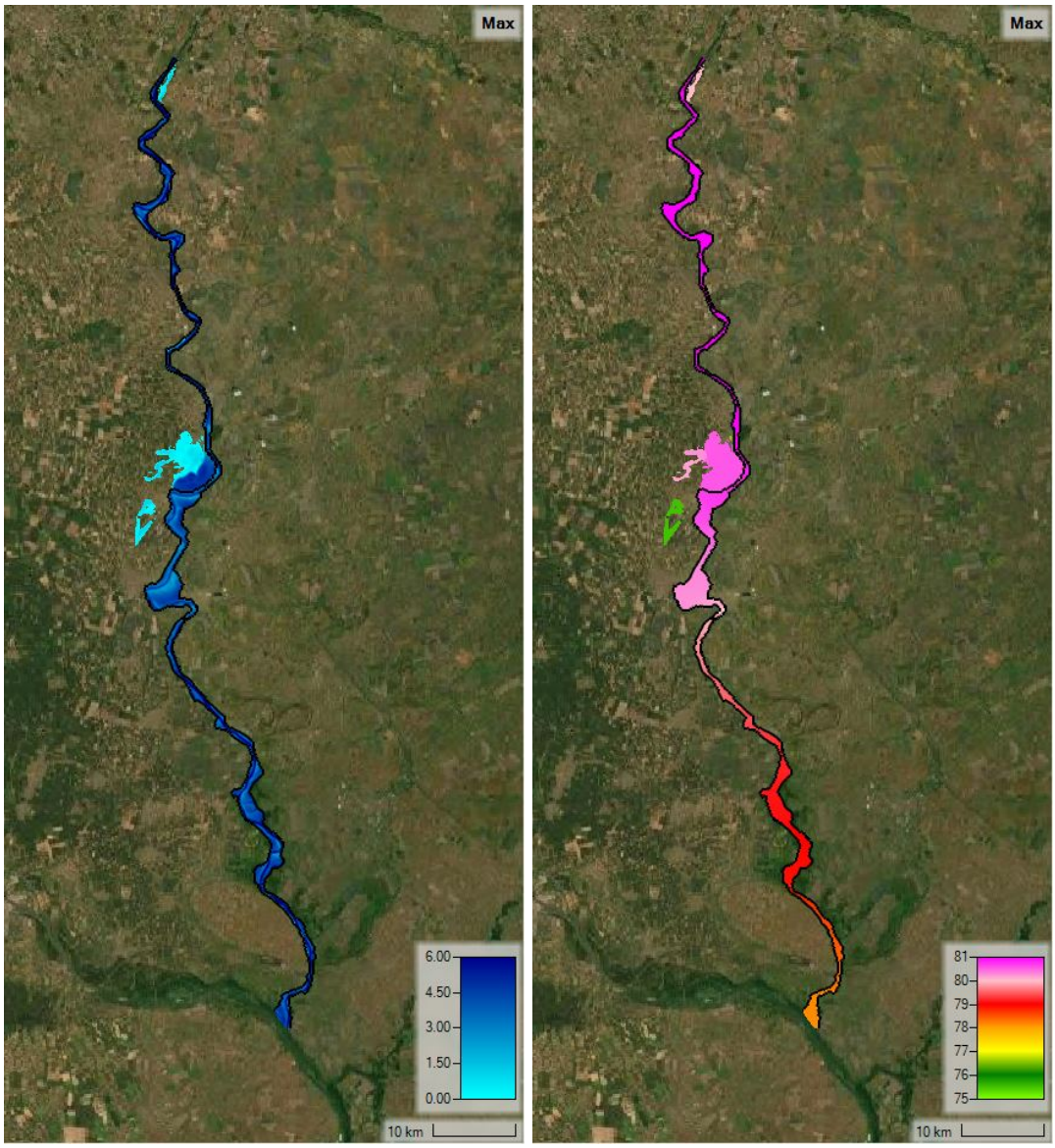

Figure C.36: Inundation depth and water surface level maps for location W3 with a return period of 1000 years.

C.13 Location W4

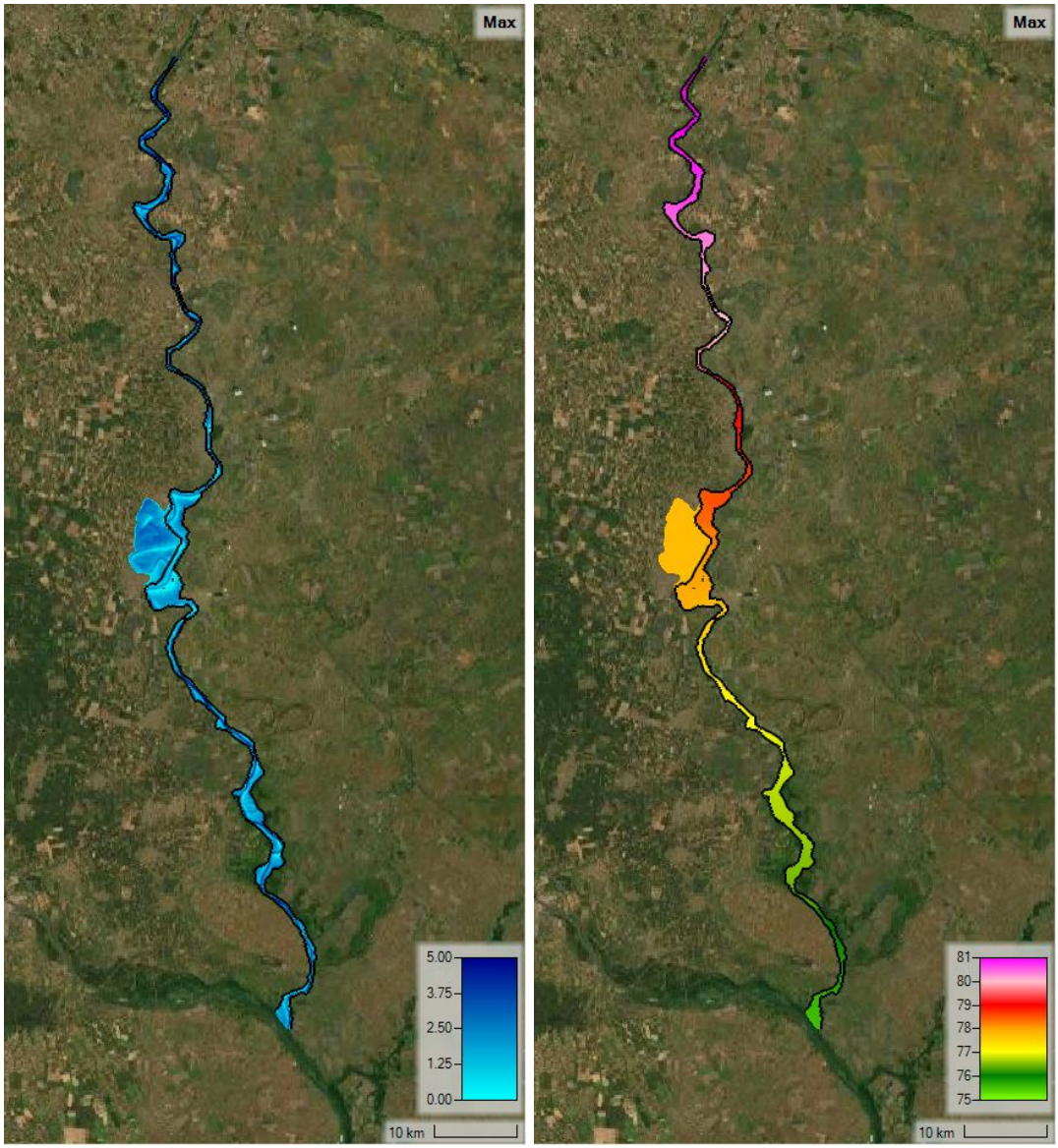

Figure C.37: Inundation depth and water surface level maps for location W4 with a return period of 10 years.

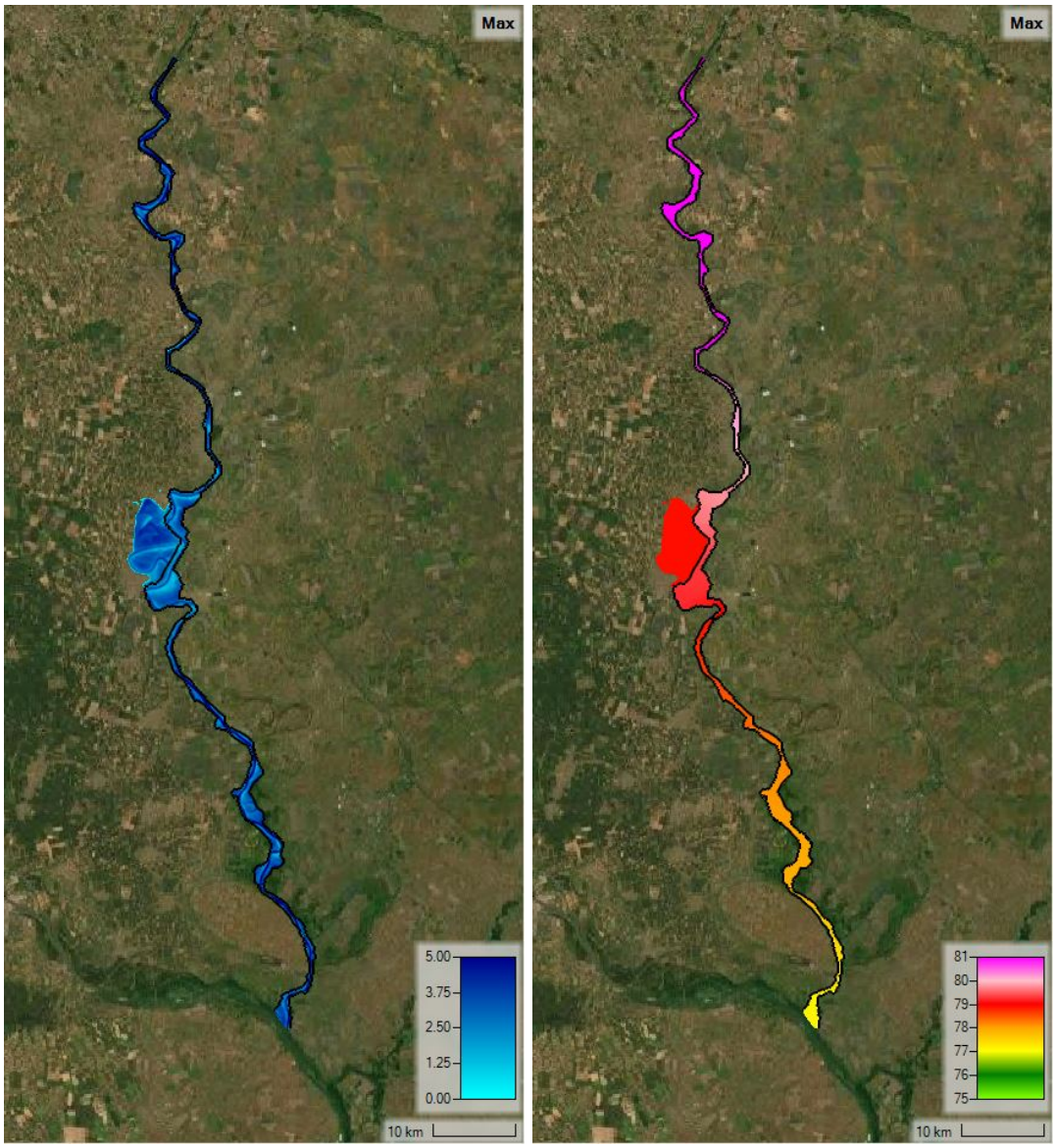

Figure C.38: Inundation depth and water surface level maps for location W4 with a return period of 100 years.

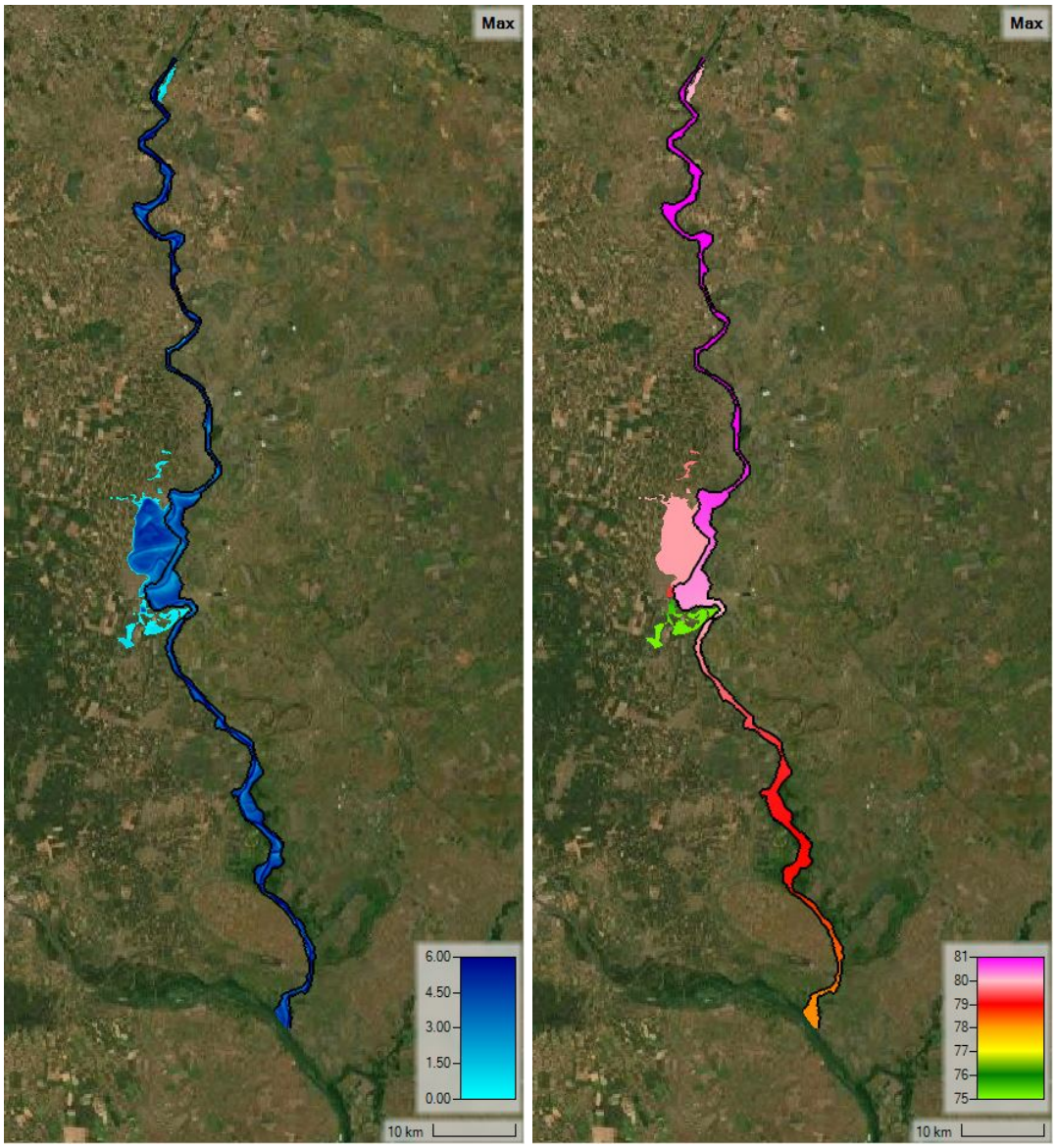

Figure C.39: Inundation depth and water surface level maps for location W4 with a return period of 1000 years.

C.14 Location W5

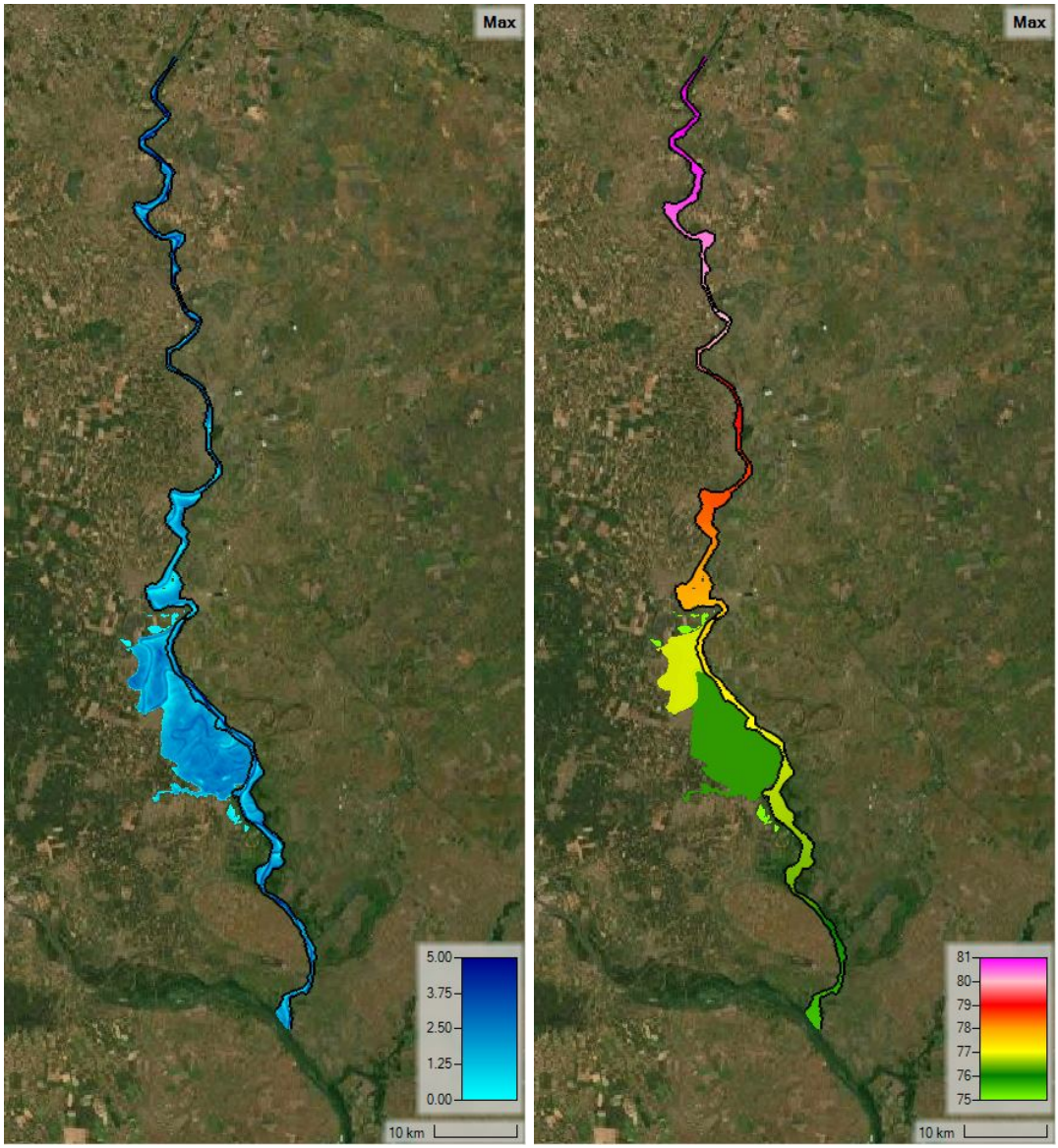

Figure C.40: Inundation depth and water surface level maps for location W5 with a return period of 10 years.

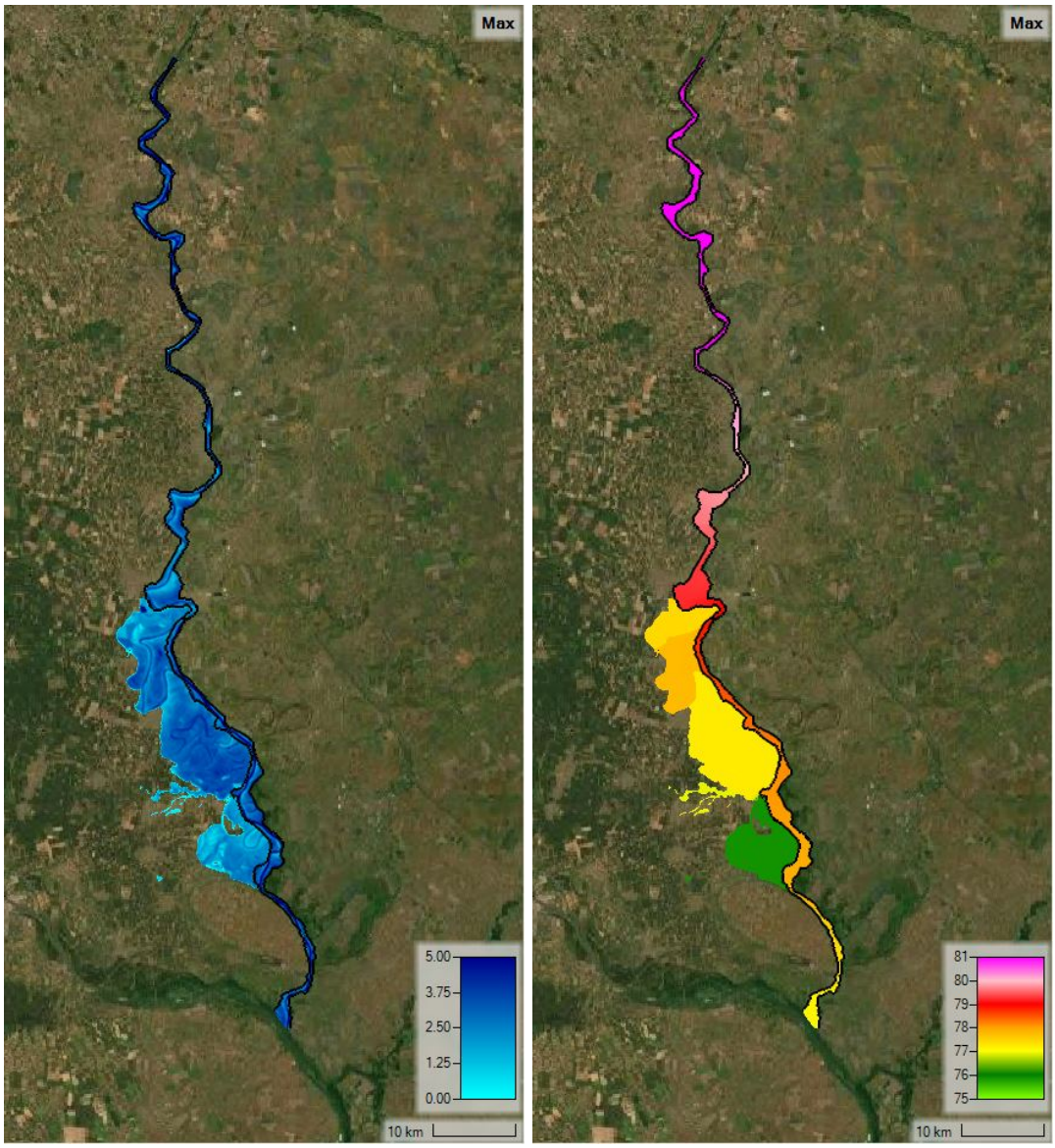

Figure C.41: Inundation depth and water surface level maps for location W5 with a return period of 100 years.

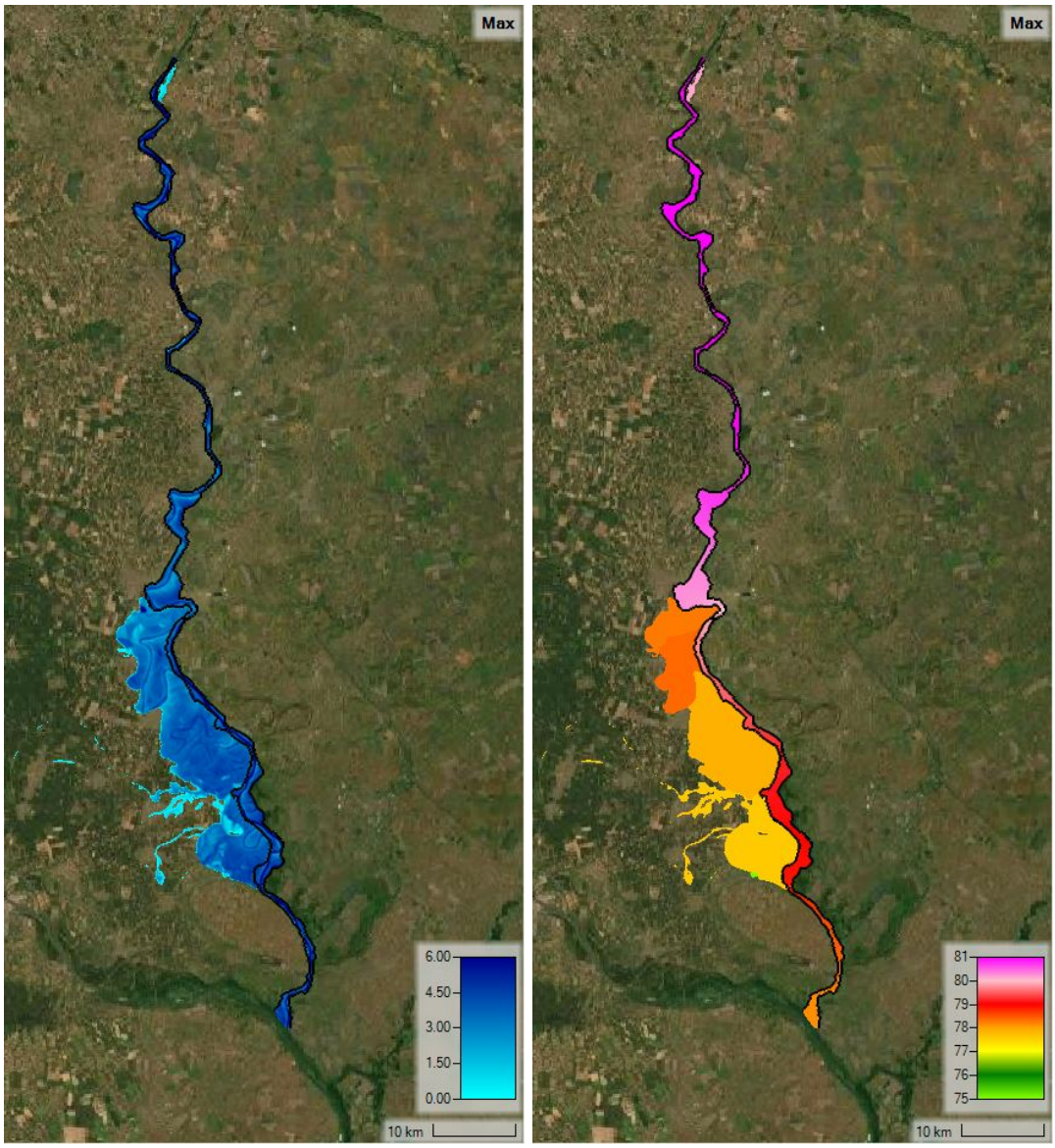

Figure C.42: Inundation depth and water surface level maps for location W5 with a return period of 1000 years.

C.15 Location W6

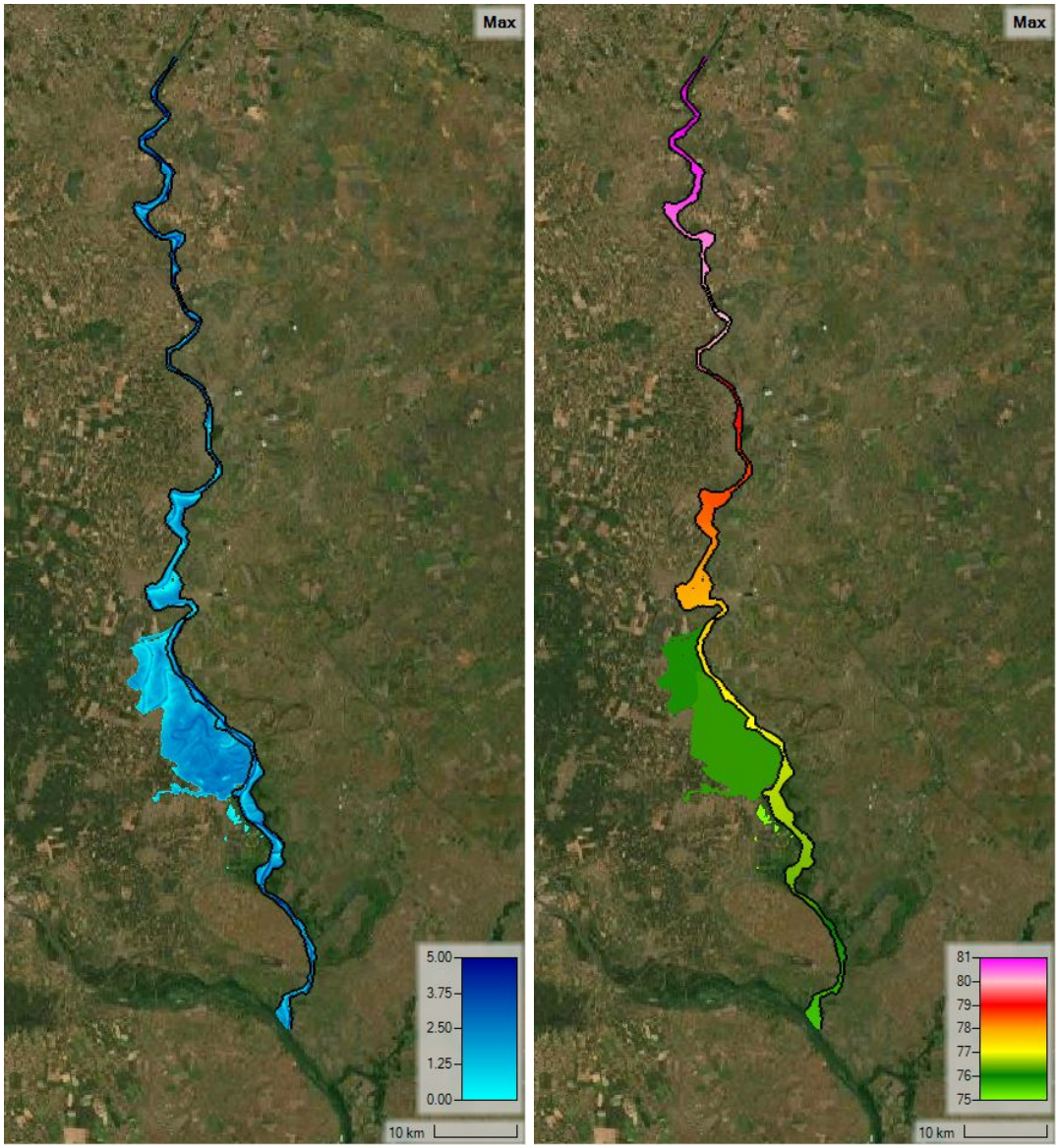

Figure C.43: Inundation depth and water surface level maps for location W6 with a return period of 10 years.

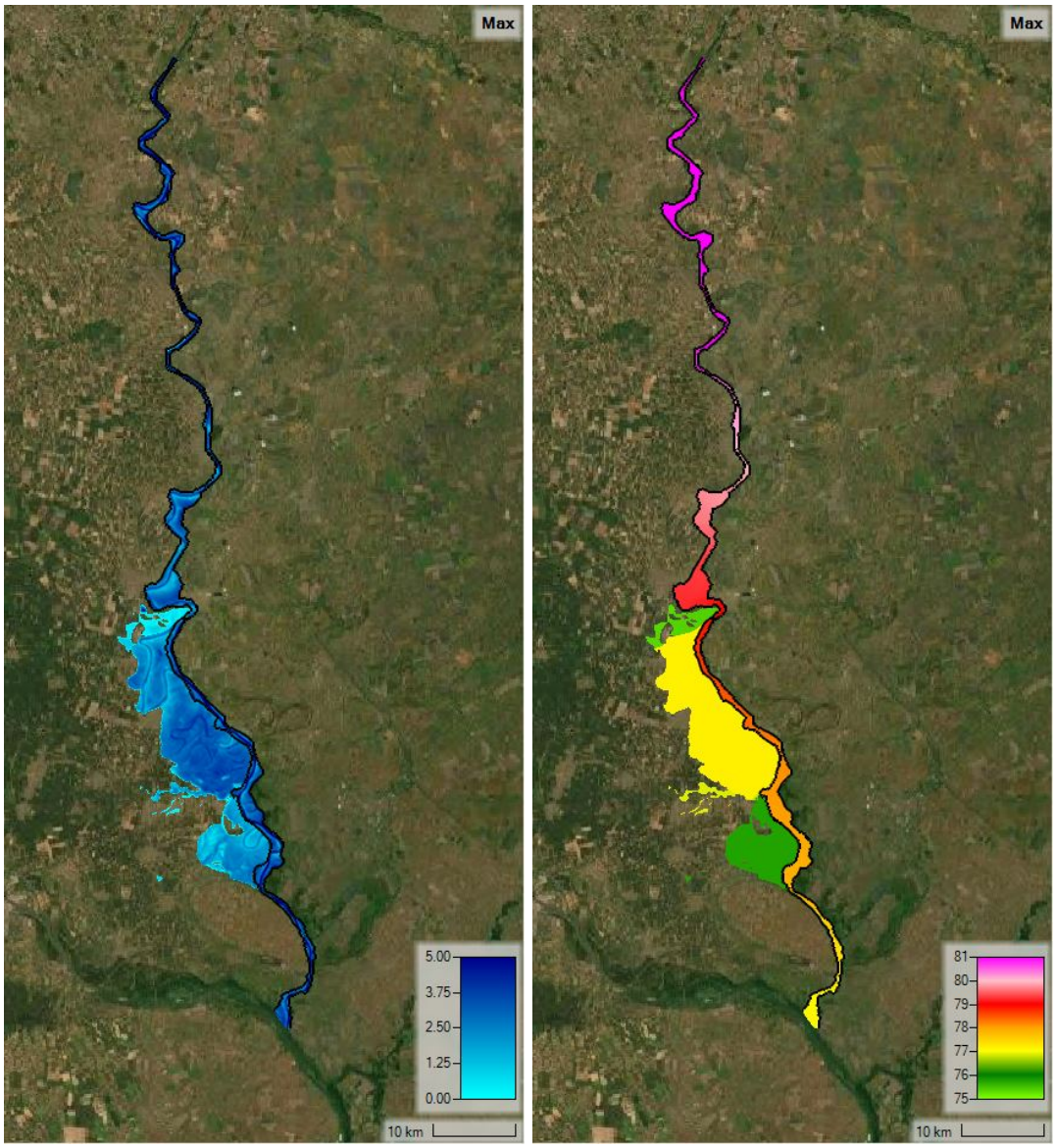

Figure C.44: Inundation depth and water surface level maps for location W6 with a return period of 100 years.

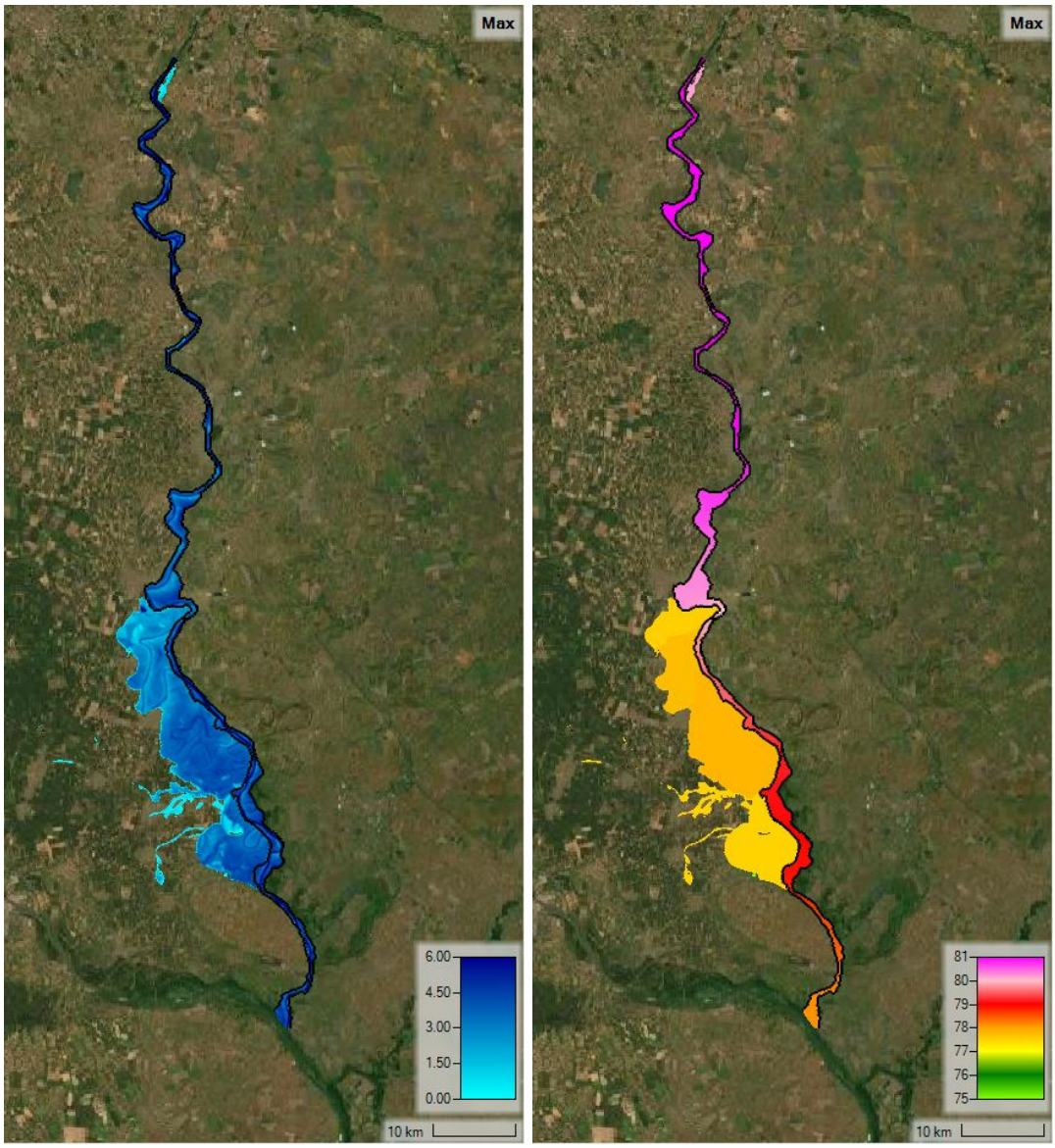

Figure C.45: Inundation depth and water surface level maps for location W6 with a return period of 1000 years.

C.16 Location W7

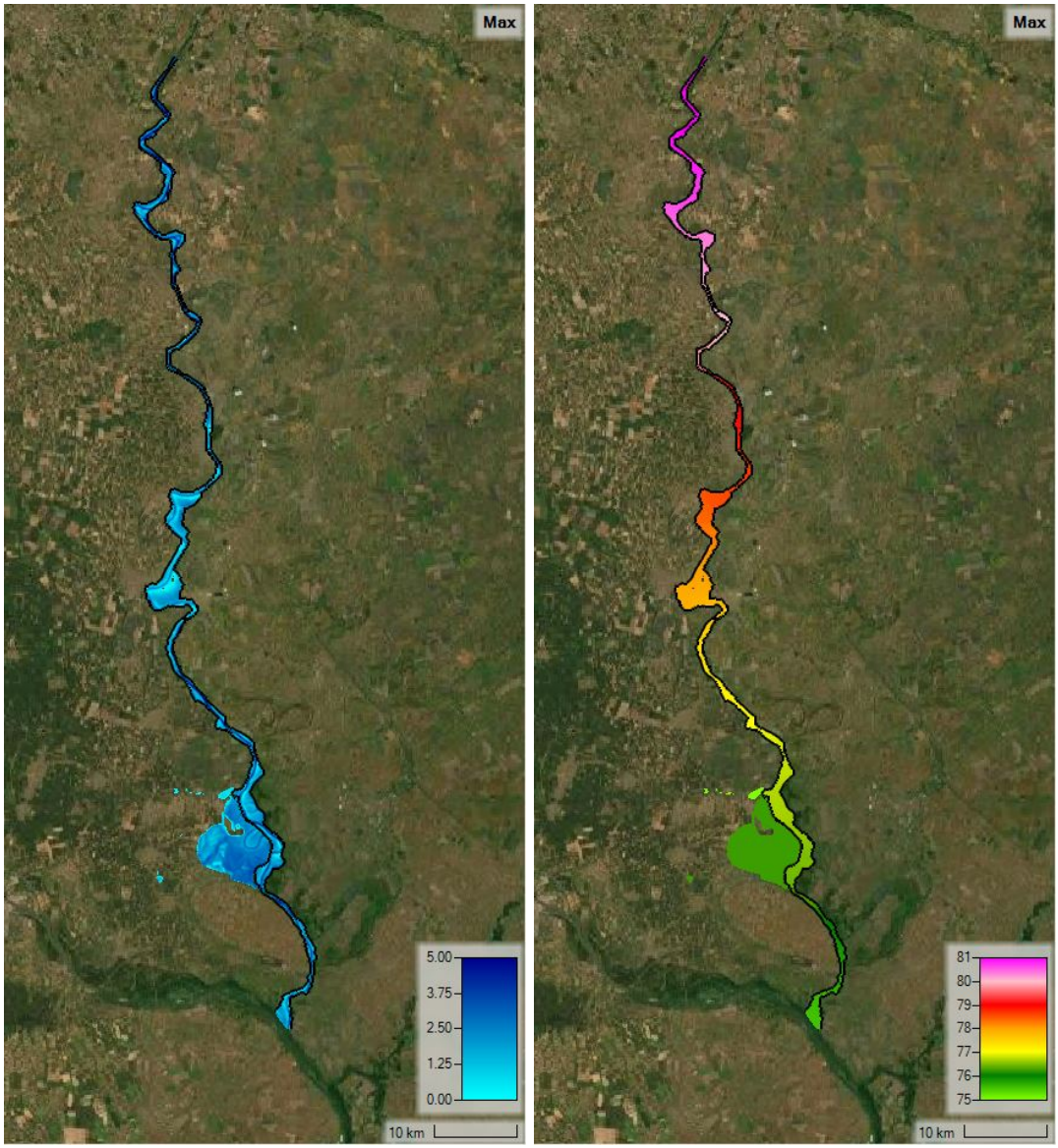

Figure C.46: Inundation depth and water surface level maps for location W7 with a return period of 10 years.

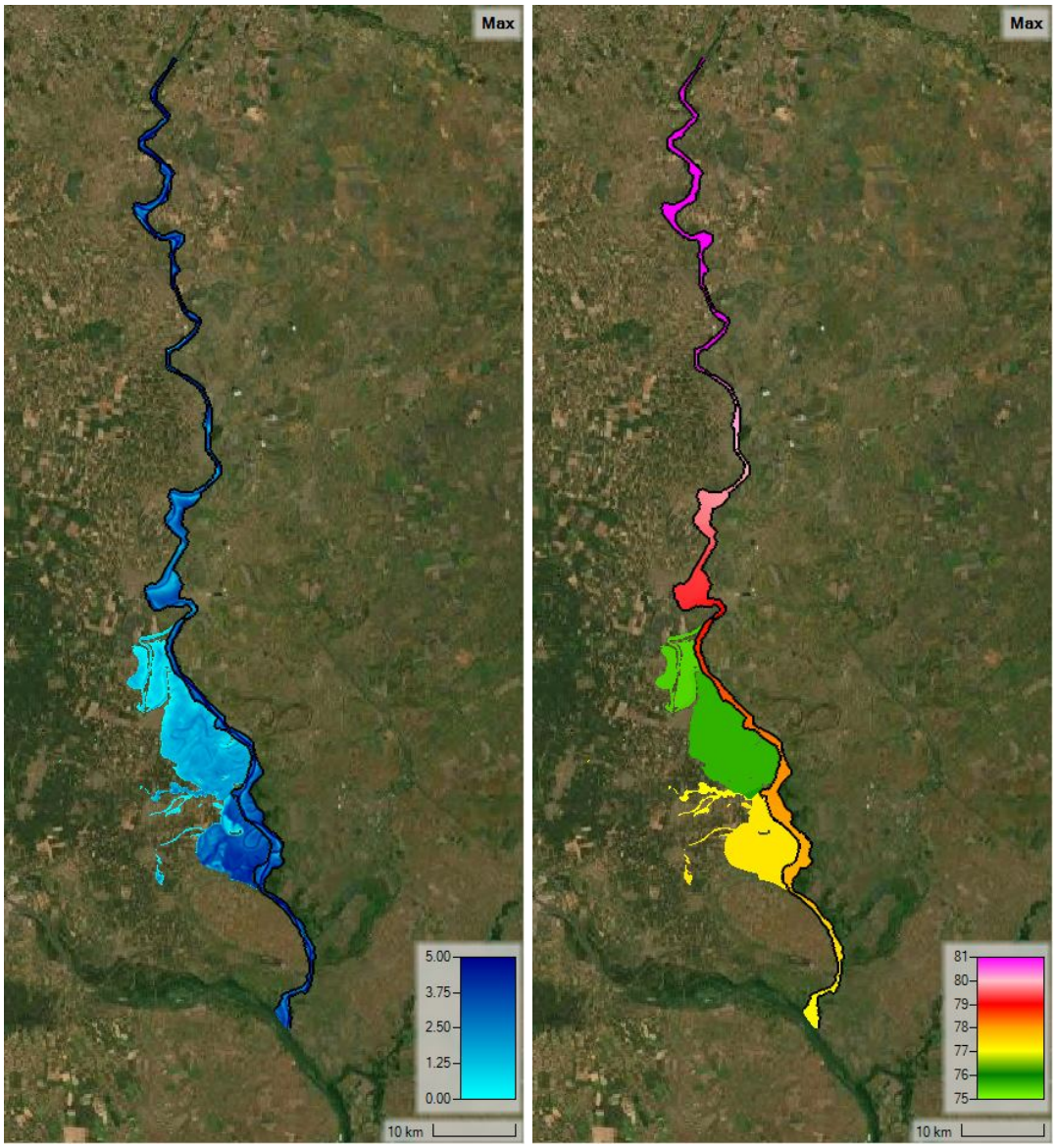

Figure C.47: Inundation depth and water surface level maps for location W7 with a return period of 100 years.

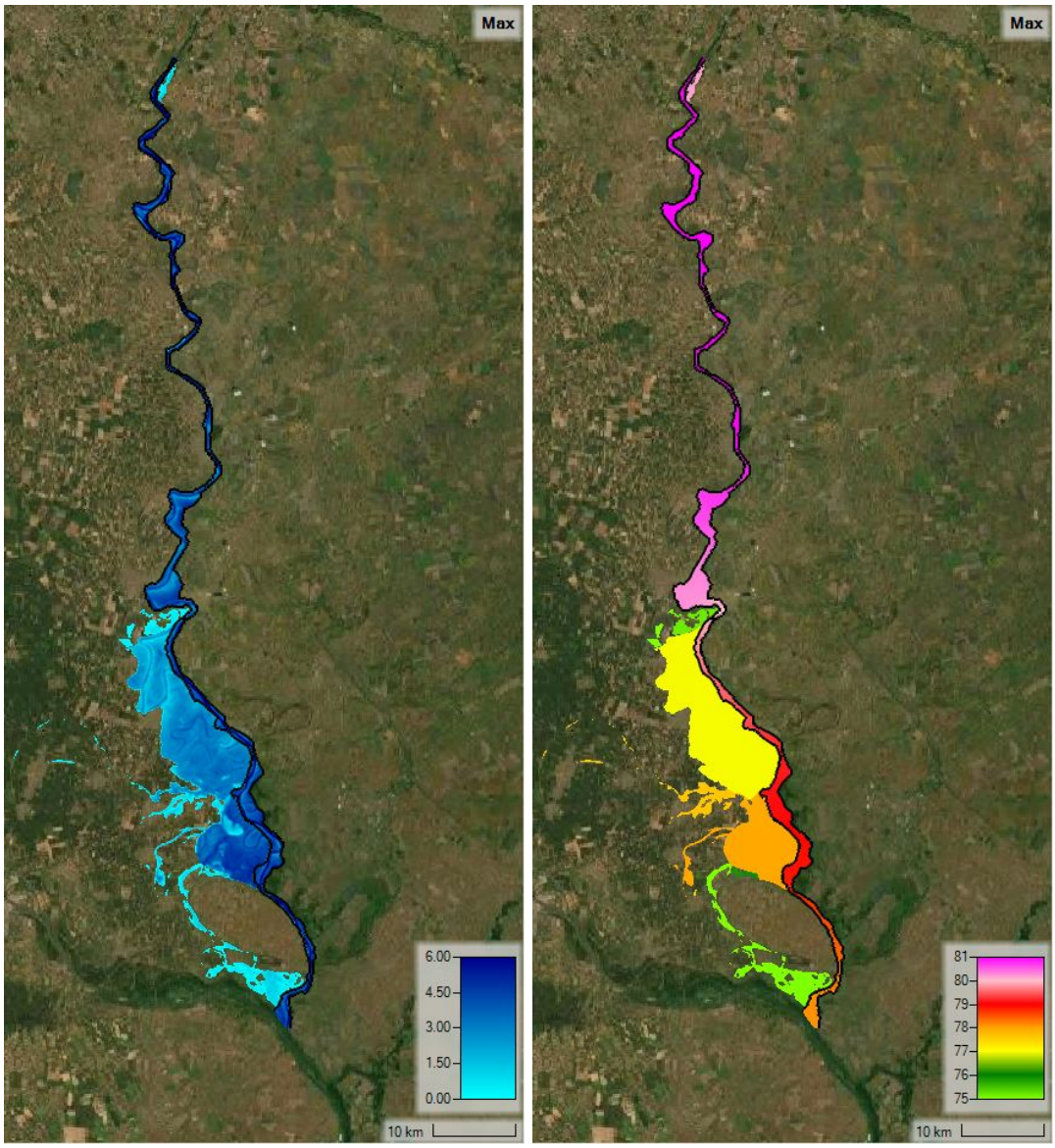

Figure C.48: Inundation depth and water surface level maps for location W7 with a return period of 1000 years.